Metalloproteinase Expression in Bone Marrow-derived Macrophages: Roles in Cell Migration

A thesis submitted to the University of East Anglia
for the degree of Doctor of Philosophy

By
Megan Murray

University of East Anglia
School of Biological Sciences
Norwich, NR4 7TJ

August 2010

Abstract

Macrophages are phagocytic leukocytes that mediate the innate immune response and can respond to lipopolysaccharide (LPS), a component of the gram negative bacterial cell wall. LPS activates pro-inflammatory signalling, triggering the release of inflammatory mediators and modulating gene expression. Matrix metalloproteinases (MMPs) are capable of degrading the extracellular matrix (ECM) whilst also mediating the proteolytic processing of growth factors, cytokines and chemokines. MMPs have long been associated with cell migration and invasion, and are therefore implicated in the macrophage response to infection and inflammation.

In this thesis the expression of metalloproteinase mRNA in murine bone marrow-derived macrophages (BMM) has been profiled in response to LPS with the use of quantitative RT-PCR (qRT-PCR). LPS induced the differential expression of several metalloproteinases in a time- and dose-dependent manner. Of particular interest was the novel down-regulation of MMP-10 mRNA following LPS treatment. As LPS is known to elicit a rapid pro-migratory macrophage response *in vitro* and *in vivo*, time-lapse microscopy was employed to study the effect of LPS on BMM migration on a two dimensional fibronectin matrix, a known MMP-10 substrate. Intriguingly, LPS was found to significantly repress BMM migration on fibronectin 24 hours post-treatment, coinciding with the down-regulation of MMP-10 expression. siRNA targeting the MMP-10 transcript mimicked the LPS-induced repression of BMM migration velocity. This repression of BMM migration could, in turn, be rescued with recombinant MMP-10 protein.

Both macrophages and metalloproteinases are associated with the process of wound healing. The type II diabetic mouse (Db/Db), a model of impaired wound healing, was utilised to investigate the expression of MMP-10 in wounded skin. Interestingly Db/Db BMMs display a significantly variation in morphology and a repressed migratory response to chemoattractant stimuli compared to their heterozygous controls. The mechanisms behind this, however, are unclear.

A potential metalloproteinase-driven mechanism has been identified by which macrophage migration in response to infection may be modulated. This has broad implications in understanding the control of macrophages in several pathologies, particularly in type II diabetes and the associated impaired wound healing response.

Acknowledgements

It is not possible to overstate my gratitude to my primary supervisor, Dr. Jelena Gavrilovic, for giving me the opportunity to join her lab and for being a constant and unflagging source of support and inspiration for the last four years. I could not have wished for a better supervisor (especially in the face of my occasional meltdowns!) and I can only hope that she has enjoyed teaching me half as much as I have enjoyed learning from her.

I am also extremely grateful to all those in the Gavrilovic lab, past and present, who welcomed me to the BMRC and taught me numerous techniques. I am particularly indebted to Dr. Damon Bevan for all his help with sectioning and staining, and for generally keeping me entertained; to Dr. Wei Shi for teaching me 'Taqman' (in a foreign language, no less); and to Dr. Natasha Baker for being a PhD student to aspire to! I would also like to thank new recruit Dr. Jon Howe for coming along, fresh from his write-up, with plenty of advice on how to retain my sanity throughout the process.

I would like to thank my industrial supervisor, Dr. Mark Fidock, for giving me the chance to experience life at Pfizer; and my advisor Dr. Mette Mogensen for her insightful comments on imaging and for operating an 'open door' policy when it came to borrowing antibodies.

Special thanks go to the late Prof. George Duncan for all his advice throughout my undergraduate degree and all too briefly during the start of my PhD.

None of this would have been possible if it weren't for the tireless emotional strength of my family. Mum, Dad and Morgain; I really don't know how you've put up with me for the last 25 years, but I love you for it and hope I've made you proud.

Finally all my love and gratitude go to Lox for his support (both emotional and financial!) and his seemingly limitless patience. Thank you for never once questioning why it's taken me *so* long to finish writing up.

List of Abbreviations

2D	-	Two Dimensional
3D	-	Three Dimensional
ABC	-	Avidin-Biotin Complex
ADAM	-	A Disintegrin and Metalloproteinase
ADAMTS	-	A Disintegrin and Metalloproteinase with Thrombospondin
AGE	-	Advanced Glycation Product
Arp2/3	-	Actin Related Protein 2/3
BMM	-	Bone Marrow-derived Macrophage
CCL	-	CC Chemokine Ligand
CCR	-	CC Chemokine Receptor
CD	-	Cluster of Differentiation
Cdc42	-	Cell Division Control Protein 42
CSF-1	-	Colony Stimulating Factor – 1
CSF-1R	-	Colony Stimulating Factor – 1 Receptor
C_T	-	Cycle Threshold
CXCL	-	CXC Chemokine Ligand
CXCR	-	CXC Chemokine Receptor
DAB	-	Diaminobenzidine
DAPI	-	4',6-diamidino-2-phenylindole
DIC	-	Differential Interference Contrast
ECM	-	Extracellular Matrix
EGF	-	Epidermal Growth Factor
FGF	-	Fibroblast Growth Factor
GAP	-	GTPase Activating Protein
GDI	-	Guanine Nucleotide Dissociation Inhibitors
GEF	-	Guanine Nucleotide Exchange Factor
GPCR	-	G-Protein Coupled Receptor

GTP	-	Guanosine Triphosphate
HDAC	-	Histone Deacetylase
HGF	-	Hepatocyte Growth Factor
HSC	-	Hematopoietic Stem Cell
HUVEC	-	Human Umbilical Vein Endothelial Cell
IGF	-	Insulin-like Growth Factor
IKK	-	IκB kinase
IL	-	Interleukin
IκB	-	Inhibitor of kappa B
LDL	-	Low Density Lipoprotein
LPS	-	Lipopolysaccharide
MAPK	-	Mitogen Activated Protein Kinase
MCP-1	-	Monocyte Chemotactic Protein – 1
MEF-2	-	Myocyte Enhancer Factor 2
miRNA	-	MicroRNA
MMP	-	Matrix Metalloproteinase
MT-MMP	-	Membrane Type – Matrix Metalloproteinase
MTOC	-	Microtubule Organising Centre
MyD88	-	Myeloid Differentiation Primary Response Gene 88
NF-κB	-	Nuclear Factor – kappa B
NGS	-	Normal Goat Serum
oxLDL	-	Oxidized Low Density Lipoprotein
PAMP	-	Pathogen Activated Molecular Pattern
PECAM	-	Platelet /Endothelial Cell Adhesion Molecule
PI3-K	-	Phosphatidylinoside-3- Kinase
PML-NB	-	Promyelocytic Leukemia Protein – Nuclear Bodies
PPR	-	Pattern Recognition Receptor
qRT-PCR	-	Quantitative Real-Time - Polymerase Chain Reaction
RNAi	-	RNA Interference

ROCK	-	Rho Kinase
ROS	-	Reactive Oxygen Species
SEM	-	Standard Error of the Mean
Shh	-	Sonic Hedgehog
siRNA	-	Small Interfering RNA
TCA	-	Trichloroacetic acid
TIMP	-	Tissue Inhibitor of Metalloproteinase
TLR	-	Toll-like Receptor
TNF-α	-	Tumour Necrosis Factor – alpha
uPA	-	Urokinase Plasminogen Activator
VCAM	-	Vascular Cell Adhesion Molecule
VEGF	-	Vascular Endothelial Growth Factor
VSMC	-	Vascular Smooth Muscle Cell
WASp	-	Wiskott-Aldrich Syndrome Protein
WAVE	-	Wiskott-Aldrich Syndrome Protein Family Verprolin Homologous Protein
WT	-	Wild Type

Table of Contents

List of Figures and Tables

Figures

Tables

Chapter 1: **Introduction**

1.1 Inflammation and the immune response

1.1.1 The innate immune system

The immune system is composed of a diverse array of responses that enable host protection against disease-causing pathogens, toxins, and allergenic substances, whilst differentiating self from non-self to maintain homeostasis. The immune system can be broadly categorised into to two subsets: innate immunity and the adaptive response.

Innate immunity includes all aspects of the host immune response that are encoded for by an organism's germline genetic code. This response is non-specific but occurs immediately following exposure to a pathogen or non-self molecule. Despite its lack of specificity and inability to confer long-lasting protection, the innate immune response is actually far more sophisticated than originally thought. The component features of the innate response are numerous and include factors secreted from cells, such as cytokines, chemokines and free radical species; bioactive molecules present in bodily fluids, including complement proteins and defensins; and membrane-bound and cytosolic receptor proteins that are able to recognise pathogen-associated molecular patterns (PAMPs) (Chaplin, 2010).

The features of the innate immune response described above fall into two main categories of functional response to pathogen invasion; the complement system and inflammation. The complement system is a biochemical cascade of zymogen activation that ultimately results in the destruction of pathogens by marking them via opsonisation and then recruiting the cells and proteins able to facilitate their lysis. The molecules resulting from the complement cascade are pro-inflammatory in nature and thus trigger the next stage in the innate immune response. The complement system also acts as a bridge between innate and adaptive immunity by influencing the behaviour and differentiation of B-cells, the principle function of which is to produce antibodies (Dunkelberger and Song, 2010).

The cellular component of inflammation is mediated by leukocytes, and can be acute, involving granulocytes; or chronic, involving monocytes and lymphocytes. Both forms of inflammation are characterised by marked vascular changes such as vasodilation and increased vessel permeability, and are the result of increased expression of pro-inflammatory factors secreted by leukocytes (Chaplin, 2010). To fully understand the inflammatory response it is important to first consider the hematopoietic cell lineage from which all leukocytes are derived.

1.1.2 The haematopoietic lineage and macrophage differentiation

1.1.2.1 Haematopoiesis

Haematopoiesis is the process through which all the cellular components of the blood derive from haematopoietic stem cells (HSC) in the bone marrow. This maintains a steady state of blood cells in the peripheral circulation of healthy organisms and also allows for the production of important immune cells in response to infection and inflammation. Haematopoietic cells can be broadly divided into three main lineages; erythroid, lymphoid and myeloid (figure 1.1) that function in oxygen transport, adaptive immunity and innate immunity, respectively. As with all stem cells, HSCs have the ability to differentiate into any one of these multiple cell lineages whilst also being responsible for replenishing the pluripotent population by a process of self-renewal (Rosmarin et al., 2005). At each stage of differentiation cell type is defined by cell surface markers and functional activity.

1.1.2.2 Macrophage differentiation

The process of differentiation from HSCs to myeloid progenitor cells, monoblasts, monocytes, and finally to macrophages does not depend on the action of one 'master regulator' transcription factor. Instead a combination of external cytokine signals regulates the developmentally ordered expression of a set of transcription factors, including PU.1 (purine-rich PU-box binding) and C/EBP (CCAAT/enhancer-binding protein)-α, which are critical in myeloid lineage commitment (Friedman, 2002) (figure 1.1). Once a monoblast has committed to the monocytic lineage it can leave the bone marrow as a peripheral blood monocyte. The cytokines that orchestrate the final stage of differentiation into tissue macrophages are also responsible for the simultaneous migration of monocytes out of the blood vasculature and into tissue. The chemokine colony stimulating factor (CSF)-1, for example, induces differentiation and proliferation of monocytes whilst also functioning as a potent chemoattractant (Pixley and Stanley, 2004).

1.1.2.3 CSF-1

Despite there being no single 'master regulator' of monocyte/macrophage differentiation, a putative hierarchy could place additional significance on CSF-1. In mice unable to express functional CSF-1 protein macrophage number is severely reduced, mice exhibit poor breeding due to impairment of ovulation and life-span is significantly reduced compared to their wild-type litter mates (Pollard, 1997; Wiktor-Jedrzejczak et al., 1990). These mice also have reduced bone marrow cellularity, with total cell number being around 10% of healthy mice. Conversely, the constitutive expression of the CSF-1 receptor (CSF-1R) is enough to trigger a change of cell fate, forcing B-lymphocyte progenitors to irreversibly 'switch' lineage to macrophages (Borzillo et al., 1990). The

over-expression of transcription factor PU.1 has a similar effect, stimulating macrophage proliferation from B-lymphoid progenitors (Friedman, 2002).

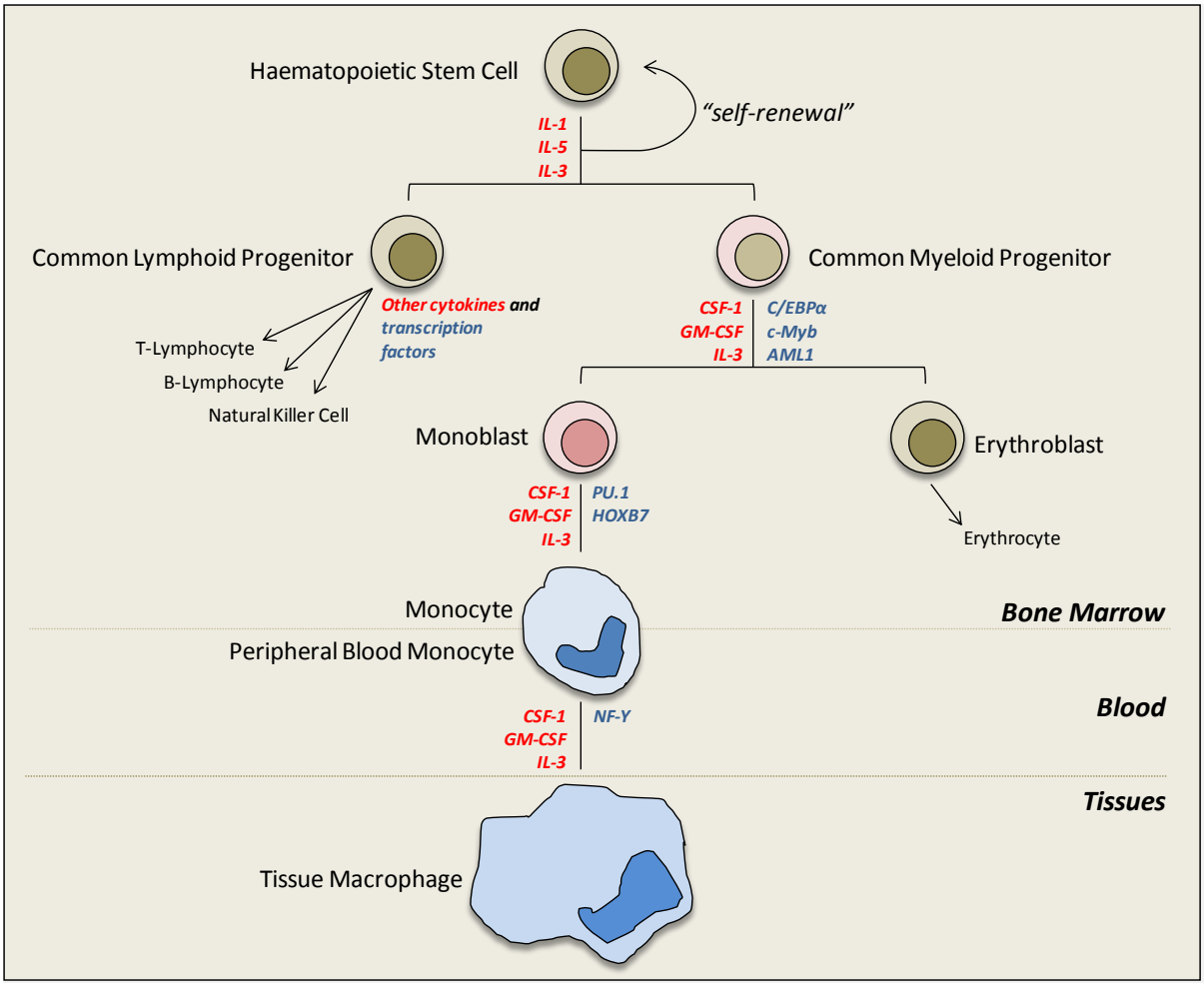

Figure 1.1 Haematopoiesis and macrophage differentiation. A simplified schematic to show the process of differentiation from haematopoietic stem cell to tissue macrophage. At each stage the key chemokines and cytokines (red), and transcription factors (blue) that drive the commitment and maturation of the myeloid lineage are indicated. AML1 – acute myeloid leukaemia 1; CSF-1 – colony stimulating factor-1; C/EBPα - CCAAT/enhancer-binding protein-α; GM-CSF – granulocyte monocyte-CSF; HOXB7 – Homeobox B7; IL – interleukin; NF-Y – nuclear transcription factor-Y; PU.1 - purine-rich PU-box binding. Information for this figure taken from (Valledor et al., 1998; Chaplin, 2010).

1.1.3 The role of peripheral blood monocytes and tissue macrophages during infection and inflammation

The primary function of the macrophage is as a phagocyte. During phagocytosis macrophages engulf and digest anything they recognise as non-self, for example, pathogens and foreign bodies. Macrophages also have the ability to also recognise dead and dying cells, removing cellular debris and necrotic tissue as a vital part of the wound healing process (Leibovich and Ross, 1975; Kong and Ge, 2008) (see Chapter 1, 1.3.2) .

1.1.3.1 Pattern recognition receptors and Pathogen associated molecular patterns: Toll-like receptors and lipopolysaccharide

Macrophages are able to recognise such a vast number of self and non-self molecules (and make decisions about how to respond to them) because they express a high number of pattern recognition receptors (PRRs) on their cell surface. PRRs are able to identify specific pathogen associated molecular patterns (PAMPs), such as lipopolysaccharide (LPS). LPS forms a major component of the bacterial outer membrane and is composed of a hydrophilic polysaccharide moiety and a fatty acid 'lipid A' hydrophobic domain. Whilst the lipid A portion is anchored to the outer membrane, the polysaccharide backbone protrudes into the host micro-environment where it can be detected and bound by macrophage PRRs. PRRs are classified according to their ligand specificity and include the toll-like receptors (TLRs). TLRs mediate cellular signalling through the cell membrane via adaptor proteins that trigger complex signalling pathways, resulting in the increased transcription of pro-inflammatory genes (Guha and Mackman, 2001).

LPS, for example, is recognised by TLR4 in complex with CD14, a cell surface glycoprotein, and myeloid differentiation protein (MD)-2 (figure 1.2). A serum lipid binding protein (LBP) transfers LPS to CD14 on the macrophage cell surface; however CD14 cannot activate pro-inflammatory signal transduction alone as it lacks transmembrane and intercellular domains. CD14 therefore presents LPS to the TLR4/MD-2 complex, initiating signal transduction via the TLR4 cytoplasmic domain (Fujihara et al., 2003). LPS-stimulated signalling via TLR4 is explored in more detail in Chapter 3.

When a macrophage recognises and binds to a pathogen via its PRRs the pathogen is then engulfed in a phagosome. Phagosomes eventually fuse with lysosomes in the cytoplasm initiating a release of enzymes, an oxidative burst and a reduction in pH in order to destroy the pathogen (Blander and Medzhitov, 2006). Waste products remain in the phagosome until they are expelled from the macrophage or integrated into the cell surface in a process known as antigen presentation whereby B-cell antibody production is stimulated (Blander and Medzhitov, 2006).

In terms of their location there are two types of macrophage involved in pathogen recognition and the immune response; resident macrophages and blood-borne monocyte-derived tissue macrophages. Resident macrophages are present in tissue at low levels and are immediately protective against invasion of pathogens and available for homeostatic clearance of cellular debris. Monocytes, however, move from the circulation into infected tissues via the process of monocyte recruitment, diapedesis and differentiation into monocyte-derived tissue macrophages.

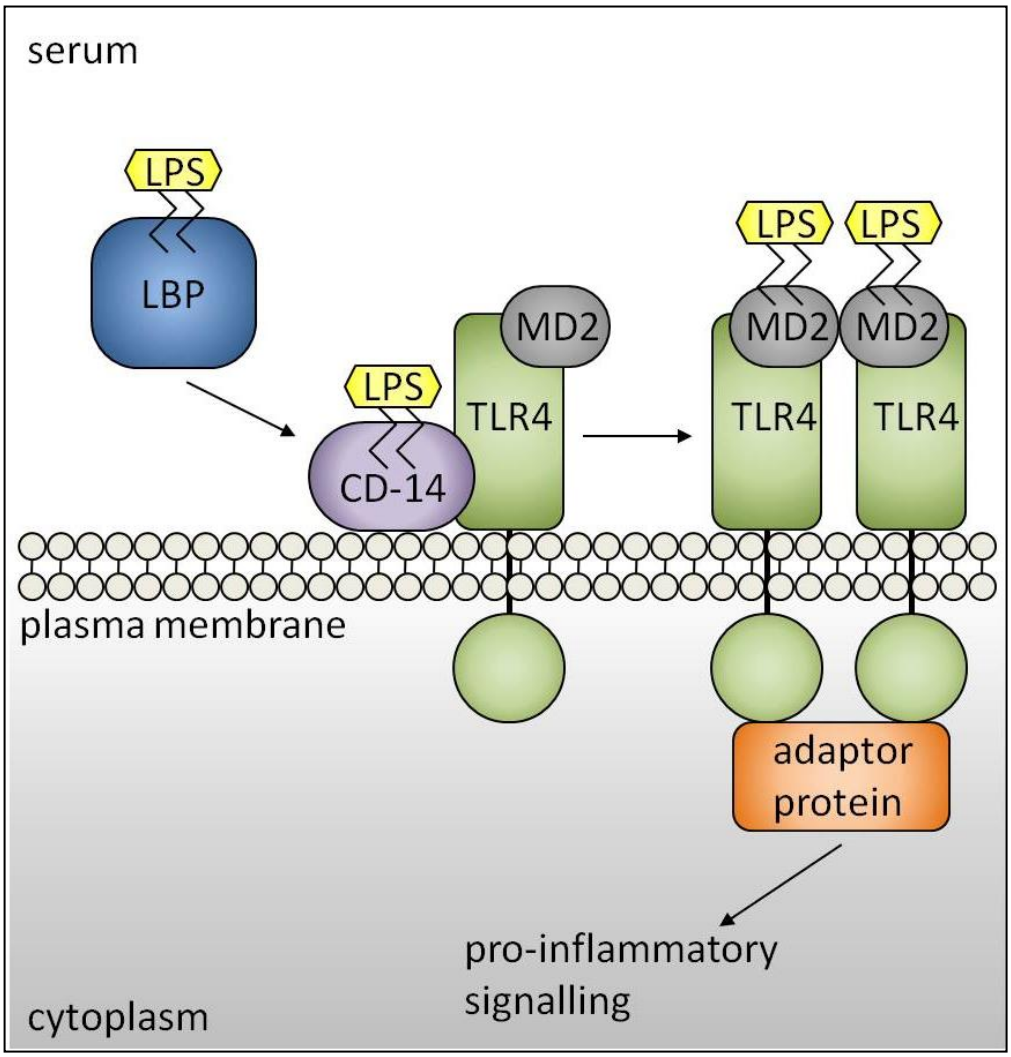

Figure 1.2 LPS recognition by TLR4 on the macrophage cell surface. LBP in the serum binds the lipid A portion of LPS, transferring LPS to CD14 on the cell surface. CD14 concentrates LPS and presents it to TLR4 in complex with accessory protein MD-2. This induces a conformational change and triggers dimerisation of TLR4. This in turn stimulates pro-inflammatory signalling, such as NF-κB, via cytosolic adaptor proteins (see Chapter 3, figure 3.1 for more detail). Information for this diagram taken from (Fujihara et al., 2003; Guha and Mackman, 2001).

1.1.4 The recruitment of monocytes and their diapedesis into sites of infection and inflammation

The recruitment of peripheral blood monocytes to sites of infection and inflammation, and their subsequent diapedesis and differentiation into tissue macrophages, is vital to tissue homeostasis and host defence. Whilst there are a small number of resident tissue macrophages in all tissues it is necessary for their presence to be massively augmented in response to pro-inflammatory stimulation. Circulating monocytes are arrested in blood vessels surrounding areas of infected or injured tissue by becoming tethered to the surface of the activated endothelium. Once attached to the lining of the blood vessel monocytes are able to first roll then 'crawl' towards the damaged tissue along a gradient of chemotactic cues before transmigration through the endothelium and basement membrane (figure 1.3).

1.1.4.1 Selectins and monocyte rolling

The process of monocyte rolling and crawling is made possible by the synchronised making and breaking of cell adhesion molecules (reviewed in (Worthylake and Burridge, 2001)). This includes the transmembrane selectins, of which there are three variants; P-, E- and L-selectin. This adhesion cascade begins with the activation of the endothelium by cytokines, such as TNF-α, which are secreted into the wound site by damaged cells and early response immune cells such as neutrophils. Activated endothelial cells express P-selectin and E-selectin, both of which bind ligands on the surface of the monocytes facilitating their loose adhesion and rolling (figure 1.3). P-selectin, for example, binds P-selectin glycoprotein ligand-1 (PSGL-1) and signals through this to activate monocyte integrin expression (Huo and Xia, 2009). Leukocytes express L-selectins that, as well as mediating leukocyte rolling on the endothelium, also allows for secondary leukocyte capture, i.e., the interaction of free flowing leukocytes with rolling leukocytes (Galkina and Ley, 2007). L-selectin also relays information about the leukocyte microenvironment via specific protein binding sites its cytoplasmic tail (reviewed in (Ivetic and Ridley, 2004)). The importance of L-selectin interaction with the cytoskeleton has been highlighted in a recent mutagenesis study. This revealed reduced L-selectin mediated tethering and a reduction in the shedding of the L-selectin ectodomain upon leukocyte activation (Ivetic et al., 2004).

1.1.4.2 Integrins mediate firm adhesion of monocytes

Integrins are heterodimeric transmembrane receptors that connect the actin cytoskeleton of the cell to the surrounding matrix proteins, mediating the firm adhesion of monocytes to the endothelium (Brakebusch and Fassler, 2003) (figure 1.4). Integrins are composed of two distinct α and β subunits both of which contain transmembrane domains. Generally, the α domain

determines the specificity of ligand binding whilst the β subunit interacts with the cytoskeleton. Variants of each subunit exist, allowing the generation of 24 unique receptors (reviewed in (Barczyk et al., 2010)). Integrins can signal in a bi-directional manner, that is they are able to mediate signals from the 'inside-out' as well as the 'outside-in'.

'Inside-out' signalling appears to act mainly to bring the α and β subunits into their active conformation through the formation of focal adhesion complexes. Focal adhesion complexes are typically composed of cytosolic proteins, for example, talin and vinculin, which form a bridge between the β integrin subunit and the actin cytoskeleton. In leukocytes, another cytoskeleton-associated protein, Paxillin, has also been shown to interact with the cytosolic domain of the α4 integrin (Alon et al., 2005). The Kindlins are a relatively novel family of integrin-related proteins. Haematopoietic lineage-specific kindlin-3, for example, has been shown to bind to β1 and β3 integrin tails triggering integrin activation and enhancing macrophage binding to fibronectin (Moser et al., 2008). Focal adhesions, as their name suggests, have been shown to be expressed at specific foci on the cell surface during two-dimensional (2D) cell adhesion. Recent studies, however, have revealed a more diffuse expression pattern of focal adhesion proteins during three-dimensional (3D) migration (Fraley et al., 2010).

Once in their active conformation integrins can mediate 'outside-in' signals in response to the extracellular environment. Integrins can bind to matrix proteins, such as fibronectin and collagens, and other cell-adhesion molecules. This allows for the firm adhesion of cells to the surrounding matrix, whilst also mediating signals that trigger changes in cell behaviour and differentiation. For example, the α4β1 integrin heterodimer expressed on leukocytes binds to vascular cell adhesion molecule (VCAM)-1 on the endothelium. The expression of VCAM-1 is up-regulated by pro-inflammatory stimuli and studies have shown that blocking VCAM-1 binding dramatically reduces the migration of monocytes across an endothelial monolayer *in vitro,* reflecting its role in adhesion (Ronald et al., 2001). Integrin α4β1 is also known to bind fibronectin, present both in a soluble form in the blood and as an insoluble matrix in both healthy and wounded tissue. Fibronectin binding stimulates the nuclear translocation of nuclear factor (NF)-κB (Roldan et al., 1992). NF-κB (discussed in detail in Chapter 3) is a transcription factor known to play a role in the differentiation of immune cells including monocytes/macrophages (Hoffmann and Baltimore, 2006).

In order for continuous crawling along the endothelium to proceed, monocyte-integrin interactions participate in a negative feedback loop that enables the detachment of old adhesions triggered by the formation of new ones. For example, the activation of αvβ3 integrin binding in

monocytes feeds back to decrease the engagement of β2 integrins in the same cell (Worthylake and Burridge, 2001). Increasingly data are emerging that implicate proteinases in the process of cell adhesion molecule cleavage. Specifically the ADAMs (a disintegrin and metalloproteinase; described in more detail in Chapter 1, 1.2), are capable of cleaving all selectins implicated in monocyte rolling and the cell adhesion molecules involved in firm adhesion and crawling (Reiss et al., 2006). For example, B-cells from the ADAM17$^{-/-}$ mouse express higher levels of L-selectin on the cell surface due to reduced ADAM mediated shedding (Le Gall et al., 2009). Recently, ADAM17 mediated shedding of L-selectin has been shown to be enhanced in activated leukocytes as a result of increased ADAM17 levels at the plasma membrane (Killock and Ivetic, 2010). In addition to its action as a sheddase at the leukocyte surface, ADAM-17 can also cleave VCAM-1 from the surface of TNF-α stimulated endothelial cells (Singh et al., 2005). In combination with the integrin negative feedback mechanism the protease mediated cleavage of cell adhesion molecules probably contributes to successful translocation of monocytes over the endothelium along the gradient of chemo-attractant.

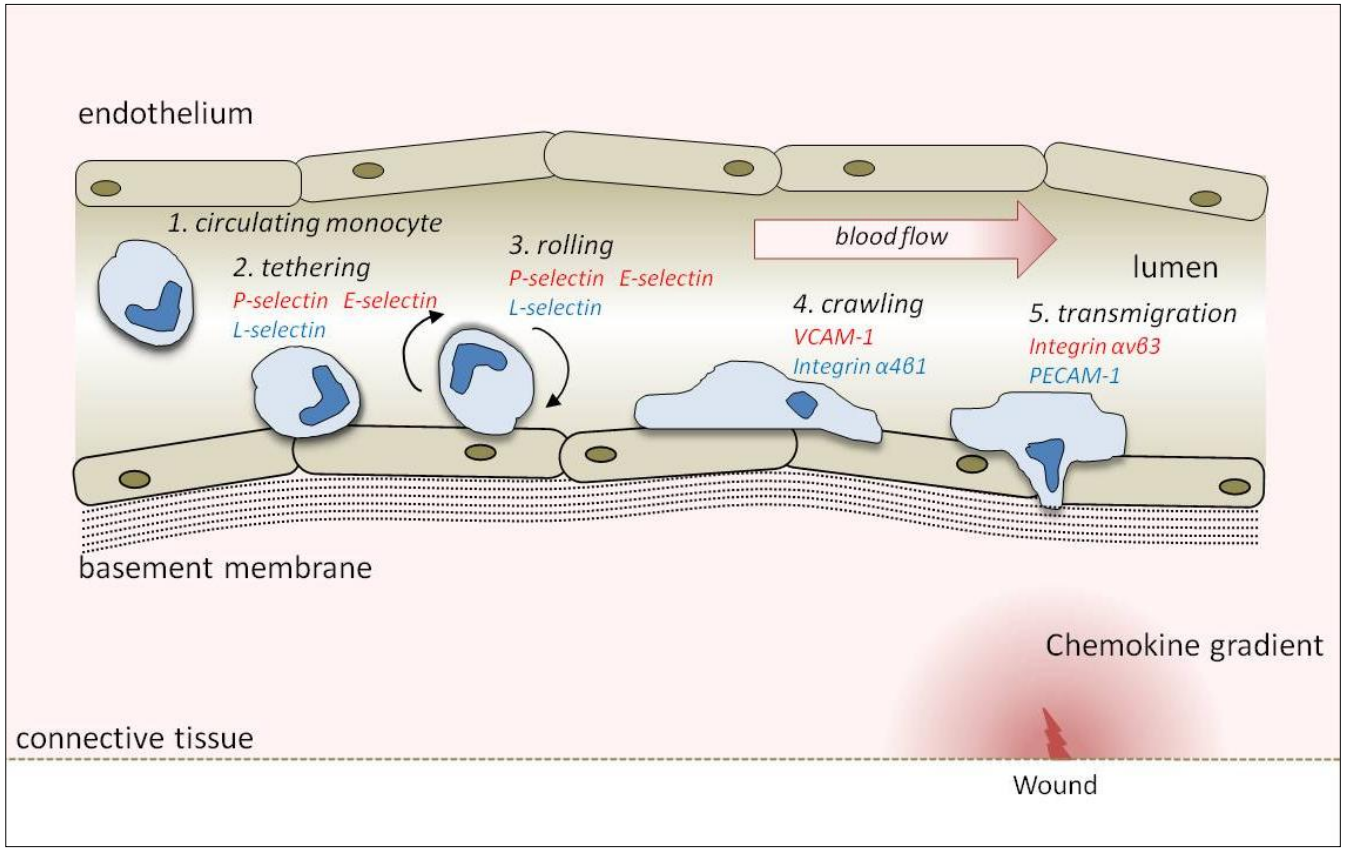

Figure 1.3 Key steps in monocyte recruitment to sites of infection and injury: the adhesion cascade. (1) Peripheral blood monocytes respond to activated endothelial cells by (2) loosely tethering to the endothelium. (3) Interaction with cell adhesion molecules triggers rolling of the monocyte along the endothelium followed by (4) firm adhesion as monocyte becomes activated and begins to take on macrophage characteristics. (5) As the gradient of chemokines becomes stronger the monocyte commences transmigration of the endothelium and basement membrane becoming a fully differentiated tissue macrophage. This process can occur under the shear flow of blood through larger vessels but more commonly takes place in smaller venules and capillaries where flow is slower and less rate-limiting. Red text indicates relevant endothelial cell adhesion molecules; blue text indicates relevant leukocyte cell adhesion molecules. Figure adapted from (Martin and Leibovich, 2005; Worthylake and Burridge, 2001).

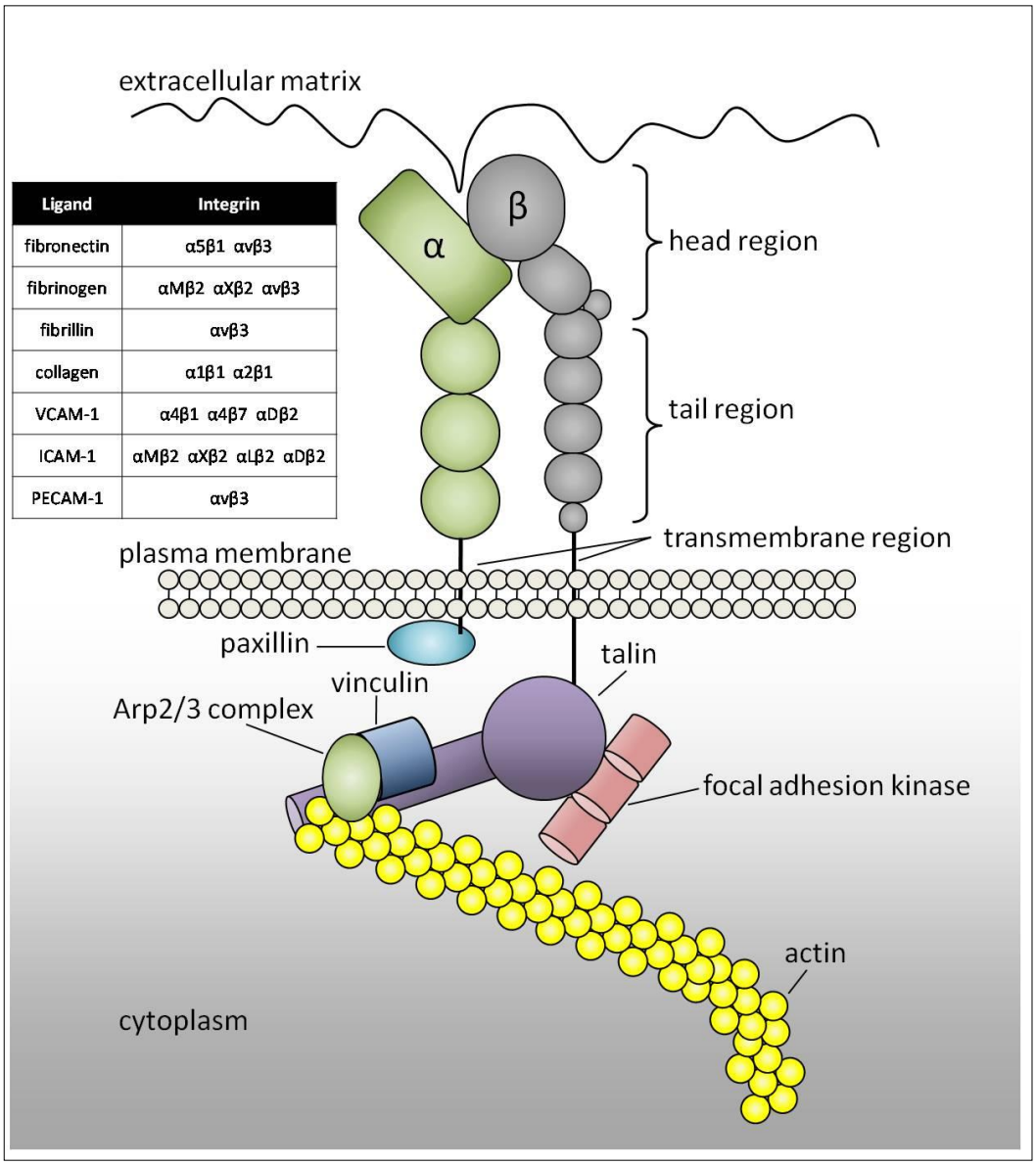

Ligand	Integrin
fibronectin	α5β1 αvβ3
fibrinogen	αMβ2 αXβ2 αvβ3
fibrillin	αvβ3
collagen	α1β1 α2β1
VCAM-1	α4β1 α4β7 αDβ2
ICAM-1	αMβ2 αXβ2 αLβ2 αDβ2
PECAM-1	αvβ3

Figure 1.4 The basic structure of the integrin heterodimer and its interaction with key focal adhesion proteins in the cytoplasm. Heterodimeric integrin receptors are composed of an α and a β subunit that are activated when 'inside-out' signalling triggers an unbending of the ligand binding head region. Talin (a focal adhesion protein) binds the cytoplasmic tail of the β subunit. Autophosphorylation of focal adhesion kinase triggers interaction between talin, vinculin and the actin cytoskeleton. Vinculin can transiently bind to the Arp2/3 complex, mediating actin polymerisation. The active integrin can now bind to ECM ligands with high affinity, triggering 'outside-in' signalling. This in turn elicits complex and cell specific signalling events that allow the cell to respond to the external environment. The table embedded shows a list of ligands common to leukocytic cells during their recruitment, and their integrin binding partners. Information for this diagram is taken from (Brakebusch and Fassler, 2003;

1.1.4.3 Endothelial transmigration

Once the activated monocyte has reached the site of infection and inflammation it must squeeze through the tight gaps between neighbouring endothelial cells and escape the blood vessel at the site of infection and/or inflammation. Perhaps the most important cell adhesion molecule implicated at this stage is platelet/endothelial cell adhesion molecule (PECAM)-1 also known as CD31 (Martin and Leibovich, 2005). PECAM-1 is a transmembrane protein expressed on the surface of most leukocytes, endothelial cells and platelets, which forms cell-cell junctions through homophilic binding. As well as its role in cell adhesion PECAM-1 is also able to interact with integrins, such as αvβ3, and appears to have important signalling properties suited to a role in transmigration (Thompson et al., 2001). *In vivo* studies using PECAM-$1^{-/-}$ mice have revealed a failure in leukocyte transmigration following pro-inflammatory IL-1β stimuli but no effect on leukocyte rolling or adhesion, with leukocyte arrest observed at the level of the perivascular basement membrane (Thompson et al., 2001).

In monocytes, as well as some endothelial and smooth muscle cells, integrins are enriched in adhesions know as podosomes (reviewed in (Linder, 2007)). These are unique in that they have the ability to degrade the surrounding matrix proteins as well as mediating adhesion. Unsurprisingly podosomes have therefore been implicated in several forms of cell transmigration, including that of activated monocytes. For example, human monocyte-derived macrophages have been found to form podosome-like structures as cells undergo an amoeboid to 3D change in migration (Van et al., 2010).

Following the transmigration of the perivascular basement membrane the process of monocyte recruitment and diapedesis into areas of infection and inflammation is complete. Throughout this process the CSF-1 expressed by the surrounding endothelial cells is continually driving monocyte differentiation to tissue macrophages. Perhaps unsurprisingly, the integrins play a role in differentiation also. For example, in un-stimulated cells the transcriptional repressor Foxp1 binds to and represses CSF-1R transcription. Engagement of αMβ2 on monocytes, however, down-regulates the expression of Foxp1 allowing differentiation to proceed (Tester et al., 2007).

1.1.5 The role of peripheral blood monocytes and tissue macrophages in disease pathologies

The aberrant recruitment of macrophages is pivotal in the development of several diseases. For example, macrophage accumulation is known to play a role in the pathogenesis and complications of type 2 diabetes; including atherosclerosis, impaired wound healing (discussed in detail in Chapter 1, 1.3, and Chapter 5) (Maruyama et al., 2007), nephropathy (Ninichuk et al., 2007) and even obesity (Weisberg et al., 2003).

1.1.5.1 Atherosclerosis

As a result of their ability to transmigrate the endothelium, in combination with their function as phagocytes, macrophages are the predominant cells involved in both the formation and destabilisation of atherosclerotic plaques in cardiovascular disease (CVD) (Takahashi et al., 2002). Unlike during response to infection, during atherogenesis endothelial cells are activated by the accumulation of low density lipoprotein (LDL), usually at sites of vessel bifurcation and curvature (Mestas and Ley, 2008). LDL is vital for the transport of cholesterol around the body, necessary for proper cell membrane structure and permeability as well as the intestinal absorption of fat soluble vitamins. Monocytes are similarly activated by components of LDL; this can trigger their differentiation into macrophages and up-regulates their expression of chemokine receptors thus increasing adhesion to the endothelium and coronary artery smooth muscle cells (Barlic et al., 2006).

Transport of LDL particles into the arterial wall can result in excessive accumulation of LDL, again at areas of branching and where shear stress is reduced. LDL particles can then become oxidised (oxLDL) and further stimulate the expression of chemokine receptor CX3CR1 (receptor for fractalkine) on the surface on monocytes (Barlic et al., 2006). The damage caused to the arterial wall by oxLDL triggers the innate immune response and, due to the increased expression of CX3CR1, excessive recruitment of monocytes to the endothelium occurs via the adhesion cascade (figure 1.3). Once transmigration of the endothelium has occurred macrophages begin uptake of the oxLDL particles via phagocytosis. Some, but not all, of these particles are degraded within phagosome of the macrophages and secreted as single LDL particles. These are eventually re-phagocytosed and converted to cholesterols triggering the transformation from macrophage to foam cell (Takahashi et al., 2002).

An accumulation of macrophage-derived foam cells can form a fatty streak in the blood vessel wall. Small fatty streaks alone are ‘clinically silent’ and can begin formation as early as the first decade of life in humans with little threat of morbidity. If the macrophage response to apoptotic

foam cells begins to fail a necrotic core may form and the fatty streak may become dangerous (Liang et al., 2007). This further stimulates immune response to the site of foam cell accumulation whereby the fatty streak increases in size, vascular smooth muscle cell proliferation and migration increases, and calcification of the surrounding tissues causes a hardening of the now fibrous plaque (Takahashi et al., 2002). As this plaque increases in size a fibrous cap can form between the fat deposits and the arterial wall, resulting in an atheroma. It is the stability of this 'cap' that determines the life-span of the atheroma and this is largely influenced by the expression of a family of proteolytic enzymes expressed by the macrophages present in the plaque shoulder (reviewed in (Newby, 2005)). This family, known as the metalloproteinases (described in detail in Chapter 1, 1.2), is able to degrade all major components of the surrounding vascular matrix, including the components of the fibrous cap. Plaque destabilisation occurs when the fibrous cap protecting the fatty core of the plaque is degraded by metalloproteinases. This can be further weakened by the constant mechanical strain of blood vessel expansion and contraction during circulation. When the plaque is weakened sufficiently it may rupture, leaking the contents of the atheroma into the blood vessel. This can cause blockage of the blood vessel lumen due to the size of the plaque fragments and the blood clotting response. Increased expression of the proteinases by macrophages has been observed in atherosclerotic plaques in vivo, for example the membrane bound matrix metalloproteinase MMP-16 (Uzui et al., 2002). There are increasing data to suggest their use as biomarkers for plaques undergoing destabilisation (Rodriguez et al., 2008).

It is clear, therefore, that the monocyte adhesion cascade and subsequent macrophage differentiation can be inappropriately activated, contributing to the pathogenesis of life-threatening cardiovascular diseases. It is through understanding the mechanisms behind monocyte and macrophage adhesion to the endothelium and the process of cell migration through basement membrane that a clear appreciation of their function during homeostasis and in disease states can be formed.

1.1.6 Immune cell migration and its regulation by the Rho GTPases

The importance of cell migration between cells and through surrounding matrices during the immune response has long been appreciated. Only recently, however, have some of the complex pathways involved in the induction and control of cell translocation been determined. For successful cell migration to take place localised and transient signalling events must lead efficiently to changes in cellular architecture in a cyclical process of lamellipodial protrusion and retraction.

1.1.6.1 Classical model of migration

The classical model of 2D cell migration (reviewed in (Ridley et al., 2003)) involves the polarization of a cell by the formation of a protruding leading edge and a trailing edge that will undergo retraction (figure 1.5). The leading edge is driven by actin polymerization and the clustering of integrins at focal adhesions with the underlying substrate. The actin monomer, G-actin, is a globular protein which forms a major component of the dynamic cytoskeletal microfilaments by assembling into polymeric filaments known as F-actin. The leading edge is characterised by large areas of dynamic lamellipodia rich in an F-actin mesh and focal adhesions. Some focal adhesions disassemble as the lamellipodia restructure but some mature and become anchors for the cell during migration, eventually dissolving as the cell migrates forward.

Throughout the migrating cell are bundles of polarised microtubules that form a structural cytoskeletal network emanating from the microtubule organizing centre (MTOC). In macrophages microtubules are highly dynamic and demonstrate an unusually rapid response to extracellular stimuli, reflective of their role in innate immunity (Robinson and Vandre, 1995). Microtubules appear to stabilise the migrating cell and have been found to be vital for macrophage recruitment to wounds *in vivo*.

The trailing edge of migrating cells is characterized by tail retraction, whereby the adhesions at the rear of the cell are synchronously disassembled. This process is driven by the targeting of dynamin, a GTPase responsible for endocytosis of adhesion components; the inhibition of myosin light chain (MLC) phosphatise and the activation of MLC kinase. This prevents the phosphorylation and activation of Myosin II, a motor protein which interacts with F-actin and transmits force along filaments to sites of adhesion (reviewed in (Vicente-Manzanares et al., 2005; Ridley et al., 2003)).

1.1.6.2 Rho, Rac and Cdc42: The RhoGTPases

The fundamental role of macrophages in the innate immune response requires an ability to mobilize rapidly in response to chemical signals, such as chemokines. The key regulators of the signalling networks controlling this response are the Rho GTPases. These are a class of the Ras

superfamily of GTP binding proteins comprising of Rho, Rac, and Cdc42, of which there are further isoforms (Bokoch, 2005). These proteins bind and hydrolyse GTP that, amongst other basic cell functions, acts as a 'molecular switch' controlling cytoskeletal dynamics and, in turn, cell motility (figure 1.6). Classically Rac is considered to mediate lamellipodia formation, Rho is thought to control the actin cytoskeleton and stress fibre formation, whilst Cdc42 organizes filopodia dynamics (Ridley, 2001).

Three isoforms of the Rho protein, RhoA, RhoB and RhoC, are present in mammals. As with all the RhoGTPases these are regulated both temporally and spatially throughout the cell. Canonical Rho signalling occurs via Rho Kinases (ROCK), and is largely thought to control cell body contraction at the trailing edge of the migrating cell by inhibiting MLC phosphatase, as explained above (Ridley, 2001). In macrophages stimulated with CSF-1 functional inhibition of Rho has been shown to induce enhanced cell spreading (including both lamellipodia and filopodia), but significantly inhibit migration speed and translocation (Allen et al., 1998a). Endogenous inhibition of Rho-ROCK signalling by the integrin αvβ3 has also been shown to induce formation of large lamellipodia and increase directional migration (Petrie et al., 2009).

In mammals Rac exists in three highly homologous isoforms: Rac1, Rac2 and Rac3 with only Rac1 and Rac2 expressed in macrophages. Despite their homology, each isoform appears to play a different role in migration. Inhibition of Rac1 in the RAW264.7 macrophage cell line, for example, results in reduced membrane ruffling and lamellipodial extension, despite no effect on migration speed, *in vitro* (Cox et al., 1997). Rac1-null mice are embryonic lethal due to migration defects and the neutrophils from Rac1 conditional knockout mice display a severely impaired response to chemotactic stimuli (Zhang et al., 2009). Conversely, endogenous activation of Rac1 by the formation of an α5β1/syndecan 4/fibronectin focal adhesion restricts its activity to the leading edge of migrating fibroblasts allowing the formation of a dominant lamellipodium (reviewed in (Petrie et al., 2009)). The importance of integrins in Rac signalling is compounded by evidence from fibroblasts expressing a β1 integrin point mutation. These cells show inhibition of Rac1 signalling and, surprisingly, more directional migration (Pankov et al., 2005). Rac2 inhibition results in reduced F-actin levels, marginally decreased migration, and reduced formation of the actin-rich adhesions, podosomes. Interestingly Rac2-null mice are viable (Wheeler et al., 2006) and conditional deletion of Rac2 in the neutrophils of mice reveals no real change in response to chemotactic stimuli other than a slight delay, perhaps a reflection of the differential dependence on Rac1 and Rac2 in these cells (Zhang et al., 2009). Rac proteins exert their effects on the leading

edge lamellipodia by signalling via the WAVE (Wiskott-Aldrich syndrome protein family verprolin-homologous protein) complex to promote actin polymerization driven by actin related protein (Arp) 2/3.

Cdc42, perhaps the least understood of the RhoGTPases, is thought to control the extension of filopodia towards the front of migrating cells by signalling through WASP (Wiskott-Aldrich syndrome protein) and activating Arp2/3 driven actin polymerization. In macrophages Cdc42-WASP signalling can be stimulated by CSF-1 and act upstream of Rac-WAVE induced lamellipodia formation (Jones, 2000). Inhibition of Cdc42 expression in macrophages does not inhibit migration altogether but prevents directional migration towards a chemoattractant (Allen et al., 1998a). In fact, Cdc42 has been shown to play a key role in maintaining microtubule stability at the leading edge, in turn promoting directional migration (Petrie et al., 2009).

All three of the Rho GTPases are therefore vital for the successful control of cell migration in response to chemotactic stimuli. Rho activation alone, however, appears to be sufficient to stabilise the monocyte-endothelial interaction during migration along the vascular endothelium and during endothelial transmigration. Interestingly, inhibition of Rho activity in TNF-α stimulated human umbilical vein endothelial cells (HUVECs) reduces monocyte adhesion to a monolayer of these cells (Wojciak-Stothard et al., 1999). This was not due to a reduced number of endothelial CAMs (VCAM-1, ICAM-1 and E-selectin) however, but instead Rho inhibition appeared to interfere with their distribution on the cell surface, preventing monocyte-binding receptor clustering. Wójciak-Stothard et al hypothesise that this is as a result of deregulated signalling to the actin cytoskeleton that would inevitably have an effect on migratory events.

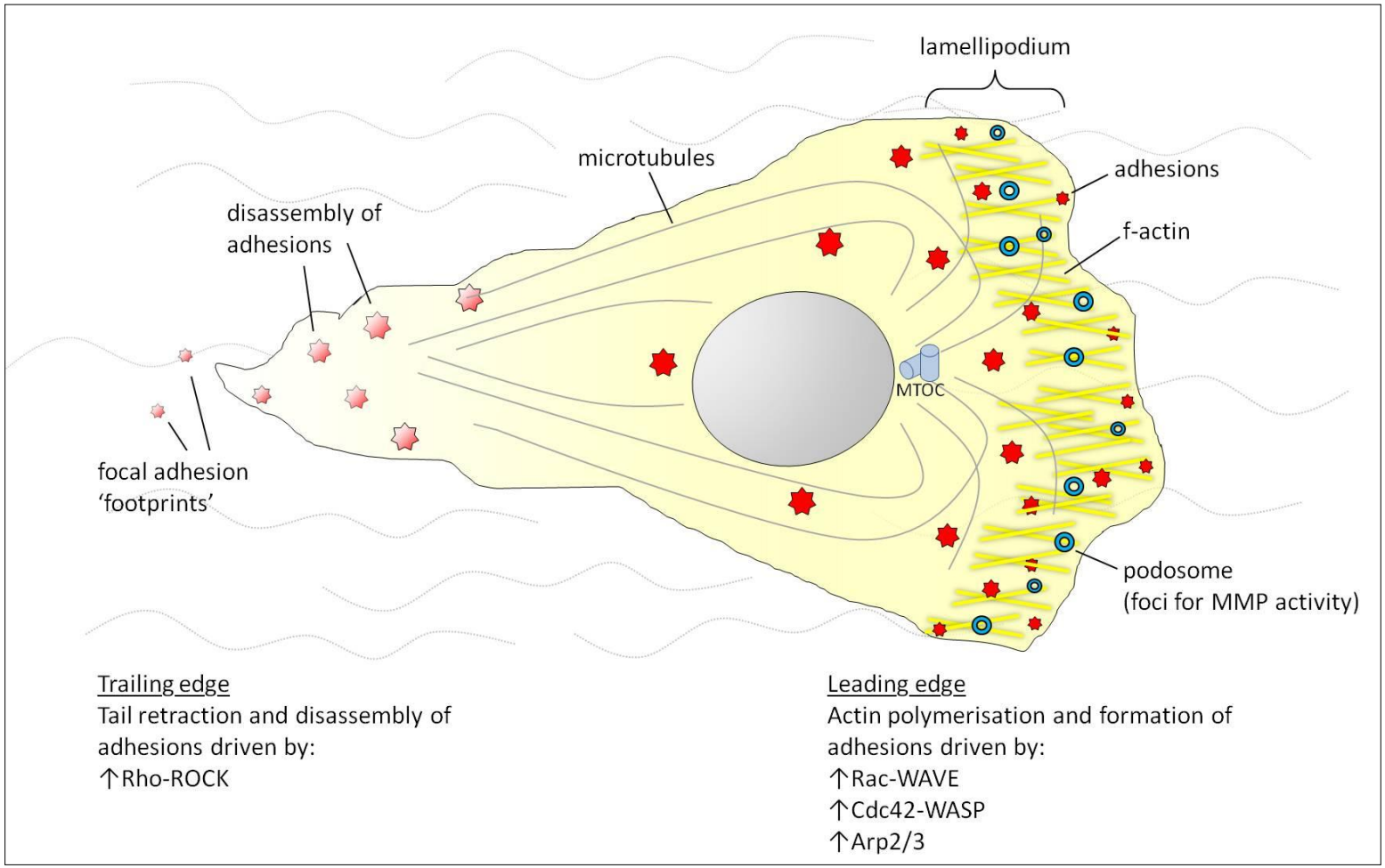

Figure 1.5 Cell polarization results in the formation of a leading and trailing edge of the cell. The Rho GTPases Rac, Rho and Cdc42 control F-actin polymerization (yellow bars) and focal adhesion assembly (red stars) at the leading edge of the cell, whilst also organizing the simultaneous disassembly of adhesions that lead to tail retraction at the trailing edge of the cell (size and shading of adhesions reflects their strength). Activation of Rho, Rac and Cdc42 triggers downstream signalling via ROCK, WAVE and WASP proteins, respectively. Information for this diagram obtained from (Ridley et al., 2003; Ridley, 2001; Linder, 2007).

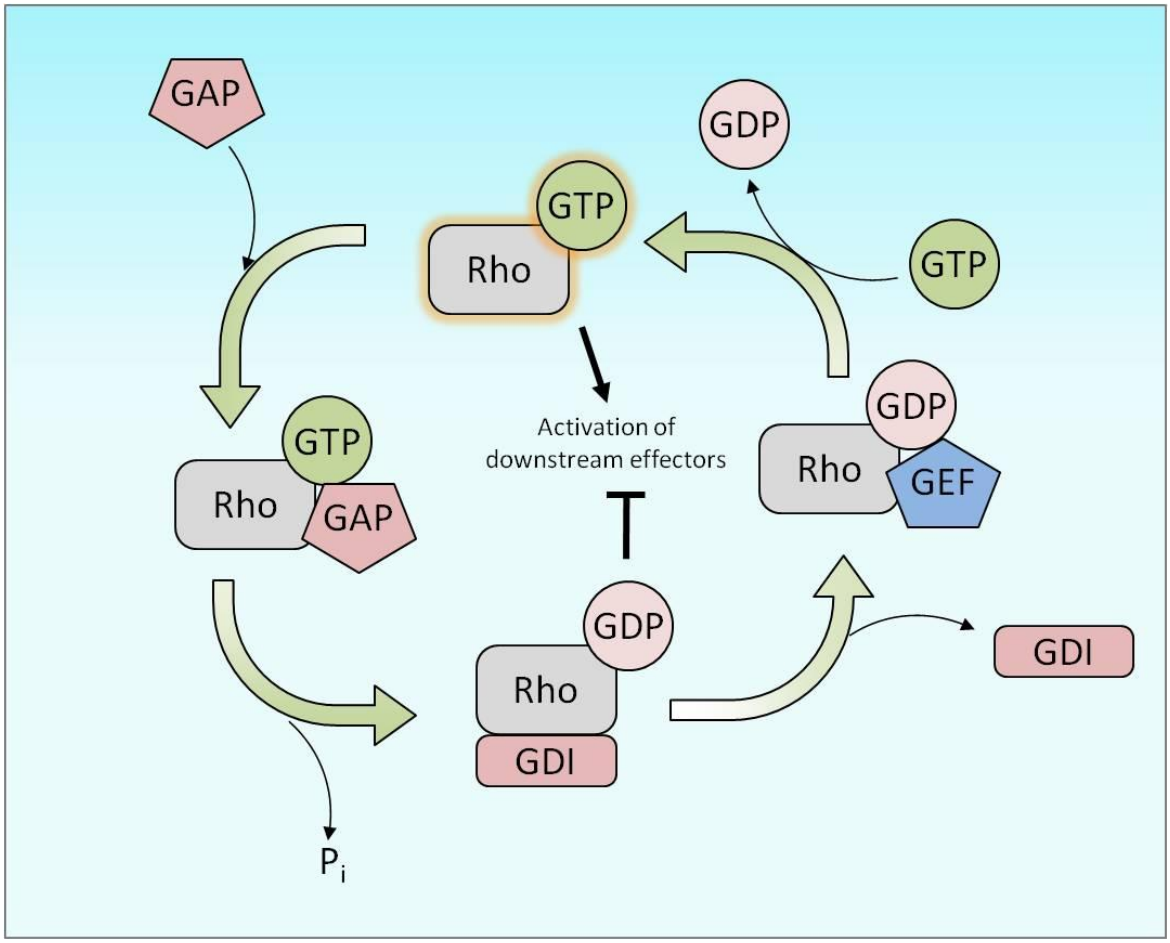

Figure 1.6 A 'molecular switch': the Rho GTPase cycle controls cytoskeletal dynamics in migrating cells. Rho GTPases cycle between an inactive GDP-bound and active GTP-bound conformation to control formation of lamellipodia (Rac), stress fibres (Rho) and filopodia (Cdc42). In their inactive GDP-bound state Rho GTPases form a complex with GDI in the cytoplasm. This blocks GTPase interaction with the plasma membrane or downstream effectors. Dissociation of GDI enables the GTPase to move closer to the plasma membrane and bind GEF. GEF is responsible for catalyzing the exchange of GDP with GTP, subsequently activating the Rho GTPase complex enabling further activation of potential downstream effectors. Active GTPase attracts the binding of GAP which accelerates the conversion of GTP back to GDP, with the release of inorganic phosphate (P_i), thus inactivating the Rho GTPase. Inactive GTPase moves back into the cytoplasm where it is bound again by GDI. **GDI** – **G**uanine nucleotide **D**issociation **I**nhibitors. **GEF** – **G**uanine nucleotide **E**xchange **F**actors. **GAP** – **G**TPase **A**ctivating **P**rotein. Information for this diagram obtained from (Petrie et al., 2009).

1.1.7 The extracellular matrix and immune cell migration

The extracellular matrix (ECM) is the connective tissue that surrounds cells and provides support. There are two main forms of ECM; interstitial matrix and the basement membrane or basal lamina, both of which are composed of aggregates of matrix proteins. The interstitial matrix forms the majority of the connective tissue between cells and acts as scaffold for migrating cells. Basement membranes, on the other hand, form sheet-like matrix barriers that separate epithelial cells from underlying mesenchymal cells. For example, basement membranes separate the epidermis from the underlying dermis in the skin (see Chapter 1, 1.3) and also provide a barrier between the endothelial cells lining blood vessels and the underlying vascular smooth muscle cells.

1.1.7.1 Extracellular matrix structure: basement membrane and interstitial matrix

The four main components of the basement membrane are laminin, non-fibrillar type IV collagen, nidogen and heparan sulphate proteoglycan (Yurchenco and Schittny, 1990). These proteins form the basement membrane architecture through specific binding interactions, with type IV collagen and laminin forming distinct networks that are bridged by nidogen and provide an anchor for heperan sulphate proteoglycan complexes (Yurchenco and Schittny, 1990). The interstitial matrix is composed mainly of fibrillar type 1 collagen, which provides physical stability and acts as a loose scaffold for other proteins to anchor themselves to. As well as collagens, the interstitial matrix also contains glycoproteins, such as vitronectin and fibronectin and proteoglycans, such as condroitin sulphate (Korpos et al., 2010). The specific structure of each type of ECM depends on its function. For example, ECM surrounding arteries and veins also contain high levels of elastin to cope with the increased blood pressure and maintain vessel integrity (Bou-Gharios et al., 2004).

1.1.7.2 Fibronectin in the extracellular matrix

Fibronectin is a major component of the interstitial matrix binding to heparin sulphate molecules and collagens. Fibronectin molecules typically exist as dimers composed of two ~250 kDa subunits linked by a disulphide bond and, due to alternative splicing, at least 20 different variants of fibronectin are present in humans (Pankov and Yamada, 2002). As a result of its solubility fibronectin can be subdivided in to two broader categories; soluble plasma fibronectin and less-soluble cellular fibronectin. Plasma fibronectin is formed by hepatocytes in the liver and this splice variant is relatively basic, for example lacking the 'EDA' domain responsible for integrin α4β7 binding (Pankov and Yamada, 2002). Cellular fibronectin on the other hand forms a much larger group including numerous cell-type specific isoforms. The basic domain structure of both plasma and cellular fibronectin are however homologous (figure 1.7). The elucidation of its domain

structure has been enabled by several proteolytic cleavage sites throughout the molecule, which may also reveal cryptic ligand binding sites. The RGD (Arg-Gly-Asp) binding site, for example, mediates the binding of α5β1 and αvβ3 and is therefore critical for fibronectin-cell interaction (Akiyama et al., 1995). Fibronectin contributes to the ECM by providing a degree of elasticity following the formation of fibrils. Fibronectin fibrillogenesis occurs following binding to integrin α5β1 that elicits the formation of a dense network of fibrils on the cell surface (reviewed in (Wierzbicka-Patynowski and Schwarzbauer, 2003)). In turn, fibronectin fibrils can trigger integrin clustering, thus further increasing local concentration and allowing cross-talk between the matrix and the cell cytoskeleton.

1.1.7.3 Extracellular matrix and leukocyte migration

The composition of blood vessel basement membrane is of particular importance to immune cell migration as this presents the first matrix barrier during extravasation from the circulation (reviewed in (Korpos et al., 2010)). Leukocytes migrating through the basement membrane do so by forming adhesions with the ECM components via the integrins (the formation of distinct focal adhesions *in vivo* is somewhat controversial however [see Chapter 1, 1.1.4.2]) and secreting proteases to breakdown the ECM barriers. Neutrophils, for example, stain positive for cleaved laminin-α4 and -α5 chains following basement membrane transmigration *in vivo* and these areas of staining co-localise with integrin α6 distribution, suggesting that a remodelling of the ECM has occurred (Wang et al., 2006). A similar study, however, has suggested that monocytes are able to traverse the basement membrane without remodelling the ECM (Voisin et al., 2009). This is understandably something of a contentious issue however, and is discussed further in Chapter 1, 1.2.5.

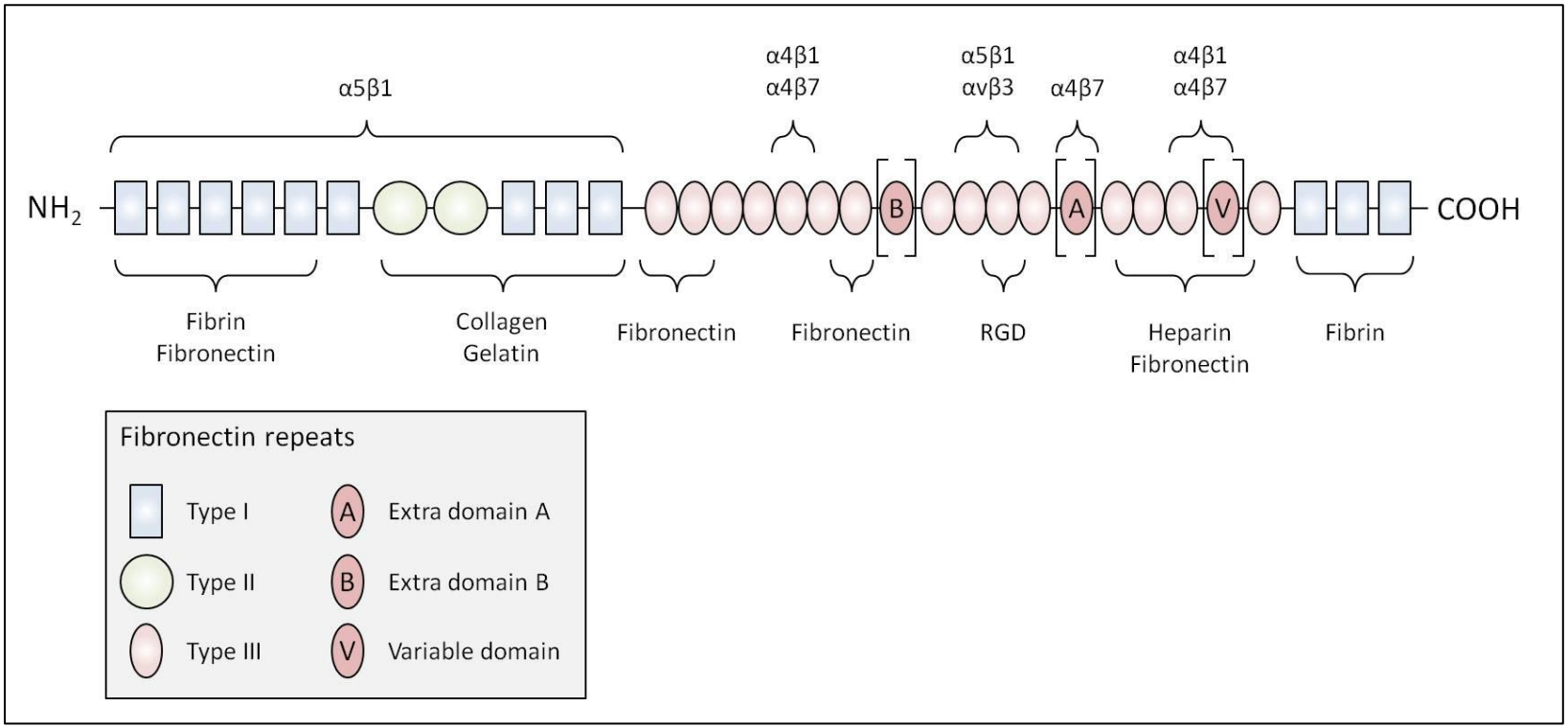

Figure 1.7 The basic domain structure of fibronectin. Fibronectin consists of three types of repeats and three alternatively sliced domains as indicated. The alternatively spliced domains present in cellular fibronectin are omitted from plasma fibronectin, thus affecting the integrin binding mediated at these sites. Integrin binding sites relevant to leukocyte-fibronectin binding are shown. Fibronectin can also bind numerous extracellular matrix proteins, including further fibronectin molecules during fibrillogenesis. Information for this diagram is taken from (Wierzbicka-Patynowski and Schwarzbauer, 2003; Pankov and Yamada, 2002).

1.2 Metalloproteinases

1.2.1 The Metalloproteinases

First classified by Rawlings and Barret (Rawlings and Barrett, 1993), the evolutionary family of proteinases is composed of four subfamilies; the serine proteinases, cysteine proteinases, aspartic proteinases and the metalloproteinases. Together these are responsible for the degradation and turnover of all connective tissue proteins in the ECM (Cawston, 1995). Whilst the aspartic and cysteine proteinases mainly act intracellularly in acidic compartments, the serine and metalloproteinase families are largely considered to work extracellularly, cleaving surrounding matrix proteins at a neutral pH (Cawston, 1995).

The metalloproteinases can be further subdivided and include the metzincin superfamily, which in turn includes the matrix metalloproteinases (MMPs), the ADAMs (a disintegrin and metalloproteinase) and the ADAMTS proteinases (ADAM with thrombospondin motifs) (Nagase et al., 2006). MMPs function as endopeptidases with broad substrate specificity and all members of the family are dependent on the presence of a zinc ion in their active site (Kahari and Saarialho-Kere, 1997). There are 23 human MMPs in total and these are conserved throughout the mammalian class of vertebrates. Table 1.1 demonstrates the further classification of these proteinases into five main functional groups due to their ECM substrate specificity; the Collagenases, Gelatinases, Stromelysins, Matrilysins and the Membrane-type MMPs; and one group of MMPs that share neither structural nor substrate specificities. More recently a role for the MMPs in the cleavage and activation of chemokines during the immune response has been established (Overall et al., 2002) and this is discussed in more detail in Chapter 5.

1.2.3 Matrix Metalloproteinase structure and activity

All 23 mammalian MMPs have similar structural domains (figure 1.8). MMPs are composed of a hydrophobic amino terminal signal sequence, a pro-peptide domain containing a conserved cysteine residue, and a catalytic domain including a zinc ion in the active site. Most MMPs (not including MMP-7 and -26) also contain a hemopexin-like c-terminal domain that includes a calcium binding site and is connected to the catalytic domain by a hinge region (Nagase et al., 2006). The MT-MMPs also either possess a transmembrane domain (MMP-14, -15, -16 and -24) or are attached to the cell surface by a glycosylphosphatidylinositol (GPI) anchor (MMP-25) (Nagase et al., 2006).

Table 1.1 The MMPs and their ECM substrates; including their exogenous activators and capacity to further activate other MMPs. Information for this table adapted from (Murphy and Knauper, 1997; Rawlings et al., 2010; Kahari and Saarialho-Kere, 1997; Chakraborti et al., 2003).

Protease	ECM Substrates	Activated by	Activator of
Collagenases			
MMP-1 (Collagenase 1)	Fibrillar collagens I, II, III, VII, VIII, X, aggrecan, serpins, α2M	Plasmin, MMP-3, MMP-10	MMP-2
MMP-8 (Collagenase-2)	Fibrilliar collagens I, II, III, aggrecan, serpins, α2M	Plasmin, MMP-3, MMP-10	No protease activation defined
MMP-13 (Collagenase-3)	Fibrillar collagens I, II, III, type IV, IX, X, XI collagens, gelatin, fibronectin, laminin, tenascin, aggrecan, serpins	Plasmin, MMP-2, MMP-3, MMP-10, MMP-14, MMP-15	MMP-2, MMP-9
Gelatinases			
MMP-2 (Gelatinase A)	Gelatin, type I and IV collagen, fibronectin, tenascin	MMP-1, MMP-7, MMP-13, MMP-14, MMP-16, MMP-17, MMP-25	MMP-9, MMP-13
MMP-9 (Gelatinase B)	Gelatin, type I, IV and XIV collagen, α2M	Plasmin, MMP-2, MMP-3, MMP-13	Plasmin
Stromelysin			
MMP-3 (Stromelysin-1)	Type IV collagen, fibronectin, aggrecan, nidogen	Plasmin, elastase	MMP-1, MMP-7, MMP-8, MMP-9, MMP-13
MMP-10 (Stromelysin-2)	Type IV collagen, fibronectin, aggrecan, nidogen	Plasmin, elastase	MMP-1, MMP-7, MMP-8, MMP-9, MMP-13
MMP-11 (Stromelysin-3)	α1-proteinase inhibitor, α2-macroglobulin	Furin	No protease activation defined
MMP-19 (Stromelysin-4)	Type IV collagen, gelatin, laminin, fibronectin, aggrecan, fibrin/fibrinogen	Trypsin	No protease activation defined
Matrilysins			
MMP-7 (Matrilysin)	Type IV collagen, fibronectin, aggrecan, nidogen, elastin, laminin, vitronectin, fibrin/fibrinogen	Plasmin, MMP-3	MMP-2
MMP-26 (Matrilysin-2)	Type IV collagen, gelatin, fibronectin, fibrin/fibrinogen	MMP-26	No protease activation defined
Membrane Type			
MMP-14 (MT1-MMP)	Type I, II and III collagen, gelatin, fibronectin, laminin, vitronectin, aggrecan	Plasmin, furin	MMP-2, MMP-13
MMP-15 (MT2-MMP)	Proteoglycan	No protease activator(s) defined	MMP-2, MMP-13
MMP-16 (MT3-MMP)	Type III collagen, fibronectin	No protease activator(s) defined	MMP-2
MMP-17 (MT4-MMP)	Gelatin, fibrin/fibrinogen	No protease activator(s) defined	MMP-2
MMP-24 (MT5-MMP)	Fibronectin, proteoglycan, gelatin	No protease activator(s) defined	MMP-2
MMP-25 (MT6-MMP)	Type IV collagen, gelatin, fibronectin, proteoglycans, laminin-1, fibrin/fibrinogen	No protease activator(s) defined	MMP-2
Other MMPs			
MMP-12 (Metalloelastase)	Type IV collagen, fibronectin, aggrecan, nidogen, elastin	Plasmin	No protease activation defined
MMP-20 (Enamelysin)	Aggrecan	No protease activator(s) defined	No protease activation defined
MMP-23	Gelatin	No protease activator(s) defined	No protease activation defined
MMP-27	No substrates defined	No protease activator(s) defined	No protease activation defined
MMP-28	Casein	No protease activator(s) defined	No protease activation defined

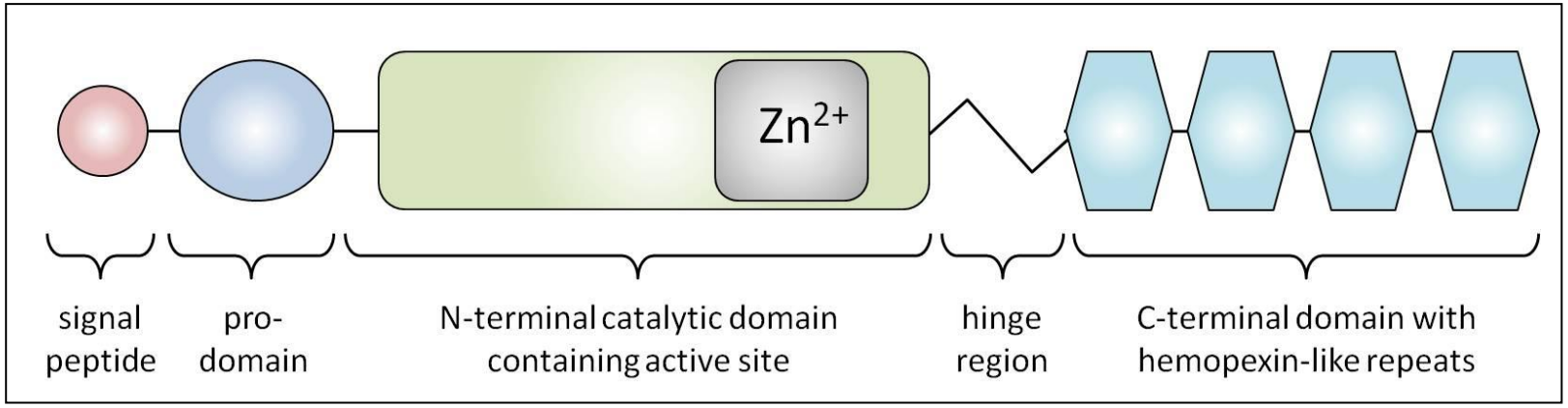

Figure 1.8 The basic domain structure of the MMPs. This configuration represents almost half of the total number of human MMPs; including MMP-1, -3, -8, -10, -11, -12, -13, -19, -20 and -27. Diagram adapted from (Nagase et al., 2006; Murphy and Knauper, 1997).

As with all proteins, the structure of an MMP determines its function and site of action. The majority of the MMPs are secreted as inactive zymogens, or pro-MMPs, and require removal of the pro-peptide domain to activate the latent enzyme. The pro-peptide domain contains a cysteine residue that directly interacts with the zinc in the active site thus preventing substrate binding. Conversely, the MT-MMPs can be activated intracellularly, before binding to the cell membrane, due to a furin-like recognition sequence in the pro-domain (Chakraborti et al., 2003). The activity of MMPs is tightly regulated in healthy tissue with a delicate balance of activation, either by other MMPs or via the plasmin-plasminogen cascade; and inhibition, by the endogenous tissue inhibitors of metalloproteinases (TIMPs).

Plasminogen is a circulating plasma protein produced in the liver. The conversion of the inactive plasminogen zymogen to active plasmin is mediated by the binding of urokinase-like plasminogen activator (uPA) to its receptor uPAR on the cell surface. This instigates the extracellular plasminogen cascade, the main function of which is fibrinolysis of blood clots. This cascade also however results in the activation of proteinases involved in cell-cell and cell-matrix interactions (Murphy et al., 1992). For example, plasmin is able to activate both proMMP-3 and -10. Active MMP-3 is further responsible for the direct activation of proMMP-1 and the sequential activation of MMP -9 (Murphy and Knauper, 1997). Thus it becomes apparent that uPA-uPAR interaction can trigger activation cascades capable of activating all latent MMPs.

1.2.4 The TIMPs: endogenous inhibitors of metalloproteinases

The endogenous tissue inhibitors of metalloproteinases, the TIMPs, are capable of inhibiting all active forms of the MMPs by forming a complex with the N-terminus of the relevant proteinase and chelating the zinc ion in the active site (Nagase et al., 2006). There are four mammalian TIMPs, numbered 1-4, which vary in efficacy and inhibitory profile (table 1.2). For example, TIMP-1 inhibits most MMPs and ADAM10 but has low inhibitory activity for most of the MT-MMPs. TIMP-3, on the other hand, has the broadest inhibitory range and is also able to inhibit several of the ADAM and ADAMTS family members (Brew and Nagase, 2010). Interestingly TIMP-3 is able to bind ECM via glycosaminoglycans whilst TIMPs-1, -2 and -4 are soluble, suggesting that their site of action is as important as that of the MMPs (Yu et al., 2000).

Gene	Location	MMP Inhibition	Other metalloproteinase interactions	Pro-MMP interaction
TIMP-1	Secreted	All, but weak inhibition of MMP-14, -16, -19, and -24. Strong inhibition of MMP-3 and 7.	ADAM10	ProMMP-9
TIMP-2	Secreted	All	ADAM12	ProMMP-2
TIMP-3	ECM bound	All	ADAM10, 12, 17, 28 and 33. ADAMTS-1, -4, and -5. Weak inhibition of ADAMTS-2.	ProMMP-2 and -9
TIMP-4	Secreted	Most	ADAM17 and 28. Weak inhibition of ADAM33.	ProMMP-2

Table 1.2 The inhibitory profile of the TIMPs; including their interaction with ADAMs, ADAMTSs and some proMMPs. Adapted from (Brew and Nagase, 2010).

TIMPs are also capable of forming non-inhibitory complexes with proMMPs via interaction of the TIMP C-terminal domain and the proMMP hemopexin-like domain. These interactions allow the TIMP molecule involved to bind simultaneously to another MMP via its N-terminal (Brew and Nagase, 2010). The functional significance of these interactions is not well understood, with the exception of TIMP-2 interaction with proMMP-2. TIMP-2 is able to bind proMMP-2 via its C-terminal domain as explained above. Concurrently TIMP-2 can bind MMP-14 (MT1-MMP) via its N-terminal domain, resulting in the formation of an MMP-14-TIMP-2-proMMP-2 membrane associated complex (Itoh et al., 2001). The components of this complex are not proteolytically active; however adjacent TIMP-2-free MMP-14 molecules, drawn into a homophilic interaction via their hemopexin domain, are able to activate the proMMP-2 by cleavage of the pro-domain (Itoh et al., 2001).

1.2.5 The role of metalloproteinases during cell migration

The metalloproteinases have long been implicated in the process of cell migration. Their primary role is to enable migratory cells to focus proteolytic activity on the ECM molecules in their path. More recently, however, the capacity for MMP-driven cleavage and activation of cryptic pro-migratory factors in the extracellular environment has also emerged.

1.2.5.1 MMPs

The dependence on broad-spectrum MMP expression for successful migration of vascular smooth muscle cells has been demonstrated by over-expression of TIMP-1 and-2. VSMC migration was inhibited both in vitro, in Transwell assays; and in vivo, in during neointimal thickening (Forough et al., 1996; Cheng et al., 1998). Similarly, the use of synthetic MMP inhibitors significantly represses migration; studies have shown the ability of monocytes to pass through a monolayer of endothelial cells in an in vitro model of the blood brain barrier to be impeded by MMP inhibition (Reijerkerk et al., 2006). Further studies into the role of specific proteinases in migration have also yielded important results. Loss of MMP-8, for example, has been shown to abrogate the migration of polymorphonuclear (PMN) leukocytes in response to LPS in MMP-$8^{-/-}$ mice (Tester et al., 2007). MMP-13 has also been found to enhance migration, inducing a four-fold increase in VSMC velocity by cleaving a type 1 collagen to substrate to its ¾ fragment (Stringa et al., 2000).

1.2.5.2 MT-MMPs

Numerous studies have also implicated the MT-MMPs (MMP-14-17, -24 and -25) in the process of basement membrane transmigration (Hotary et al., 2006; Cao et al., 2004; Sithu et al., 2007). Despite this, the true extent of their contribution has been a source of controversy of late. Given that MT-MMPs are anchored to the cell membrane it seems intuitive that they would imbue the cell with a focussed proteolytic power that would be more difficult to achieve with diffusible secreted MMPs. This requirement for MT1, MT2 and MT3-MMP has been demonstrated by the migration of neoplastic cells across the basement membrane during cancer metastasis (Hotary et al., 2006). Hotary et al employ siRNA knock-down of this triad of proteinases to demonstrate their necessity for cancer cell invasion and migration in intact *ex vivo* basement membrane. Similarly, knock-down of MT1-MMP alone in primary human blood monocytes prevents their transendothelial migration *in vitro*, whilst adenovirus driven over-expression of MT1-MMP enhances it (Sithu et al., 2007). Conversely, it has been claimed that fibrosarcoma and T-lymphocyte cells, treated with a broad-spectrum protease inhibitor *in vitro*, *are* able to retain their basement membrane invasive properties by migrating in a proteinase-independent 'amoeboid-like' fashion rather than the classical mesenchymal style of locomotion (Wolf et al., 2003a; Wolf et al., 2003b). Further to this, *in vivo* studies have revealed a preference for neutrophils and monocytes to transmigrate the endothelium of murine cremasteric venules at areas of low matrix protein expression suggesting the expression of MMPs alone is insufficient for breakdown of the basement membrane (Wang et al., 2006; Voisin et al., 2009). Voisin et al also show that inhibition of MMP-2 and -9 activities had no effect on monocyte migration in this model.

To counter the argument for MMP-independent cell migration it is important to understand that, despite inhibition of the gelatinases in the model used by Voisin et al, activity of all other MMPs, including the MT-MMPs, remains. This in no way rules out the role of any other MMP in this *in vivo* model of transendothelial migration. Also, in a murine model of central nervous system inflammation, expression of MMP-2 and -9 by macrophages has been shown to be vital for basement membrane transmigration in the brain and the spinal cord suggesting that the requirement for proteinases is site-specific (Agrawal et al., 2006). Subsequent studies have also challenged the proteinase-independent 'amoeboid-like' migration hypothesis. Sabeh et al (2009) have shown definitively that proteinase-independent migration is an artefact of ECM substrate pore size rather than a biologically relevant migratory phenotype. Specifically, pepsin-extracted type I collagen matrices lack the specific cross-linked structure found in native collagen and thus allow for cell migration even when MMP-14 is absent (Sabeh et al., 2009). Migration through reconstituted native type I collagen however is totally dependent on this metalloproteinase.

1.2.5.3 ADAM and ADAMTS families

Another group of metalloproteinase molecules that appear to play a role in cell migration are the ADAMs and the ADAMTSs. Their pro-migratory activity is primarily mediated by their interaction with cell surface proteins such as the integrins and cell adhesion molecules. ADAM28, for example, is able to interact with and bind to integrin α4β1 via its disintegrin domain, implying that it either plays a role in cell-cell adhesion or sequestering the active protease to the cell surface (Bridges et al., 2002). ADAM28 has also been shown to enhance leukocyte adhesion to endothelial cells *in vitro*, via binding to P-selectin on the surface of endothelial cells (Shimoda et al., 2007). P-selectin is known to play a role in leukocyte rolling along the blood vessel lumen (see Chapter 1, 1.1.4.1) and Shimoda et al suggest that ADAM28 enhances its function in leukocyte transmigration. Similarly, ADAM17 has been found to play a role in the recruitment of leukocytes to the endothelium lining blood vessels via its action as a sheddase for VCAM-1. Knockdown of ADAM17 leads to a reduction of VCAM-1 ectodomain shedding in response to pro-inflammatory stimulation (Singh et al., 2005). As soluble VCAM-1 is a known chemoattractant for T-cells (Kitani et al., 1998) it seems that ADAM17 may play an important role in the migration of these cells during the immune response. In earlier studies ADAM17 had been shown to mediate ectodomain shedding of pro-inflammatory TNF-α, earning the moniker TNF-α-converting enzyme (TACE) (Black et al., 1997). More recently Fraktalkine/CX3CL1 has been identified as an ADAM17 substrate, also a potent pro-inflammatory factor (Garton et al., 2001).

The function of the ADAMTS family in cell migration is less well understood, however recent research has uncovered some important roles. ADAMTS7, for example, is strongly expressed in VSMC both *in vivo* and *in vitro*, and its over-expression is associated with increased neointima formation and VSMC migration (Wang et al., 2009). As with the MMPs and ADAMs, the function of the ADAMTSs appears to be site specific. For instance, ADAMTS1 is significantly up-regulated following skin and nerve injury (Krampert et al., 2005). In particular, ADAMTS1 is strongly expressed by macrophages in skin early in the wounding process and keratinocytes later on. Exposure of fibroblasts and endothelial cells to recombinant ADAMTS1 revealed modulation of migration in both cell types. Interestingly, low levels of ADAMTS1 appear to enhance migration whilst high levels inhibit it. Krampert el al also shown that this action is dependent on ADAMTS1 activity, again suggesting it is the proteolytic function of this molecule that is implicated in migration.

1.2.6 MMP expression in macrophages

In humans, macrophages and their monocytic precursors have been shown to express the majority of the mammalian MMPs, with MMP-1, -3, -9, -10, -12, -14, -19 and -25 expressed preferentially (Webster and Crowe, 2006). The induction of MMPs in macrophages is principally driven by pro-inflammatory stimuli, such as TNF-α, the colony stimulating factors, LPS, and the interferons. For example, both TNF-α and M-CSF stimulate a dose- and time-dependent increase in MMP-16 mRNA expression in human monocyte derived macrophages (Uzui et al., 2002). Similarly, MMP-7 is constitutively expressed in human bone marrow-derived monocytes, but secretion is further stimulated in the presence of LPS (Busiek et al., 1992). Interestingly, levels of MMP expression can also vary during differentiation from monocyte to macrophage. In human peripheral blood monocytes stimulated to differentiate with phorbol 12-myristate 12-acetate (PMA) or M-CSF, secretion of proMMP-9 increased along with hallmarks of monocyte differentiation such as cell adhesion and spreading (Xie et al., 1998).

The capacity of macrophages and monocytes to produce an increased level and range of MMPs reflects their function within tissue. By secreting matrix degrading enzymes, these cells are able to participate in the remodelling of the ECM in response to immune status. This is particularly evident when investigating the interaction between monocytes and endothelial cells as a model of their extravasation from the blood vessel in response to pro-inflammatory stimuli. Co-culture techniques, for example, have revealed a dependence on MMP-14 expression by human blood

peripheral monocytes for migration through TNF-α stimulated endothelial monolayers (Matias-Roman et al., 2005). Not only did Matias-Roman et al detect enhanced MMP-14 expression during monocyte/endothelium transmigration but MMP-14 was also observed to cluster at the leading edge of these cells where they suggest it exerts its proteolytic activity of fibronectin. Similarly broad spectrum MMP inhibition *in vivo* is shown to reduce monocyte extravasation due to a decrease in endothelial gap formation and loss of tight junction proteins (Reijerkerk et al., 2006). Again, this appears to be the result of proteolytic degradation although the specific metalloproteinase(s) involved were not elucidated.

As well as expressing MMPs during normal homeostatic processes, macrophages have been shown to aberrantly express proteinases in diseased tissues, such as atherosclerotic plaques and chronic wounds. This is covered in detail in Chapter 1, 1.3 and 1.4.

1.3 The wound healing response

1.3.1 Skin structure and function

Mammalian skin is comprised of three primary layers of cells that provide an anatomical barrier to protect against pathogens, regulate body temperature and control evaporation (figure 1.9). Skin is the largest member of the largest organ system in mammals, the integumentary system (Breitkreutz et al., 2009). This system also includes other external protective features such as the hair and nails.

1.3.1.1 Epidermis

The epidermis is the outermost layer of the mammalian skin. This acts as an immediate barrier to pathogens and other foreign objects in the external environment as well as guarding against evaporation and loss of solutes, whilst also providing a waterproof layer (reviewed in (Madison, 2003)). The epidermis is formed from a layer of squamous stratified epithelial cells interspersed with Merkel cells (somatosensory receptors), melanocytes (pigment producing cells), langerhans cells (antigen presenting) and, predominantly, keratinocytes. The outermost layer of the epidermis, the stratum corneum, is composed of fully differentiated keratinocytes that have migrated outwards through the strata, become enucleated, loaded with keratin filaments, and embedded in an extracellular lipid matrix (Madison, 2003). Eventually these cells die due to a lack of blood supply and are sloughed off in a process known as desquamination. The cycle of keratinocyte differentiation continues constantly, replenishing the epidermal layer and maintaining its barrier function (reviewed in (Proksch et al., 2008)).

1.3.1.2 Dermis

Beneath the epidermis lies a basement membrane and then the dermis. The dermis is largely acellular, consisting mainly of connective tissue composed of collagen interspersed with cellular structures such as the mechanosensory nerve endings, hair follicles, sebaceous glands, and blood and lymphatic vessels. Interestingly, a recent study revealed that approximately 60% of the cells in the dermis of mouse skin are macrophages, staining positive for macrophage-specific markers (Dupasquier et al., 2004), whereas previously fibroblasts had been thought to make up the majority. This suggests that the dermal layer plays a far greater role in the steady-state immune response than has previously been estimated.

The dermis can be subdivided into two further layers, the papillary region and the slightly thicker reticular region, which is separated by a vascular interface (figure 1.9; reviewed in (Sorrell and

Caplan, 2004)). The papillary dermis is arranged into finger-like structures, or papillae, that protrude towards the epidermis and provide a greater surface area for interaction between these two layers. The collagen fibres present in the papillary region are poorly organised and are composed mainly of type I and III collagen, although non-fibrillar collagens XII and XVI are also present. There is also a high concentration of decorin, a proteoglycan, and microfibril associated versican present in the papillary region. The reticular dermis extends deep into the skin and has an even lower concentration of cells than the papillary region. The composition of ECM in this layer of dermis differs from that of the papillary region with thicker, well-organised bundles of mainly type 1 collagen. Decorin is also present, although in a more dispersed pattern than is seen in the papillary region, and versican is expressed in association with elastic fibres rather than microfibrils (Sorrell and Caplan, 2004). The presence of these ECM components add strength to the dermis whilst also providing a scaffold for migrating cells and also enabling storage of water and solutes in the skin (Sorrell and Caplan, 2004).

1.3.1.3 Hypodermis

The innermost layer of the skin is known as the hypodermis, or the subcutaneous adipose layer. This is composed mainly of adipocytes and loose connective tissue but also contains macrophages and larger cellular structures such as blood and lymph vessels and nerve fibres. The main functions of the hypodermis appear to be fat storage, for energy and thermoregulation, and to connect the skin to the underlying muscle (Kanitakis, 2002). Recently however the endocrine function of adipose tissue has become the focus of much research, revealing an important role for adipocytes in the progression of pro-inflammatory diseases (Yeop et al., 2010), such as type II diabetes and related complications, for example impaired dermal wound healing (Goren et al., 2007; Nascimento and Costa, 2006).

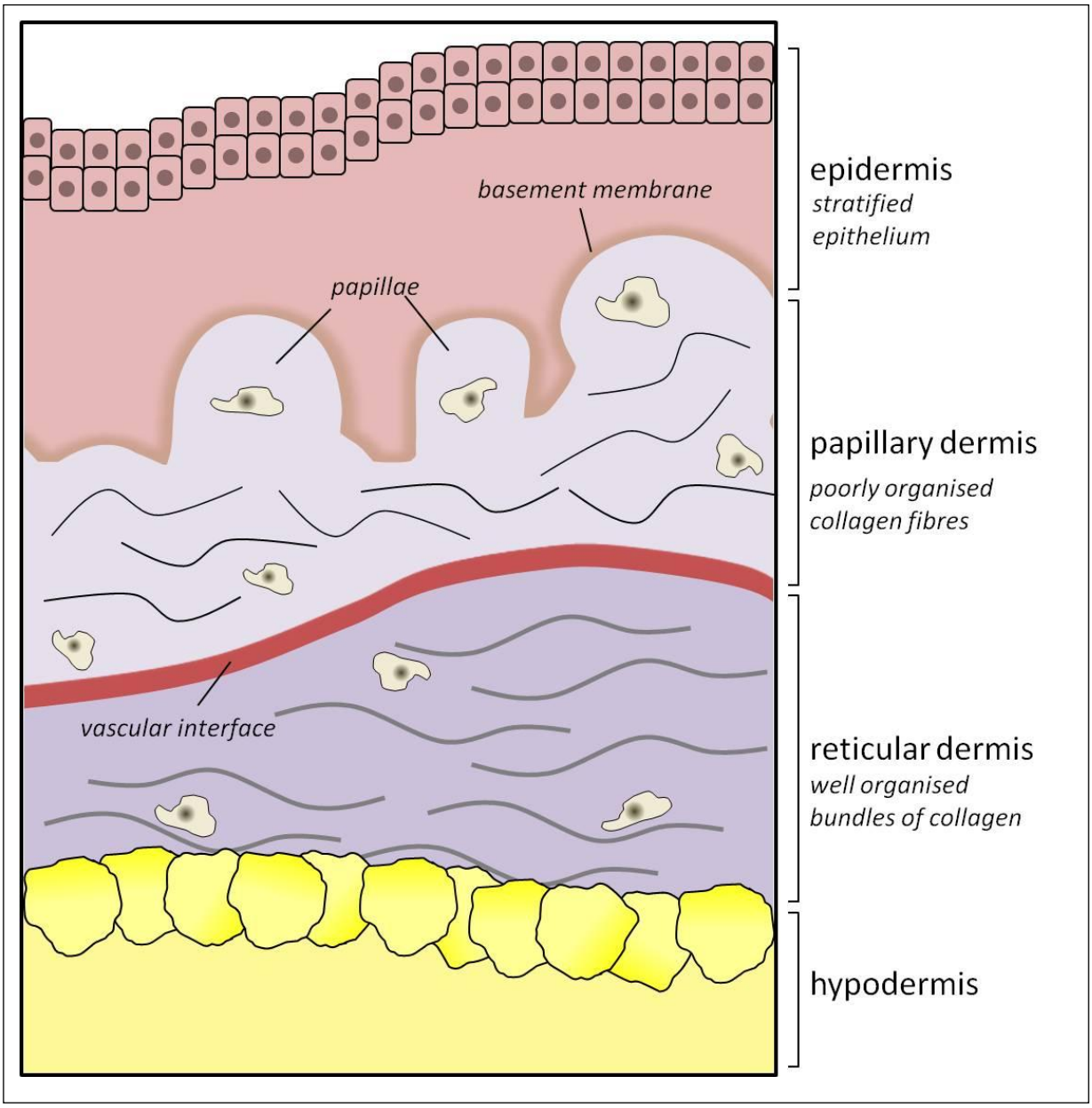

Figure 1.9 The mammalian skin structure. The skin is composed of three main layers: the epidermis, dermis and hypodermis. The epidermis is mainly formed from layers of stratified squamous epithelial cells providing a barrier to the external environment. In between the epidermis and the dermis is a basement membrane. The dermis can be subdivided into the papillary dermis and the reticular dermis, separated by a vascular interface. The papillary dermis protrudes into the epidermis with papillae, providing increased surface area for interaction. The connective tissue of the dermis is mainly composed of collagen, which is poorly organised in the papillary layer but more tightly ordered in the reticular dermis. The dermis is largely acellular although there are more cells present in the papillary layer than the reticular dermis. The hypodermis contains mainly adipocytes for fat storage and is the innermost layer of the skin. Information for this diagram obtained from (Sorrell and Caplan, 2004).

1.3.2 Wound healing and the multistep inflammatory cascade

Wound healing is the process by which the skin repairs itself after injury (figure 1.10). Immediately following wounding the healing process begins with an initial pro-inflammatory response. This is followed by a phase of proliferation and culminates with the remodelling of the dermis and epidermis to restore the protective barrier provided by the skin.

1.3.2.1 The multistep inflammatory cascade

The wound healing response involves numerous cell types that are deployed to the site of injury in exquisitely timed succession (table 1.3). This process is orchestrated by an equally complex sequence of chemoattractant signals secreted by both the injured tissue and the cells participating in the wound healing response. Immediately after wounding, platelets are released from damaged blood vessels and come into contact with ECM components and other factors released from damaged endothelium, such as von Willebrand factor (vWF). This stimulates platelets to bind to one another in aggregates allowing blood clots to form. These aggregates are strengthened by soluble fibrinogen that cross-links to form a fibrin clot and acts as a scaffold for migratory cells involved in the subsequent stages of wound healing (Martin and Leibovich, 2005).

Neutrophils are the first leukocytic cells to arrive at the site of injury (figure 1.10 A). Neutrophil diapedesis and migration is stimulated by chemokines released from endothelium exposed to pathogens during wounding. This process can be mimicked *in vitro* by exposing human endothelial cells to LPS, resulting in an up regulation in IL-8 transcription (Goetzl et al., 1996). The role of neutrophils is to phagocytose pathogens and enzymatically digest them within phagolysosomes. Neutrophils are also able to produce an oxidative burst that further aids their antimicrobial action; a process that appears to be intrinsically linked to the control of their migration (Zhang et al., 2009).

Macrophages arrive shortly after neutrophils as the second influx of leukocytes to the wound site, using the fibrin clot as a scaffold for their migration (figure 1.10 B). Their diapedesis into the wounded tissue and subsequent differentiation from monocytes is triggered by numerous growth factors. Perhaps the most important of these is macrophage chemotactic protein (MCP)-1, expressed by vascular endothelium, smooth muscles cells and fibroblasts (reviewed in (Deshmane et al., 2009)). Genetic deletion of MCP-1 and its receptor is not lethal although severe abnormalities in monocyte recruitment and chemokine expression are observed (Lu et al., 1998). Macrophages in the wound also respond to the presence of PAMPs, such as LPS, peptidoglycan and unmethylated CpG motifs that can stimulate their activation and migration (Guha and

Mackman, 2001; Sweet et al., 2002). Like neutrophils, the primary role of macrophages in wound healing is as phagocytes. Macrophages not only engulf pathogens but also clear the wound of spent neutrophils via PECAM-1 mediated cell-cell recognition. Unlike neutrophils however, the action of macrophages has been shown to be absolutely necessary for wound healing (Leibovich and Ross, 1975; Danen et al., 2002).

1.3.2.2 The proliferation phase

Activation of fibroblast migration into wounded tissues marks the end of the pro-inflammatory phase of wound healing and the beginning of the proliferative phase. Fibroblasts migrate into the wound using the fibrin clot as scaffold. They then lay down a collagen-rich matrix allowing for further migration, and form granulation tissue composed mainly of fibronectin. A small proportion of fibroblasts in dermal wounds continue to differentiate into myofibroblasts and provide a contractile force to close to the wound (Sorrell and Caplan, 2004). The majority of the fibroblasts, however, further contribute to the wound healing process by secreting growth factors to stimulate angiogenesis and keratinocyte migration.

Fibroblasts contribute to angiogenesis in two ways. Firstly, fibroblasts secrete chemoattractants such as vascular endothelial growth factor (VEGF) and hepatocyte growth factor (HGF) that stimulate the migration and proliferation of endothelial cells during angiogenesis (Bou-Gharios et al., 2004). Secondly, fibroblasts contribute to the structure of new blood vessels by laying down ECM and, in the case of much deeper wounds, forming the outer layer of blood vessels greater than 5 mm in diameter (Bou-Gharios et al., 2004).

Keratinocyte migration and subsequent re-epithelialisation is the final stage of the proliferative phase of wound healing. Keratinocytes respond to several growth factors during the re-epithelialisation of a wound. For example, fibroblast growth factors (FGFs) and platelet derived growth factor (PDGF) have been shown to stimulate significantly greater closure of dermal wounds in mice (Greenhalgh et al., 1990). Re-epithelialisation is also made possible by the expression of MMPs in keratinocytes. *In vitro*, MMP-1 has been found to be expressed by keratinocytes migrating on a type 1 collagen matrix, whilst in vivo studies have revealed the expression of MMP-10 in the basal keratinocytes of wounded epithelium (Rechardt et al., 2000; Madlener et al., 1996). The expression of MMPs in keratinocytes and other cells in wounded skin is disused further in Chapter 5.

1.3.2.3 Tissue remodelling

The final stage of wound healing takes the greatest amount of time and persists even after the re-epithelialisation is complete. The remodelling phase can last up to a year and results in the formation of scar tissue as matrix is laid down in place of granulation tissue (figure 1.10 C; reviewed in (Velnar et al., 2009)). The key feature of this is the thickening of collagen bundles, increasing the tensile strength of the wound. A delicate balance between synthesis and degradation of ECM components is struck during remodelling, with an increase in TIMP expression resulting in a decrease in MMP activity (Kahari and Saarialho-Kere, 1997). The various cells involved in the earlier wound healing stages are depleted by apoptosis so that fibroblast density is reduced, growth of capillaries stops and only resident macrophages remain (Velnar et al., 2009).

Due to the complex nature of the wound healing process and the multiple cells types involved it is perhaps unsurprising that several disease states include impaired wound healing as a secondary complication. For example, any disease affecting the circulation and causing ischemia, such as atherosclerosis, will prevent the proper deployment of the cells involved in wound healing. Similarly immune suppression will delay the wound healing process, particularly the pro-inflammatory phase, and is a symptom of human immunodeficiency virus (HIV) induced acquired immunodeficiency syndrome (AIDS). Perhaps the most common pathology associated with impaired wound healing, and one that is rapidly becoming more prevalent, is type II diabetes (Campbell, 2009).

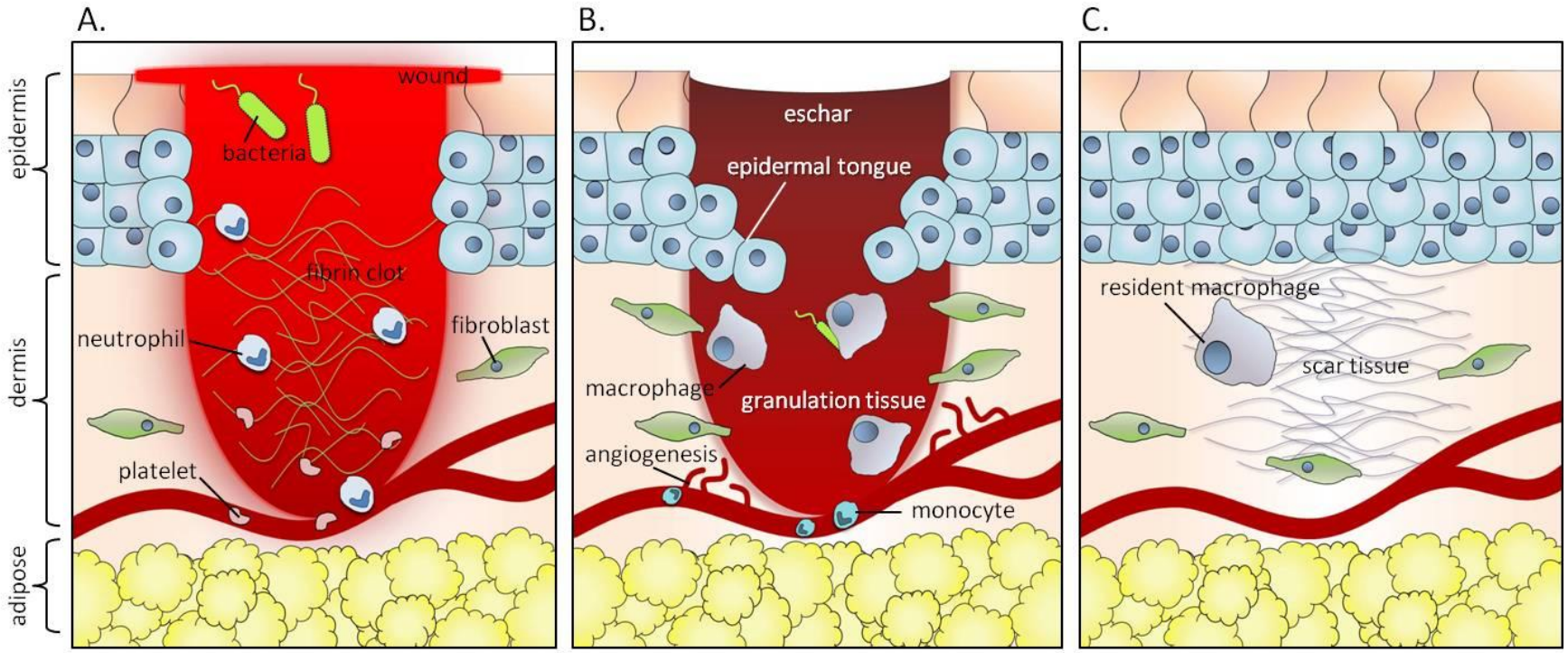

Figure 1.10 The wound healing response. Wound healing in healthy tissue takes place in three primary stages. (A) Immediately following wounding platelets are released from the blood and form a fibrin clot. The first stage of wound healing is pro-inflammatory and involves a massive influx of immune cells, beginning with neutrophils, which migrate into the wound using the fibrin clot as a scaffold and clear the wound of pathogens. (B) Following neutrophils monocyte-derived macrophages migrate into the wound clearing any remaining pathogens whilst also engulfing spent neutrophils and cell debris. The proliferation phase begins as fibroblasts migrate into the wound and lay down granulation tissue rich in ECM components. Fibroblasts also secrete cytokines that trigger angiogenesis thus increasing blood flow to the wounded tissue. Keratinocyte migration also triggers wound closure and contributes to the advancing epidermal tongue. (C) The final stage of wound healing continues after re-epithelialisation is complete and involved the remodelling of wounded tissue and formation of scar tissue. Fibroblast proliferation stops and growth of new capillaries is arrested. Resident macrophages remain but all other wound responsive cells are cleared by apoptosis. Information for this diagram taken from (Gurtner et al., 2008)

Cell type	Source	Function in wound healing	Responds to…
Platelets	Damaged blood vessels	Form an aggregate mass aiding blood clotting	*Collagen, vWF, Tissue Factor, Thrombin* – in blood and released from damaged endothelial cells
Neutrophils	Diapedesis from blood vessels	Anti-microbial: phagocytosis and oxidative burst	*IL-8 (CXCL8), CXCL5, CXCL1, IFN-γ, C5a* – expressed by epithelial cells, fibroblasts, endothelial cells
Macrophages	Diapedesis of circulating monocytes from blood vessels Some resident in tissue	Secondary influx of phagocytes: clears wound of ECM, cell debris, spent neutrophils and any remaining pathogens	*MCP-1 (CCL2), CCL3, CCL5, PDGF, TGF-β* – expressed by platelets, neutrophils and damaged endothelium *PAMPs* – on the surface of pathogens
Fibroblasts	Connective tissue at the wound edges	Formation of granulation tissue and later wound contraction	*EGF, PDGF, FGF-1, FGF-2* – expressed by macrophages, keratinocytes and damaged endothelium
Endothelial cells	Nearby blood vessels	Angiogenic sprouting (Earlier activation allows for diapedesis)	*VEGF, HGF, PDGF, FGF-1, FGF-2, TGF-β, IL-8* – expressed by macrophages, smooth muscles cells, T-lymphocytes, other endothelial cells.
Keratinocytes	Epidermal wound edges	Re-epithelialisation of open wound	*TGF-β, KGF, EGF, FGF-1, FGF-2* – expressed by macrophages, fibroblasts, smooth muscle cells, other keratinocytes Lack of contact inhibition from other keratinocytes at the wound edge

0-3 days

3-12 days

3 days – 6 months +

Table 1.3 Cells deployed during the multistep inflammatory cascade. Numerous cells are stimulated during the wound healing response and the precise timing of their deployment is vital for efficient resolution of injury, infection and subsequent inflammation. The cells involved are listed from earliest to latest induction and the approximate period during which they are active is indicated by arrows. C5a – complement component 5a, EGF – epidermal growth factor, FGF – fibroblast growth factor, IL-8 – interleukin-8, IFN-γ – interferon-γ, KGF – keratinocyte growth factor, MCP-1 macrophage chemotactic protein-1, PDGF – platelet derived growth factor, TGF-β – transforming growth factor-β, VEGF – vascular endothelial growth factor, vWF – von Willebrand Factor. Adapted from (Martin and Leibovich, 2005) with information drawn from (Esche et al., 2005).

1.4 Type II Diabetes

1.4.1 Type II diabetes and the diabetic milieu

Diabetes mellitus, often just referred to as diabetes, is a disease characterised by high blood glucose levels due to a deregulation of the hormone insulin. There are two types of diabetes, type I and type II.

1.4.1.1 Comparing type I and type II diabetes

Type I diabetes is the result of the autoimmune destruction of insulin-producing pancreatic beta cells and is fatal unless treated with a strict regime of exogenous insulin administration. Type II diabetes, conversely, is characterised by an inability to respond to endogenously produced insulin, termed insulin resistance, and is considered to be a metabolic disorder rather than an autoimmune disease. Like type I diabetes, type II is characterised by increased blood glucose, however patients usually do not lose the ability to produce insulin. Therefore, the first line of treatment for type II diabetes is lifestyle modification as obesity and physical inactivity strongly correlate to increased prevalence of the disease (reviewed in (Campbell, 2009)). Following this a regimen of oral anti-diabetes drugs, anti-hypertensive medications and anti-dyslipidemic agents can be prescribed. Type II diabetes is by far the more common of the two variants, accounting for more than 90% of cases, and is increasing in incidence to epidemic levels (Zimmet et al., 2001). Despite being preventable and treatable type II diabetes still imposes a huge burden on health systems world-wide. Therefore a better understanding of its pathogenesis and the subsequent co-morbidities is necessary to reduce its prevalence.

1.4.1.2 The diabetic milieu and insulin resistance

There are a number of factors that can trigger the development of type II diabetes. For example lifestyle; including diet, weight and physical activity; genetics, pre-existing medical conditions and even certain medications can contribute to the constant low-grade pro-inflammatory microenvironment known as the diabetic milieu (figure 1.11).

Lifestyle is perhaps the most important aetiological factor contributing to increased risk of diabetes, particularly in terms of the recent epidemic (reviewed in (Mozaffarian et al., 2009)). Increased intake of food containing saturated fatty acids can lead to increased levels of circulating LDLs, which, combined with a sedentary lifestyle, can lead to obesity and prolonged dislipidemia, both of which strongly correlate to insulin resistance (Haffner and Miettinen, 1997). Insulin resistance is a condition whereby tissues that would usually respond to insulin, such as muscle,

liver and fat, are no longer able to. In a healthy individual increased blood glucose triggers insulin production in turn triggering uptake of blood glucose and circulating fatty acids and their conversion to glycogen and triglycerides, respectively. Insulin resistance therefore results in increased blood glucose and levels of circulating fatty acids.

Both increased blood glucose and circulating fatty acids trigger pro-inflammatory events associated with the diabetic milieu (figure 1.11). For example, even transient hyperglycemia has been shown to trigger a lasting up-regulation of NF-κB in aortic endothelial cells *in vitro* (El-Osta et al., 2008). Similarly, NF-κB expression was induced in adipocytes and fibroblast cells following exposure to saturated fatty acids, whilst treatment with unsaturated fatty acids decreased NF-κB (Yeop et al., 2010). This increase in pro-inflammatory gene expression leads to macrophage activation and expression of certain cytokines and chemokines. It has been shown, for example, that high glucose significantly increased the levels of MCP-1, TNF-α, IL-1β and β2 integrins expressed by a monocytic cell line (Shanmugam et al., 2003). Interestingly secretion of pro-inflammatory nitric oxide was also significantly increased in macrophages from the type II diabetic mouse model, db/db, compared to its non-diabetic heterozygous counterpart, db/+, suggesting a deregulation of pro-inflammatory events in the diabetic phenotype (Zykova et al., 2000).

It is clear that monocytes and macrophages respond to increased levels of pro-inflammatory cytokines by proliferating and migrating towards the source in excess. It is the deregulation of these otherwise normal macrophage functions, attributable to their exposure to the diabetic milieu, which contributes to the pathology of several secondary complications of type II diabetes.

1.4.2 Macrophage expression of metalloproteinases in type II diabetes

Macrophages play an important role in the resolution of inflammation. It is to be expected, therefore, that the chronic inflammation associated with the diabetic milieu should further trigger aberrant macrophage activation and migration, contributing to co-morbidities, such as impaired wound healing and atherosclerosis (figure 1.11). Metalloproteinases expressed by macrophages play an important role in cell migration (see Chapter 1, 1.2.5) and degradation of ECM, both of which are key features of wound healing and atherosclerosis.

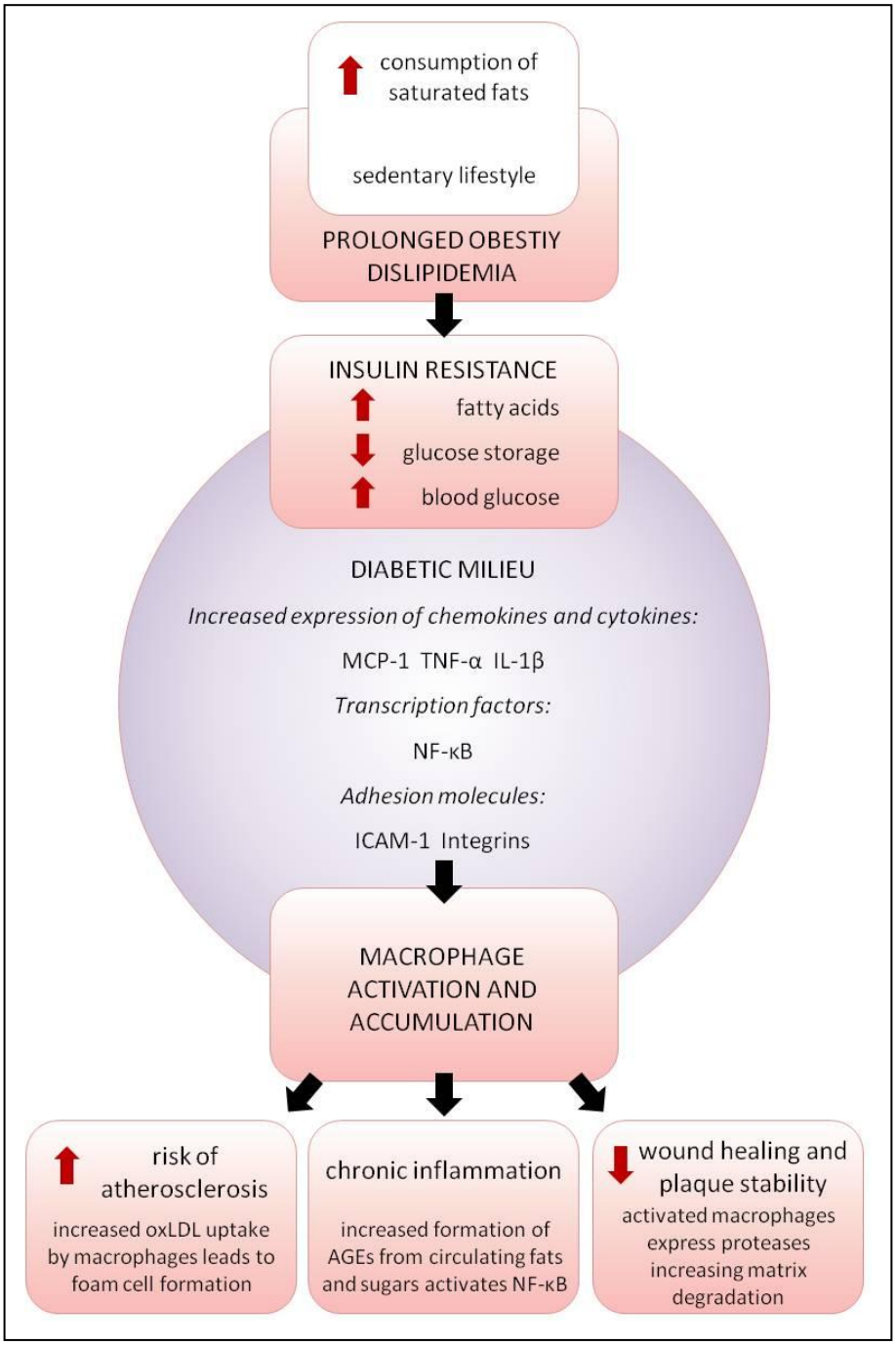

Figure 1.11 The diabetic milieu and secondary complications of type II diabetes. Poor diet and a sedentary lifestyle lead to prolonged obesity and dislipidemia, which can trigger insulin resistance. Insulin resistance is characterised by hyperglycaemia and an increase in circulating fatty acids converted from glucose that is unable to be stored. This stimulates enhanced expression of chemoattractants, transcription factors and adhesion molecules that activate macrophages. Macrophage accumulation contributes to chronic inflammation due to their expression of pro-inflammatory factors such as TNF-α. Risk of atherosclerotic plaque development is the result of macrophage foam cell formation. The proteases secreted by macrophages degrade matrix proteins leading to plaque rupture and impaired wound healing. Information for this diagram taken from (Haffner and Miettinen, 1997; Wall et al., 2002)

1.4.2.1 Impaired wound healing and metalloproteinases

Impaired wound healing is one of the most common secondary complications attributable to type II diabetes and typically manifests as ulcerations seen frequently on the feet and the legs of diabetic patients. 'Diabetic foot', as it is more commonly known, first develops as a result of another complication of type II diabetes; peripheral neuropathy. Neuropathies result from damage to the microvasculature supplying blood to the nerves and lead to loss of peripheral sensation, i.e., in the hands and feet. Loss of sensation means that small wounds can often go unnoticed, especially in the feet, and can rapidly form chronic ulcers.

Evidence that deregulation of macrophage number is responsible for the delayed healing of chronic wounds has been shown by rescuing wound healing using mouse models of type II diabetes; the naturally occurring leptin receptor-deficient db/db mouse and the leptin-deficient ob/ob mouse. Leptin (encoded by the *ob* gene) is a hormone that acts on the hypothalamus to regulate satiety. Loss of Leptin or its receptor (*obr*) results in uncontrolled food intake, thus inducing a type II diabetic phenotype (Chen et al., 1996) including the propensity for delayed wound healing. More recently studies have revealed leptin to have a direct effect on immune cell recruitment in both mice and humans (Goren et al., 2003) suggesting a mechanism by which healing is impaired.

Left untreated, full thickness dermal wounds in db/db mouse skin take significantly longer to heal than those of non-diabetic heterozygous (db/+) control wounds and macrophage infiltration is significantly delayed. This can be partially rescued by the application of PDGF, FGF (Greenhalgh et al., 1990), and HGF (Bevan et al., 2004), of which PDGF and HGF were found to increase macrophage infiltration to the wounds. Interestingly, in ob/ob wounds, repressing pro-inflammatory TNF-α signalling with the application of an anti-TNF-α monoclonal antibody (mAb) was found to decrease inflammation and rescue impaired rate of wound re-epithelialisation (Goren et al., 2007). This suggests a delicate balance must be struck between the need for macrophages during wound healing and their expression of inflammatory cytokines in the chronic ulcer.

There is a wealth of data supporting the need for tight regulation of metalloproteinase expression in healing wounds. Differential expression of the gelatinases, MMP-2 and -9, for example, has been observed in both mouse and human chronic diabetic wounds (Wall et al., 2002). A putative role for MMP-14 in monocyte migration has also been demonstrated, with the use of an anti-MMP-14 mAb. The inhibition of MMP-14 activity represses monocyte migration on a fibronectin

matrix and through an endothelial monolayer (Matias-Roman et al., 2005). Enhanced expression of MMP-14 has been found in isolated human dermal fibroblasts as a result of increased TNF-α and MMP-2 activation (Han et al., 2001). This suggests a mechanism by which prolonged TNF-α expression contributes to MMP-driven deregulation of macrophage migration.

There is also evidence of ADAMTS function in wound healing. For example, ADAMTS-1 is expressed by macrophages at relatively low levels in non-diabetic wounded tissue and contributes to enhanced migration of keratinocytes and endothelial cells (Krampert et al., 2005). Krampert et al also show however that increased levels of ADAMTS-1, as seen in diabetic wounded tissue, actually represses migration by inhibiting the action of FGF-2. This again highlights the need for balance of factors in chronic wounds and suggests there is much more to learn before we can fully appreciate the complex mechanisms controlling wound healing in type II diabetes.

1.4.2.2 Atherosclerosis and metalloproteinases

The role of macrophages in the pathogenesis of CVD and atherosclerosis is well understood (see Chapter 1, 1.1.4). Atherosclerosis is a serious disease, but is clinically silent for the majority of its progression. Atherosclerotic plaques only become clinically relevant when they pose an immediate risk of blood vessel occlusion or of rupture. Plaque rupture and intimal thickening, which can lead to occlusion, are caused in part by the over expression of metalloproteinases in macrophages and foam cells that form the majority of the atheroma (Newby, 2005). This is particularly relevant in diabetic patients as their plaques are typically more advanced and more prone to rupture (Liang et al., 2007).

The macrophage-derived foam cells that contribute to the lipid laden core of an atherosclerotic plaque are known to exhibit increased expression of various MMPs. For example, whilst MMP-2 is expressed constitutively in both healthy alveolar macrophages and aortic macrophage foam cells extracted from rabbits, only the foam cells expressed MMP-1 and -3 (Galis et al., 1995). Similarly, enhanced expression of MMP-16 has also been reported in the macrophages of advanced atherosclerotic plaques *in vivo*, whilst its expression can be up-regulated by treatment with oxLDL and TNF-α in macrophages *in vitro* (Uzui et al., 2002). The db/db type II diabetic mouse model is also useful for studying metalloproteinase expression in atherosclerosis, when crossed with the hypercholesterolemic ApoE-null mouse. Compared to non-diabetic ApoE-null controls, for example, these mice develop atheromas more quickly and express enhanced levels of active

MMP-9 (Wendt et al., 2006). These studies suggest that MMPs may have potential as biomarkers of imminent plaque rupture or as an indication of prognosis in heart disease patients.

Interestingly, a lack of macrophage MMP expression appears to stabilise plaques rather than prevent their formation altogether. For example, research has shown that transplant of MMP-14-null bone marrow into mice deficient in the LDL receptor can lead to increased accumulation of collagen in atherosclerotic plaques and a concurrent decrease in macrophage MMP-1 activity (Schneider et al., 2008). Despite there being no effect on the size of the atheroma or its macrophage composition, loss of MMP-14 did enhance stability of plaques, thus further confirming the importance of macrophage MMP expression for the potential of plaque rupture. This corresponds to a recent study into levels of TIMP-3 in atherosclerotic plaques. Expression of TIMP-3 was found to be dramatically reduced in macrophage foam cells collected from an *in vivo* model of foam cell accumulation (Johnson et al., 2008). Interestingly, immunohistochemical analysis of atheromas from cholesterol-fed rabbits also revealed differential expression of TIMP-3, with higher levels associated with the stable cap and lower levels present in the deep, less stable layers of the plaque. Johnson et al propose that TIMP-3 expression inversely correlates with that of MMP-14 in plaques and highlight the significance of a TIMP-3/MMP-14 balance in the progression of atherosclerosis.

Just as in impaired wound healing, there is also a role for the ADAMTS family in atherosclerotic plaque rupture. Expression of ADAMTS4 and 8 co-localised with macrophage-rich areas in immunohistochemical analyses of atherosclerotic plaque in mice (Wagsater et al., 2007). Wagsater et al also showed that ADAMTS-4 and -8 increase in expression during monocyte to macrophage differentiation and in response to TNF-α and IFN-γ stimulation, although it is not yet clear what their relevant substrates are in the atherosclerotic plaque.

These studies confirm the need to better understand macrophage expression of metalloproteinases in atherosclerosis, however there must be caution in considering the use of metalloproteinase inhibitors to prevent destabilisation of plaques. As well as macrophages, VSMCs express metalloproteinases to aid their migration towards atheromas (Newby, 2007). VSMCs however are thought to strengthen, rather than destabilise, the plaque, thus contributing another layer of complexity to the pathology of type II diabetes.

1.5 Summary

The role of macrophages in inflammation and the immune response is well understood. Their function as phagocytes to clear the wound of pathogens and cell debris has long been appreciated and more recent studies have elucidated the role of macrophages in expression of important cytokines and chemokines. Similarly, the signalling pathways involved in macrophage response to infection have been well studied, for example, knowledge of the activation of TLR4 by LPS and the subsequent nuclear translocation of NF-κB has triggered a wealth of publications investigating the targets of this transcription factor.

Despite an expanding knowledge-base, there is still a need to better appreciate the role of the metalloproteinases in infection and inflammation, particularly in the case of monocyte and macrophage migration. Aberrant macrophage migration and expression of metalloproteinases has been shown to contribute to a number of secondary complications of type II diabetes, such as atherosclerosis and chronic wounds. The growing prevalence of this entirely preventable disease only serves to highlight the need to understand its pathogenesis.

Due to the number of different metalloproteinase genes, their broad expression profile, and their numerous functions in varying diseases, it is important to take a systematic approach when studying them. By profiling individual metalloproteinases in macrophages it is possible to narrow down the search for relevant genes that may serve as potential biomarkers or even drug targets.

1.6 Aims of thesis

In this thesis I aim to explore the expression of the metalloproteinases in murine bone marrow-derived macrophages; including all the MMPs and TIMPs, and some key ADAMs and ADAMTSs. In doing this I aim to produce a potential protease signature for these macrophages, both at basal levels and in response to pro-inflammatory LPS stimulation. I also aim to perform miRNA microarray analysis of bone marrow-derived macrophages, again both at basal levels and following stimulation.

Following on from the proteinase and miRNA profile analysis I aim to investigate the migratory phenotype of bone marrow-derived macrophages on different ECM components, both with and without LPS stimulation. I will examine the possible functional role of any differentially regulated metalloproteinases or miRNAs in migration, as identified by the profile analysis.

As macrophages are key players in the various secondary complications of type II diabetes, I aim to investigate the expression of metalloproteinases in tissues from the type II diabetic mouse (db/db) and its non-diabetic counterpart (db/+). Specifically, I will look at the expression of any proteinases highlighted in the original profile analysis in db/db bone marrow-derived macrophages and during a model of impaired wound healing that is well established in our laboratory. I also plan to investigate the migratory phenotype of bone marrow-derived macrophages from the db/db mouse in response to chemoattractant stimuli in an attempt to reveal any inherent defects in diabetic macrophage motility.

Chapter 2: **Materials and Methods**

2.1 Materials

Unless otherwise stated all chemical reagents were purchased from Sigma-Aldrich Inc., all tissue culture reagents from Gibco Invitrogen Corportation and all tissue culture plastics from Nunc Thermo Fisher Scientific.

2.2 Cell Culture

The RAW264.7 macrophage cell line (TIB-71 ATCC) was grown in Dublecco's Modified Eagle Medium (DMEM) high glucose liquid medium, containing 100 units/ml Penicillin/Streptomycin antibiotic, 5 mM L-Glutamine, supplemented with 10% (v/v) Fetal Calf Serum (FCS; Biosera). Cells were incubated at 37°C, 5% CO_2 and split 1:3 roughly every three days, using an 18mm blade Cell Scraper (BD Falcon) to remove adherent cells. Before experiments were set up RAW264.7 were centrifuged at 1000 r.c.f for 5 minutes and re-suspended at the density stated.

2.2.1 Bone Marrow-derived Macrophage Model System

This protocol and much kind advice was provided by Dr. Parag Bhavsar and Prof. Anne Ridley, King's College, London

C57Bl/6 mice, bred in the Disease Modelling Unit, UEA, were killed by CO_2 suffocation under schedule 1 of the 1986 Animals Scientific Procedures Act and Bone Marrow-derived Macrophages (BMM) were isolated from the femurs and tibias of the mice as previously described (Walker et al., 1985). Briefly, bone marrow was flushed from the bone cavity with a 21g needle and syringe containing macrophage medium consisting of Roswell Park Memorial Institute (RPMI) 1640 liquid medium containing 100 units/ml Penicillin/Streptomycin antibiotic, 5 mM L-Glutamine, 1% (v/v) sodium pyruvate, 0.5% (v/v) nonessential amino acids, 24 µM tissue culture grade β-mercaptoethanol, supplemented with 10% (v/v) FCS and 10% (v/v) L929-cell-conditioned medium (LCM) as a source of Colony Stimulating Factor-1 (CSF-1). Cell number in bone marrow flush was counted (see Appendix, table 8.1) and 10 x 10^6 cells were plated onto 100 mm diameter Bacteriological Petri Dishes (BD Falcon) in 10ml macrophage medium. After three days of incubation at 37°C, 5% CO_2, the non-adherent population was aspirated and re-plated at the same density, with fresh macrophage medium. The adherent population was discarded. After a further five days culture non-adherent cells were aspirated and discarded, whilst remaining adherent BMMs were removed by scraping. Before experiments were performed BMM were centrifuged at 1000 r.c.f for 5 minutes and re-suspended at the density stated.

The L929 fibroblast cell line (a gift from Anne Ridley) was grown in DMEM high glucose liquid medium, containing 100 units/ml Penicillin/Streptomycin antibiotic, 5 mM L-Glutamine, 1% (v/v) Sodium Pyruvate, supplemented with 10% (v/v) FCS. Initially cells were grown in non-vented closed-system 75 cm^2 tissue culture plastic flasks (TPP) at 37°C, 5% CO_2 with the cap open. When cells reached confluencey flask caps were closed to allow them to condition the medium with CSF-1 in a closed system. After 2 weeks the conditioned medium was harvested and filtered using 0.2µm pore Mini Filters (Vivascience AG), aliquoted into volumes of 5ml and stored at 4°C for no longer than 3 months. For continued culture cells were split 1:5, roughly every three days with the cap open. Adherent cells were removed using 2ml 0.5% (v/v) Trypsin/EDTA per 75 cm^2 flask.

2.3 Trypan Blue Exclusion Assay of Cell Viability

Macrophage cell suspension was diluted 1:1 with Trypan Blue, a vital dye solution. Dead cells with damaged membranes take up the dye, appearing blue when viewed under a microscope, whilst live cells with intact membranes remain unstained. The resulting cell suspension was loaded onto a haemocytometer and the number of live (unstained) versus dead (stained) cells were counted. The percentage viability was calculated for all macrophage treatments.

2.4 Macrophage Treatments

Unless stated otherwise, all experiments were carried out on RAW264.7 or BMMs in the relevant tissue culture medium described above in the presence of 0.2% FCS.

2.4.1 LPS (a TLR4 agonist)

A 1 mg/ml stock solution of Lipopolysaccharide purified from *E. coli* (LPS) were diluted in the appropriate medium to concentrations of either 2, 20 and or 200 ng/ml as indicated and added to an equal volume of macrophage cell suspension resulting in final LPS concentrations of 1, 10 or 100 ng/ml, respectively. Macrophages were seeded into 24 or 48 well plates at densities of 0.5 x 10^6 and 0.25 x 10^6 cells per well, respectively. Cells remained exposed to LPS for the duration of the experiment stated, before total RNA purification or protein extraction.

2.4.2 Recombinant mouse TNFα (a pro-inflammatory cytokine)

Lyophilised recombinant mouse TNF alpha (rmTNFα) was reconstituted in sterile dH_2O to a concentration of 1 µg/ml, then stored at -20°C. This stock solution was further diluted in the appropriate medium containing 10% (v/v) FCS as a carrier protein to concentrations of 2, 20 and

200 ng/ml as indicated and added to an equal volume of macrophage cell suspension resulting in final rmTNFα concentrations of 1, 10 and 100 ng/ml. Macrophages were seeded into 24 or 48 well plates at densities of 0.5 x 10^6 and 0.25 x 10^6 cells per well, respectively. Cells remained exposed to rmTNFα for the duration of the experiment stated, before total RNA purification or protein extraction.

2.4.3 BMS-345541 and BAY 11-7082 (IκB kinase inhibitors)

Solid BMS-345541 was dissolved in DMSO to a concentration of 1 mg/ml, then stored at -20°C. This stock solution was further diluted in the appropriate medium to concentrations of 10, 20 and 30 μg/ml as indicated and added to an equal volume of macrophage cell suspension resulting in final BMS-345541 concentrations of 5, 10 and 15 μg/ml. Solid BAY 11-7082 was dissolved in DMSO to a concentration of 10 mg/ml, then stored at -20°C. This stock solution was further diluted in the appropriate medium to concentrations of 0.4, 4 and 40 μg/ml as indicated and added to an equal volume of macrophage cell suspension resulting in final BAY 11-7082 concentrations of 0.2, 2 and 20 μg/ml. Macrophages were seeded into 24 or 48 well plates at densities of 0.5 x 10^6 and 0.25 x 10^6 cells per well, respectively, and exposed to BMS-345541 or BAY 11-7082 for 1 hour prior to LPS treatment. Following this, all BMS-345541 and BAY 11-7082 was removed from cells and LPS was added as above.

2.4.4 Actinomycin D (inhibitor of transcription)

A 1 mg/ml stock solution of Actinomycin D was diluted in the appropriate medium to a concentration of 10 μg/ml and added to an equal volume of macrophage cell suspension resulting in a final Actinomycin D concentration of 5 μg/ml. Macrophages were seeded into 24 or 48 well plates at densities of 0.5 x 10^6 and 0.25 x 10^6 cells per well, respectively, with Actinomycin D for 45 minutes. Following this, all Actinomycin D was removed from cells and LPS was added as above.

2.4.5 D-Glucose and D-Mannitol

A 450 mg/ml stock solution of D-Glucose was diluted in the appropriate medium to give working concentrations of 200 mg/ml (11 mM – equivalent to wild type blood glucose)and 720 mg/ml (40 mM – equivalent to blood glucose levels found in the diabetic mouse). A 180 mg/ml stock solution of D-Mannitol was diluted in the appropriated medium to give a single working concentration of 720 mg/ml (40 mM – to mimic maximum equivalent D-glucose concentration). After three days of initial BMM culture the non-adherent macrophage population was aspirated and 10 x 10^6 of these cells were plated onto 100 mm diameter Bacteriological Petri Dishes in 10ml macrophage medium

containing D-glucose. Differentiation of BMM continued as described above before cells were prepared for immunocytochemistry.

2.4.6 Recombinant Human MMP-10

The concentration of a stock solution of recombinant human MMP-10 (rhMMP-10; a kind gift from A.D. Rowan (Barksby et al., 2006)) was determined to be 360 ng/ml with the Human MMP-10 Quantikine ELISA kit (R&D systems). Stock rhMMP-10 was diluted in the appropriate medium to give a working concentration of 2.8 ng/ml. Macrophages were seeded into 24 well plates at a density of 25 x 10^3 cells per well and were treated with rhMMP-10 6 hours before time-lapse microscopy of the cells began.

2.4.7 siRNA

5 nmol lyophilised siGENOME SMARTpool siRNA (Dharmacon; see Table 2.1) targeting mouse MMP-10 was dissolved in 250 µl siRNA Suspension Buffer (Qiagen) to a concentration of 20 µM. Any aggregates that were formed during lyophilisation were disrupted by heating for 1 minute at 90˚C, followed by 60 minutes incubation at 37C˚. siGENOME SMARTpool siRNA and AllStars Negative Control (Qiagen) scrambled siRNA were then stored at -20˚C. siRNAs were diluted in 100 µl of the appropriate medium (serum free) to a working concentration of 15 nM and 1.5 µl of HiPerfect Transfection Reagent (Qiagen) was added. Samples were incubated for 5 minutes to allow transfection complexes to form. Macrophages were seeded at a density of 15 x 10^3 cells per well into 96 well plates or 25 x 10^3 cells per well into fibronectin coated 24 well plates 24 hours prior to transfection. siRNA and HiPerfect Transfection Reagent were added 'drop-wise' to the cells and remained on the cells for 24 hours before total RNA extraction and protein extraction, or before time-lapse microscopy began.

	Sequence 5' – 3'
siGENOME SMARTpool siRNA 'Mouse-MMP-10'	GGGAAGUCCUAUUCUUUAA
	GAAUUGAGCCACAAGUUGA
	GAGAUGUUCACUUCGAUGA
	CCUCAGGGACCAACUUAUU
AllStars Negative Control 'Scrambled siRNA'	Alexa488 labelled - sequence not provided

Table 2.1 siRNA sequences as supplied by Dharmacon.

2.4.8 LNA modified Oligonucliotides: Anti-miRs

5 nmol miRCURY locked nucleic acid (LNA) Knockdown oligonucleotide (Exiqon; see Table 2.2) targeting mouse miR-155 and a 5 nmol Scramble-miR LNA oligonucleotide (Exiqon) in a 25 nM suspension were diluted in 100 µl of appropriate medium (serum free) to a working concentration of 50 nM. 1.5 µl of HiPerfect Transfection Reagent was added and samples were incubated for 5 minutes to allow transfection complexes to form. Macrophages were seeded at a density of 25 x 10^3 cells per well into fibronectin coated 24 well plates 24 hours prior to transfection. Transfection complexes were added 'drop-wise' to the cells and remained on the cells for at least 24 hours before the start of time-lapse microscopy began. 1 hour after transfection, stock solutions of LPS were diluted to a concentration of 1 µg/ml in the appropriate medium and further diluted to a working concentration of 10 ng/ml in the wells containing the miRCURY LNA transfected cells.

	Sequence 5' – 3'
miRCURY LNA Knockdown 'mmu-miR-155'	/56-FAM/ACCCCTATCACAATTAGCATTAA
miRCURY LNA Knockdown 'Scramble-miR'	GTGTAACACGTCTATACGCCCA

Table 2.2 LNA anti-miR sequences as supplied by Exiqon.

2.5 Total RNA purification

Total RNA was purified from macrophage cell lysates using the RNeasy Minikit (Qiagen) according to the manufacturer's instructions. Briefly, culture medium was removed from adherent macrophages and cells were lysed in a highly denaturing guanidine thiocyanate buffer with β-mercaptoethanol. Lysate was further homogenized by passing through a 21 g needle and syringe. Later, β-mercaptoethanol and the homogenization step were omitted at the manufactures instructions and were found to have no adverse effect on RNA yield. 70% (v/v) ethanol was added to the homogenate to promote RNA binding to the silica-gel based membrane of the RNeasy mini spin column. Following this the membrane was washed and treated with DNase to degrade any DNA contaminants. To remove cell contaminants and further bind RNA to the membrane, a series of washes with high salt buffers was performed. After the membrane was dried, purified RNA was eluted in RNase-free water for storage at -20°C. All binding, washing and elution steps were performed at 15,000 r.c.f in a microcentrifuge at room temperature. RNA yield was measured using the Nanodrop ND-100 spectrophotometer (Nanodrop technologies) at 260 and 280 nm. A 260/280 nm ratio of 1.8 – 2.0 was considered acceptable purity. The normal ranges of mRNA yield for each macrophage cell line are shown in Table 2.3.

Cell Type	Normal Range of mRNA yield	Cell Number
RAW264.7	150 – 250 ng/µl	0.5 x 10^6
BMM	50 - 150 ng/µl	0.25 x 10^6

Table 2.3 Range of mRNA yield from RAW264.7 cell line and primary BMMs after total RNA purification.

2.6 Reverse Transcription

250 ng - 1 µg of purified mRNA in a 10 µl volume was reverse transcribed to complementary DNA (cDNA) using Random Primers (Promega), dNTP Mix (Bioline) and Superscript II ® Reverse Transcriptase in a 20 µl reaction according to the manufacturer's instructions. Briefly, 250 ng/ml random primers and 100 mM dNTP was added to each sample and heated at 65˚C for 5 minutes to denature the mRNA secondary structure. Samples were then immediately transferred to ice to prevent secondary structures reforming and to allow random primers to anneal to mRNA. Following this 250 mM 5 x first strand buffer, 0.1 M DDT, 200 U/µl reverse transcriptase and analytical grade H_2O, to bring the volume to 20 µl, were added to each sample and heated at 42˚C for 50 minutes to allow first strand cDNA synthesis, followed by 70˚C for 15 minutes to inactivate the reaction. Later, Superscript II ® Reverse Transcriptase was replaced with 200 U/µl Moloney Murine Leukemia Virus Reverse Transcriptase (M-MLV RT; Promega) with no adverse effect on reverse transcription efficiency.

2.7 Quantitative Real Time – PCR

Quantitative real-time PCR (qRT-PCR) reactions were performed using the 7500 Fast RT-PCR System (Applied Biosystems) according to the manufacturer's instructions. Each reaction contained the equivalent of 5 - 10 ng reverse transcribed mRNA (1 ng mRNA for the 18S control analyses), 8.33 µl QuantiTect probe PCR Master Mix (Qiagen), 100nM each of the forward and reverse primer (see Appendix, table 8.2) and 200nM of probe in a volume of 25 µl per reaction. Each reaction was performed for 2 minutes at 50°C and 10 minutes at 95°C to activate the Taq DNA polymerase component of the master mix, followed by 40 cycles, each consisting of 15 seconds melting at 95°C, and 1 minute annealing and extending at 60°C. The ribosomal gene 18S was used as an endogenous control to normalize differences in total reverse transcribed mRNA in each sample. Standard curves for each PCR reaction were prepared covering a range equivalent to 20 – 0.625ng of mRNA (4 to 0.125ng for 18S analyses) and relative levels of target cDNA within

each sample were determined, normalized to the 18S cDNA for that sample. Any samples with an 18S value varying more than 1 C_Ts from the mean were omitted (see Figure 2.1). Data is therefore represented as the level of target mRNA relative to the level of 18S mRNA in that sample, or converted to fold change in expression relative to 18S. Statistical analysis of gene expression changes between two sets of data was performed using the two-tailed Student's T-test on sample groups no smaller than n = 3.

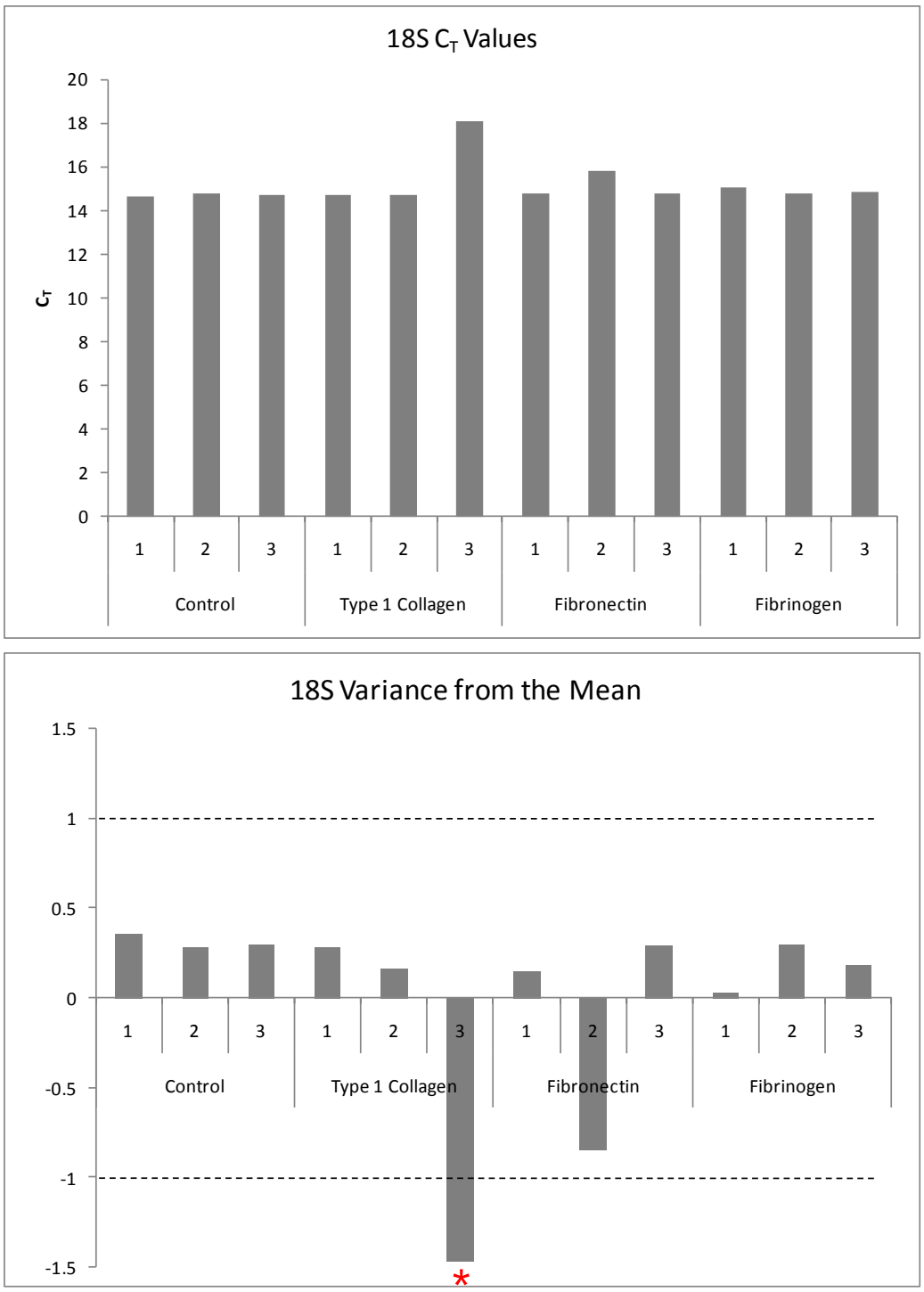

Figure 2.1 Example 18S C_T values and variance from the mean. The variance from the mean of all samples was calculated and plotted to indicate which samples, if any, vary more than 1 C_T from the mean value. In this case, sample 3; Type 1 collagen (indicated by *) varies almost 1.5 C_T from the mean.

2.8 Trichloroacetic Acid Precipitation of Proteins from Cell Culture Supernatant

500 µl of cold 10% (v/v) trichloroacetic acid (TCA) was added to 1 ml of cell supernatant, incubated on ice for 1 hour and then centrifuged for 15 minutes, 13,000 r.c.f, at 4˚C to collect protein pellet. Following this, protein pellets were washed with cold acetone to remove excess TCA, vortexed and then collected again by further centrifugation. Acetone was removed and pellets were air-dried before resuspension in 1x SDS-PAGE Reducing Final Sample Buffer (0.625 M Tris pH 6.8, 2% (v/v) SDS, 2% (v/v) of 10% Bromophenyl blue (dissolved in EtOH), 10% (v/v) Glycerol, 15% β-mercaptoethanol, 6 M urea).

2.9 Extraction of Protein from Tissue Samples

Snap frozen tissue sections were fully immersed in cold extraction buffer (10 mM Tris-HCL pH7.6, 10 mM NaCl, 3 mM $MgCl_2$, 1% (v/v) NP-40) and finely cut up with scissors. Tissue was then fully disrupted with ball barings using the TissueLyser II (Qiagen). Samples were incubated on ice for 1 hour, with gentle vortexing every 15 minutes. Finally, samples were centrifuged for 1.5 minutes at 10,000 r.c.f and supernatants were collected. Protein concentration was determined by the Bicinchoninic acid (BCA) Protein Assay Kit (Pierce) according to the manufacturer's instructions. Briefly, samples and a series of Bovine Serum Albumin (BSA) standards were combined with reagents from the BCA assay kit, creating an alkaline environment for the chelation of copper with protein reducing Cu^{2+} to Cu^{1+}. BCA reacts with the Cu^{1+} to produce a water soluble purple precipitate, the absorbance of which was read immediately with an MRX Microplate Reader (Dynatech Laboratories) at 550 nm primary wavelength. Protein extracts were then diluted to allow for equal loading onto polyacrylamide gels.

2.10 Western Blotting

TCA precipitated or RSB extracted protein samples were diluted 1:5 with 4x reducing sample buffer (0.625 M Tris pH 6.8, 2% [v/v] SDS, 2% [v/v] of 10% Bromophenyl blue [dissolved in EtOH], 10% [v/v] Glycerol, 20% [v/v] β-mercaptoethanol) and denatured by boiling for 5 minutes. Samples, along with pre-stained Precision Plus Protein All Blue Standards (BIO-RAD), were loaded into a 6% SDS-polyacrylamide stacking gel (6% [v/v] acrylamide/bis [BIO-RAD], 25% [v/v] 0.5M Tris buffer pH 6.8) and resolved in a 10% SDS-polyacrylamide gel (10% [v/v] acrylamide/bis [BIO-RAD], 25% [v/v] 1.5 M Tris buffer pH 8.8) in the presence of 1 x running buffer (35 mM Tris, 274 mM Glycine, 5 mM SDS). Proteins were transferred onto PVDF membrane (BIO-RAD) by semi-dry

blotting with semi-dry transfer buffer (25 mM Tris, 192 mM Glycine, 20% (v/v) MeOH, 0.13 mM SDS). Membranes were blocked in a 2x non-fat dry milk solution (25 mM Tris pH 7.4, 150 mM NaCl, 0.05% (v/v) Tween-20, 5% (v/v) non-fat dry milk) and incubated with primary antibody diluted in 1x non-fat dry milk solution. Membranes were washed in a 1x western wash buffer (25 mM Tris pH 7.4, 150 mM NaCl, 0.05% (v/v) Tween-20) for 5 x 5 minutes and blocked again before incubation with a horseradish peroxidise (HRP) conjugated secondary antibody, also diluted in 1x non-fat dry milk solution. Membranes were washed in 1 x western wash buffer for a further 5 x 5 minutes before 5 minutes incubation with Amersham ECL Western Blotting Detection Reagents (GE Healthcare). Membranes were then exposed to x-ray film and developed in an autoradiograph film processor (Xograph Healthcare Ltd.) to qualitatively measure the HRP catalysed chemiluminescent signal.

2.11 ELISA

The concentration of mTNFα in cell culture supernatants and cell lysates was determined with the solid phase sandwich Murine TNFα ELISA Kit (Diaclone Research) according to the manufacturer's instructions. Briefly, a serial dilution of a mTNFα standard was made providing a range of concentrations from 1000 pg/ml to 31.25 pg/ml. 200 µl of standards and samples were pipetted into microtitre strip wells coated with a monoclonal antibody against mTNFα and incubated for 2 hours at room temperature. Wells were washed three times with the washing buffer provided before addition of 50 µl biotinylated polyclonal anti-mTNFα antibody to all wells. A further 1 hour incubation was followed by washing as before and the addition of 100 µl streptavidin conjugated HRP. Wells were incubated for 30 minutes to allow biotin-streptavidin binding and washed again to remove unbound streptavidin-HRP before addition of 100 µl chromogen tetramethylbenzidine (TMB; containing H_2O_2) and a further 30 minutes incubation at room temperature in the dark. In the presence of H_2O_2, HRP catalyses the production of a water soluble blue precipitate from TMB. To stop the HRP catalysed reaction, 100 µl H_2SO_4 stop reagent was added to each well to acidify and denature HRP, producing a yellow colour change. Absorbance was read immediately with an MRX Microplate Reader at 450 nm primary wavelength.

2.12 Cell Migration Assay and Time-lapse Microscopy

24 well plates were coated with Type 1 Rat Tail Collagen (BD Biosciences), Human Plasma Fibrinogen (Calbiochem) or Bovine Plasma Fibronectin (Calbiochem) at the concentrations given

(see Table 2.4) for at least one hour before cell seeding and washed with sterile 1x PBS, or left uncoated. 2.5 x 10^5 cells were seeded into 24 well plates then incubated at 37°C, 5% CO_2 and allowed to adhere. Treatment agents were administered as described above before cells were transferred to a motorised stage within a controlled environment chamber at 37˚C, 5% CO_2.

For gas equilibration and to prevent formation of bubbles µ-Slide Chemotaxis chambers (Ibidi GmbH; Figure 2.2) and cell culture media were kept in 5% CO_2 overnight before experiments were performed. 6 x 10^3 cells in 6 µl culture medium were applied to the observation channel and allowed to adhere before 40 µl culture medium was added to both reservoirs. 30 minutes before time-lapse microscopy began, 18 µl of either recombinant mouse CSF-1 (rmCSF-1; R&D Systems), recombinant mouse Monocyte Chemoattractant Protein – 1 (rmMCP-1; R&D Systems) or 1x PBS control was applied to one reservoir to create a gradient of chemoattractant across the observation channel (see Table 2.4).

Cells were imaged every 10 minutes for 17 hours (unless stated otherwise) with a monochrome Axioplan CCD camera (Zeiss) attached to a widefield, Axiovert 200M inverted light microscope (Zeiss) using Axiovision software. Cell migration velocity and distance (accumulated and Euclidean; figure 2.3) was tracked and analysed using the ImageJ (NIH) plug-ins 'Manual Tracking' (F. Cordelières, Institute Curie, France) and 'Chemotaxis and Migration Tool' (Trapp and Horn, Ibidi GmbH).

Chemoattractant	Concentration Applied	Concentration at Cells
rmCSF-1	600 ng/ml	198 ng/ml (taken as 200 ng/ml)
rmMCP-1	600 ng/ml	198 ng/ml (taken as 200 ng/ml)

Table 2.4 Concentration of chemoattractant applied to Ibidi µ-Slide chemotaxis chambers and the concentration at which the gradient reaches the cells.

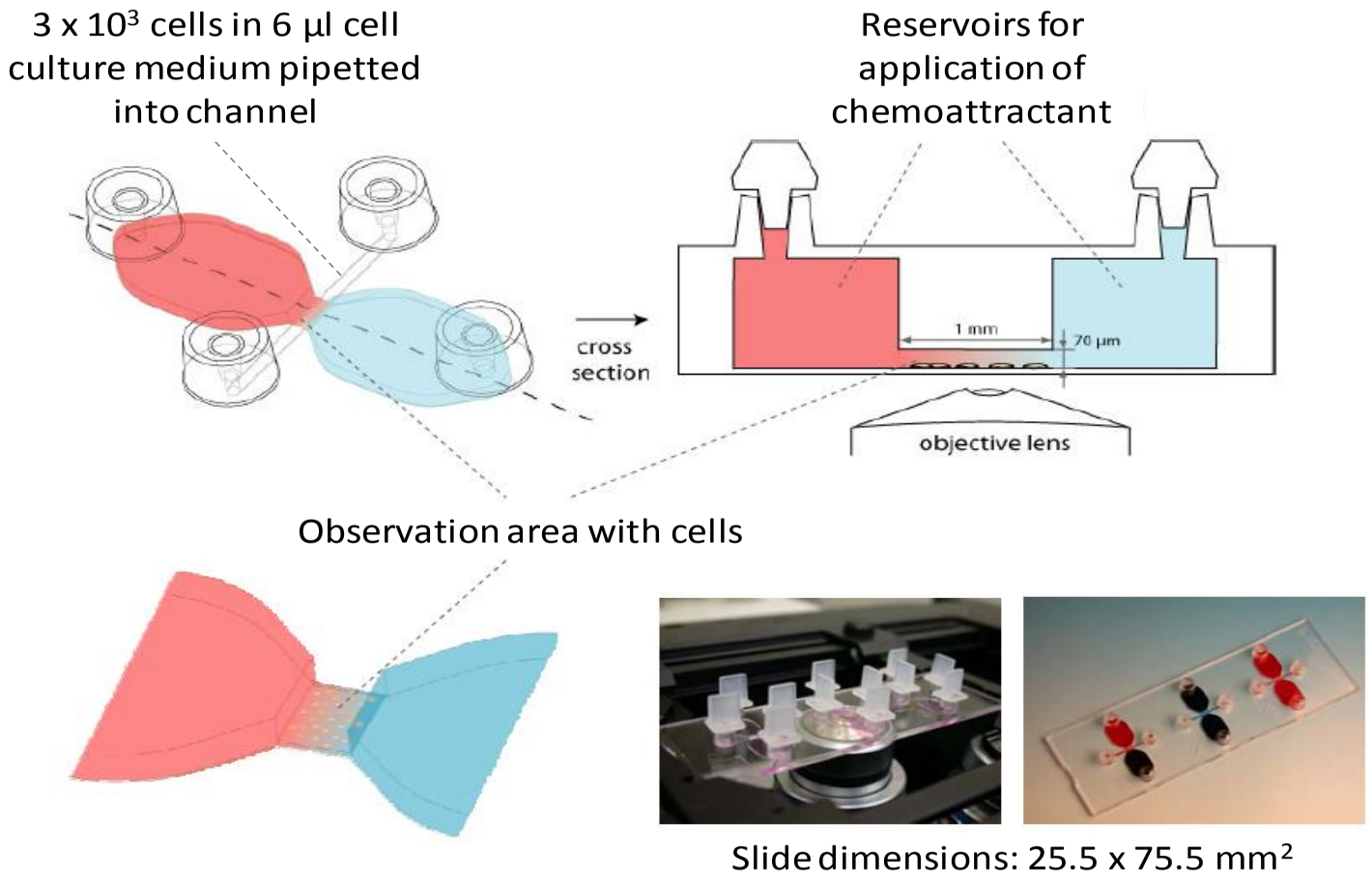

Figure 2.2 Diagram to illustrate use of Ibidi µ-Slide chemotaxis chamber. Using bevelled end pipette tips, cell suspension is loaded into the observation channel via the pipette adaptors and allowed to adhere before reservoirs are topped up with cell culture medium. Chemoattractants were applied to one reservoir creating a linear gradient across the 1mm observation area that is stable for up to 48 hours. The gradient is such that 33% of the chemoattractant concentration applied reaches the cells. During cell culture and timelapse microscopy, plugs are inserted into the pipette adaptors and µ-Slides are kept in a humidity chamber to prevent evaporation of cell culture medium or formation of bubbles. Adapeted from manufacturer's instructions (www.ibidi.com).

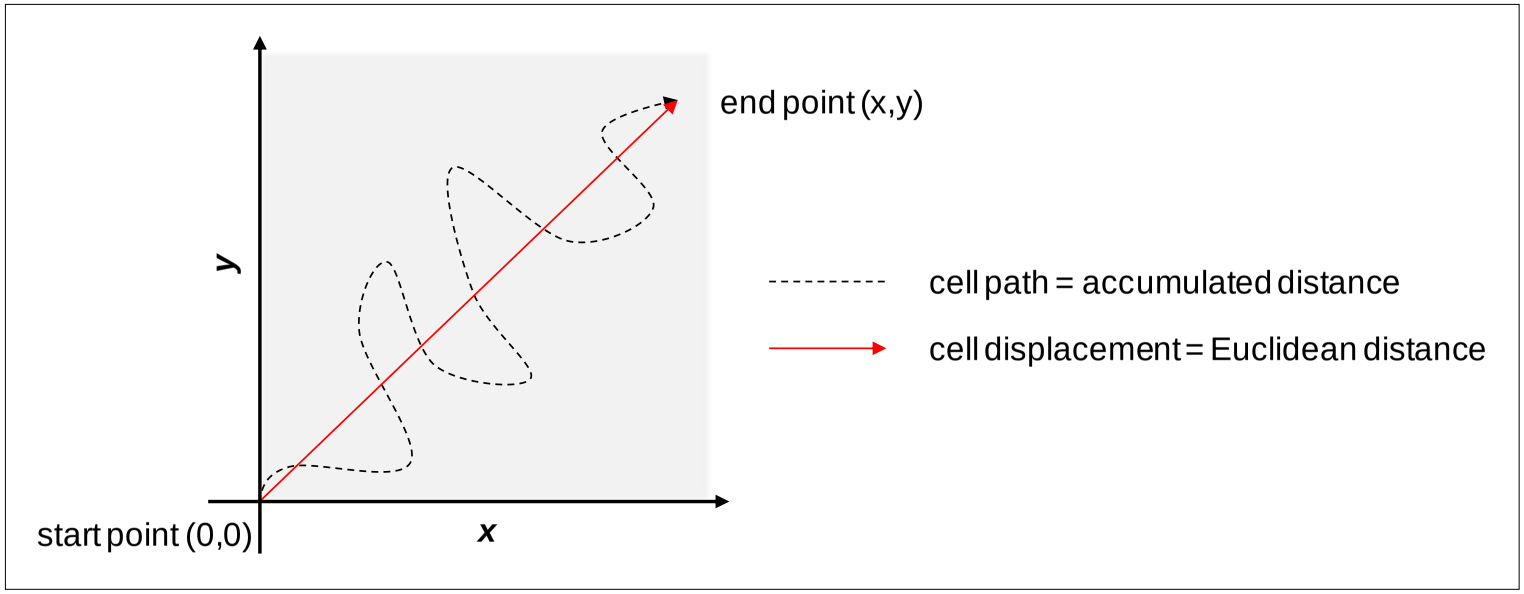

Figure 2.3 Cell migration: accumulated and Euclidean distance. Distance of cell migration can be expressed as accumulated distance, which is equal to the path of cell migration, or Euclidean distance, which is equal to cell displacement (x,y) from startpoint (0,0). The 'directionality' of migration (also known as persistence) is calculated as Euclidean distance/accumulated distance. Migration was tracked and analysed using the ImageJ (NIH) plugins 'Manual Tracking' (F. Cordelières, Institute Curie, France) and 'Chemotaxis and Migration Tool' (Trapp and Horn, Ibidi GmbH).

2.13 2D and 3D Cell Culture

2.13.1 2D Cell Culture

24 or 48 well plates were coated with Type 1 Rat Tail Collagen (in 0.02 M acetic acid), Human Plasma Fibrinogen (in PBS) or Bovine Plasma Fibronectin (in PBS) at the concentration stated (see Table 2.4) and incubated for 1 hour at room temperature. Following this, wells were washed twice with 1x sterile PBS. Cells were resuspended in cell culture medium + 0.2% (v/v) FCS at 1 x 10^6 cells/ml and plated out onto adsorbed matrix components.

2.13.2 3D Type 1 Collagen

Working on ice, 300 µl collagen solutions were prepared from a 3.66 mg/ml stock solution of type 1 collagen, 10% (v/v) 10 x sterile PBS, 1M NaOH (equal to volume of collagen) and sterile analytical grade water (up to desired final volume). The 10 x sterile PBS and sterile analytical grade water were combined with 1M NaOH before the type 1 collagen was added, diluting it to the concentration stated (see Table 2.4). Immediately after the type 1 collagen was added, 6 x 10^3 cells were resuspended in the solution which was then plated out into 48 well plates and incubated at 37˚C, 5% CO_2 for 30 minutes. Once gels had set, a volume of cell culture medium + 0.2% (v/v) FCS equal to the volume of the gel was added.

2.13.3 3D Plasminogen-depleted Fibrinogen/Fibrin

Working on ice, 300 µl Human Plasminogen-depleted Fibrinogen (Calbiochem) solutions were prepared from a 25 mg/ml stock diluted to the concentration stated (see Table 2.5) with serum-free cell culture medium. 0.15 NIH units of Bovine Plasma Thrombin was added in a 0.1% (w/v) BSA carrier solution and 6 x 10^3 cells were resuspended in this final solution. Subsequently cells were plated out into 48 well plates and incubated at 37˚C, 5% CO_2 for 30 minutes. Once gels had set, a volume of cell culture medium + 0.2% (v/v) FCS equal to the volume of the gel was added. N.B. Bovine FCS was omitted and plasminogen-depleted fibronectin was used for 3D gels to avoid the introduction of plasminogen to the solution. Plasmin, the active form of plasminogen, has serine protease activity and is able to degrade insoluble fibrin to fibrinogen, thus solubilising the 3D gel.

2.13.4 3D Plasma Fibronectin in a Type 1 Collagen gel

Working on ice, a 3D type 1 collagen gel was prepared as described above. Before 1M NaOH, a 200 µg/ml stock solution of plasma fibronectin was diluted to the concentration stated (see Table 2.4) in the sterile analytical grade water component of the gel. Cells were resuspended in the solution at 2 x 10^6 cells/ml, plated out into 24 or 48 well plates and incubated at 37˚C, 5% CO_2 for 30

minutes. Once gels had set, a volume of cell culture medium + 0.2% (v/v) FCS equal to the volume of the gel was added.

Matrix Component	2D concentration	3D concentration
Type 1 Rat Tail Collagen	10 µg/ml	1 mg/ml
Human Plasma Fibrinogen	10 µg/ml	ND
Human Plasminogen-depleted Fibrinogen	ND	2.5 mg/ml
Bovine Plasma Fibronectin	10 µg/ml	10 µg/ml (in a Type 1 Collagen gel)

Table 2.5 Concentration of matrix components used to create a 2D coating or 3D gel.

2.14 Full thickness excisional wounding

Wounding procedures were kindly carried out by Dr. Damon Bevan in the Disease Modelling Unit, UEA under project licence no. PPL80/1799, essentially as described in Bevan et al. (2004)(Bevan et al., 2004).

Genetically diabetic (C57BL/KsOlaHsd, db/db) mice and their non-diabetic heterozygote control (db/+) were obtained from Harlan UK Limited. All mice were maintained on a standard laboratory diet and water *ad libitum*. Experiments were carried out using animals aged between 7 – 16 weeks old and controls were age-matched wherever possible. Mice were anaesthetized by halothane and N_2O inhalation and all subsequent wounding procedures were carried out on a heated table. The dorsal region of the animal was shaved and sterilized using Isopropyl Wipes (Johnson and Johnson). Using sterile 0.6 cm punch biopsies (Stiefel Laboratories), two full-thickness excisional wounds were created on each dorsolateral flank of the db/db mice, equidistant from the midline. As the db/+ mice are considerably smaller than their diabetic counterparts a single wound was created on each dorsolateral flank of these animals. Wounds were separated by a margin of at least 10 mm. Immediately after wounding, a transparent semi-permeable dressing (Bioclusive, Johnson and Johnson) was applied over all wounds and firmly secured using a surgical adhesive (Vetbond, 3M). The covering was applied such that the wounds were completely isolated from one another. Mice were housed separately after wounding to minimise chance of infection.

2.15 Tissue Embedding and Sectioning

Tissue embedding and sectioning of fresh tissue was largely carried out by, or under the supervision of, Dr. Damon Bevan, UEA.

After the indicated number of days wounded mice were killed by CO_2 suffocation according to Schedule 1 of the 1986 Animals Scientific Procedures Act. Immediately following this a blood glucose test (Accu-Chek, Roche) was performed and mice were weighed to confirm diabetic or non-diabetic phenotype (see Table 2.6). Wounded and non-wounded control tissue was excised from the mice and either immersed in RNAlater (Ambion) for subsequent RNA extraction; embedded in Tissue-Tek Optimum Cutting Temperature (OCT) compound (Sakura) and snap frozen in liquid nitrogen; or cultured as tissue explants in 24 well plates containing 1ml DMEM high glucose liquid medium, containing 100 units/ml Penicillin/Streptomycin antibiotic, 5 mM L-Glutamine, supplemented with 10% (v/v) FCS for 24 hours incubated at 37˚C, 5% CO_2, treated with 100 ng/ml LPS +/- 5 µM Monensin Sodium Salt. Subsequently, tissue explants were cut in half, one half embedded in OCT and one half immersed in RNAlater as above and stored at -20˚C. Wounds embedded in OCT compound were cut into 10 µm sections with the Microm HM560 Cryostar cryostat (Thermo Scientific), mounted on 26 x 76 mm Glass Microscope Slides (Surgipath) and stored at -20˚C prior to immunohistochemistry and immunofluorescence.

Phenotype	Quantity	Blood Glucose Range	Weight Range
db/db	12	17.4 - ≥33 mmol/L	32 - 48.5 g
db/+	10	2.7 - 6.8 mmol/L	23.6 - 32.7

Table 2.6 Blood glucose and weight range of Db/Db and Db/+ mice indicates diabetic phenotype in Db/Db mice.

2.16 Immunocytochemistry

For antibody dilutions see Table 2.7. All incubations were carried out at room temperature unless otherwise stated.

2.16.1 Cell Surface F4/80

F4/80 is a murine macrophage-specific cell surface glycoprotein that is used extensively to characterise populations of macrophages (McKnight et al., 1996).

2×10^4 cells in a 40 µl drop were plated onto 13mm glass coverslips (Chance Propper Ltd.) in 24 well plates and allowed to adhere for 1 hour. 500 µl cell culture medium was added with treatments as indicated and cells were incubated at 37˚C, 5% CO_2 overnight. The following day coverslips were removed from the 24 well plate and cells were fixed with a 4% (w/v) Paraformaldehyde solution for 5 minutes and washed quickly in 1x PBS. Non-specific protein binding and Fc receptor binding was blocked by incubating the cells for 30 minutes in a 10% (v/v) normal goat serum (NGS) solution. Without washing, cells were then incubated with Rat anti-Mouse F4/80 monoclonal IgG primary antibody diluted in a 1% (v/v) NGS solution for 30 minutes. Following this, cells were washed extensively in 1x PBS to remove unbound primary antibody before a further 30 minutes incubation with Goat anti-Rat Alexa-Fluor 488 polyclonal IgG secondary antibody. Cells were washed extensively as before and then incubated with DAPI for 5 minutes. Finally cells were washed quickly in 1x PBS and mounted onto microscope slides with Hydromount Mounting Medium.

2.16.2 MMP-10 and MMP-12

2×10^4 cells in a 40 µl drop were plated onto 13mm glass coverslips in 24 well plates and allowed at adhere for 1 hour. 500 µl cell culture medium was added with treatments as indicated and cells were incubated at 37˚C, 5% CO_2 overnight. The following day cells were treated with 5 µM Monensin Sodium Salt to block intracellular protein transport, sequestering secreted proteins within the cytoplasm (Hembry et al., 1986). After 3 hours incubation cells were fixed with a 4% (w/v) Paraformaldehyde solution for 5 minutes and washed quickly in 1x PBS. Cell membranes were permeablised with a 0.1% (v/v) Triton X-100 solution for 5 minutes and washed quickly in 1x PBS. Non-specific protein binding and Fc receptor binding was blocked by incubating the cells for 30 minutes in a 10% (v/v) NGS solution or 10% (v/v) NDS. Without washing, cells were then incubated with either Rabbit anti-Human/Mouse MMP-12 polyclonal primary antibody (BIOMOL) or Sheep anti-Mouse D248/6 MMP-10 polyclonal primary antibody (a kind gift from Ros Hembry – 'homemade' (Bord et al., 1998)) diluted in a 1% (v/v) NGS or NDS solution for 30 minutes. Following this, cells were washed extensively in 1x PBS to remove unbound primary antibody before a further 30 minutes incubation with Goat anti-Rabbit Alexa-Fluor 488 conjugated polyclonal IgG secondary antibody (Molecular Probes) or Donkey anti-Sheep Alexa-Fluor 488 conjugated polyclonal IgG secondary antibody. Cells were washed extensively as before and then incubated with DAPI for 5 minutes. Finally cells were washed quickly in 1x PBS and mounted onto microscope slides with Hydromount Mounting Medium.

2.16.3 Cytoskeletal Components

2 x 10^4 cells in 40 µl were plated onto 13mm glass coverslips in 24 well plates and allowed at adhere for 1 hour. 500 µl cell culture medium was added with treatments as indicated and cells were incubated at 37˚C, 5% CO_2 overnight. The following day cells were fixed with ice cold Methanol/10% MES (100nM 4-Morpholineethanesulfonic acid sodium salt [MES], 1mM Ethylene-bis[oxyethylenenitrilo]tetraacetic acid [EGTA], 1mM $MgSO_4$) solution for 5 minutes at -20˚C and washed quickly in 1% (v/v) NGS. Cell membranes were permeablised with a 1% NP40 detergent solution for 5 minutes and washed quickly as before. Non-specific protein binding and Fc receptor binding was blocked by incubating the cells for 30 minutes in a 10% (v/v) NGS. Without washing, cells were then incubated with Rat anti-Mouse α-Tubulin monoclonal IgG antibody (AbD Serotec), Rabbit anti-Mouse Arp2 (a kind gift from Dr. Mette Mogensen, UEA – 'homemade'), Rabbit anti-Mouse β-Actin polyclonal IgG antibody (AbCam), Rabbit anti-Mouse Non-Muscle Myosin Heavy Chain II-A polyclonal IgG antibody (MHC-IIA; Covance) or combinations thereof diluted in a 1% (v/v) NGS for 1 hour. Following this, cells were washed extensively in 1% NGS to remove unbound primary antibody before a further 30 minutes incubation with Goat anti-Rabbit Alexa-Fluor 488 conjugated polyclonal IgG secondary antibody, Goat anti-Rabbit Alexa-Fluor 568 conjugated polyclonal IgG secondary antibody (Molecular Probes) or Goat anti-Rat Alexa-Fluor 633 conjugated polyclonal IgG secondary antibody (Molecular Probes). Cells were washed extensively as before and then incubated with DAPI for 5 minutes. Finally cells were washed quickly in 1x PBS and mounted onto microscope slides with Hydromount Mounting Medium. Double labelling of cytoskeletal components was achieved by combining primary antibodies raised in different species simultaneously or sequential application of primary antibodies raised in the same species.

Primary antibodies against α-tubulin, β-actin and Arp2 were a kind gift from Dr Mette Mogensen.

2.16.4 Immunofluorescence in tissue sections

10 µm sections of wounded or non-wounded tissue were removed from -20˚C and allowed to reach room temperature before sections were outlined with a hydrophobic ImmEdge barrier pen (Vector Labs). Tissue was fixed with a 4% (w/v) Paraformaldehyde solution for 10 minutes and washed quickly in 1x PBS then permeablised in a 0.2% (v/v) Tween-20 solution for 30 minutes and washed quickly again. Non-specific protein binding was blocked by incubating the sections for at least 30 minutes in 4% (v/v) BSA, 4% (v/v) Normal Goat Serum (NGS) or Normal Donkey Serum (NDS). Without washing, tissue was then incubated with Rat anti-Mouse F4/80 monoclonal IgG primary antibody (AbD Serotec), or Sheep anti-Mouse IW13 MMP-10 polyclonal primary antibody (a kind gift from Ros Hembry – 'homemade' (Bord et al., 1998)) diluted in a 4% (v/v) BSA/4% (v/v)

NGS/ 0.2% (v/v) Tween-20 solution overnight at 4˚C. The following day tissue was washed extensively in 1x PBS to remove unbound primary antibody before a further 1 hour incubation with Goat anti-Rat Alexa-Fluor 488 polyclonal IgG secondary antibody (Molecular Probes) or Donkey anti-Sheep Alexa-Fluor 488 conjugated polyclonal IgG secondary antibody (Molecular Probes). Cells were washed extensively as before and then incubated with 4′,6-Diamidino-2-phenylindole dihydrochloride (DAPI) for 5 minutes. Finally tissue was washed quickly in 1x PBS and mounted onto 26 x 76 mm Glass Microscopy Slides (Surgipath) with Hydromount Mounting Medium (National Diagnostics).

2.16.5 Immunohistochemistry in tissue sections

Tissue sections were fixed, permeablised and treated with primary antibody as described above, blocking with 4% (v/v) BSA/4% (v/v) Normal Rabbit Serum (NRS; DAKO). The following day tissue was washed extensively in 1x PBS to remove unbound primary antibody before a further 1 hour incubation with Biotinylated Rabbit anti-Rat polyclonal IgG secondary antibody (DAKO) or Biotinylated Rabbit anti-Goat polyclonal IgG secondary antibody (DAKO). Tissue was washed extensively as before then treated for 30 minutes with the VECTASTAIN Elite ABC kit (Vector Labs) which contains an optimised Avadin/Biotinylated HRP enzyme Complex (ABC) that irreversibly binds to the biotinylated secondary antibodies. Following this incubation the sections were washed quickly in 1x PBS before the addition of Diaminobenzidine (DAB) and H_2O_2 as supplied in the DAB Peroxidase Substrate Kit (Vector Labs). In the presence of H_2O_2, HRP converts DAB to an insoluble brown precipitate allowing visualisation of the antigen of interest. Optimum incubation time with DAB Substrate kit components varied but was no longer than 5 minutes. Tissue was observed constantly and then immersed in dH_2O to stop the reaction. Tissue was dehydrated with sequential immersion in 70% (v/v) EtOH for 30 seconds, 100% (v/v) EtOH for 30 seconds followed by a final 5 minute incubation with 100% (v/v) EtOH. Tissue was mounted onto microscope slides with DEPEX Mounting Medium (Electron Microscopy Sciences).

2.16.6 Haematoxylin Counterstain

Before fixation tissue was counterstained for 30 seconds with Harris' Haematoxylin (Surgipath) to resolve areas rich in nucleic acid, such as the cell nucleus.

Antibody	Concentration used
Rat anti-Mouse F4/80 monoclonal primary	1:500
Sheep anti-Mouse IW13 MMP-10 polyclonal primary	1:1000
Sheep anti-Mouse D248/6 MMP-10 polyclonal primary	1:3690
Rabbit anti- Mouse MMP-12 polyclonal primary	1:150
Rat anti-Mouse α-Tubulin monoclonal primary	1:200
Rabbit anti-Mouse Arp2 polyclonal primary	1:200
Rabbit anti-Mouse β-Actin polyclonal primary	1:200
Rabbit anti-Mouse Non-Muscle Myosin Heavy Chain II-A polyclonal primary	1:500
Goat anti-Rat Alexa-Fluor 488 polyclonal secondary	1:1000
Goat anti-Rabbit Alexa-Fluor 488 conjugated polyclonal secondary	1:1000
Donkey anti-Sheep Alexa-Fluor 488 conjugated polyclonal secondary	1:1000
Goat anti-Rabbit Alexa-Fluor 568 conjugated polyclonal secondary	1:1000
Goat anti-Rat Alexa-Fluor 633 conjugated polyclonal secondary	1:1000
Biotinylated Rabbit anti-Rat polyclonal secondary	1:1000
Biotinylated Rabbit anti-Goat polyclonal secondary	1:1000

Table 2.7 Concentrations of primary and secondary antibodies used for immunocytochemistry.

2.17 Taqman Low Density Array for MicroRNAs

RAW264.7 cells were grown to confluency in 75 cm^2 tissue culture flasks at a density of roughly 10 x 10^6 cells, and treated with 100 ng/ml LPS, 10 µg/ml BMS-345541, 4 µg/ml BAY 11-7082 or combinations thereof. Cells were incubated at 37˚C, 5% CO_2 for 4 hours before cells were removed from the flasks with a cell scraper and centrifuged at 1000 r.c.f for 5 minutes. Supernatant was discarded and cell pellets were snap frozen in liquid Nitrogen.

Murine microRNA microarray was outsourced to Aros Applied Technology AS, Denmark. Briefly, RNA was extracted from cell pellets and subjected to quality control before 1 ng total RNA was reverse transcribed to cDNA using primers specific to the Taqman ® Rodent MicroRNA A + B Cards Set v2.0 (Applied Biosystems). Each card contains 364 microRNA assays enabling quantitation of 518 unique mouse microRNAs and 303 unique rat microRNAs (see Appendix, figure 8.1). Three endogenous control assays for each species are included on each array as well as one unrelated negative control to aid in data normalization.

Data was analysed using the $2^{-\Delta\Delta CT}$ algorithm with great help from Dr. Oona Adams, Pfizer UK.

Chapter 3: **Lipopolysaccharide induces differential metalloproteinase expression in murine macrophages**

3.1 Introduction

3.1.1 Metalloproteinase expression in monocytes and macrophages

The long-held hypothesis that migratory cells focus extracellular matrix (ECM) degrading proteinases at the leading edge has led to a wealth of studies revealing the role of the matrix metalloproteinases (MMPs) in path clearance (Murphy and Gavrilovic, 1999), including their ability to expose cryptic ECM pro-migratory sites (Stringa et al., 2000; Davis et al., 2000). More recently an additional role for the MMPs and other proteinases in the cleavage and activation of pro-inflammatory chemokines has been explored (Dean et al., 2008). When considering the macrophage response to infection and inflammation it becomes clear that both modes of MMP action are relevant.

When circulating monocytes are exposed to the relevant pro-inflammatory signals they bind the endothelium and extravasate through gaps between neighbouring endothelial cells (Worthylake and Burridge, 2001). This process has been shown to be MMP-dependent, for example, studies using monocytic and neutrophil cell lines in Transwell© migration assays have revealed that the interaction between MMP-9 and leukocyte β2 integrins is essential for the translocation of these cells across a β2-ligand coated Transwell© membrane, towards a TNF-α gradient (Stefanidakis et al., 2004). Following extravasation, monocytes must transmigrate through the surrounding basement membrane in order to differentiate into tissue macrophages and migrate towards areas of infection or inflammation (Luster et al., 2005). Again, this process appears to be MMP-dependent; with the use of siRNA it has been shown that expression of MT1-MMP/MMP-14 is essential for the migration of monocytes through endothelial cells *in vivo* (Sithu et al., 2007).

3.1.2 LPS/NF-κB induced metalloproteinase expression in monocytes and macrophages

Macrophage activation in response to the bacterial endotoxin LPS via toll-like receptor (TLR) 4 is well-characterised (explained in detail in Chapter 1, 1.1.3). It is perhaps only in the last fifteen years that research has begun to elucidate the molecular mechanisms by which LPS is able to regulate expression of proteases in macrophages and other blood cells, focusing on the role of the transcription factor nuclear factor (NF)-κB. Figure 3.1 shows the canonical pathway of NF-κB activation and nuclear translocation triggered by LPS-TLR4 binding on the surface of monocytes and macrophages. Despite an early focus on its involvement in the expression of antibodies by B-cells (Hoffmann and Baltimore, 2006), NF-κB has been shown to play another important role in the transcription of MMPs in various other leukocytic cell types. For example, in the pro-monocytic

cell line U937 LPS stimulated expression of MMP-1 has been shown to be blocked by inhibition of the NF-κB signalling cascade *in vitro* (Nareika et al., 2005). Similarly, by inhibiting the proteasomal degradation of cytosolic IκB *in vitro* the translocation of NF-κB to the nucleus of LPS stimulated human peripheral blood mononuclear cells has been revealed to be crucial in the production of MMP-9 (Lu and Wahl, 2005).

In vivo and *ex vivo* studies have also revealed a clear relationship between LPS and MMP expression in a variety of tissues. For example, MMP-7 and MMP-10 have been shown to be induced in the airway epithelium of mice infected with the gram-negative bacterium *Pseudomonas aeruginosa* (Kassim et al., 2007). Analysis of known key gene interaction networks involved in host response to infection with *P. aeruginosa* revealed the involvement of NF-κB in the regulation of both MMPs. Human organ-cultured full-thickness skin biopsies, stimulated with the well characterised NF-κB stimulus and effector TNF-α, have also been found to express both the 'pro' and active forms of MMP-2 (Han et al., 2001). Similarly, dermal fibroblasts cultured from these tissue explants were shown to express both MMP-2 and MT1-MMP in response to TNF-α, which could be blocked by a compound that inhibits the translocation of NF-κB to the nucleus.

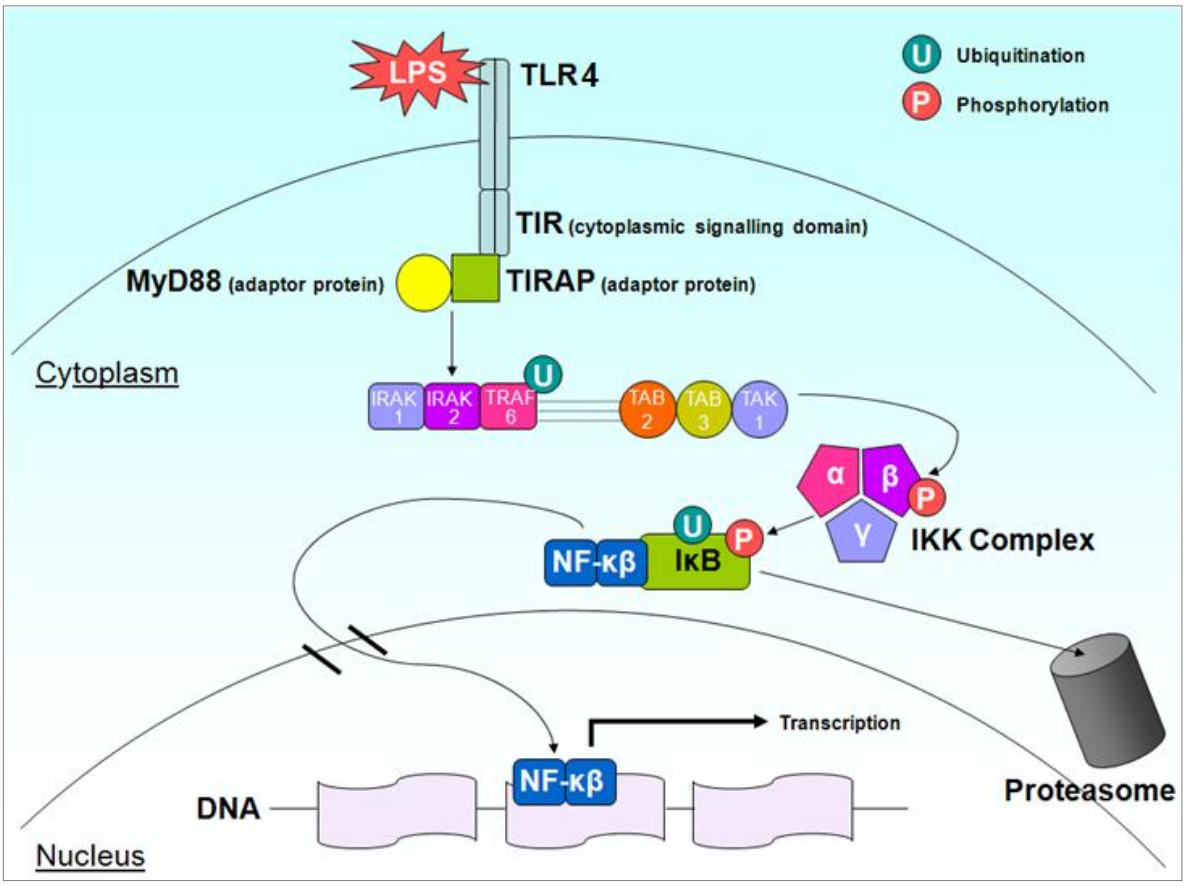

Figure 3.1 LPS binds TLR4 activating nuclear translocation of the transcription factor NF-κB: The canonical/MyD88 dependent pathway. LPS binds TLR4, triggering dimerisation. The intracellular domain of the TLR is now able to associate with the adaptor protein MyD88, either directly via TIR (a cytoplasmic signaling domain), or indirectly via TIRAP. This interaction allows for the formation of the IRAK1-IRAK2-TRAF6 complex. Subsequent ubiquitination of TRAF6 allows for binding with the TAB2-TAB3-TAK1 trimer. This activates TAK1, which is now able to phosphorylate IKKβ of the IKK complex – the core convergence of most NF-κB activation pathways. Phosphorylated IKKβ in turn phosphorylates the inhibitory IκB protein, targeting it for ubiquitination and degradation by the proteasome. NF-κB is now liberated and is free to translocate to the nucleus where it is able to bind to DNA and activate the transcription of relevant genes. MyD88 - Myeloid differentiation primary response gene 88, TIR - Toll - IL-1 receptor, TIRAP – Toll - IL-1 receptor domain containing adaptor protein, IRAK - IL-1 receptor associated kinase, TRAF - TNF receptor associated factor, TAB – TGF-β activated kinase-1, TAK - TAK1-binding proteins, IKK - IκB kinase. Information for this diagram was assembled from (Guha and Mackman, 2001; Hoffmann and Baltimore, 2006).

3.1.3 The role of the HDACs in LPS – stimulated expression of metalloproteinases

It is only relatively recently that the role of the chromatin remodelling histone deacetylases (HDACs) has been considered in a pro-inflammatory setting, such as response to LPS. HDACs are categorised into three classes based on their sequence homology; Class I, Class II and Class III. It is the Class II HDACs; 4, 5 and 7, that seem particularly relevant to the molecular mechanisms controlling response to LPS. For example, LPS has been shown to transiently repress then induce these three HDACs in bone marrow-derived macrophages over a 24 hour period (Aung et al., 2006). Classically HDACs function to deacetylate histone groups encouraging high affinity binding between histones and the DNA backbone. This condenses DNA structure preventing transcription factors accessing promoter regions, thus inhibiting transcription of mRNA. Class II HDACs also interact directly with transcription factors themselves to inhibit gene expression. The transcription factor Myocyte Enhancer Factor (MEF)-2, for example, known to be induced by LPS in the RAW264.7 macrophage-like cell line (Han et al., 1997), is prevented from binding to the MMP-10 promoter by HDAC7 in human aortic endothelial cells (Chang et al., 2006). This relationship has further been elucidated with the finding that Transforming Growth Factor (TGF)-β is able to up-regulate MMP-10 expression by activating MEF2 and promoting the proteasome-dependent degradation of HDAC4, 5 and 7 (Ishikawa et al., 2010b).

3.2 Aims

In order to approach this well established area of research we chose to complete a full profile of lipopolysaccharide (LPS) stimulated and unstimulated murine bone marrow-derived macrophage MMPs including some ADAMs (**A** **D**isintegrin **A**nd **M**etalloproteinase), ADAMTSs (ADAM with **T**hrombo**S**pondin motif) and their endogenous inhibitors, the TIMPs (**T**issue **I**nhibitors of **M**etallo**P**roteinases). By performing this analysis we aim to reveal a potential protease signature for bone marrow-derived macrophages.

In this chapter we also aim to confirm the temporal regulation of class II HDACs 4, 5 and 7 in bone marrow-derived macrophages by LPS seen in Aung et al (2006), and subsequently relate this to the expression of the MMPs in these cells.

3.3 Results

3.3.1 LPS induced metalloproteinase mRNA in RAW264.7 and bone marrow-derived macrophages reveals distinct expression profiles

Bone marrow-derived macrophages (BMMs) and the RAW264.7 macrophage cell line were exposed to 1, 10 or 100 ng/ml lipopolysaccharide (LPS) for 24 hours before total RNA was extracted and quantitative RT-PCR (qRT-PCR) performed. A summary of change in metalloproteinase mRNA expression in response to 100 ng/ml LPS is shown in Table 3.1. This includes expression of all MMPs and TIMPs and the levels of key ADAM and ADAMTS mRNA. For reference, and because we wished to focus on this family of metalloproteinases more carefully, a heat map profile of the change in MMP cycle threshold (C_T) range in response to LPS in RAW264.7 macrophages and BMMs was compiled (figure 3.2). Overall levels of metalloproteinase mRNA expression appear to vary between the two types of macrophage; however there are some interesting similarities that will be discussed further. For example, MMP-9 and -12 are the most highly expressed in both types of macrophage. The range of C_T values for MMP-9 is between 23 – 28 in BMMs and 23 – 25 in RAW264.7 whilst the range for MMP-12, also known as macrophage metalloelastase, is between 21 – 22 in BMMs and ≤ 20 – 22 in RAW264.7. MMP-1b, -7, -16, -17, -20, -24; TIMP-3 and -4; ADAM9 and 28; and ADAMTS8 show no expression in either type of macrophage.

Relative MMP mRNA expression normalised to 18s for the genes that show a change of at least 1 C_T in response to the highest concentration of LPS in RAW264.7 and BMMs reveals further similarities and variations in expression profile (Figures 3.3 – 3.4). In both RAW264.7 macrophages and BMMs MMP-11 (figure 3.3 C, 3.4 D), -14 (figure 3.3 E, 3.4 F), and -25 (figure 3.3 G, 3.4 H) appear to be regulated by LPS in similar trends. MMP-11 shows a small but significant dose-dependent reduction in expression in response to LPS. MMP-14 and -25, both members of the 'membrane type' family of MMPs, show a similar trend for induction of expression in response to LPS that appears to peak at 10 ng/ml, although levels of significance vary. The remaining MMPs shown in figures 2.2 – 2.3 serve to highlight the difference in expression profile between the two types of macrophage. MMP-2, for example, can be seen to be induced by 100 ng/ml LPS in BMMs (figure 3.4 A) whereas no expression is seen in RAW264.7 macrophages. Conversely, MMP-3 is induced by 10 and 100 ng/ml LPS in RAW264.7 macrophages (figure 3.3 A) whilst no expression is seen in BMMs. In the case of certain MMPs it seems that BMMs are more responsive to LPS than

the RAW264.7 macrophages. In this initial profile both MMP-10 and -12 appear significantly down regulated in BMMs in response to LPS, albeit with a stronger response to all concentrations of LPS seen for MMP-10. In RAW264.7 both MMP-10 and -12 are expressed highly but are not regulated by LPS (see table 3.1).

This profile of metalloproteinase expression was performed once with triplicate samples.

Gene	+ LPS		Average C_T	Average C_T + LPS	Average C_T	Average C_T + LPS
	RAW264.7	BMM	RAW264.7		BMM	
MMP-1b	x	x	-	-	-	-
MMP-2	x	↑	-	-	36.5	32.5
MMP-3	↑	x	38.3	30.9	-	-
MMP-7	x	x	-	-	-	-
MMP-8	↑	↔	33.4	30.6	31.5	32.0
MMP-9	↔	↑	25.0	24.9	27.4	24.5
MMP-10	↔	↓	27.1	27.5	32.5	38.8
MMP-11	↓	↓	34.3	35.7	33.0	34.4
MMP-12	↔	↓	20.9	20.9	21.5	22.7
MMP-13	↑	↔	28.9	25.3	29.5	29.4
MMP-14	↑	↑	36.5	33.7	27.6	22.1
MMP-15	↔	↓	33.8	33.3	22.3	25.5
MMP-16	x	x	-	-	-	-
MMP-17	x	x	-	-	-	-
MMP-19	↔	↔	32.3	33.1	27.0	27.5
MMP-20	x	x	-	-	-	-
MMP-21	↓	x	31.0	32.1	-	-
MMP-23	↔	x	34.2	33.6	-	-
MMP-24	x	x	-	-	-	-
MMP-25	↑	↑	30.6	28.9	33.7	32.7
MMP-27	x	↓	-	-	30.2	34.7
MMP-28	↑	↔	35.0	32.5	32.5	32.7
TIMP-1	x	↑	-	-	26.5	25.2
TIMP-2	↔	↓	25.6	26.0	23.4	25.1
TIMP-3	x	x	-	-	-	-
TIMP-4	x	x	-	-	-	-
ADAM8	↔	↔	25.1	24.3	24.6	25.4
ADAM9	x	x	-	-	-	-
ADAM10	↔	↔	25.6	25.7	26.6	27.2
ADAM12	↔	x	33.3	33.6	-	-
ADAM15	↔	↔	24.1	23.8	26.8	27.3
ADAM17	↔	↔	27.7	28.5	25.7	25.1
ADAM28	x	x	-	-	-	-
ADAM33	↑	↔	36.4	34.1	32.8	33.5
ADAMTS1	↔	↓	28.2	28.8	34.2	36.7
ADAMTS4	↑	↑	33.1	29.3	35.8	33.7
ADAMTS8	x	x	-	-	-	-

Table 3.1 Summary of change in metalloproteinase expression in response to LPS. qRT-PCR was performed on triplicate samples of cDNA extracted from RAW264.7 and BMMs treated with 100 ng/ml LPS. Resulting average C_T values were analysed and any value ≥35 was deemed to indicate no expression. Unless LPS treatment brought C_T values to within the detectable range, lack of expression is indicated with 'x'. ↑ indicates increased expression by at least 1 C_T, ↓ indicates decreased expression by at least 1 C_T and ↔ indicates no change in expression in response to 100 ng/ml LPS.

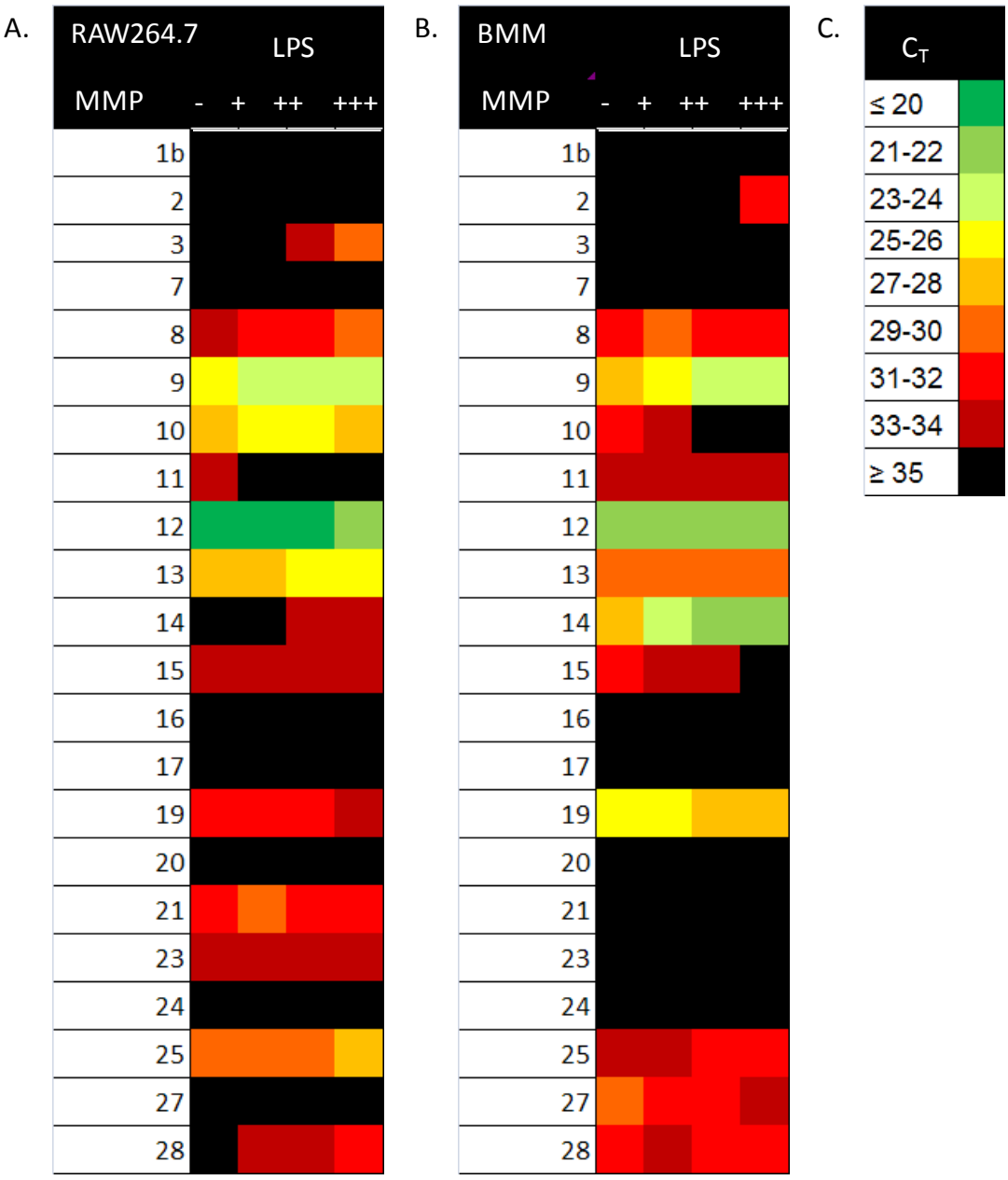

Figure 3.2 Heat maps of matrix metalloproteinase C_T range in RAW264.7 macrophages and BMMs in response to LPS. qRT-PCR was performed on triplicate samples of cDNA extracted from (A) RAW264.7 and (B) BMMs treated with increasing concentrations of LPS for 24 hours. (C) C_T values were converted to a representative colour, black indicating no expression (≥ 35) and green indicating very high expression (≤ 20). - = untreated, + = 1 ng/ml LPS, ++ = 10 ng/ml LPS, +++ = 100 ng/ml LPS.

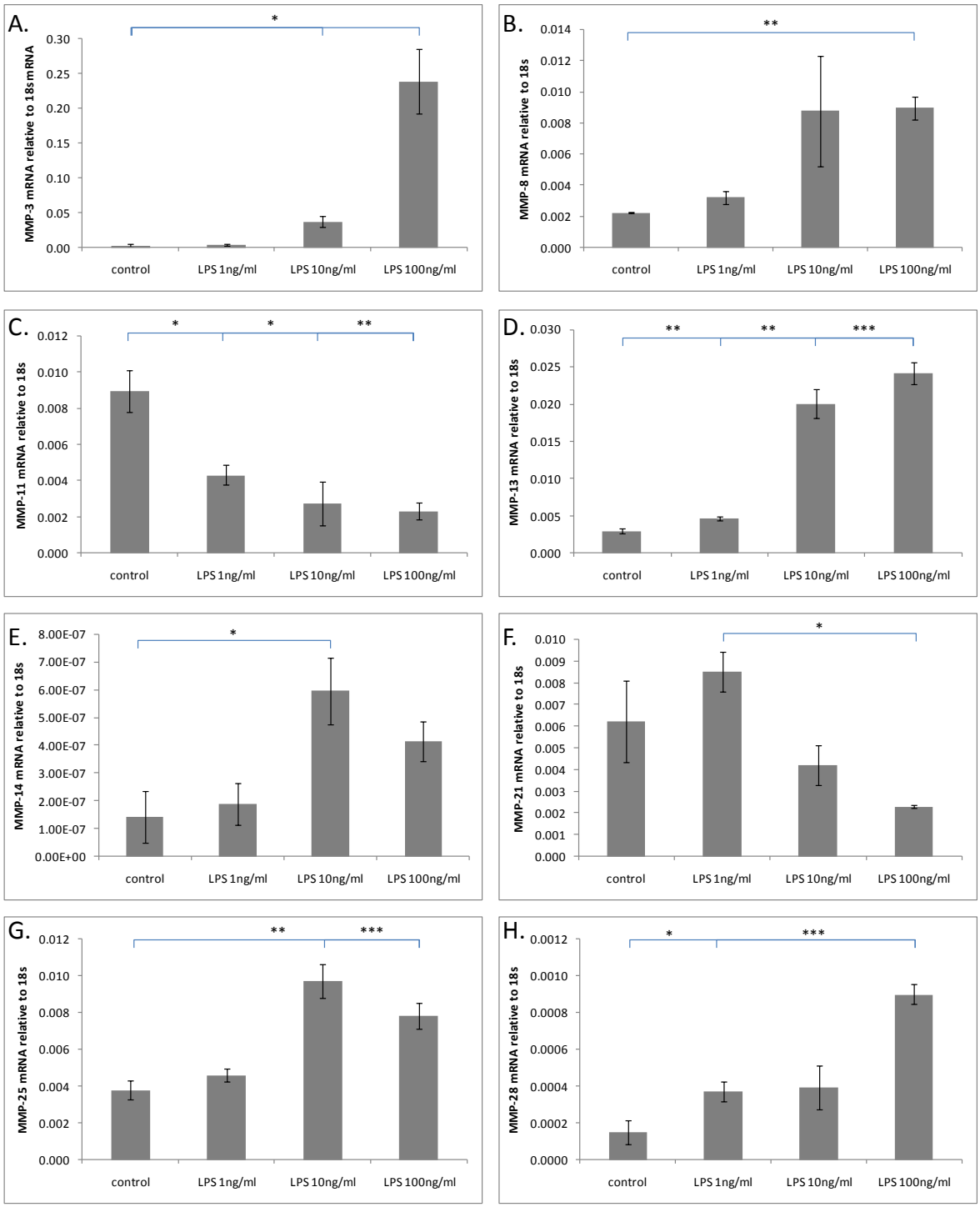

Figure 3.3 Relative MMP expression in RAW264.7 macrophages in response to LPS. (A-H) qRT-PCR was performed on cDNA extracted from RAW264.7 macrophages treated with increasing concentrations of LPS for 24 hours. Data was analysed by relative quantification and normalized to 18S endogenous control. Each bar represents the mean of 3 samples ± SEM. Statistical significance was determined using the Student's t-test. * $p \leq 0.05$, ** $p \leq 0.01$ *** $p \leq 0.001$.

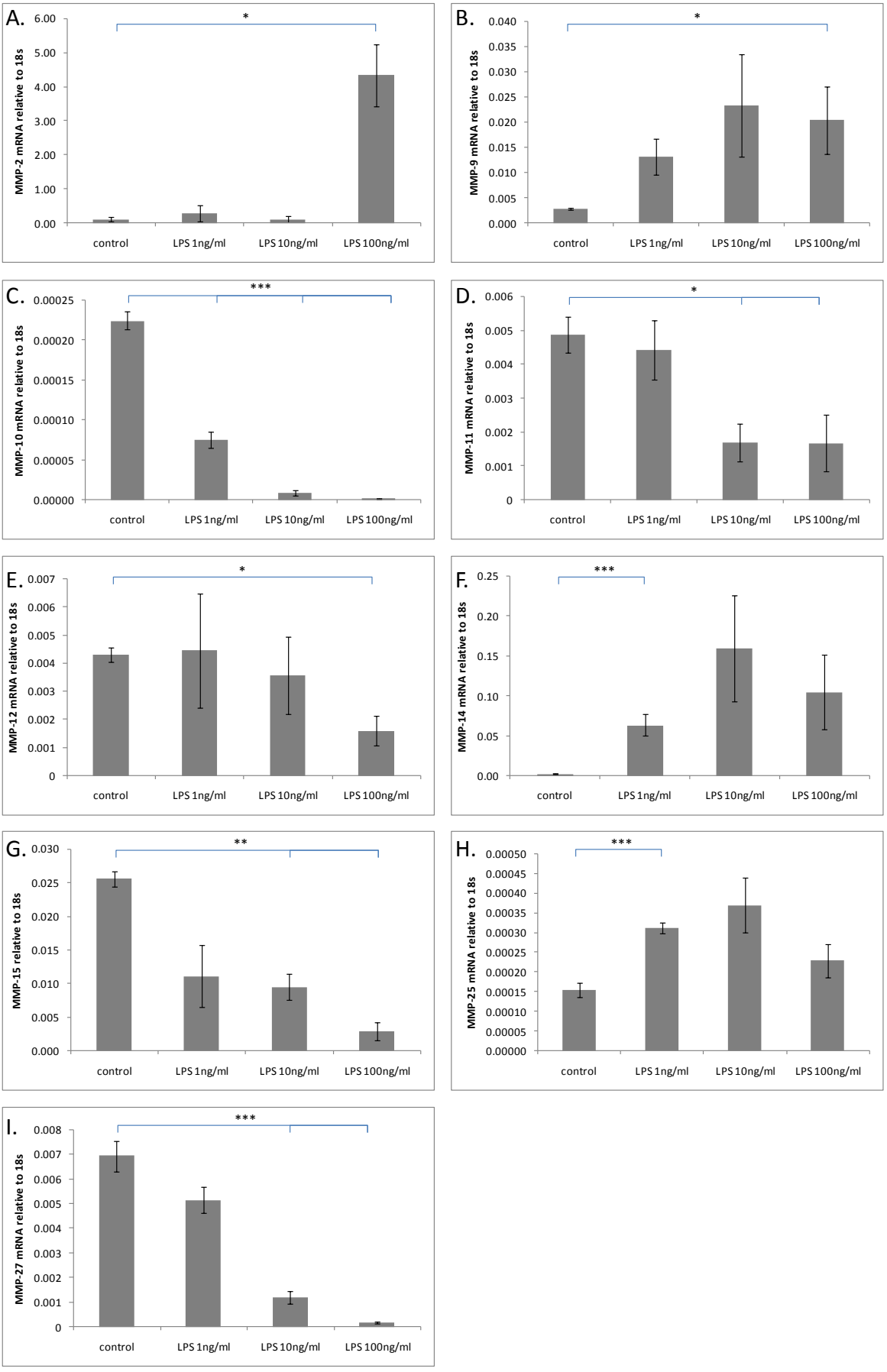
A.
MMP-2 mRNA relative to 18s
6.00
5.00
4.00
3.00
2.00
1.00
0.00
*
control
LPS 1ng/ml
LPS 10ng/ml
LPS 100ng/ml
B.
MMP-9 mRNA relative to 18s
0.040
0.035
0.030
0.025
0.020
0.015
0.010
0.005
0.000
*
control
LPS 1ng/ml
LPS 10ng/ml
LPS 100ng/ml
C.
MMP-10 mRNA relative to 18s
0.00025
0.00020
0.00015
0.00010
0.00005
0.00000
***
control
LPS 1ng/ml
LPS 10ng/ml
LPS 100ng/ml
D.
MMP-11 mRNA relative to 18s
0.006
0.005
0.004
0.003
0.002
0.001
0
*
control
LPS 1ng/ml
LPS 10ng/ml
LPS 100ng/ml
E.
MMP-12 mRNA relative to 18s
0.007
0.006
0.005
0.004
0.003
0.002
0.001
0
*
control
LPS 1ng/ml
LPS 10ng/ml
LPS 100ng/ml
F.
MMP-14 mRNA relative to 18s
0.25
0.20
0.15
0.10
0.05
0.00
***
control
LPS 1ng/ml
LPS 10ng/ml
LPS 100ng/ml
G.
MMP-15 relative to 18s
0.030
0.025
0.020
0.015
0.010
0.005
0.000
**
control
LPS 1ng/ml
LPS 10ng/ml
LPS 100ng/ml
H.
MMP-25 mRNA relative to 18s
0.00050
0.00045
0.00040
0.00035
0.00030
0.00025
0.00020
0.00015
0.00010
0.00005
0.00000
***
control
LPS 1ng/ml
LPS 10ng/ml
LPS 100ng/ml
I.
MMP-27 mRNA relative to 18s
0.008
0.007
0.006
0.005
0.004
0.003
0.002
0.001
0
***
control
LPS 1ng/ml
LPS 10ng/ml
LPS 100ng/ml

Figure 3.4 Relative MMP expression in BMMs in response to LPS. (A-I) qRT-PCR was performed on cDNA extracted from BMMs treated with increasing concentrations of LPS for 24 hours. Data was analysed by relative quantification and normalized to 18S endogenous control. Each bar represents the mean of 3 samples ± SEM. Statistical significance was determined using the Student's t-test. * $p \leq 0.05$, ** $p \leq 0.01$ *** $p \leq 0.001$.

3.3.2 MMP-10 mRNA expression is significantly down-regulated in macrophages 24 hours post-LPS stimulation

To further investigate the macrophage response to LPS we chose to focus on the surprising down regulation of MMP-10 seen in BMMs. LPS-induced modulation of MMP-10 has been seen previously in monocytes derived from human peripheral blood mononuclear cells, however this study revealed an up-regulation of MMP-10 mRNA (Bar-Or et al., 2003). As shown above, MMP-10 mRNA is strongly down-regulated 24 hours post – LPS stimulation in BMMs. In order to confirm this result BMMs were again exposed to 100 ng/ml LPS for 24 hours before qRT-PCR for MMP-10. This assay was also repeated for RAW264.7 macrophages despite seeing no change in MMP-10 mRNA levels in the initial profile (figure 3.3). Again, LPS is shown to drive significant repression of MMP-10 mRNA in BMM (figure 3.5 B, D). Interestingly, in repeating this analysis we *also* found MMP-10 mRNA in RAW264.7 macrophages to be repressed (figure 3.5 A, C). This analysis of expression has been performed five times in BMMs and four times in RAW264.7 macrophages with reproducible results. This suggests that the initial lack of LPS-driven MMP-10 mRNA repression in RAW264.7 macrophages was anomalous.

Despite the similarity in BMM and RAW264.7 macrophage MMP-10 expression in response to LPS seen above, the C_T values shown in figure 3.5 reveal clear differences in overall expression level. As we consider a C_T value of ≥ 35 to signify the end of the linear range of PCR amplification for a gene it can be said that MMP-10 mRNA levels are undetectable in BMMs treated with 100 ng/ml LPS (range 37.19 – 38.72). In RAW264.7 macrophages however MMP-10 expression is still detectable following 100ng/ml LPS treatment (range 33.19 – 33.47), although significantly decreased compared to untreated control.

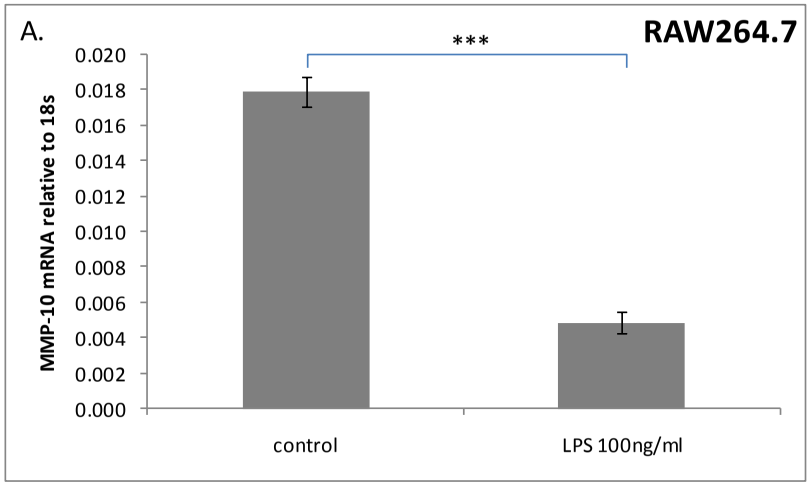

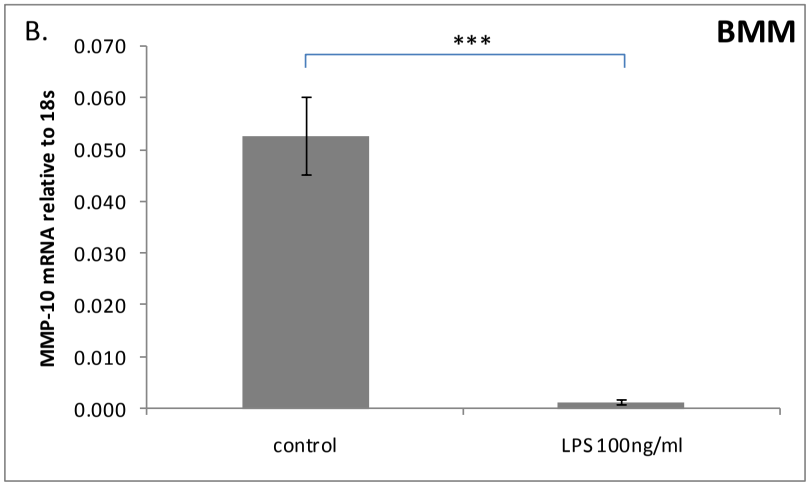

C.

Treatment	C_T value 1	C_T value 2	C_T value 3
Control	31.55	31.31	31.49
LPS 100 ng/ml	33.29	33.18	33.47

D.

Treatment	C_T value 1	C_T value 2	C_T value 3
Control	32.49	32.89	33.33
LPS 100 ng/ml	37.19	38.09	38.72

Figure 3.5 LPS represses relative expression of MMP-10 in BMMs and RAW264.7 macrophages. qRT-PCR was performed on (A) RAW264.7 macrophages and (C) BMMs 24 hours post – LPS stimulation. Data was analysed by relative quantification and normalized to 18S. (B, D) Corresponding CT values are shown. Each bar represents the mean of 3 samples ± SEM. Statistical significance was determined using the Student's t-test. *** $p \leq 0.001$.

3.3.3 MMP-10 mRNA expression is significantly up-regulated in macrophages 4 hours post – LPS stimulation

To this point all MMP-10 mRNA quantification has been carried out at the relatively late time point of 24 hours post-LPS stimulation. A time course of macrophage response to LPS stimulation with qRT-PCR analysis of MMP-10 mRNA levels at 4, 8, 16 and 24 hours was performed in RAW264.7 macrophages (figure 3.6). Interestingly this revealed a trend towards an increase in MMP-10 mRNA expression at the 4 hour time point (lack of significance due to anomalous 18S - confirmed as significant in a subsequent experiment, see figure 3.8) whilst also confirming the significant down-regulation of MMP-10 mRNA at 24 hours. At 8 and 16 hours no significant change in expression was observed. LPS also induced a significant increase in MMP-10 mRNA in BMMs, though at the even earlier time point of 3 hours (figure 3.7). Although there still appears to be a trend for up regulation of MMP-10 mRNA in BMMs 4 hours post-LPS stimulation this is no longer statistically significant.

This temporal regulation of MMP-10 mRNA following LPS stimulation has been observed three times in RAW264.7 macrophages and twice in BMMs with all experiments performed in triplicate.

To determine whether LPS has an effect on mRNA stability we incubated RAW264.7 macrophages with Actinomycin D, an inhibitor of mRNA transcription (figure 3.8). In the absence of Actinomycin D LPS was able to significantly induce MMP-10 mRNA at 4 hours as expected. When RAW264.7 macrophages were pre-incubated with Actinomycin D for 45 minutes before stimulation with LPS for 4 hours, no change in MMP-10 expression was seen. This suggests that up regulation of MMP-10 in RAW264.7 macrophages 4 hours post-LPS stimulation is likely to be due to enhancement of transcriptional activity, rather than an LPS-induced increase in mRNA stability. This was repeated with LPS stimulation for 24 hours; however RNA yield was too poor to perform qRT-PCR due to the toxicity of Actinomycin D at this time-point. Viability of RAW264.7 macrophages was assessed via the trypan blue exclusion assay revealing ≤ 12% live cells after 24 hours with both Actinomycin D and LPS stimulation.

This analysis of transcriptional activity has only been performed once in RAW264.7 macrophages, in triplicate, and not confirmed in BMMs.

A.

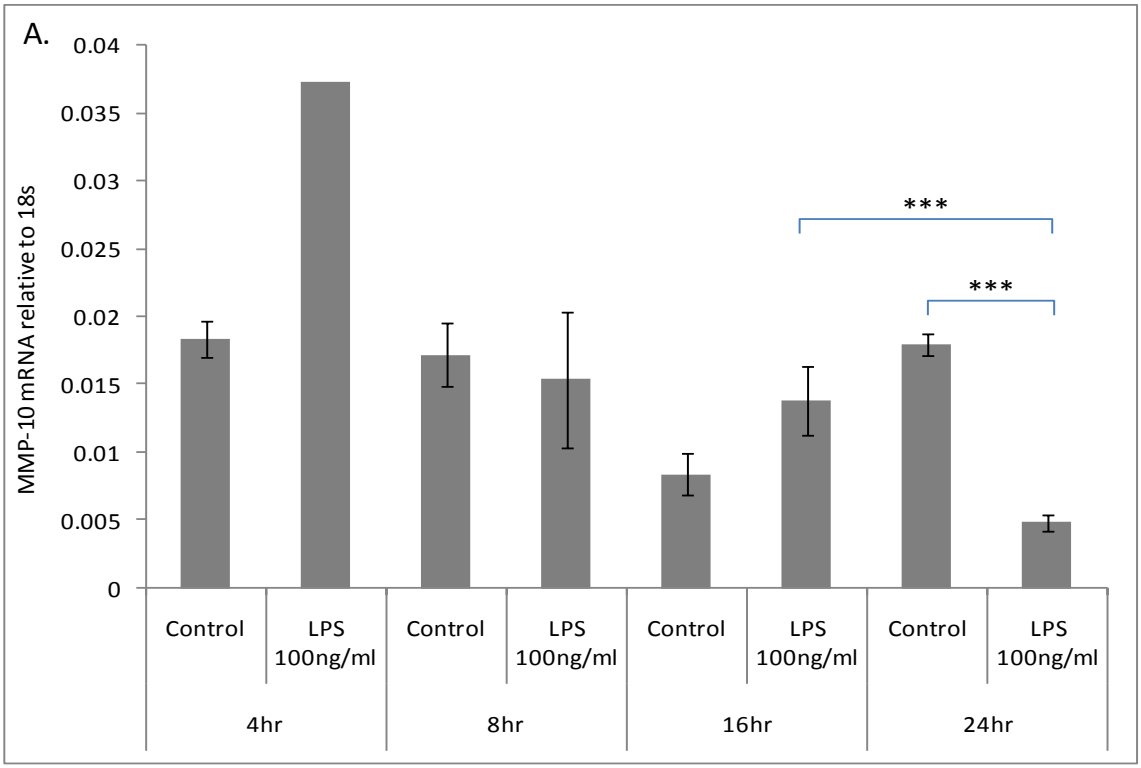

B.

	Treatment	C_T value 1	C_T value 2	C_T value 3
4 hr	Control	31.3	31.3	31.4
	LPS 100 ng/ml	30.7	30.7	30.7†
8 hr	Control	31.5	31.2	31.3
	LPS 100 ng/ml	31.0	31.3	32.5
16 hr	Control	31.9	32.5	32.4
	LPS 100 ng/ml	32.8	31.5	31.5
24hr	Control	31.6	31.3	31.5
	LPS 100 ng/ml	33.3	33.2	33.5

Figure 3.6 Relative expression of MMP-10 normalized to 18S in RAW264.7 macrophages at 4, 8, 16 and 24 hours post-LPS stimulation. (A) qRT-PCR was performed on RAW264.7 macrophages. Data was analysed by relative quantification and normalized to 18S. (B) Corresponding C_T values are shown. Each bar represents the mean of 3 samples ± SEM. Statistical significance was determined using the Student's t-test. *** $p \leq 0.001$. † indicates 18S C_T value varied more than 1.5 C_Ts from the mean and was therefore excluded from analysis.

A.

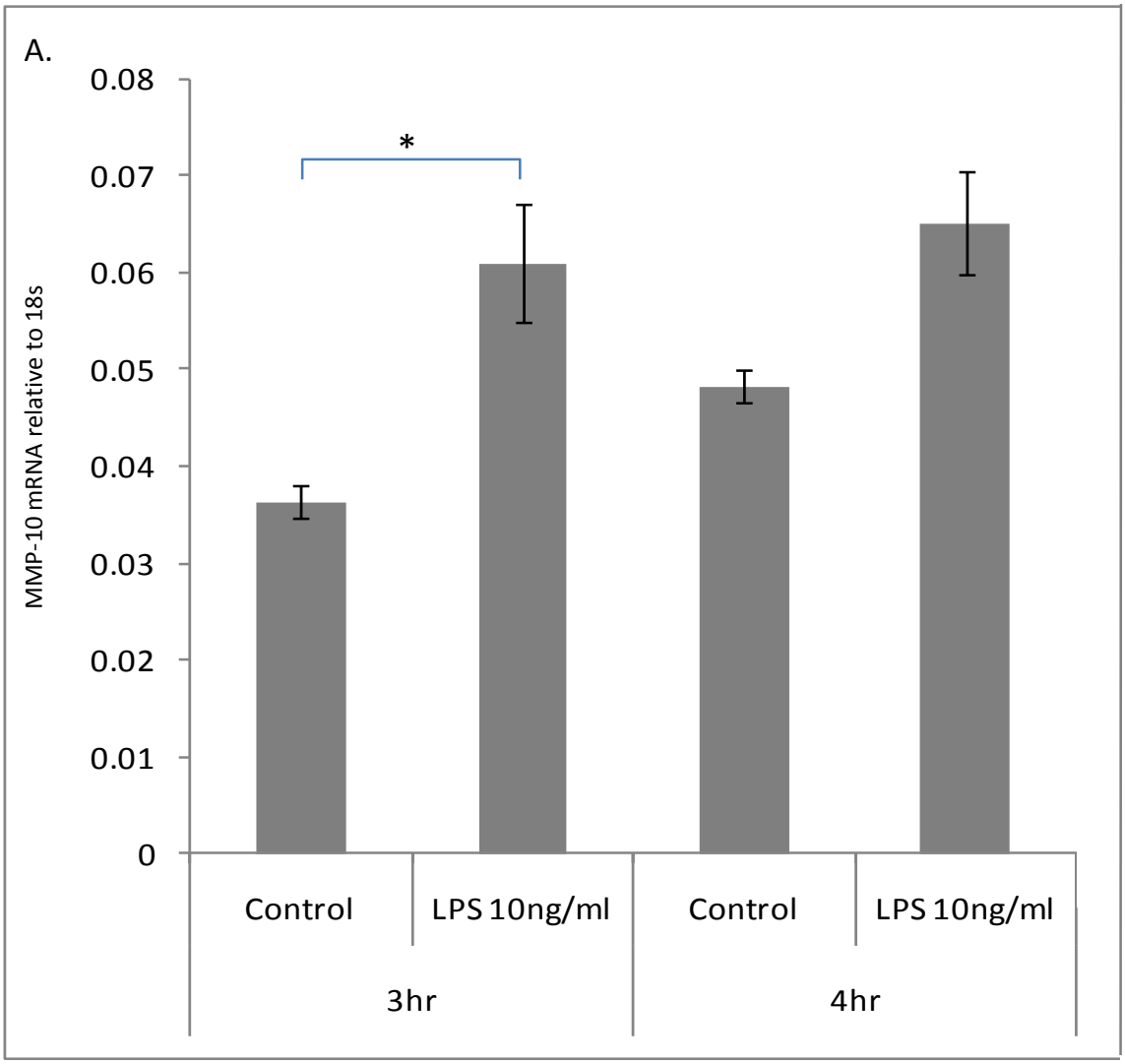

B.

	Treatment	C_T value 1	C_T value 2	C_T value 3
3hr	Control	32.7	33.2	32.6
	LPS 10ng/ml	31.4	32.0	31.8
4hr	Control	32.2	32.0	32.2
	LPS 10ng/ml	31.6	31.5	31.8

Figure 3.7 Relative expression of MMP-10 normalized to 18S in BMMs at 3 and 4 hours post-LPS stimulation. (A) qRT-PCR was performed on BMMs. Data was analysed by relative quantification and normalized to 18S. (B) Corresponding C_T values are shown. Each bar represents the mean of 3 samples ± SEM. Statistical significance was determined using the Student's t-test. * $p \leq 0.05$

A.

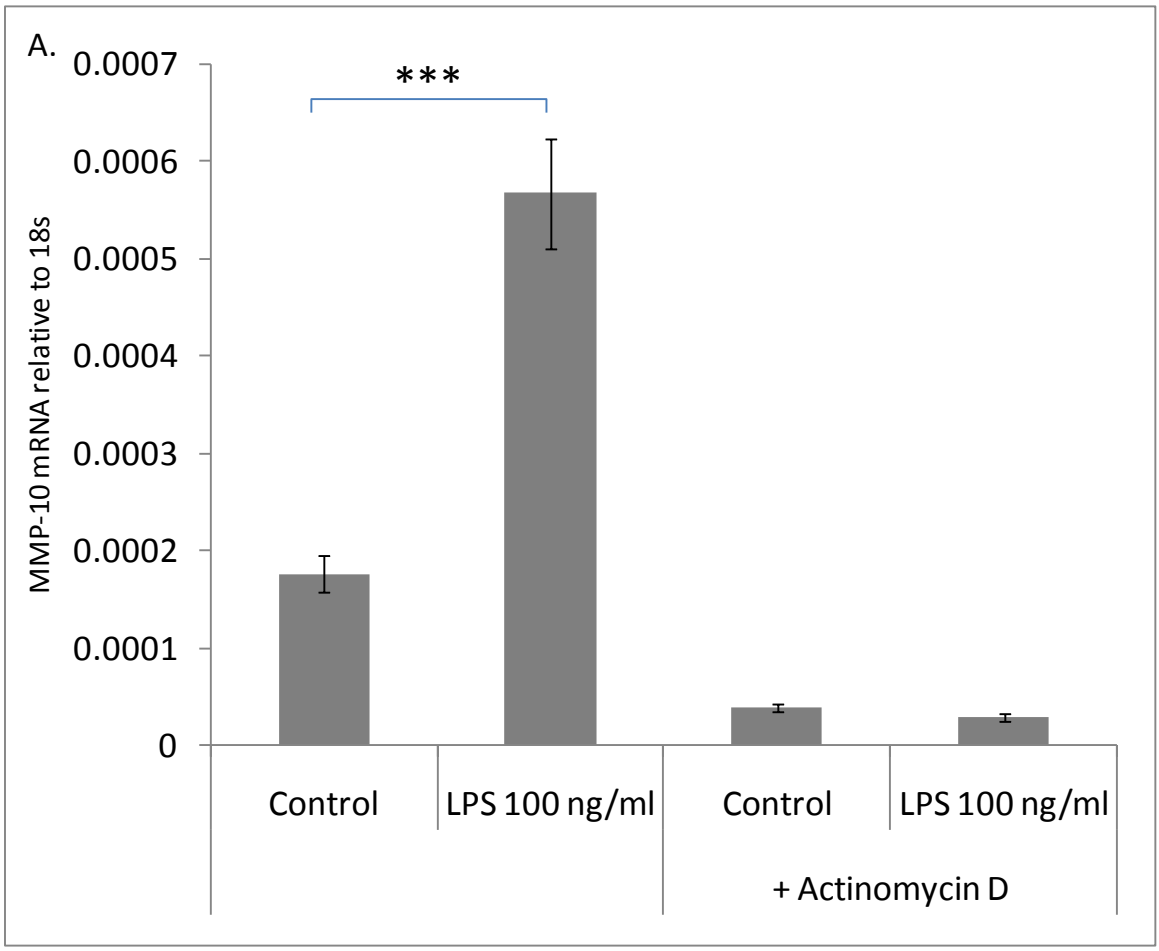

B.

Treatment	Ct value 1	Ct value 2	Ct value 3
Control	33.8	33.5	33.3
LPS 100ng/ml	32.1	31.6	31.9
Actinomycin D	35.3	35.5	35.9
Actinomycin D + LPS 100ng/ml	36.0	36.5	35.9

Figure 3.8 Induction of MMP-10 mRNA expression 4 hours post-LPS is blocked by inhibition of transcription with Actinomycin D in RAW264.7 macrophages. Actinomycin D was applied for 45 minutes and then removed before the experiment began. (A) qRT-PCR was performed on RAW264.7 macrophages. Data was analysed by relative quantification and normalized to 18S. (B) Corresponding C_T values are shown. Each bar represents the mean of 3 samples ± SEM. Statistical significance was determined using the Student's t-test. *** $p \leq 0.001$.

3.3.4 Immunocytochemistry of MMP-10 protein in LPS treated macrophages

To confirm that LPS-induced regulation of MMP-10 mRNA is translated into a change in MMP-10 protein expression RAW264.7 macrophages (figure 3.9) and BMMs (figure 3.10) were cultured on glass cover-slips for 24 hours stimulation with LPS and three hours incubation with 5 µM monensin sodium salt before being immuno-stained with D248/6 anti-MMP-10 polyclonal antibody. Both types of macrophage show strong positive staining for MMP-10 when untreated (figure 3.9 A, B and 3.10 A, B). This staining is markedly reduced following LPS stimulation for 24 hours (figure 3.9 D, E and 3.10 D, E). Secondary antibody only controls (figure 3.9 C, F and 3.14 C, F) reveal minimal non-specific secondary antibody binding and autofluorescence.

High magnification images of both RAW264.7 macrophages and BMMs allow for comparison of MMP-10 protein distribution (figure 3.11). In both cell types staining appears punctate throughout the cytoplasm with some concentration around the nuclei. This is particularly evident in the RAW264.7 macrophages where staining appears to concentrate further next to the nucleus, perhaps in the Golgi apparatus. In both cases there also appears to be punctate staining on the surrounding matrix.

RAW264.7 macrophages were immuno-stained for MMP-10 4 hours after LPS stimulation to investigate whether the induction of MMP-10 mRNA at this time-point is translated into a detectable change in protein. No obvious increase in MMP-10 protein after 4 hours LPS stimulation was observed (figure 3.12 A, B). In this experiment there also appears to be more non-specific secondary antibody binding or autofluorescence from the secondary antibody only control (figure 3.12 C).

To confirm that the regulation of MMP-10 protein we have seen is not caused by a global effect of LPS on protein level, RAW264.7 macrophages were immuno-stained with antibodies against MMP-12 (figure 3.13) which is highly expressed but minimally regulated by LPS in both RAW264.7 macrophages and BMM, as shown in figure 3.1. Both untreated cells (figure 3.13 A) and those stimulated with LPS for 24 hours (figure 3.13 B) show high levels of MMP-12 expression in a similar punctate pattern to that seen for MMP-10.

Each analysis of MMP-10 and MMP-12 protein expression was performed once with all experiments performed in triplicate.

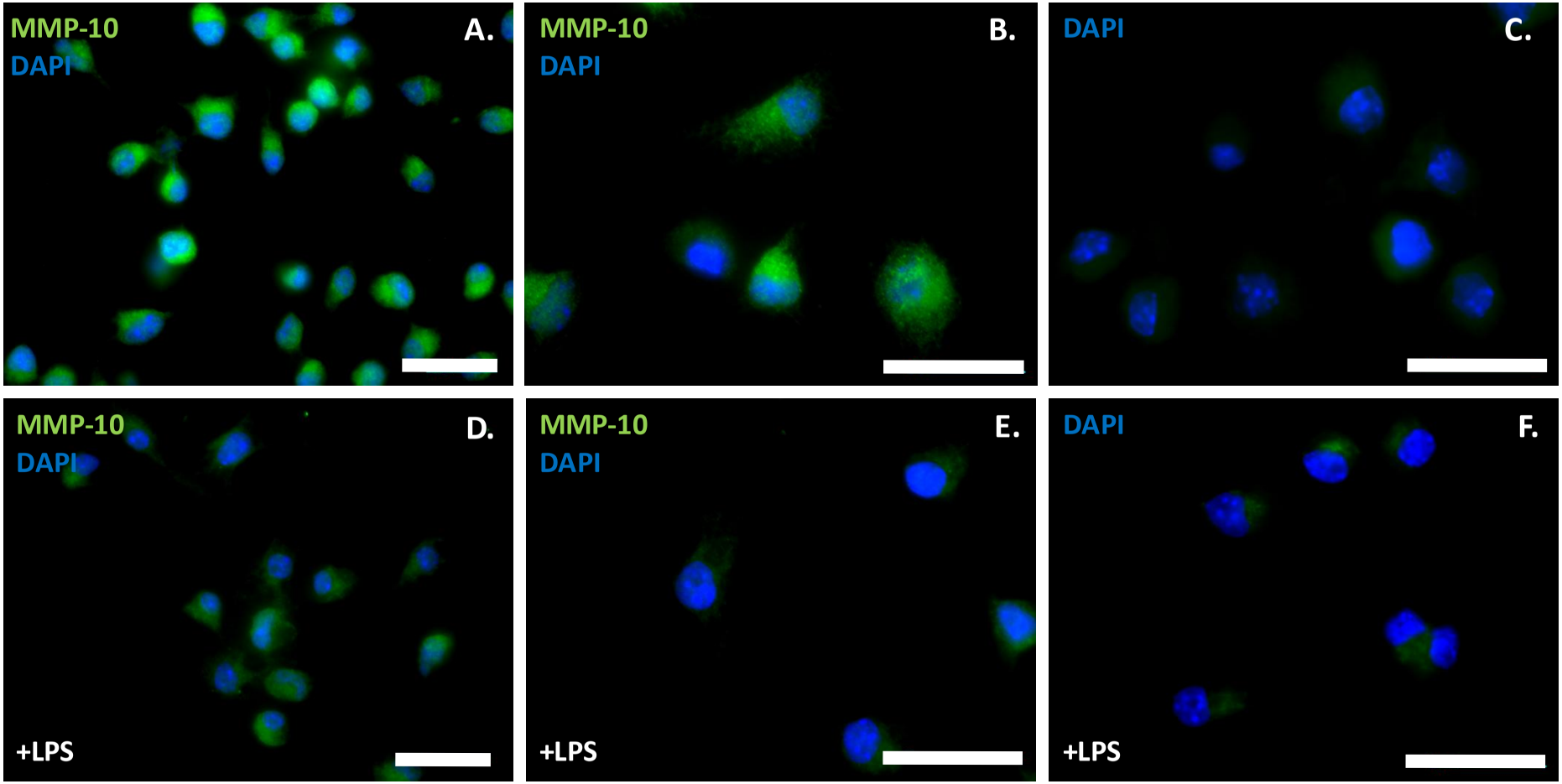

Figure 3.9 Immunocytochemical staining for MMP-10 protein in RAW264.7 macrophages 24 hours post-LPS stimulation. Cells were cultured on glass cover-slips for 24 hours before stimulation with LPS for a further 24 hours. (A, B): Unstimulated RAW264.7 macrophages. (D, E): RAW264.7 macrophage 24 hours post LPS stimulation. (C, F): secondary antibody only control. Scale bar = 25 µm. Images captured at fixed exposure.

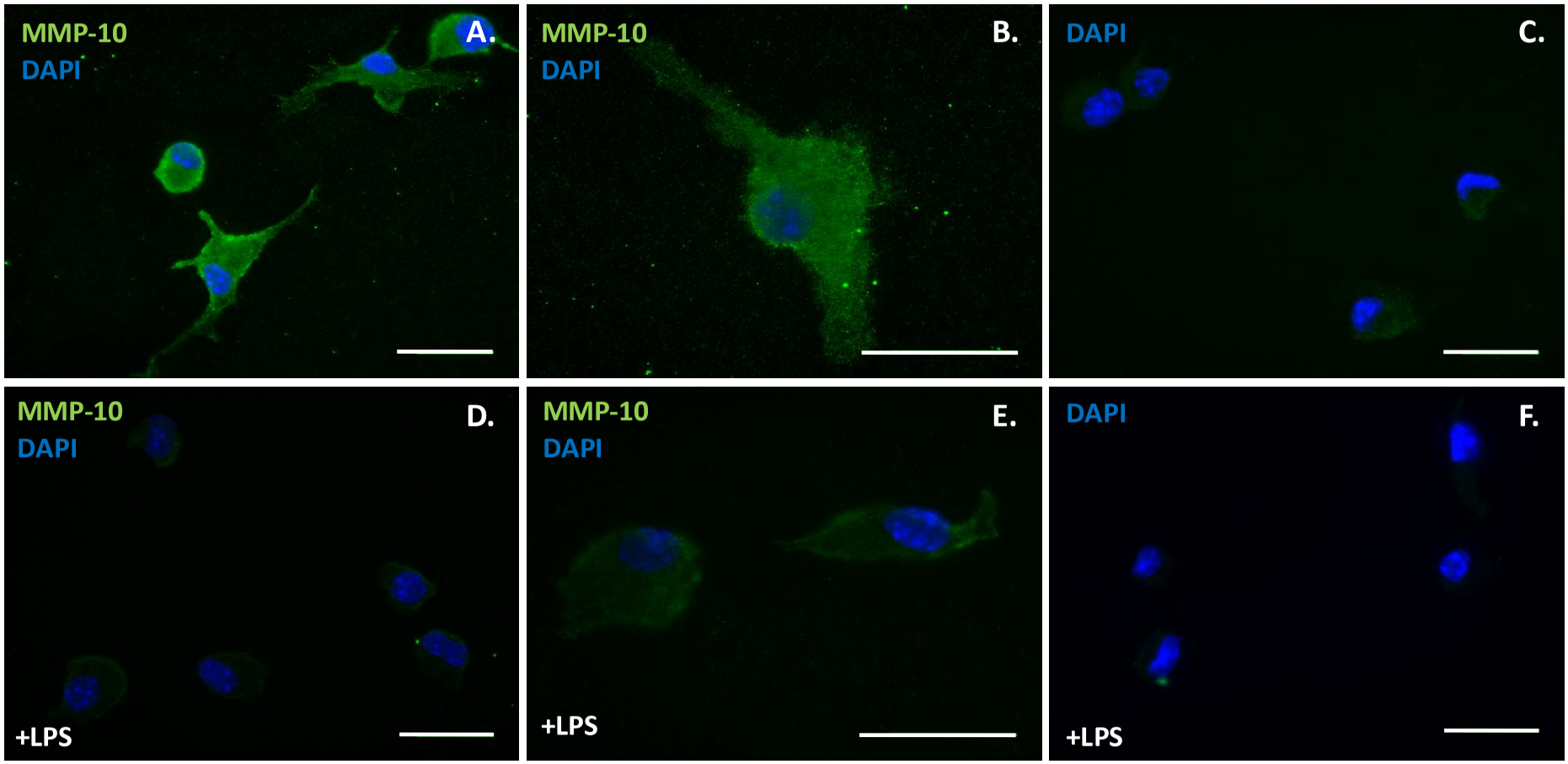

Figure 3.10 Immunocytochemical staining for MMP-10 protein in BMMs 24 hours post-LPS stimulation. Cells were cultured on glass cover-slips for 24 hours before stimulation with LPS for a further 24 hours. (A, B): Unstimulated BMMs. (D, E): BMMs 24 hours post LPS stimulation. (C, F): secondary antibody only control. Scale bar = 25 µm. Images captured at fixed exposure.

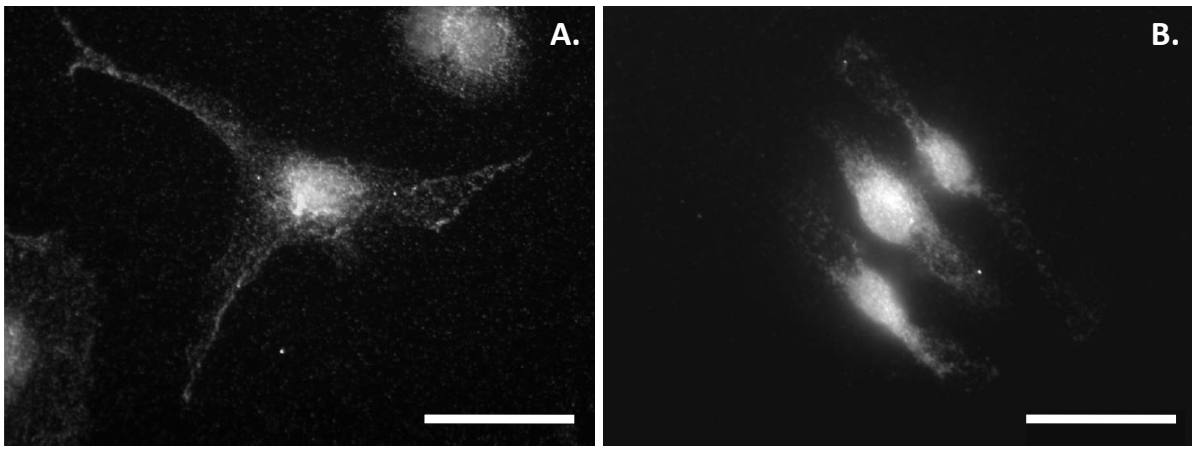

Figure 3.11 Comparing unstimulated RAW264.7 macrophage and BMM immunocytochemical staining for MMP-10 protein. MMP-10 positive staining appears punctuate with possible concentration around the Golgi apparatus, in both (A) BMMs and (B) RAW264.7 macrophages. Scale bar = 25 µm.

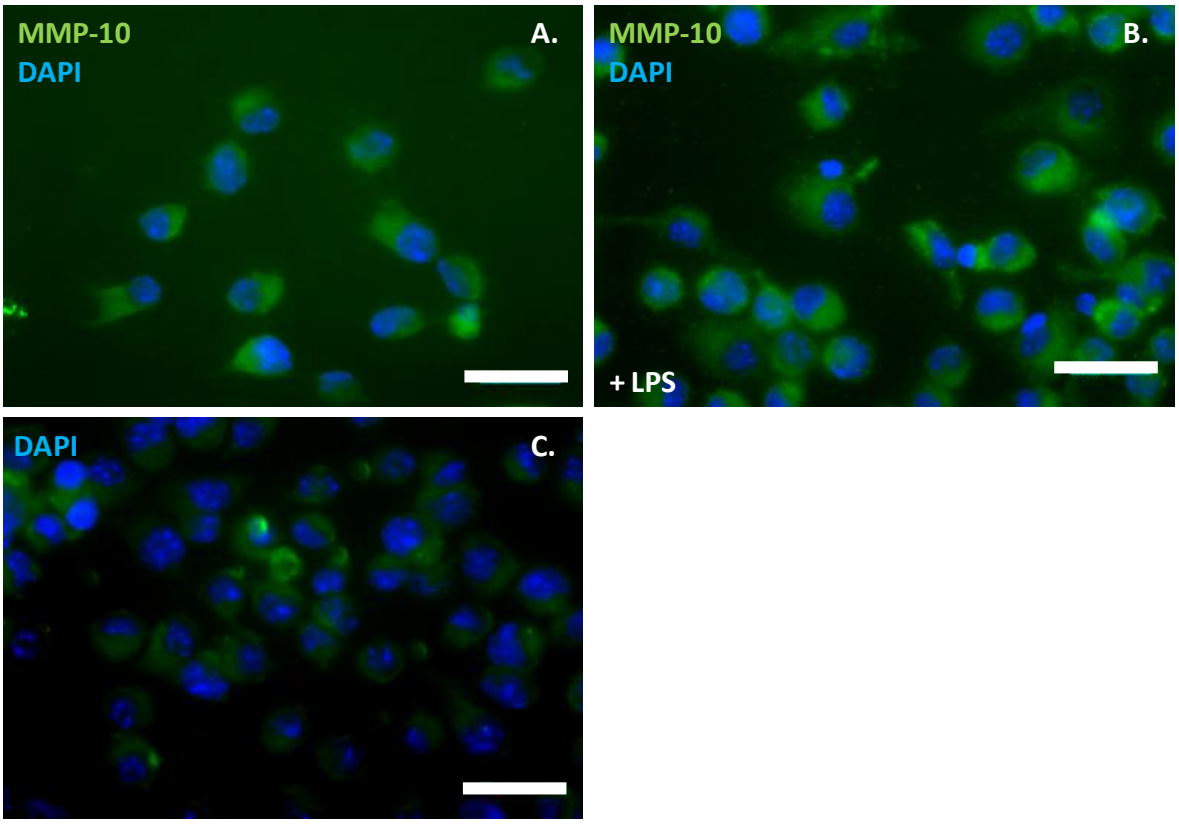

Figure 3.12 Immunocytochemical staining for MMP-10 protein in RAW264.7 macrophages 4 hours post-LPS stimulation. Cells were cultured on glass cover-slips for 24 hours before stimulation with LPS for a further 4 hours**.** **(**A) Unstimulated RAW264.7 macrophages. (B) RAW264.7 macrophages 4 hours post LPS stimulation. (C) Secondary antibody only control. Scale bar = 25 µm. Images captured at fixed exposure.

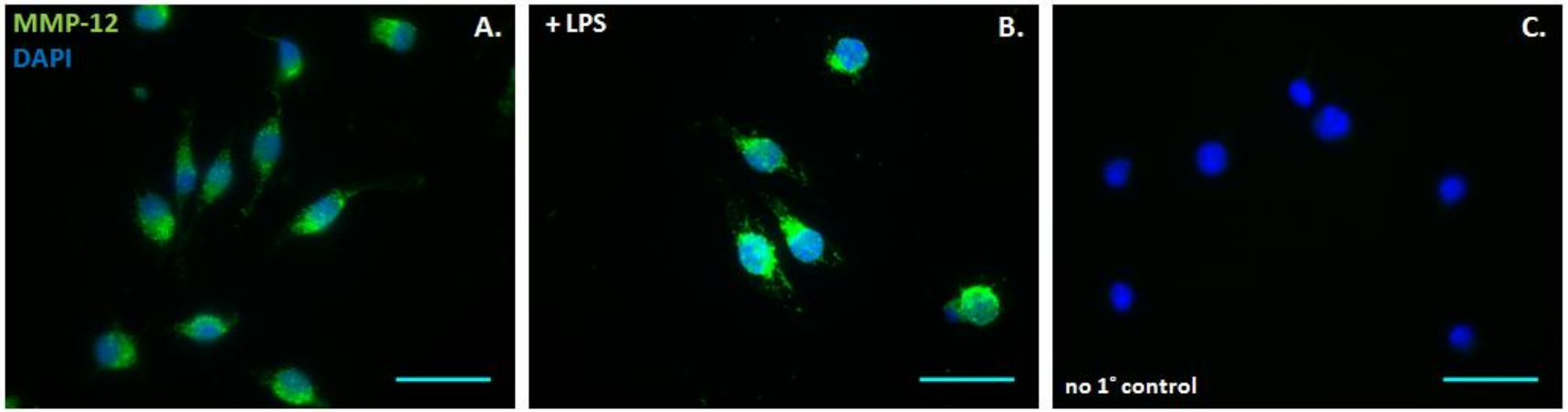

Figure 3.13 Immunocytochemical staining for MMP-12 protein in RAW264.7 macrophages 24 hours post LPS stimulation. Cells were cultured on glass cover-slips for 24 hours before stimulation with LPS for a further 24 hours. A: Unstimulated RAW264.7 macrophages. B: RAW264.7 macrophages 24 hours post LPS stimulation. C: Secondary antibody only control. Scale bar = 25 µm. Images captured at fixed exposure.

3.3.5 Western Blot analysis of LPS induced macrophage MMP-10 protein regulation is inconclusive

Western blot analyses of cumulative MMP-10 protein present in TCA precipitated RAW264.7 macrophage supernatant 4 or 24 hours post-LPS stimulation was performed (figure 3.14). Preliminary blots with IW13 MMP-10 polyclonal primary antibody revealed this to be more effective in western blots than the D248/6 MMP-10 primary antibody used for immunocytochemistry (data not shown). There appears to be no change in cumulative secreted MMP-10 protein at both 4 and 24 hours post-LPS stimulation compared with unstimulated control macrophages. A small up-regulation in overall cumulative MMP-10 protein concentration is apparent from 4 to 24 hours. Predicted pro- and active murine MMP-10 protein sizes are 57 and 47 KDa, respectively. On this blot MMP-10 protein appears to run at a slightly higher molecular weight, approximately 65 KDa. A band at approximately 90 KDa is also present on the 24 hour blot. This could reflect non-specific binding due to the presence of 0.2% serum. It is difficult to drawn any definitive conclusions however as the wells appear overloaded with protein.

The blot shown is representative of three experiments. No loading control is available for secreted proteins; however equal volumes of TCA precipitate were loaded into each well.

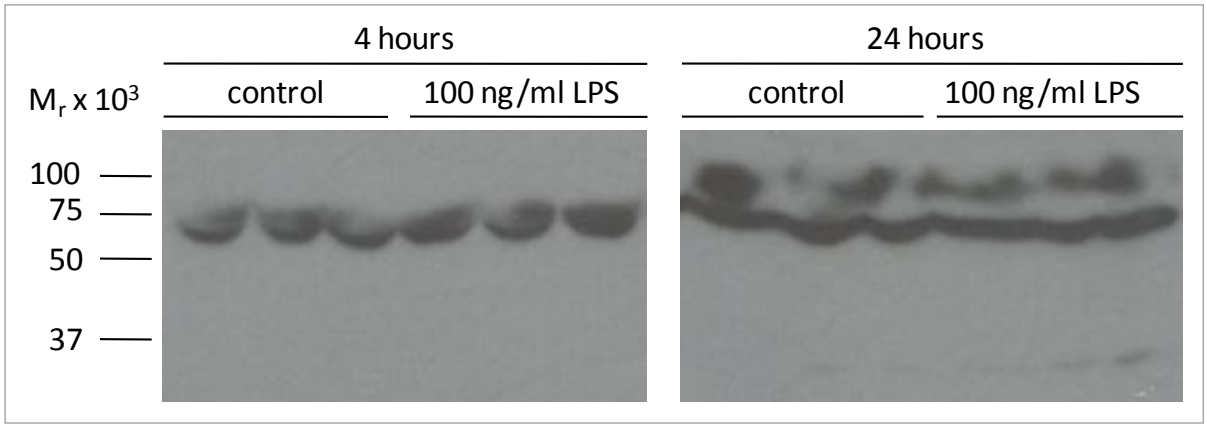

Figure 3.14 Western blot of RAW264.7 macrophage supernatant for cumulative MMP-10 protein 4 and 24 hours post-LPS stimulation. RAW264.7 macrophages were plated at the same density per well and transferred to 0.2% serum medium for the duration of the experiment. Supernatants were removed and 1 ml TCA precipitated. One fifth of each precipitate was loaded per well. Positions of BioRad Precision Plus protein standards are indicated.

Western blot analysis of cumulative MMP-10 protein present in TCA precipitated BMM supernatant 24 hours post-LPS stimulation was also performed, revealing an apparent increase in MMP-10 protein in BMMs 24 hours post-LPS stimulation (figure 3.15). Samples were resolved and detected as above, this time including a positive control of rhMMP-10. Both untreated and LPS-stimulated BMMs appear to express MMP-10 although the signal is much stronger for the stimulated cells. Overloading of the well makes it difficult to resolve any specific band sizes. It appears, however that neither sample shows detection of the smaller active form of MMP-10.

The blot shown represents one experiment. No loading control is available for secreted proteins; however equal volumes of TCA precipitate were loaded into each well.

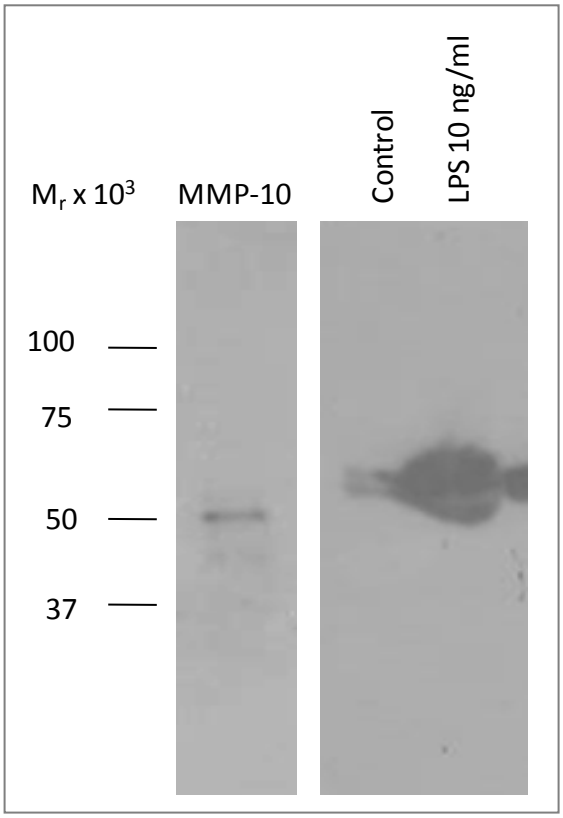

Figure 3.15 Western blot of BMM supernatant for cumulative MMP-10 protein 24 hours post-LPS stimulation. BMM were plated at the same density per well and transferred to 0.2% serum medium for the duration of the experiment. Supernatants were removed and 0.5 ml TCA precipitated. One fifth of each precipitate was loaded per well. 2.5 ng of rhMMP-10 was loaded to one well as a positive control. Positions of BioRad Precision Plus protein standards are indicated.

3.3.6 LPS stimulated MMP-10 regulation in macrophages may be controlled via the NF-κB signalling pathway

In order to better understand how LPS stimulation of macrophages results in MMP-10 modulation the signalling pathways activated by LPS/Toll-like receptor 4 (TLR4) interactions were investigated. qRT-PCR performed on LPS stimulated RAW264.7 macrophages and BMMs after 3, 4 and 24 hours reveals regulation of murine tumour necrosis factor – alpha (mTNF-α), a key player in the TLR4-Nuclear factor kappa B (NF-κB) signalling axis (figure 3.16). Significant induction of mTNF-α in BMMs following 3 hours stimulation with LPS is sustained until at least 24 hours post-LPS (figure 3.16 A, B). Similar results were observed in RAW264.7 macrophages at 4 and 24 hours post-LPS stimulation (figure 3.16 C, D).

This analysis of expression has been performed four times in BMMs and three times in RAW264.7 macrophages with reproducible results and all experiments performed in triplicate.

A.

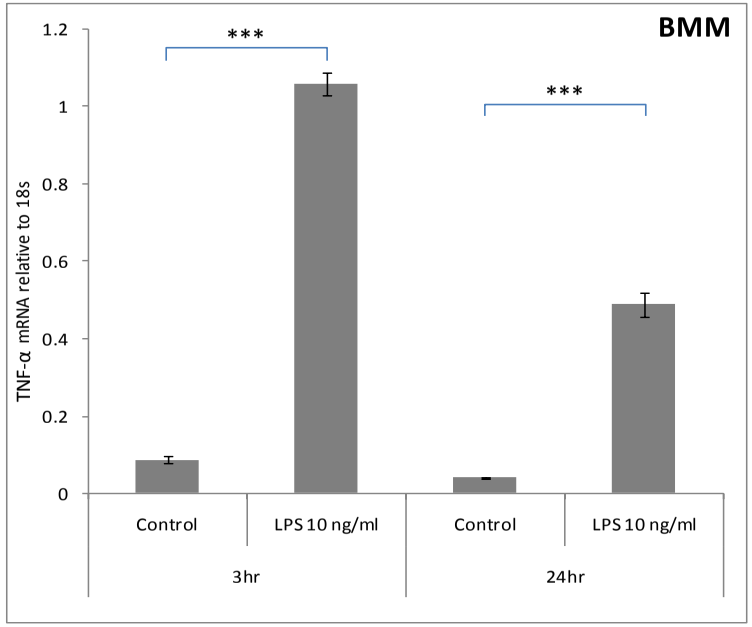

B.

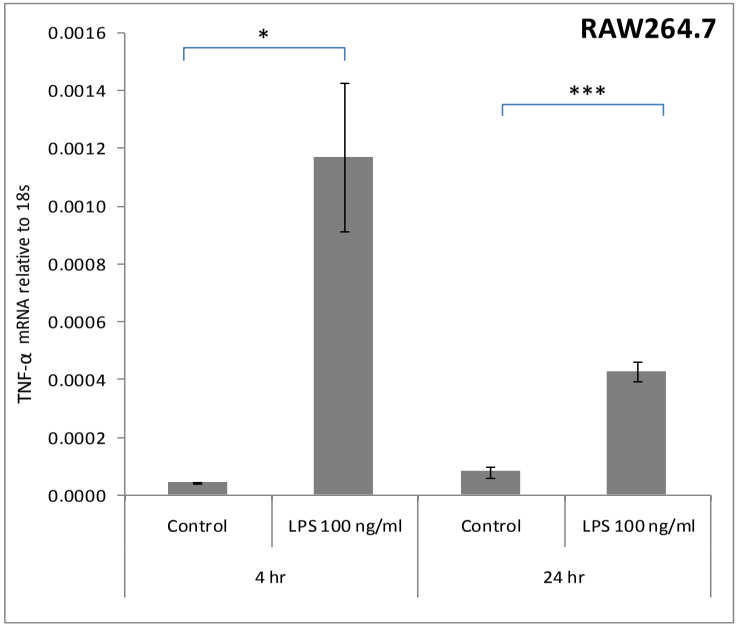

C.

	Treatment	Ct value 1	Ct value 2	Ct value 3
3 hr	Control	26.15	26.09	26.13
	LPS 10ng/ml	21.7	22.05	21.64
24 hr	Control	27.13	27.08	27.26
	LPS 10ng/ml	23.18	22.92	23.15

D.

	Treatment	Ct value 1	Ct value 2	Ct value 3
4 hr	Control	25.45	25.7	25.72
	LPS 100 ng/ml	20.45	20.85	21.04
24 hr	Control	24.83	24.18	25.07
	LPS 100 ng/ml	22.1	22.13	22.3

Figure 3.16 Relative expression of mTNF-α mRNA normalized to 18S in BMMs at 3 and 24 hours, and RAW264.7 macrophages at 4 and 24 hours post-LPS stimulation. qRT-PCR was performed on cDNA extracted from (A) BMMs and (C) RAW264.7 macrophages. Data was analysed by relative quantification and normalized to 18S. (B, D) Corresponding C_T values are shown. Each bar represents the mean of 3 samples ± SEM. Statistical significance was determined using the Student's t-test. * $p \leq 0.05$, *** $p \leq 0.001$.

An inhibitor of the TLR4-NF-κB signalling axis was utilised to further investigate the effect of LPS on RAW264.7 macrophage TNF-α and MMP-10 mRNA expression. At 4 hours post-LPS the induction of mTNF-α was significantly repressed by the IκB kinase inhibitor BMS-345541 (5 μg/ml), although expression of mTNF-α was still significantly greater than control samples (figure 3.17). LPS-driven induction of mTNF-α was also significantly inhibited by 10 μg/ml BMS-345541 and this is no longer significantly greater than control, suggesting a dose dependent response to increasing levels of inhibitor. Neither concentration of BMS-345541 appeared to have an effect on endogenous mTNF-α expression. At 24 hours post-LPS stimulation neither concentration of BMS-345541 had a significant inhibitory effect on LPS-driven induction of mTNF-α expression, despite a trend for reduction in mTNF-α mRNA with 10 μg/ml inhibitor (figure 3.18) compared with LPS treatment alone. Again, the inhibitor had no effect on endogenous mTNF-α expression.

The expression of MMP-10 mRNA in RAW264.7 in the presence of BMS-345541 was analysed 24 hours post-LPS stimulation (figure 3.19). A trend toward reversal of LPS-driven MMP-10 repression with 5 μg/ml BMS-345541 was observed, although MMP-10 mRNA levels were still significantly less than in untreated macrophages. Treatment of LPS-stimulated RAW264.7 macrophages with 10 μg/ml BMS-345541 results in a reversal in repression of MMP-10; MMP-10 mRNA levels are no longer significantly repressed compared to untreated macrophages and are significantly higher than in samples treated with 5 μg/ml BMS-345541. Endogenous levels of MMP-10 were not affected by either concentration of inhibitor.

A.

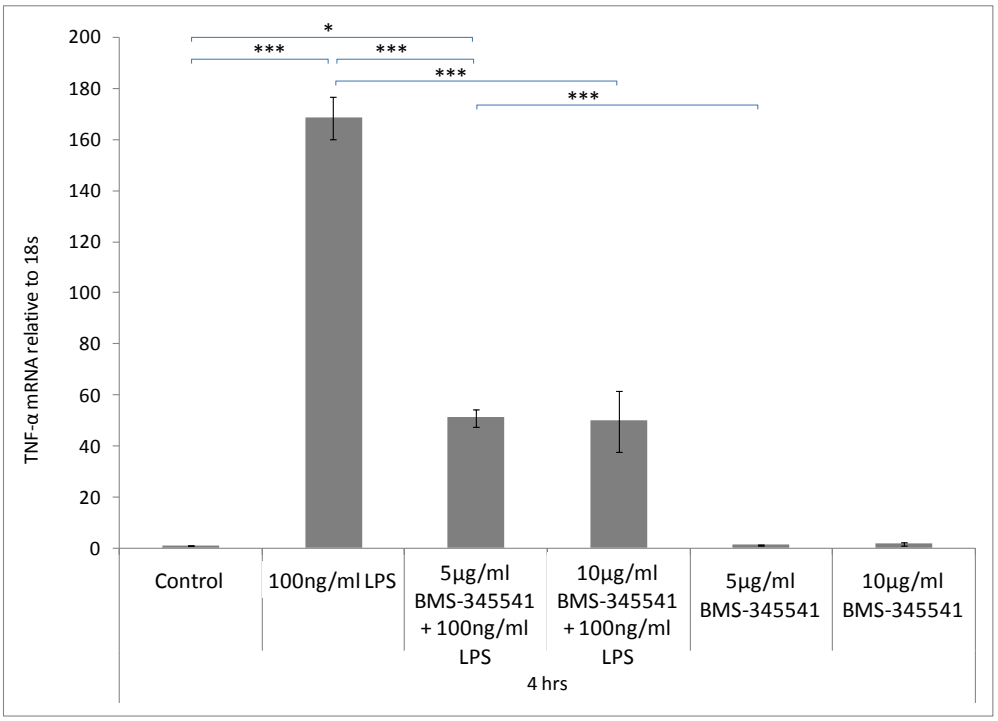

B.

	Treatment	Ct value 1	Ct value 2	Ct value 3
4hr	Control	28.28	28.61	28.24
	LPS 100ng/ml	20.88	20.96	20.95
	5µl/ml BMS-345541 + LPS 100ng/ml	22.93	22.66	22.45
	10µl/ml BMS-345541 + LPS 100ng/ml	23.29	23.24	22.95
	5µl/ml BMS-345541	27.5	28.76	28.59
	10µl/ml BMS-345541	28.51	28.14	29.49

Figure 3.17 Effect of IκB kinase inhibitor BMS-345541 on relative expression of mTNF-α mRNA in RAW264.7 macrophages at 4 hours post-LPS stimulation normalized to 18S. (A) qRT-PCR was performed on cDNA extracted from RAW264.7 macrophages 4 hours post-LPS stimulation. Data was analysed by relative quantification and normalized to 18S. (B) Corresponding C_T values are shown. Each bar represents the mean of 3 samples ± SEM. Statistical significance was determined using the Student's t-test. * $p \leq 0.05$, ** $p \leq 0.01$, *** $p \leq 0.001$.

A.

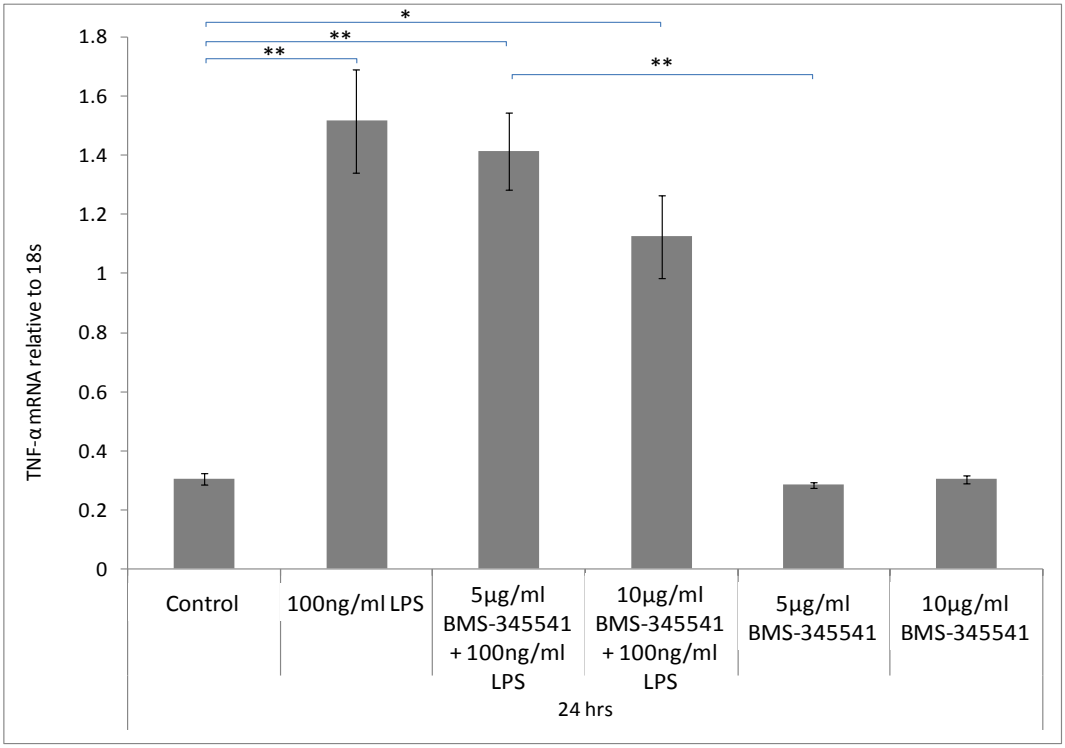

B.

	Treatment	Ct value 1	Ct value 2	Ct value 3
24hr	Control	28.4	28.1	28.2
	LPS 100ng/ml	25.1	24.8	24.5
	5µl/ml BMS-345541 + LPS 100ng/ml	24.4	24.7	24.7
	10µl/ml BMS-345541 + LPS 100ng/ml	25.0	25.5	25.1
	5µl/ml BMS-345541	28.5	28.8	28.4
	10µl/ml BMS-345541	28.2	28.4	28.3†

Figure 3.18 Effect of BMS-345541 on relative expression of mTNF-α mRNA normalized to 18S in RAW264.7 macrophages at 24 hours post-LPS stimulation. (A) qRT-PCR was performed on cDNA extracted from RAW264.7 macrophages 24 hours post-LPS stimulation. Data was analysed by relative quantification and normalized to 18S. (B) Corresponding C_T values are shown. Each bar represents the mean of 3 samples ± SEM. Statistical significance was determined using the Student's t-test. * $p \leq 0.05$, ** $p \leq 0.01$, *** $p \leq 0.001$. † indicates 18S C_T value varied more than 1.5 C_Ts from the mean and was therefore excluded from analysis

A.

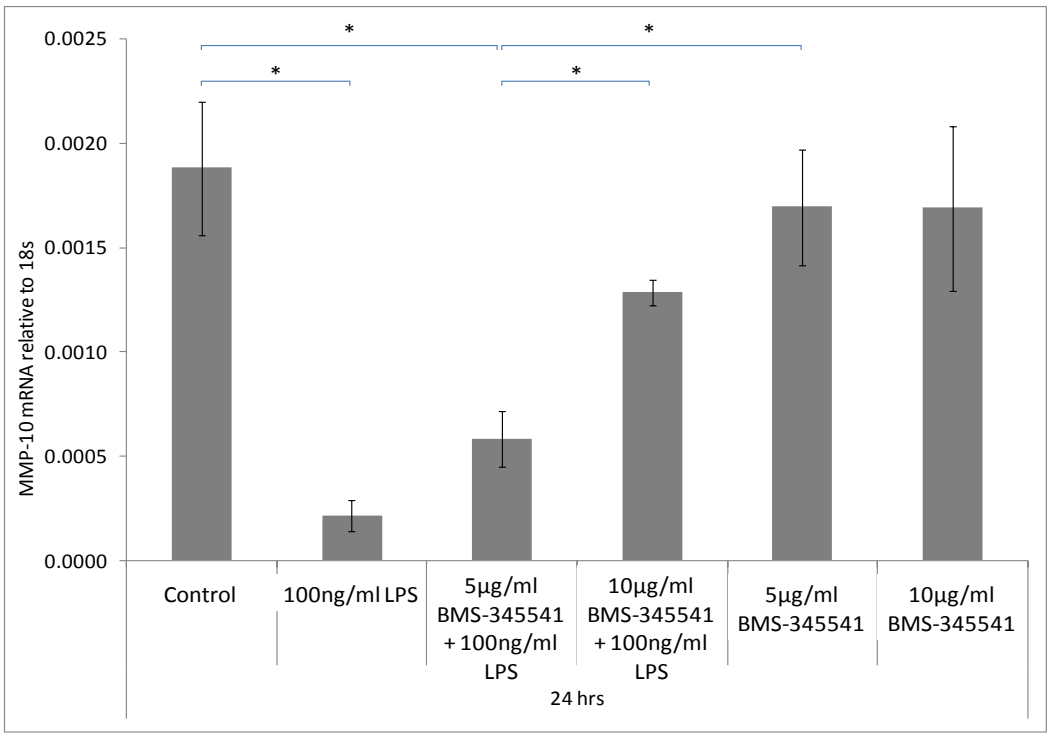

B.

	Treatment	Ct value 1	Ct value 2	Ct value 3
24hr	Control	32.8	33.6	33.3
	LPS 100ng/ml	37.0	37.0	35.2
	5µl/ml BMS-345541 + LPS 100ng/ml	34.4	35.3	34.7
	10µl/ml BMS-345541 + LPS 100ng/ml	34.0	33.6	33.7
	5µl/ml BMS-345541	33.5	34.0	32.9
	10µl/ml BMS-345541	33.8	33.0	33.4†

Figure 3.19 Effect of BMS-345541 on relative expression of MMP-10 mRNA normalized to 18S in RAW264.7 macrophages at 24 hours post-LPS stimulation. (A) qRT-PCR was performed on cDNA extracted from RAW264.7 macrophages 24 hours post-LPS stimulation. Data was analysed by relative quantification and normalized to 18S. (B) Corresponding C_T values are shown. Each bar represents the mean of 3 samples ± SEM. Statistical significance was determined using the Student's t-test. * $p \leq 0.05$. † indicates 18S C_T value varied more than 1.5 C_Ts from the mean and was therefore excluded from analysis

BMS-345541 was also used to investigate control of mTNF-α and MMP-10 in BMMs 3 hours post-LPS (figure 3.20). qRT-PCR for mTNF-α reveals a trend towards repression 3 hours post-LPS with 10 μg/ml BMS-345541, although this is not significant compared to BMMs stimulated with LPS alone (figure 3.20 A). Expression of endogenous mTNF-α shows a trend toward decrease with BMS-345541 compared to untreated cells, evident from C_T values (figure 3.20 C). qRT-PCR for MMP-10 (C) reveals a significant repression of LPS induced expression 3 hours post-LPS with 10 μg/ml BMS-345541. C_T values (D) reveal that this repression brings levels of MMP-10 mRNA back down to almost that of untreated BMMs. Interestingly 10 μg/ml BMS-345541 also shows a strong trend toward repression of endogenous levels of MMP-10 expressed by BMMs, compared to untreated BMMs. Again, significance could not be determined due to low 'n' number.

All results shown for RAW264.7 macrophages represent two experiments with reproducible results whilst results shown for BMMs represent one experiment, with all experiments performed in triplicate.

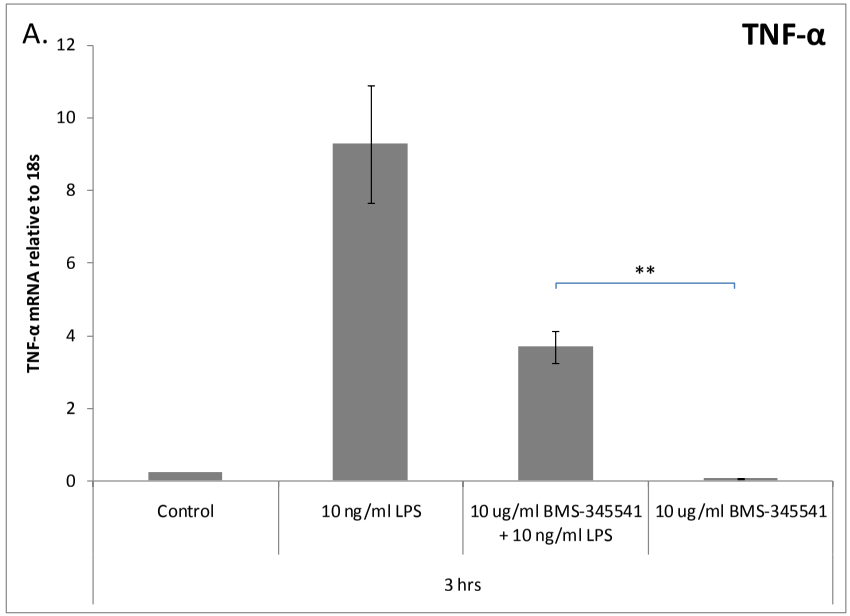

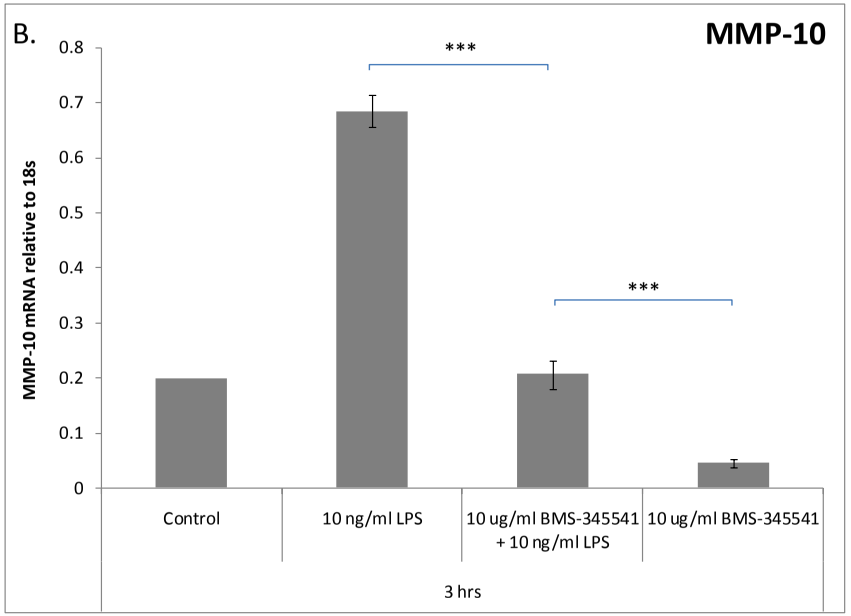

C.

	Treatment	Ct value 1	Ct value 2	Ct value 3
3hr	Control	26.7	27.0†	26.0
	10 ng/ml LPS	22.3	22.5	22.8
	10µl/ml BMS-345541 + 10ng/ml LPS	23.8	24.1	23.6
	10µl/ml BMS-345541	27.2	28.3	28.5

D.

	Treatment	Ct value 1	Ct value 2	Ct value 3
3hr	Control	33.3	33.7†	33.2
	10 ng/ml LPS	31.3	31.0	31.2
	10µl/ml BMS-345541 + 10ng/ml LPS	33.8	34.2	33.4
	10µl/ml BMS-345541	33.1	31.9	33.1

Figure 3.20 Effect of BMS-345541 on relative expression of mTNF-α and MMP-10 mRNA normalized to 18S in BMMs 3 hours post-LPS stimulation. qRT-PCR was performed on cDNA extracted from BMMs 3 hours post-LPS stimulation. Data was analysed by relative quantification and normalized to 18S for (A) mTNF-α and (B) MMP-10. (C, D) Corresponding C_T values are shown. Each bar represents the mean of 3 samples ± SEM. Statistical significance was determined using the Student's t-test. ** $p \leq 0.01$, *** $p \leq 0.001$. † indicates 18S C_T value varied more than 1.5 C_Ts from the mean and was therefore excluded from analysis

3.3.7 A potential role for class II Histone Deacetylases in macrophage MMP-10 expression in response to LPS

Previous research has shown an inverse relationship between MMP-10 and expression of the class II histone deacetylase HDAC7 in the endothelium during angiogenesis and development (Ha et al., 2008) (Chang et al., 2006). In light of this correlation, mRNA expression levels of class II HDACs 4, 5 and 7 were analysed in LPS-stimulated macrophages (figure 3.21). As already demonstrated, MMP-10 mRNA expression decreases significantly in response to increasing concentrations of LPS (figure 3.21 A, see also figure 3.4 C). In the same samples however the level of HDAC7 mRNA does not vary significantly, despite a marginal trend for decreased expression (figure 3.20 B). This relationship is also seen in RAW264.7 macrophages (figure 3.22); MMP-10 mRNA expression is significantly down-regulated 24 hours post – LPS (figure 3.22 A) but there is no significant change in HDAC7 expression in the same samples (figure 3.22 B).

The analysis of HDAC7 mRNA in BMMs represents two experiments with reproducible results. The equivalent results shown for RAW264.7 macrophages represent three experiments.

HDAC4 and 5, as with HDAC7, are able to interact with the MEF2 transcriptional activator and have been shown to be regulated in LPS-stimulated macrophages (Aung et al., 2006). Figures 3.23 and 3.24 show the expression of MMP-10 and HDAC4 and HDAC5 in BMMs and RAW264.7 macrophages 24 hours post-LPS stimulation. As with HDAC7, there appears to be no significant change in HDAC4 mRNA expression with LPS in either BMMs or RAW264.7 cells (figure 3.23 A, 3.24 A), despite a slight trend for down regulation in BMMs. HDAC5 expression however follows the pattern of MMP-10 mRNA in the same samples; in both BMMs and RAW264.7 macrophages there is a statistically significant repression in HDAC5 mRNA 24 hours post – LPS (figure 3.23 C, E; 3.24 C, E).

The analysis of HDAC4 and 5 in BMMs was performed only once. The data shown for expression of HDAC4 and 5 in RAW264.7 macrophages represents two experiments with reproducible results and all experiments performed in triplicate.

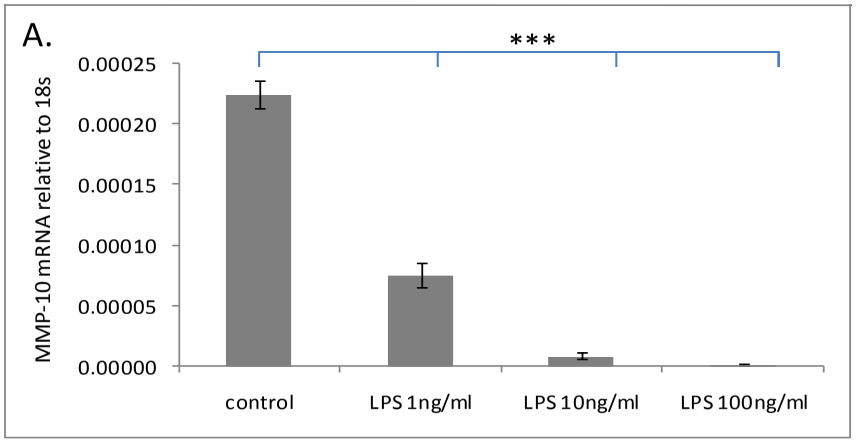

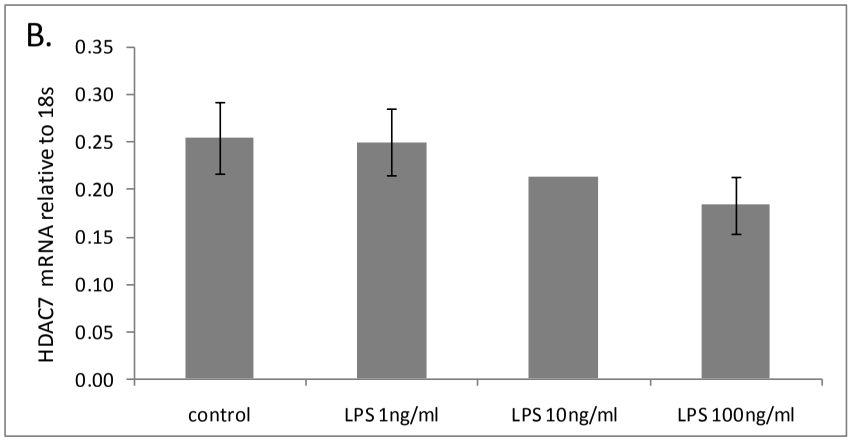

C.

Treatment	C_T value 1	C_T value 2	C_T value 3
Control	32.37	32.41	32.62
LPS 1 ng/ml	34.09	33.82	34.96
LPS 10 ng/ml	36.68	37.82	36.28
LPS 100 ng/ml	38.6	37.86	40

D.

Treatment	C_T value 1	C_T value 2	C_T value 3
Control	30.48	29.8	29.27
LPS 1 ng/ml	29.55	30.04	30.37
LPS 10 ng/ml	†	30.78	30.24
LPS 100 ng/ml	30.19	30.19	31.38

Figure 3.21 Relative expression of MMP-10 and HDAC7 mRNA normalized to 18S in BMMs 24 hours post-LPS stimulation. qRT-PCR was performed on cDNA extracted from BMMs 24 hours post-LPS stimulation for (A) MMP-10 and (B) HDAC7. Data was analysed by relative quantification and normalized to 18S. (C, D)Corresponding C_T values are shown. Each bar represents the mean of 3 samples ± SEM. Statistical significance was determined using the Student's t-test. *** $p \leq 0.001$. † indicates failure of RT-PCR for this sample.

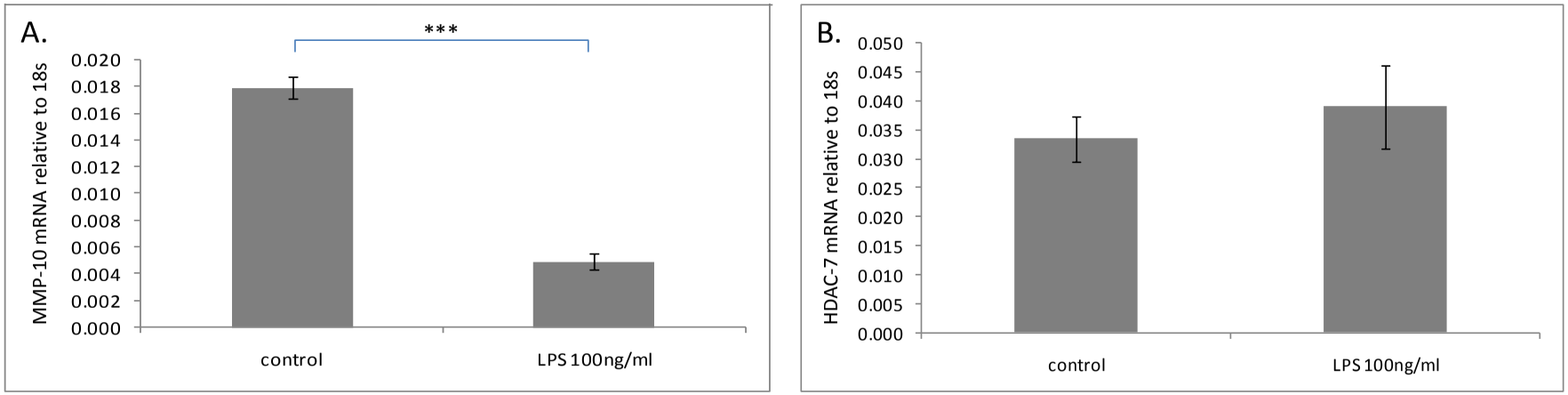

C.

Treatment	C_T value 1	C_T value 2	C_T value 3
Control	31.55	31.31	31.49
LPS 100 ng/ml	33.29	33.18	33.47

D.

Treatment	C_T value 1	C_T value 2	C_T value 3
Control	33.78	34.59	34.26
LPS 100 ng/ml	33.69	33.76	34.59

Figure 3.22 Relative expression of MMP-10 and HDAC7 mRNA normalized to 18S in RAW264.7 macrophages 24 hours post-LPS stimulation. qRT-PCR was performed on cDNA extracted from BMMs for (A) MMP-10 and (B) HDAC7. Data was analysed by relative quantification and normalized to 18S. (C, D) Corresponding C_T values are shown. Each bar represents the mean of 3 samples ± SEM. Statistical significance was determined using the Student's t-test. *** $p \leq 0.001$.

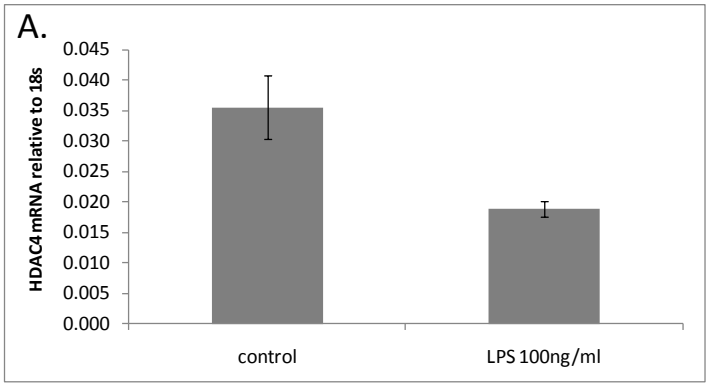

B.

Treatment	C_T value 1	C_T value 2	C_T value 3
Control	25.51	26.25	25.49
LPS 100 ng/ml	27.04	26.57	26.59

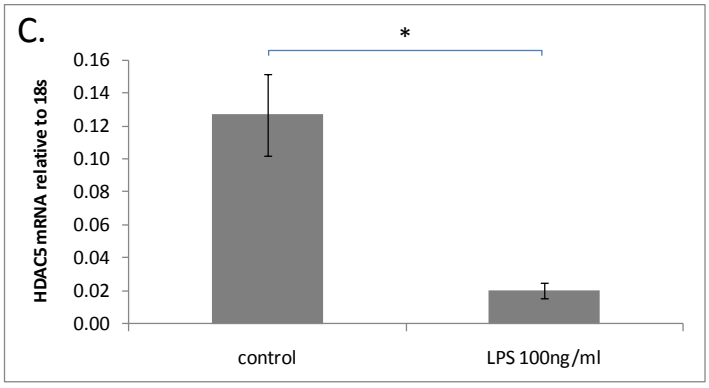

D.

Treatment	C_T value 1	C_T value 2	C_T value 3
Control	23.85	24.56	23.81
LPS 100 ng/ml	26.62	25.64	26.3

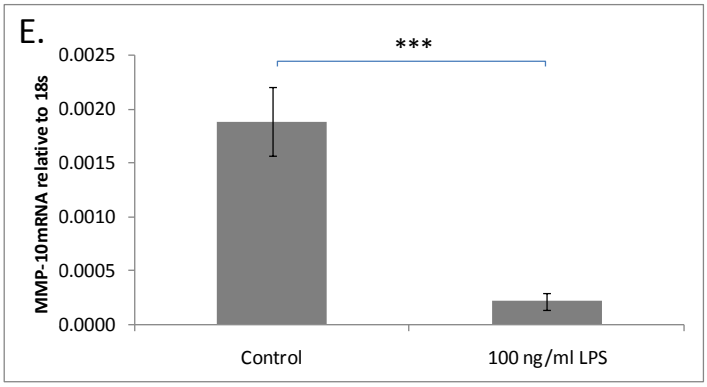

F.

Treatment	C_T value 1	C_T value 2	C_T value 3
Control	32.84	33.55	33.29
LPS 100 ng/ml	37.03	36.99	35.19

Figure 3.23 Relative expression of HDAC4, HDAC5 and MMP-10 mRNA normalized to 18S in BMMs 24 hours post-LPS stimulation. qRT-PCR was performed on cDNA extracted from BMMs for (A) HDAC4, (C) HDAC5 and (E) MMP-10 mRNA. Data was analysed by relative quantification and normalized to 18S. (B, D, F) Corresponding C_T values are shown. Each bar represents the mean of 3 samples ± SEM. Statistical significance was determined using the Student's t-test. * $p \leq 0.05$, ** $p \leq 0.01$.

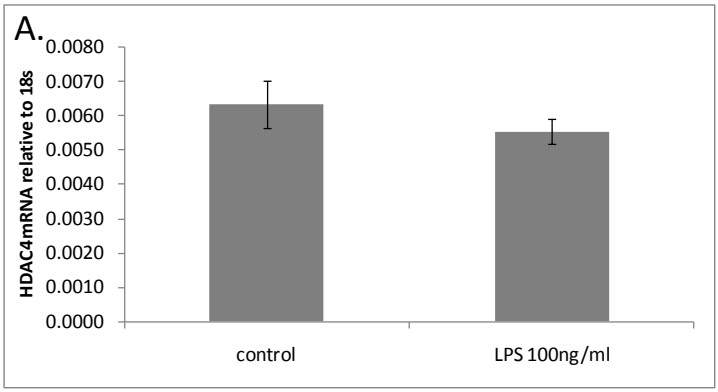

B.

Treatment	C_T value1	C_T value2	C_T value3
Control	31.51	31.66	32.14
LPS 100 ng/ml	32.08	31.81	32.2

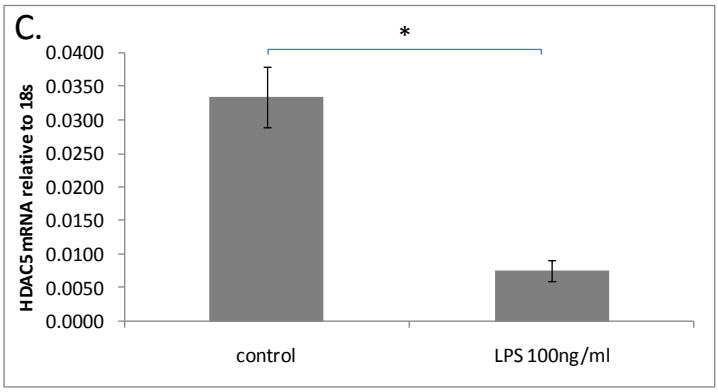

D.

Treatment	C_T value1	C_T value2	C_T value3
Control	27.39	27.4	27.89
LPS 100 ng/ml	29.42	28.96	29.75

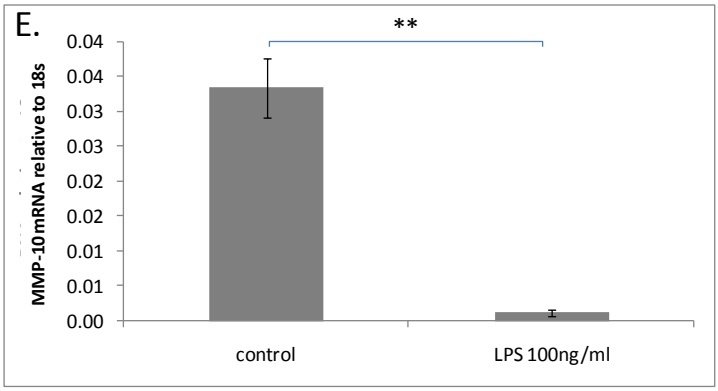

F.

Treatment	C_T value1	C_T value2	C_T value3
Control	32.49	32.89	30.54
LPS 100 ng/ml	37.19	38.09	38.72

Figure 3.24 Relative expression of HDAC4, HDAC5 and MMP-10 mRNA normalized to 18S in RAW264.7 macrophages 24 hours post-LPS stimulation. qRT-PCR was performed on cDNA extracted from RAW264.7 macrophages for (A) HDAC4, (C) HDAC5 and (E) MMP-10 mRNA. Data was analysed by relative quantification and normalized to 18S. (B, D, E) Corresponding C_T values are shown. Each bar represents the mean of 3 samples ± SEM. Statistical significance was determined using the Student's t-test. * $p \leq 0.05$, ** $p \leq 0.01$.

3.4 Discussion

In this chapter an extensive profile of all MMPs and TIMPs is reported in both BMMs and RAW264.7 macrophages, in response to LPS. Previous investigations into MMP expression in monocytes and macrophages have hinted at similar results (Bar-Or et al., 2003; Suzuki et al., 2000; Ho et al., 2008). For example, in primary human monocytes MMP-10 mRNA is markedly induced after 3 hours LPS stimulation (Ho et al., 2008), reflecting the results observed at 4 hours post-LPS in RAW264.7 and 3 hours post-LPS in BMMs (figures 3.6 and 3.7, respectively). LPS-driven induction of MMP-10 mRNA has also been observed in different cell types; in human umbilical vein endothelial cells (HUVECs) microarrays have shown MMP-10 to be induced at least two-fold following 3 to 7 hours LPS exposure (Zhao et al., 2001; Norata et al., 2004). This suggests that endothelium exposed to infection *in vivo* may secrete MMP-10 concomitantly with macrophages during the immune response, potentially aiding their extravasation and transmigration. Whilst this early induction of MMP-10 mRNA in response to LPS is well established, the repression observed 24 hours post-LPS in BMMs appears to be novel.

In BMMs the induction of MMP-10 mRNA at 3 hours post-LPS was repressed by the highly selective IκB kinase allosteric site inhibitor BMS-345541 (figure 3.20 B). This inhibits the translocation of transcription factor NF-κB into the nucleus by preventing the phosphorylation and subsequent ubiquitination of IκB in the cytoplasm (Burke et al., 2003). Interestingly the LPS-driven repression of MMP-10 mRNA observed 24 hours post-LPS was also reversed with BMS-345541 (figure 3.19). Despite there being little evidence to suggest that NF-κB interacts directly with the MMP-10 promoter (MatInspector (Cartharius et al., 2005)), these results suggest that NF-κB drives both the early induction and late repression of MMP-10 mRNA. It is difficult to reconcile these two ostensibly conflicting events, however, without considering other potential mechanisms of MMP-10 regulation.

Recent literature suggests a novel regulatory pathway for LPS-driven MMP expression, including MMP-10, in macrophages (Kim et al., 2010). Kim et al have shown that induction of MMP-10 mRNA in RAW264.7 and murine peritoneal macrophages up to 9 hours post-LPS can be inhibited with siRNA targeting NADPH oxidase-2 (Nox-2) reactive oxygen species (ROS). Macrophages, along with other immune cells, generate Nox-2 during the 'respiratory burst' following phagocytosis of pathogens. In turn Nox-2 catalyses the production of superoxides, such as H_2O_2, that are capable of killing bacteria. This implies that the generation of superoxides by Nox-2 is intrinsically linked to

the expression of MMPs in an immune setting, possibly delaying regulation of specific proteases until after phagocytosis. Perhaps unsurprisingly NF-κB has also been shown to respond to oxidative stress. It is known that H_2O_2 activates NF-κB nuclear translocation via the canonical/MyD88 dependent pathway, much like LPS (figure 3.25, (Gloire et al., 2006)).

An extensive search of the literature reveals little reference to MMP-10 regulation at 24 hours post-LPS in macrophages. In fact, by this relatively late time point any change in MMP expression is unlikely to be due to the direct effect of LPS, but instead may be the result of regulation further down-stream. For example, the transcription factor MEF-2, a direct activator of MMP-10 mRNA transcription, can be inhibited by the action of class II histone deacetylase, HDAC7, subsequently repressing MMP-10 in endothelial cells (Chang et al., 2006). As MEF-2 is known to be induced by LPS in macrophages (Han et al., 1997) it seems reasonable to hypothesise that the late repression of MMP-10 in BMMs may be due to inhibition of MEF2, potentially via the increased action of HDAC7. Analysis of HDAC7 mRNA however revealed no change in expression in RAW264.7 macrophages or BMMs 24 hours post LPS, despite the expected repression of MMP-10 (figures 3.21 and 3.22). There was also no significant change in expression of another class II histone deacetylase, HDAC4. A significant repression in HDAC5 mRNA was observed however in both BMMs and RAW264.7 macrophages 24 hours post-LPS (figures 3.23 and 3.24), which conflicts with previous observations in BMMs (Aung et al., 2006). However, the BMMs harvested by Aung et al were cultured without a selection stage and stimulated with LPS from a *Salmonella* strain, rather than *E. coli*, which may go some way to explaining their conflicting results. Due to the compelling support for this LPS/HDAC/MMP-10 regulation hypothesis in the literature however it would be important to repeat these experiments, particularly in BMMs as HDAC mRNA was examined only once in these cells.

Despite the evidence for LPS-driven class II HDAC mRNA regulation in BMMs described above there is also data supporting a potential mechanism by which HDAC7 protein is sequestered, preventing it from interacting with the MEF2 without altering its transcription. HDAC7 has been found to co-localise with promyelocytic leukemia protein (PML) nuclear bodies (NBs) in epithelial and endothelial cells (Gao et al., 2008). PML NBs are sub-nuclear compartments that play a role in transcriptional regulation, amongst other process. Gao et al have shown increased PML NB formation and co-localisation with HDAC7 following TNF-α and LPS treatment. Once HDAC7 is sequestered by the PML NBs in the nucleus it can no longer interact with and inhibit MEF2 transcription factor, leaving MEF2 free to activate MMP-10 transcription. As the levels of LPS

present in culture medium and the TNF-α expressed by the cells falls, it is reasonable to assume that HDAC7 will eventually disassociate from PML NBs allowing it to bind to and inhibit MEF2 once more. This suggests a method by which HDAC7 protein can mediate the expression of MMP-10 mRNA without levels of HDAC7 mRNA varying in response to LPS.

In order to further develop some of the preliminary data presented in this chapter it is important to consider the use of alternative techniques, especially in the analysis of MMP-10 protein expression. The limitations of the Western blots are clear and infer little about the true changes in MMP-10 expression, whilst also indicating a discrepancy between MMP-10 mRNA expression and protein secretion. It may be possible to optimise the protocol; for example, adjusting the volume of protein loaded; however the harsh precipitation techniques that lead to poor Western blot resolution are unavoidable. Whilst immunofluorescence reveals a clear down-regulation in MMP-10 protein expression 24 hours post-LPS, employing alternative assays, such as ELISA or fluorescence activated cell sorting (FACS), would provide a more quantitative result, despite not allowing for differentiation between pro- and active-MMP forms. At the time of writing no commercial murine MMP-10 ELISAs are available, however it would be possible to develop one using the polyclonal MMP-10 antibody utilised throughout this chapter.

Chapter 4: **Modulation of MMP-10 expression alters macrophage migratory phenotype**

4.1 Introduction

4.1.1 The role of metalloproteinases in cell migration

The fundamental role of macrophages in the innate immune response requires an ability to mobilize rapidly in response to external signals, such as chemokines, or a change in the surrounding extracellular matrix (ECM). The key regulators controlling this response are the Rho GTPases, a family of GTP binding proteins that control the dynamics of the cell cytoskeleton (described in detail in Chapter 1, 1.1.6).

The structure of the cytoskeleton in macrophages is greatly influenced by the composition of the ECM, affecting both the persistence and directionality of macrophage migration *in vivo*. Migration is routinely modelled *in vitro* using two-dimensional (2D) coatings of matrix components. Current concepts of cell migration and cell-matrix interactions were largely established in 2D models as these provide relatively high-throughput results which are easily visualized. Macrophages are perhaps one of the few cell types that encounter an environment where 2D migration occurs *in vivo*. Before blood monocytes differentiate into tissue macrophages they must first adhere to the 2D layer of activated endothelium lining the blood vessel lumen; rolling then crawling along it to sites of infection and injury before commencing diapedesis through the endothelial cell junctions and transmigrating the 3D basement membrane (see Chapter 1, 1.1.4). The role of the Rho GTPases in this process is fairly well understood. For example, RhoA has been shown to be vital for monocyte tail retraction during migration on a monolayer of endothelial cells (Worthylake et al., 2001). The function of MMPs in this setting has also long been of interest. The transmigration of leukocytic cells through the endothelial blood-brain barrier, for example, has been shown to depend on the action of MMPs on the tight junction protein, Occludin (Reijerkerk et al., 2006). Reijerkerk et al suggest that Occludin, a tight junction specific protein associated with decreased monolayer permeability, can be degraded by MMPs during leukocyte diapedesis but they do not speculate which MMP may be involved.

Further advances in our understanding of protease-dependent cell migration have come from studies assessing expression of the MMPs during migration on, or through, various matrix components that would be present in or around sites of diapedesis. For example, co-transfection of MMP-2 and MT1-MMP/MMP-14 into a kidney cell-line has been shown to increase digestion of FITC-labelled 2D fibronectin, as seen in 'tracks' left by migrating cells. Interestingly, subsequent treatment with recombinant TIMP-2 inhibited fibronectin degradation but not cell migration (Cao

et al., 2004). MT1-MMP/MMP-14 has also been found to co-localise with areas of collagen degradation at F-actin rich foci during the migration of a fibrosarcoma cell line through fibrillar collagen (Friedl and Wolf, 2009).

In migrating macrophages specifically, MMP activity appears to be mainly focused around actin-rich adhesions called podosomes. These are thought to aid degradation of the ECM, thus playing a role in cell migration and invasion. In hematopoietic lineage-derived osteoclasts, for example, MMP-9 and MT1-MMP/MMP-14 have been localized to podosomes and it has been hypothesized that microtubules may traffic MMPs to the cell surface at sites of podosome formation (Linder, 2007). A recent study has suggested that podosomes form dendritic cell protrusions containing MT1-MMP/MMP-14 allowing for specific areas of gelatin degradation (Gawden-Bone et al., 2010). Gawden-Bone et al hypothesise that myosin II-driven podosome formation and MT1-MMP/MMP-14 localization to the podosome are expressly coupled to allow for tissue degradation and migration. Perhaps most relevant to this chapter is the recent finding that podosomes are downregulated in dendritic cells by LPS-induced TLR4 signalling in an MMP-dependent manner, subsequently reducing their migratory capacity (West et al., 2008).

4.1.2 MicroRNAs in cell migration

MicroRNAs (miRNAs) are short, ~22 nucleotide, RNA molecules that can bind to complementary mRNA sequences in the 3' untranslated region (UTR) of target transcripts. MiRNA biogenesis takes place in the nucleus with RNA polymerase II mediating the transcription of 'primary' pri-miRNA stem-loop precursors. These precursors are processed and exported out of the nucleus where, after further processing to their mature miRNA form, they are able to interact with mRNA (Pasquinelli et al., 2005). MiRNA binding triggers the function of an RNA-induced silencing complex (RISC) that drives the repression or cleavage of target mRNA.

MicroRNAs have the ability to regulate the expression of a diverse and abundant number of targets at a post-transcriptional level and data suggesting they play a role in cell migration is emerging. For example, constitutive expression of microRNA (miR)-146b has been shown to significantly reduce the migration and invasion of a human glioma cell line in an *in vitro* wound healing model and through three-dimensional matrigel (Xia et al., 2009). Conversely, in a murine epithelial cell line stably expressing miR-155, cell migration was observed to have nearly doubled in Boyden chamber and scratch wounding assays as a result of RhoA targeting (Kong et al., 2008).

MiR-155 has been shown to play a fundamental role in macrophage function, regulating differentiation and immune response. For example, miR-155 is up-regulated in primary murine macrophages in response to pro-inflammatory stimuli such as interferon (IFN)-β and via toll-like receptor (TLR) signalling with lipopolysaccharide (LPS) (O'Connell et al., 2007). Increased expression of miR-155 leads to higher levels of the tumour necrosis factor (TNF)-α transcript in an NF-κB-dependent manner (Tili et al., 2007), whilst enforced expression of miR-155 is mouse bone marrow *in vivo* triggers a myeloproliferative disorder characterized by an overabundance of macrophages (O'Connell et al., 2008). A recent study has shown an array of LPS-responsive genes to be further regulated following knock-down of miR-155 (Ceppi et al., 2009). For example, several MMPs were shown to increase in expression, including MMP-10.

4.2 Aims

In this chapter the migratory phenotype of bone marrow-derived macrophages is analysed in response to LPS on a variety of 2D ECM substrates; specifically type 1 collagen, plasma fibrinogen and plasma fibronectin. Given that MMP-10 has been shown to be repressed following 24 hours stimulation with LPS (see Chapter 3) the function of this specific protease in LPS-induced macrophage migration is explored with the use of siRNA targeting the MMP-10 transcript.

In Chapter 3 the LPS-driven repression of MMP-10 at 24 hours is shown to be NF-κB-dependent. As the action of miR-155 in macrophages also appears to be dependent on NF-κB signalling (Tili et al., 2007), and MMP-10 regulation may fall downstream of miR-155 (Ceppi et al., 2009), a potential relationship between miR-155 and LPS-induced macrophage migration is also explored with the use of antisense locked nucleic acid (LNA) oligonucleotides targeting miR-155

4.3 Results

4.3.1 Lipopolysaccharide and components of the extracellular matrix alter the migratory phenotype of bone marrow-derived macrophages

BMMs were cultured in 2D on thin coatings of several physiologically relevant extracellular matrix (ECM) components for 24 hours before time-lapse microscopy was performed and cell migration tracked and quantified. Phase contrast images of BMMs show the gross morphology of the macrophages cultured on type 1 collagen, plasma fibrinogen and plasma fibronectin with 0.2% fetal calf serum alone as a control (figure 4.1) Morphology was most dramatically altered by culture on type 1 collagen; cells appear small and round with very little obvious adhesion to the matrix component (figure 4.1 B). With 0.2% serum alone, or on plasma fibrinogen or fibronectin, BMMs have areas of lamellipodia and large protrusions, and vary in size and shape.

To further investigate macrophage response to 2D ECM components time-lapse microscopy was performed with images of BMMs captured every 10 minutes for 17 hours. When cultured on fibrinogen and fibronectin, velocity and accumulated distance of BMM migration varied very little compared with the 0.2% serum control (figure 4.2 A, B). This is unsurprising when we consider their similar morphologies (figure 4.1 A, C, D). There is a clear trend for repression of migration velocity and accumulated distance, however, on type 1 collagen; this is not statistically significant despite the stark difference in macrophage morphology on this substrate. Interestingly it is only when comparing the effect of ECM components on Euclidean distance migrated that we see a significant difference between the migratory phenotype of the BMMs on fibrinogen and fibronectin. Euclidean distance travelled by macrophages on fibronectin is significantly greater than that of macrophages on fibrinogen, type 1 collagen or with 0.2% serum alone (figure 4.2 C). This suggests that presence of this substrate triggers more directional persistence in these cells.

Plots of BMM trajectory on each ECM substrate reflect the quantitative results described above (figure 4.3). The migratory pattern of BMMs on fibrinogen, for example, varies little from that of cells exposed to 0.2% serum alone (figure 4.3 A, C). The trend for decreased migration velocity and distance on type 1 collagen is also reflected in the corresponding migration plot (figure 4.3 B), with three anomalous trajectories possibly accounting for the lack of significance seen in figure 4.2 A and B. Finally, the trajectory of BMMs on fibronectin (figure 4.3 D) clearly emulates the significantly increased Euclidean distance seen in figure 4.2 C. This initial profile of migratory phenotype was performed once.

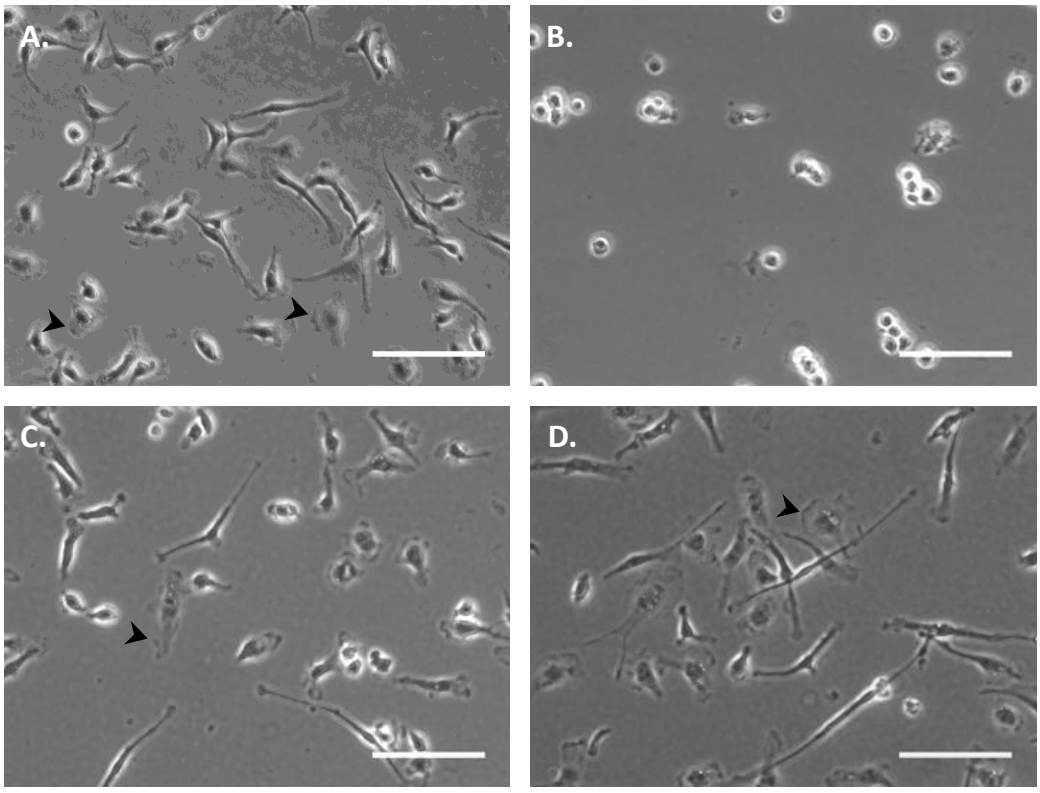

Figure 4.1 Phase contrast images of BMMs reveal changes in gross morphology in response to ECM components. Phase contrast images of BMMs after 24 hours culture with (A) 0.2% fetal calf serum, or on (B) type 1 collagen, (C) plasma fibrinogen and (D) plasma fibronectin. Arrowhead indicates lamellipodia. Scale bar = 150 µm.

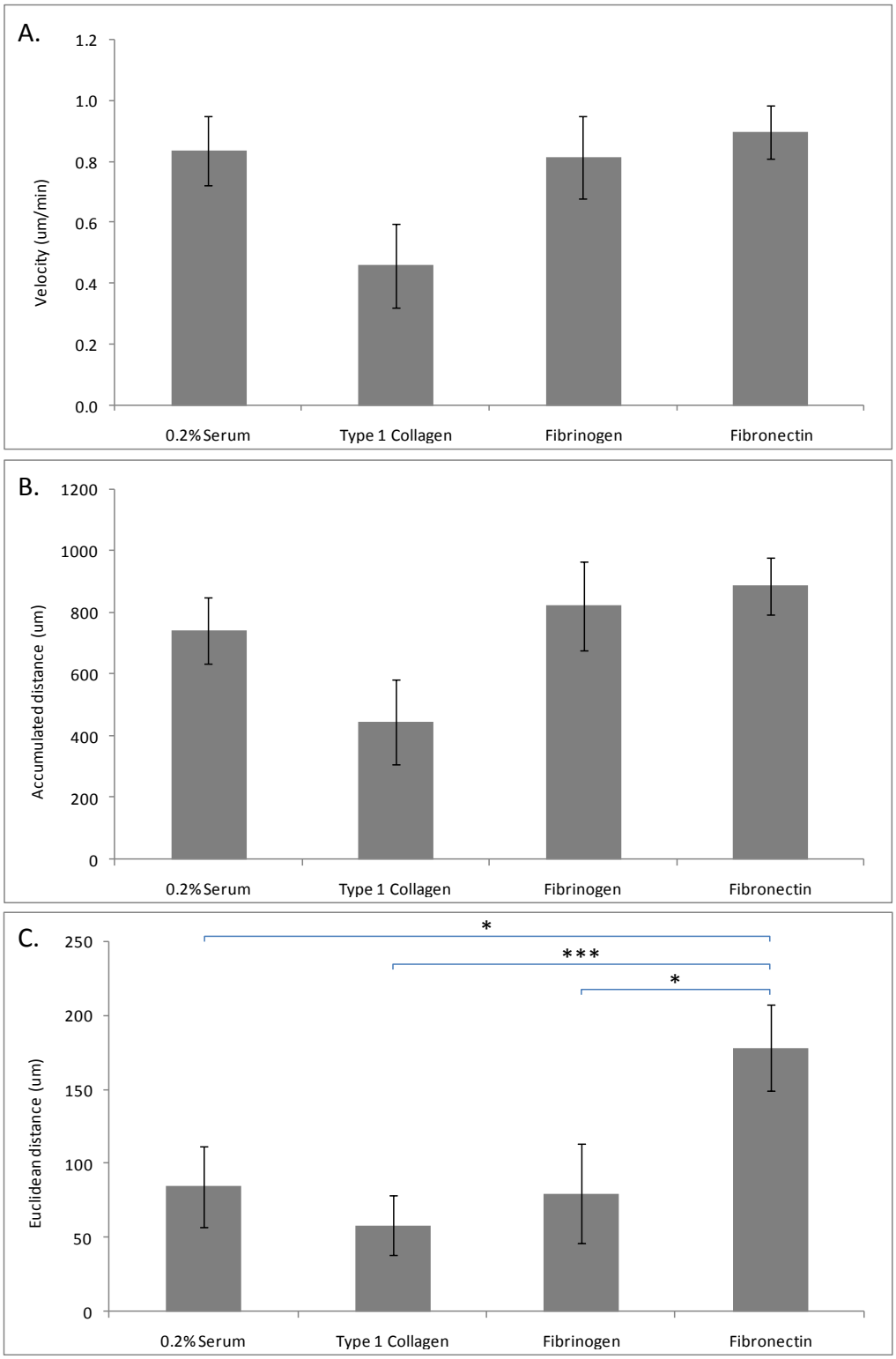

Figure 4.2 ECM components affect BMM migratory phenotype. Time-lapse images of BMMs on type 1 collagen, plasma fibrinogen and plasma fibronectin were captured every 10 minutes over a 17 hour period. 0.2% fetal calf serum acted as a control. (A) Migration velocity, (B) accumulated distance and (C) Euclidean distance of BMMs were analyzed with ImageJ processing software. Each bar represents the mean of 10 cells ± SEM. Statistical significance was determined using the Student's t-test. * $p \leq 0.05$, *** $p \leq 0.001$.

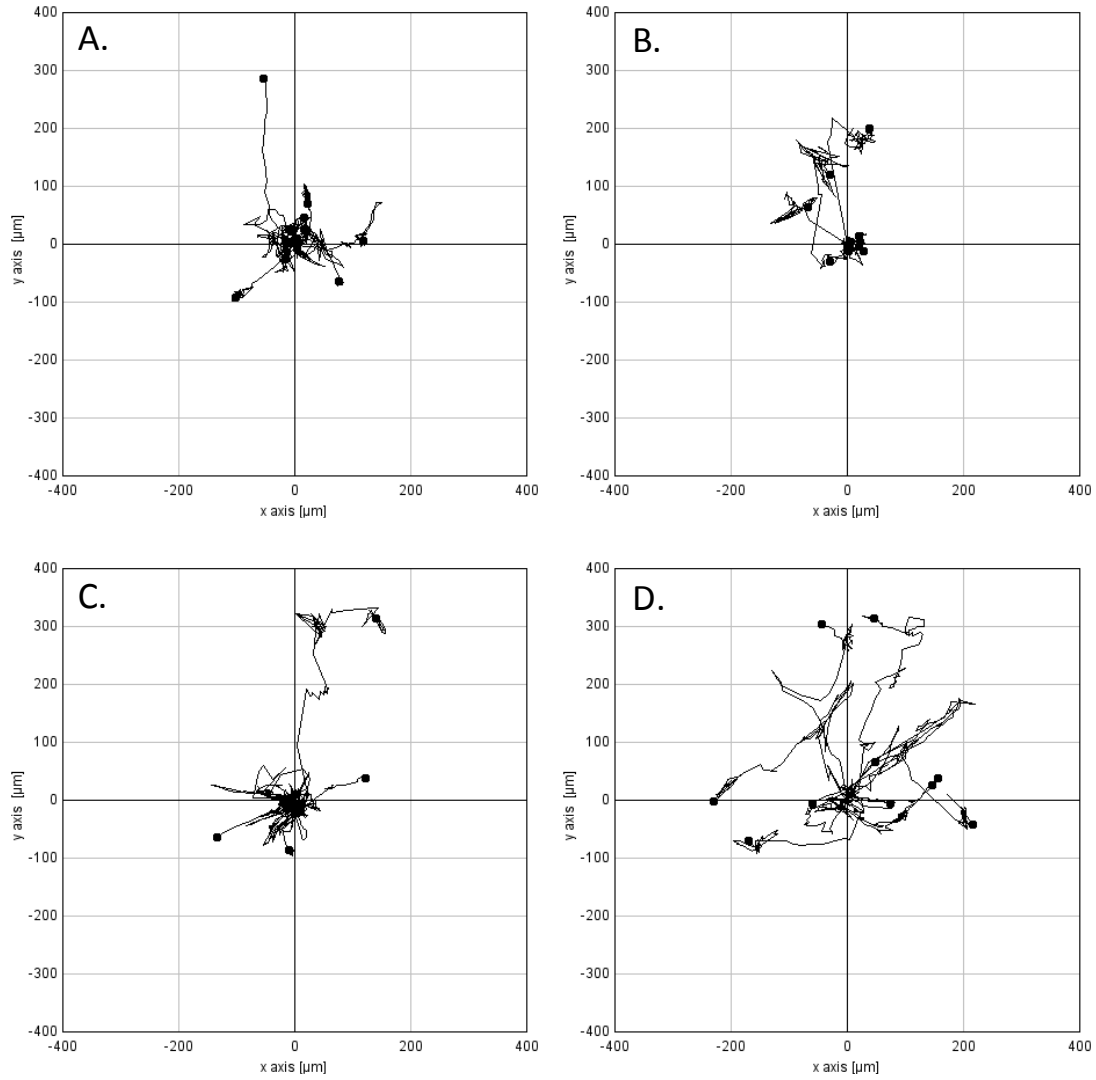

Figure 4.3 Plots of BMM migration trajectory on ECM components reflect migration velocity and distance. Cell trajectories were derived from time-lapse images of BMMs on (B) type 1 collagen, (C) plasma fibrinogen and (D) plasma fibronectin were captured every 10 minutes over a 17 hour period. (A) 0.2% fetal calf serum acted as a control. The migration of 10 cells per substrate was analyzed with ImageJ processing software.

To model the migratory phenotype of BMMs with relevance to the role of macrophages in response to infection, cells were cultured in 2D on plasma fibrinogen or plasma fibronectin in the presence of 10 ng/ml LPS for 24 hours before time lapse microscopy was performed and cell migration tracked. Phase contrast images of BMMs cultured either with 0.2% fetal calf serum with or without LPS; on plasma fibrinogen with or without LPS; or on plasma fibronectin with or

without LPS reveal variations in gross morphology (figure 4.4). Irrespective of their substrate, the morphology of the BMMs is affected by the presence of LPS; a high proportion of LPS treated BMMs appear to have longer and more numerous protrusions, more membrane ruffles and large areas of lamellipodia compared to their unstimulated controls (figure 4.4 B, D, F). The LPS treated cells on fibronectin in particular appear to have the largest proportion of lamellipodia per cell (figure 4.4 F).

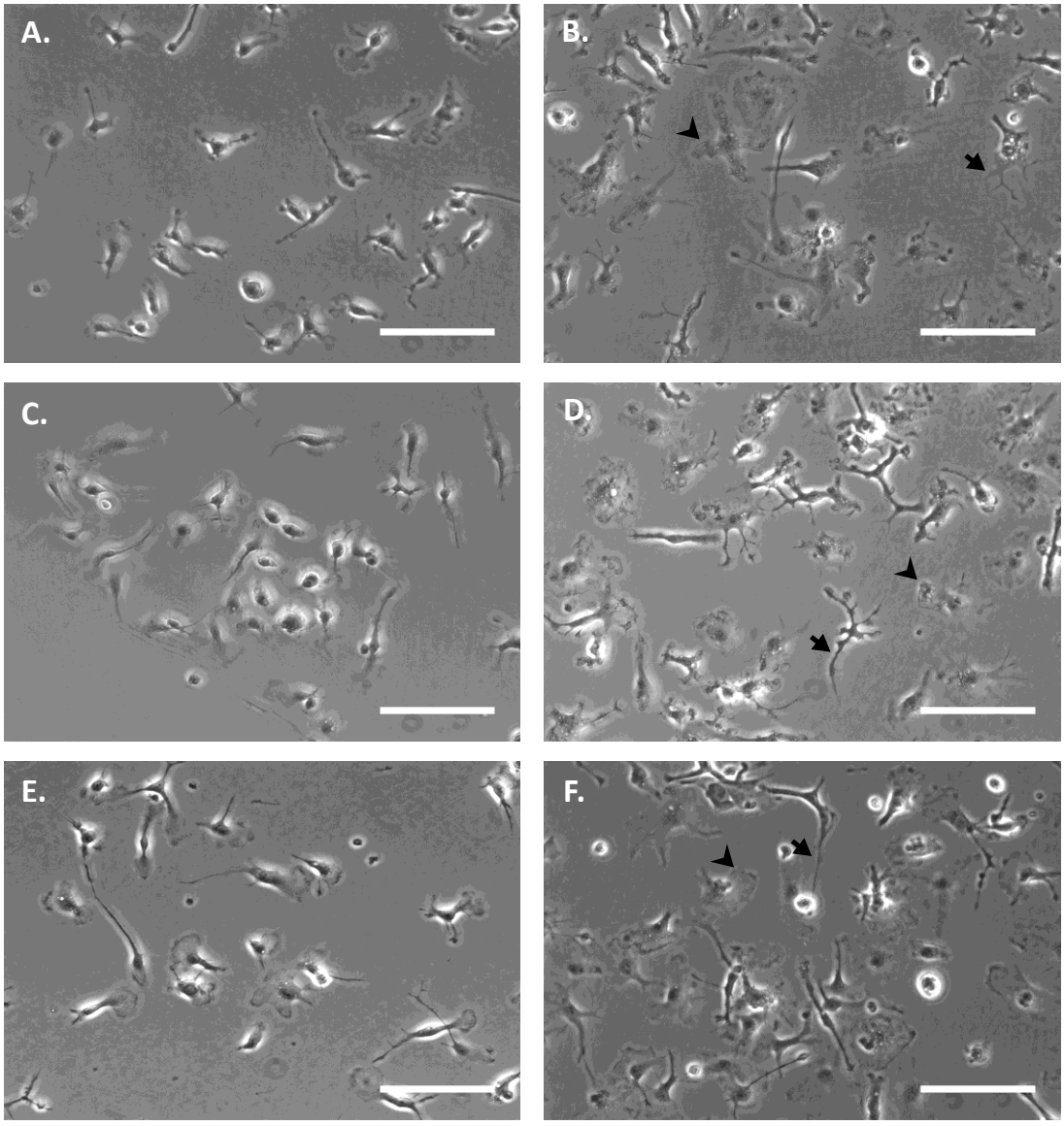

Figure 4.4 Phase contrast images of BMMs reveal changes in gross morphology in response to LPS. Phase contrast images of BMMs after 24 hours culture with (A) 0.2% fetal calf serum, (B) 0.2% fetal calf serum with 10 ng/ml LPS, or on (C) plasma fibrinogen, (D) plasma fibrinogen with 10 ng/ml LPS, (E) plasma fibronectin or (F) plasma fibronectin with LPS. Arrowheads indicate lamellipodia. Arrows indicate protrusions. Scale bar = 150 μm.

Velocity and distance migrated was also analysed with and without LPS pre-treatment (figure 4.5). When cultured without LPS we see a similar pattern in BMM migratory phenotype on fibrinogen and fibronectin and with 0.2% Serum alone as that observed in figure 4.2; there is a slight trend toward increased migratory velocity and accumulated distance for BMMs on fibronectin. Again there appears to be trend toward increase in Euclidean distance migrated by unstimulated cells on fibronectin, although in this case it is not statistically significant (figure 4.5 C). When stimulated with 10 ng/ml LPS, BMMs on fibrinogen, fibronectin, and with 0.2% serum alone appear to lose their migratory capacity. This is particularly evident on fibronectin, showing a statistically significant drop in migration velocity and accumulated distance (figure 4.5 A, B). Interestingly, stimulation with LPS appears to provoke more directional persistence in migration with BMMs on fibrinogen and in 0.2% serum alone showing a trend toward increased Euclidean distance. No such trend is observed for cells on fibronectin however (figure 4.5 C). Again, Plots of BMM trajectory on each ECM substrate reflect the velocity and distance quantified (figure 4.6). In particular these echo the increased persistence in BMM migration on fibrinogen and with 0.2% serum treated with LPS (figure 4.6 B, D).

The initial assay of macrophage morphology and migration in response to LPS was performed once. The significant down regulation of BMM migration velocity and distance on fibronectin with LPS pre-treatment has been reproduced three times.

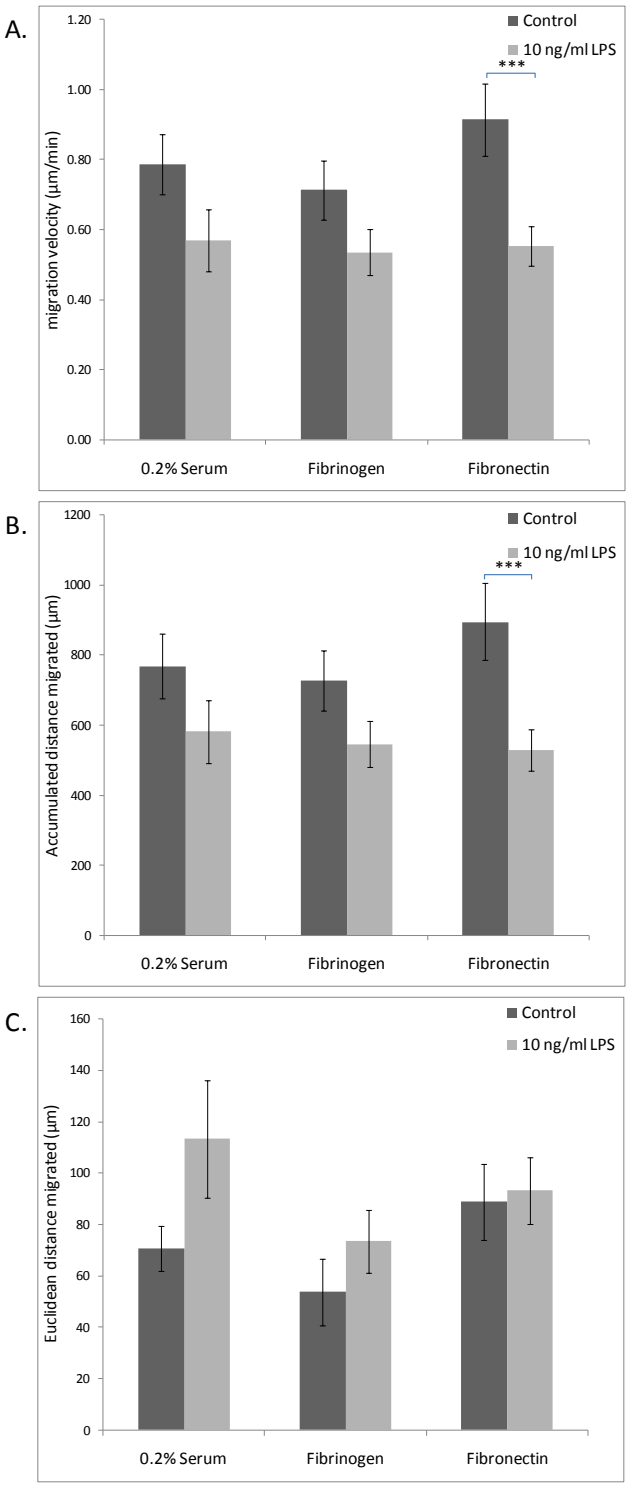

Figure 4.5 LPS effects BMM migratory phenotype. Time-lapse images of BMMs on plasma fibrinogen and plasma fibronectin stimulated with LPS were captured every 10 minutes over a 17 hour period. 0.2% fetal calf serum acted as a control. (A) Migration velocity, (B) accumulated distance and (C) Euclidean distance of BMMs were analyzed with ImageJ processing software. Each bar represents the mean of 17 cells ± SEM. Statistical significance was determined using the Student's t-test. *** $p \leq 0.001$.

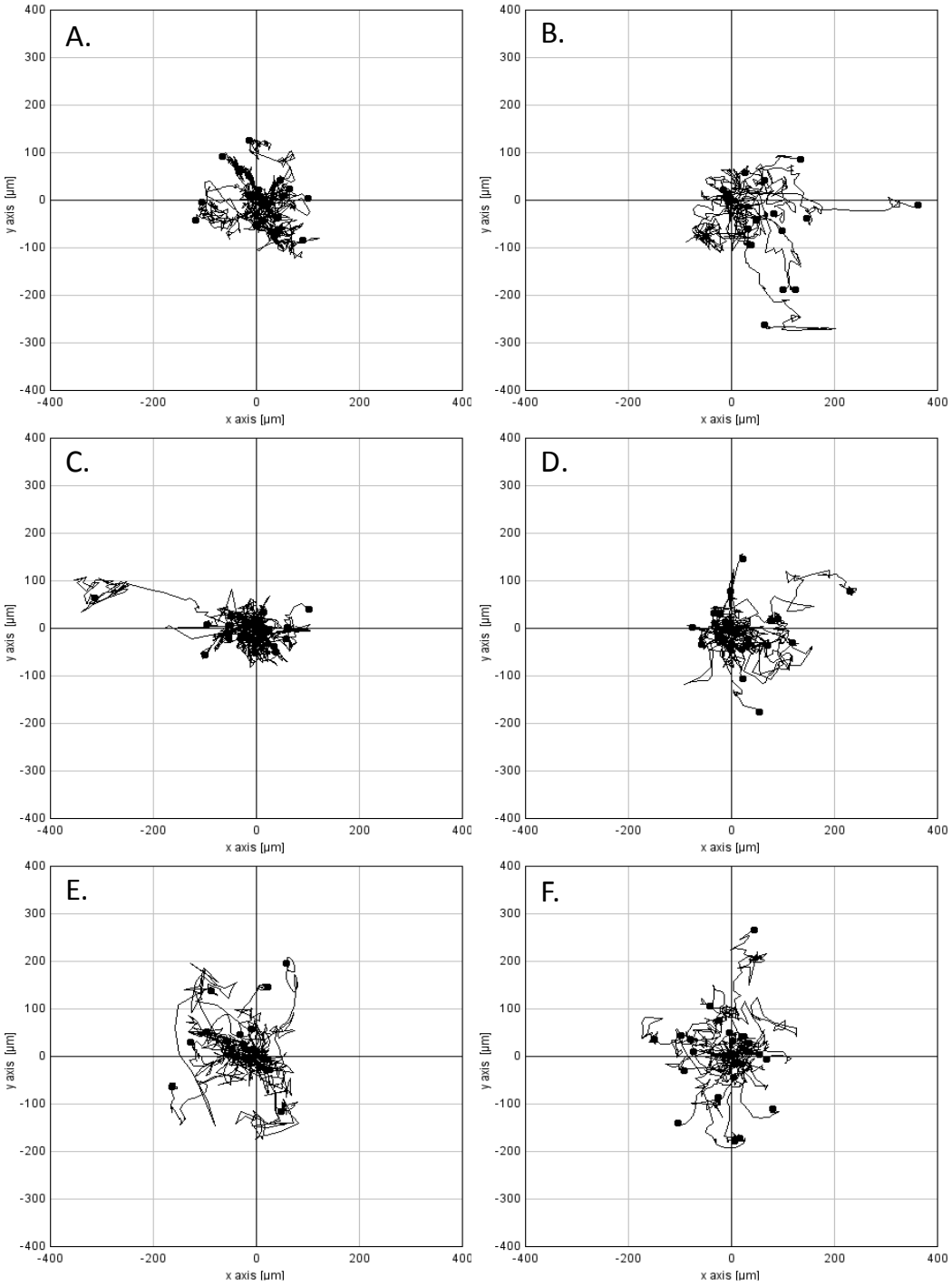

Figure 4.6 Plots of BMM trajectory on ECM components reflect migration velocity and distance. Cell trajectories were derived from time-lapse images of BMMs after 24 hours culture with (A) 0.2% fetal calf serum, (B) 0.2% fetal calf serum with 10 ng/ml LPS, or on (C) plasma fibrinogen, (D) plasma fibrinogen with 10 ng/ml LPS, (E) plasma fibronectin or (F) plasma fibronectin with LPS were captured every 10 minutes over a 17 hour period. The migration of 17 cells per substrate was analyzed with ImageJ processing software.

4.3.2 Successful transfection and knockdown of MMP-10 in bone marrow-derived macrophages with siRNA

In order to investigate the potential role of MMP-10 expression on macrophage migratory phenotype a gene silencing approach was taken. BMMs were transfected with siRNA targeting the murine MMP-10 transcript (siMMP-10) in 10% serum to preserve viability. As a control against non-specific effects of transfection BMMs were also transfected with an Alexa488 fluorophore tagged scrambled siRNA (siScrambled). This enabled visualisation of successful transfection and quantification of transfection efficiency (figure 4.7). Transfection of BMMs with both 25 nM and 15 nM siScrambled results in a successful incorporation into the cytoplasm of BMMs with an efficiency of 70.3% and 61.2 %, respectively (figure 4.7). Minimal autofluorescence could be seen from untransfected cells (data not shown).

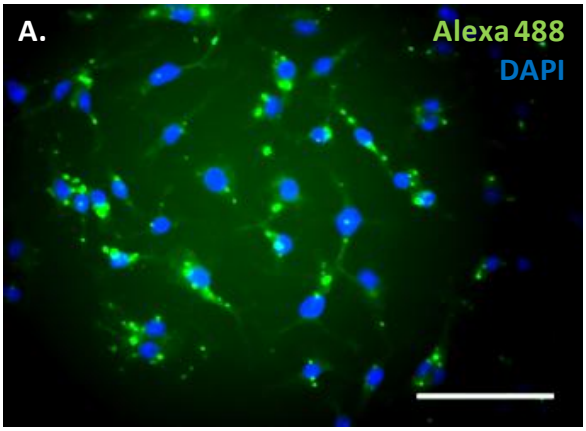

B.		Total Cells	Transfected Cells	Transfection Efficiency
15nM	1	44	22	50.0%
	2	17	14	82.4%
	3	43	22	51.2%
average				**61.2%**
25nM	1	49	37	75.5%
	2	50	31	62.0%
	3	49	36	73.5%
average				**70.3%**

Figure 4.7 Quantification of BMM transfection efficiency with Alexa488 flurophore tagged scrambled siRNA. BMMs were cultured in an Ibidi 18 well µ-Slide before transfection with 25 nM or 15 nM siScrambled for 24 hours. Cells were fixed and DAPI stained before transfection efficiency was calculated. (A) BMMs transfected with Alexa 488-tagged 15 nM siScrambled are shown. (B) Transfection efficiency was calculated as the average of percentage cells transfected for three fields of view.

To confirm knock down of MMP-10 mRNA and protein in siMMP-10 transfected BMMs qRT-PCR (figure 4.8) and immunocytochemistry (figure 4.9) were performed. Preliminary experiments revealed greater repression of MMP-10 in BMMs treated with 15 nM siMMP-10, as opposed to 25 nM (data not shown). For this reason only 15 nM siMMP-10 transfection was repeated in triplicate for qRT-PCR as shown. qRT-PCR reveals a significant reduction in MMP-10 mRNA expression

following 15 nM siMMP-10 transfection compared to 15 nM siScramled control (figure 4.8). There is a trend toward repression of MMP-10 compared with control cells (also in 10% serum). This is not statistically significant but the corresponding C_T values indicate that there is a repression in expression in all three samples (figure 4.8 B).

MMP-10 immunostaining of BMMs was markedly reduced following siMMP-10 transfection (figure 4.9). As seen in Chapter 3, these macrophages show a strong punctuate staining for MMP-10 when untreated. The extent of MMP-10 protein repression varies between fields of view reflecting the less than 100% transfection efficiency (data not shown).

Successful transfection of the Alexa488 fluorophore tagged siScrambled has been seen in three out of three experiments. qRT-PCR of MMP-10 mRNA has been performed three times, revealing successful knockdown of MMP-10 with all experiments performed in triplicate, whilst immunohistochemical analysis of MMP-10 protein knockdown has been performed once.

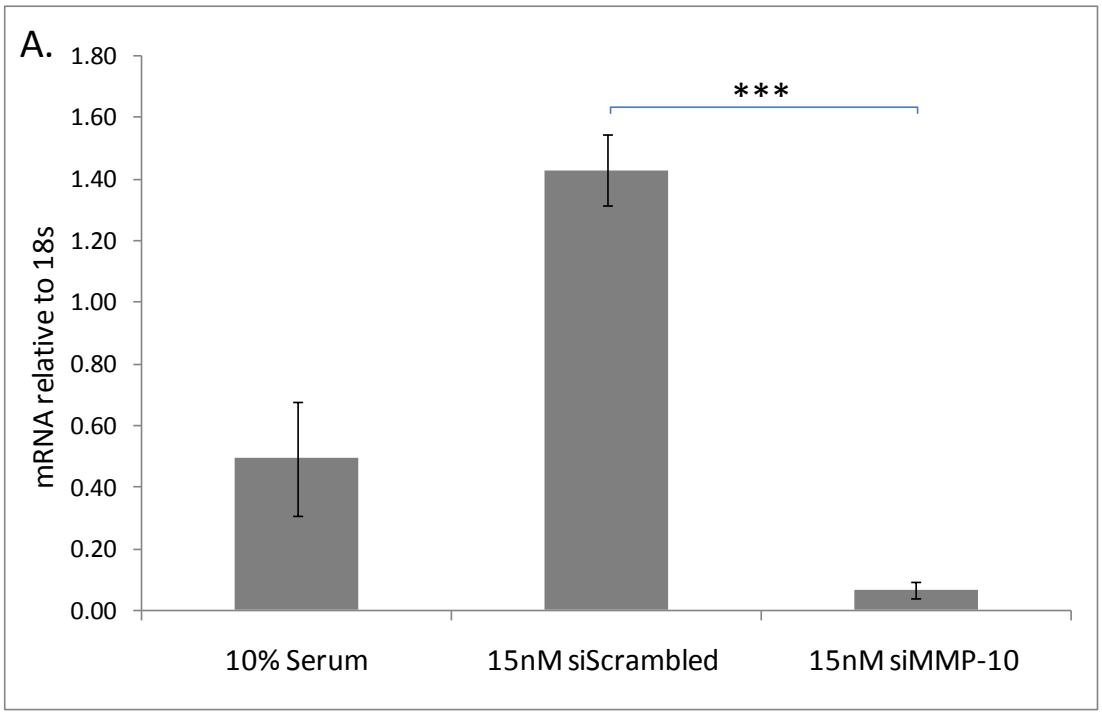

B.

Treatment	C_T value 1	C_T value 2	C_T value 3
10% Serum	35.38	34.36	33.61
15nM siScrambled	33.27	33.21	33.27
15nM siMMP-10	37.29	38.64	37.30

Figure 4.8 qRT-PCR for MMP-10 in BMMs transfected with siMMP-10. Cells were treated with 15 nM siRNA targeting the MMP-10 transcript for 24 hours before RNA was extracted and qRT-PCR was performed. (A) Data was analysed by relative quantification and normalized to 18S. (B) Corresponding CT values are shown. Each bar represents the mean of 3 samples ± SEM. Statistical significance was determined using the Student's t-test. *** $p \leq 0.001$.

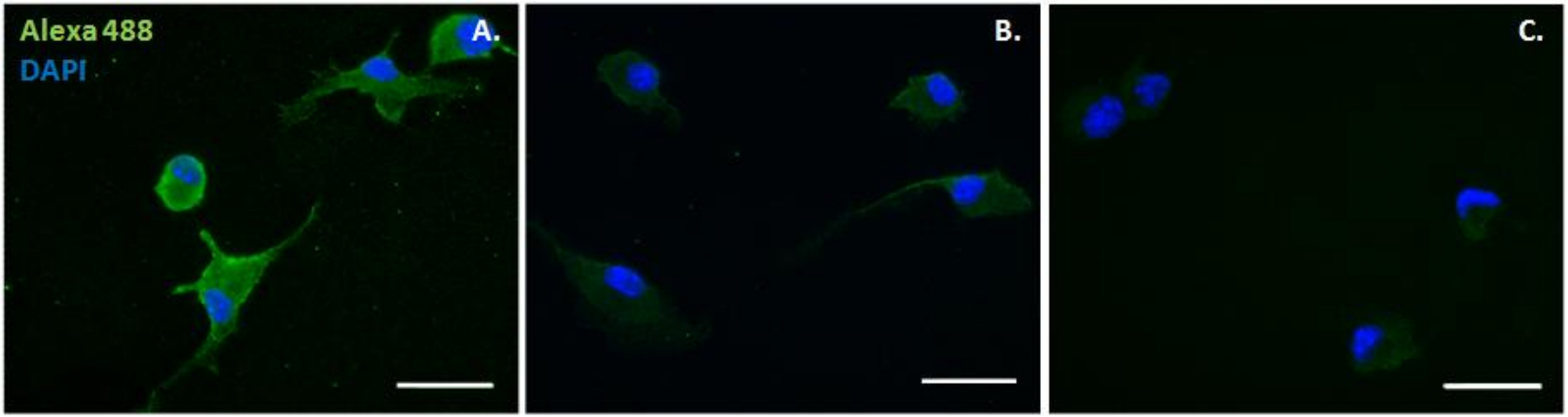

Figure 4.9 Immunocytochemical staining for MMP-10 in BMMs transfected with siMMP-10. Cells were cultured on glass cover slips for 24 hours before transfection with 15 nM siRNA targeting the MMP-10 transcript for a further 24 hours. (A) Untreated BMMs. (B) BMMs transfected with siMMP-10 for 24 hours. (C) Untreated secondary only control. Scale bar = 25 µM

4.3.3 siRNA driven repression of MMP-10 alters the migratory phenotype of bone marrow-derived macrophages on fibronectin

Having established the efficacy of siMMP-10 in BMMs, time lapse migration assays were performed with transfected cells as above. It is important to note that all subsequent experiments were performed in 10% serum to preserve cell viability in the presence of siRNA. Again, the gross morphology of BMMs seems to be most drastically altered in LPS-stimulated cells (figure 4.10 G), however both concentrations of siMMP-10 appear to have some effect on cell size and shape. BMMs transfected with 25 nM siMMP-10 appear to have far fewer protrusions and far greater areas of lamellipodia compared to their controls (figure 4.10 C), similar to the LPS-stimulated cells. BMMs transfected with 15 nM siMMP-10 do not appear to have such a dramatically altered phenotype (figure 4.10 F), however cell protrusions do appear shorter compared to their controls. SiScrambled and the transfection vehicle alone appear to have no effect on gross cell morphology.

Again, velocity and distance migrated were analysed for siMMP-10 transfected BMMs on fibronectin (figure 4.11). This verifies the significant reduction in migration velocity and accumulated distance of LPS-stimulated BMMs compared with those in 10% serum alone. Interestingly in this instance there also appears to be a trend for reduction in Euclidean distance travelled by LPS-stimulated BMMs compared with 10% serum (figure 4.11 C). A small but significant repression in macrophage migration velocity, accumulated distance and Euclidean distance in both 25 nM and 15 nM siMMP-10 transfected cells compared with their siScrambled controls was also observed. These observations are consistent with the LPS-induced repression of both MMP-10 expression and migration in BMMs on fibronectin. Corresponding migration plots showing the trajectories of 25 individual cells clearly reflect the reduction in migration distance quantified for 25 nM siMMP-10, 15 nM siMMP-10 and LPS treated macrophages (figure 4.12).

Significant reduction in BMM migration velocity and accumulated distance in siMMP-10 transfected cells has been seen in assays performed with BMMs extracted from three different mice. Data shown here is representative of cells from one mouse per phenotype.

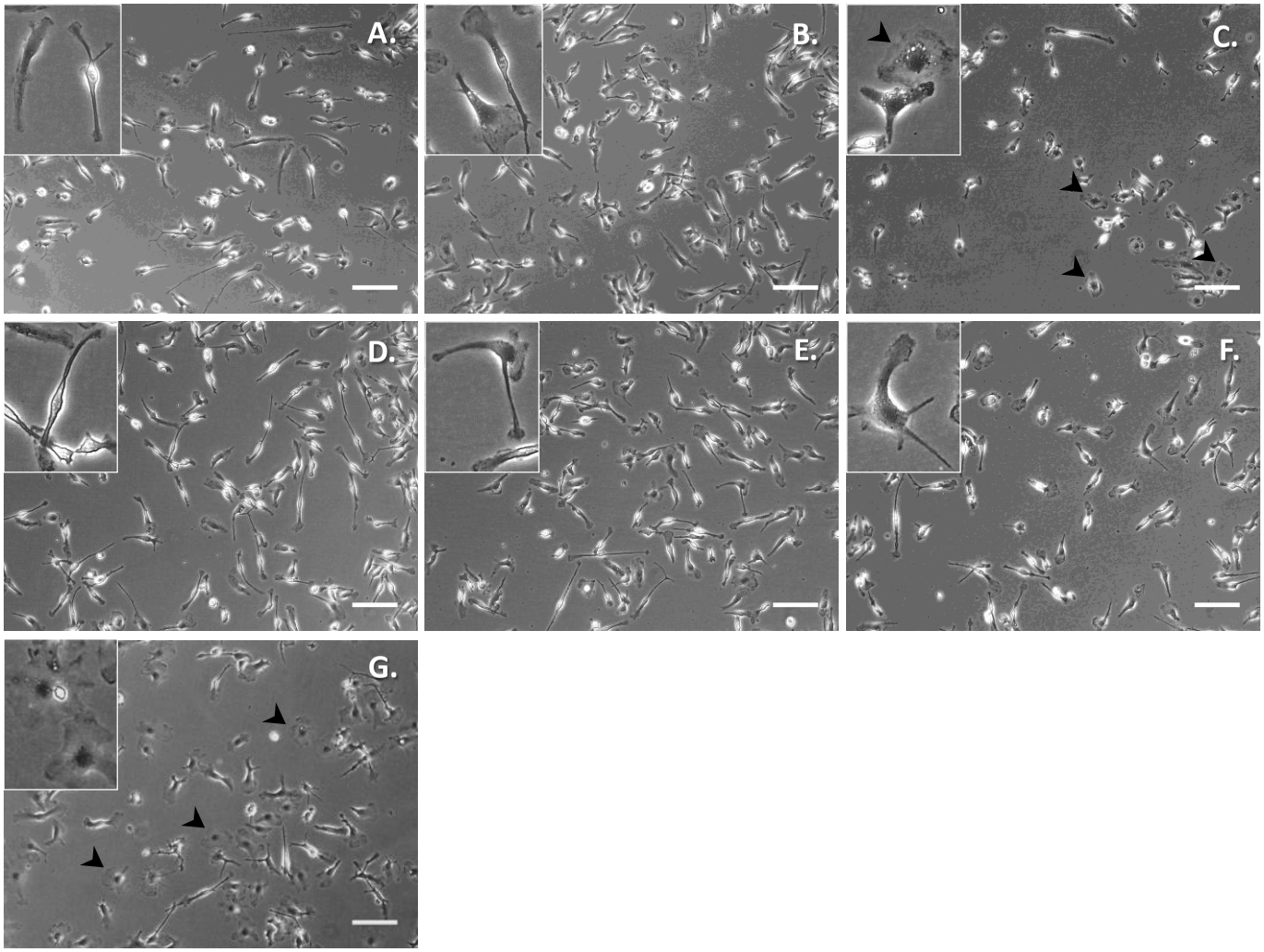

Figure 4.10 Phase contrast images of BMMs reveal changes in gross morphology in response to siMMP-10 and LPS. Phase contrast images of BMMs on fibronectin after 24 hours culture with (A) 10% fetal calf serum, or 10% fetal calf serum with either (B) 25 nM siScrambled, (C) 25 nM siMMP-10, (D) transfection vehicle control, (E) 15 nM siScrambled, (F) 15 nM siMMP-10 or (G) 10 ng/ml LPS. Arrowheads indicate lamellipodia. Scale bar = 150 µm. Insets cropped from original image.

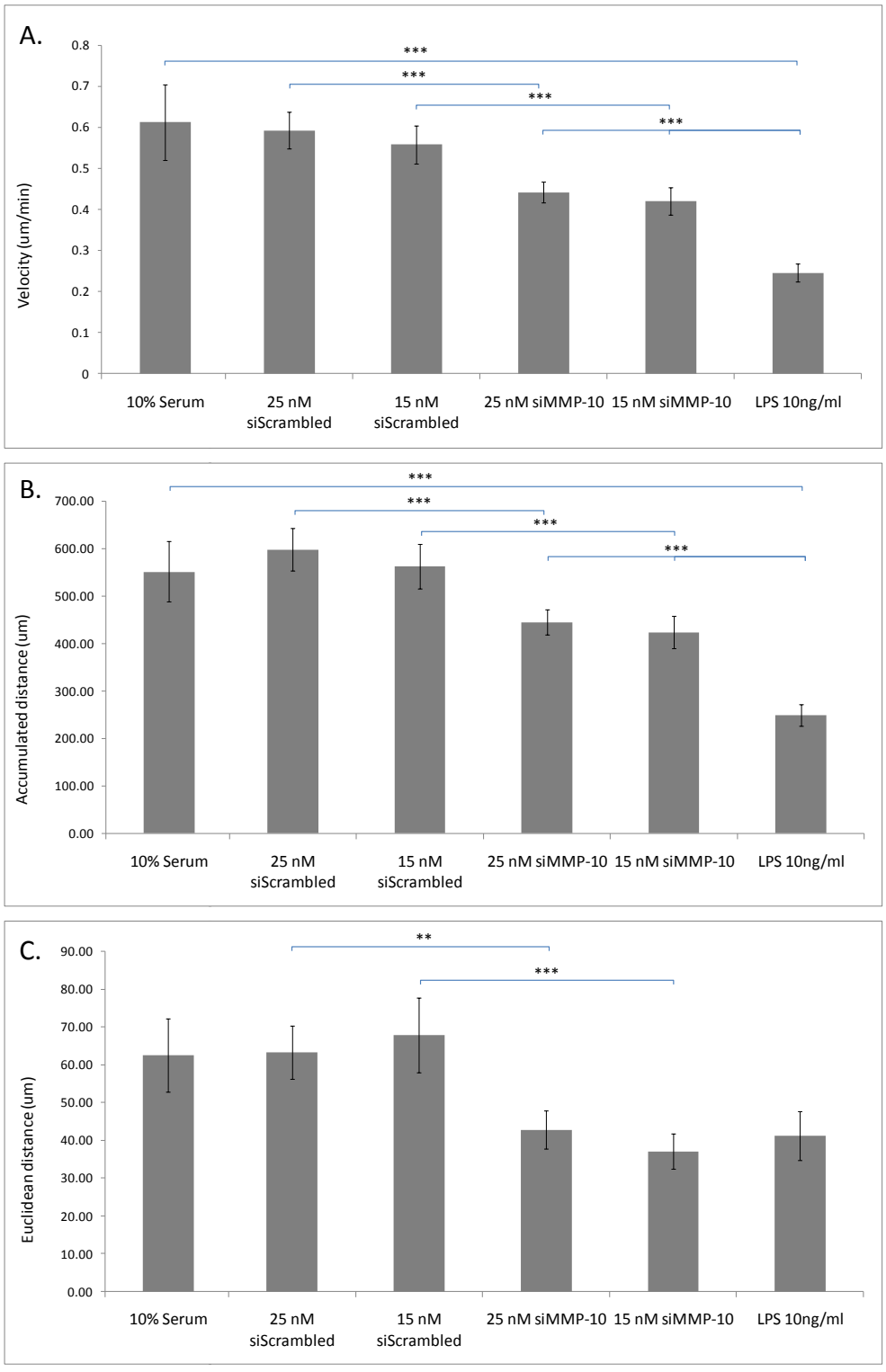

Figure 4.11 siMMP-10 and LPS effect BMM migratory phenotype. Time-lapse images of BMMs on plasma fibronectin transfected with siMMP-10 or stimulated with LPS were captured every 10 minutes over a 17 hour period. (A) Migration velocity, (B) accumulated distance and (C) Euclidean distance of BMMs were analyzed with ImageJ processing software. Each bar represents the mean of 50 cells ± SEM. Statistical significance was determined using the Student's t-test. ** $p \leq 0.01$, *** $p \leq 0.001$.

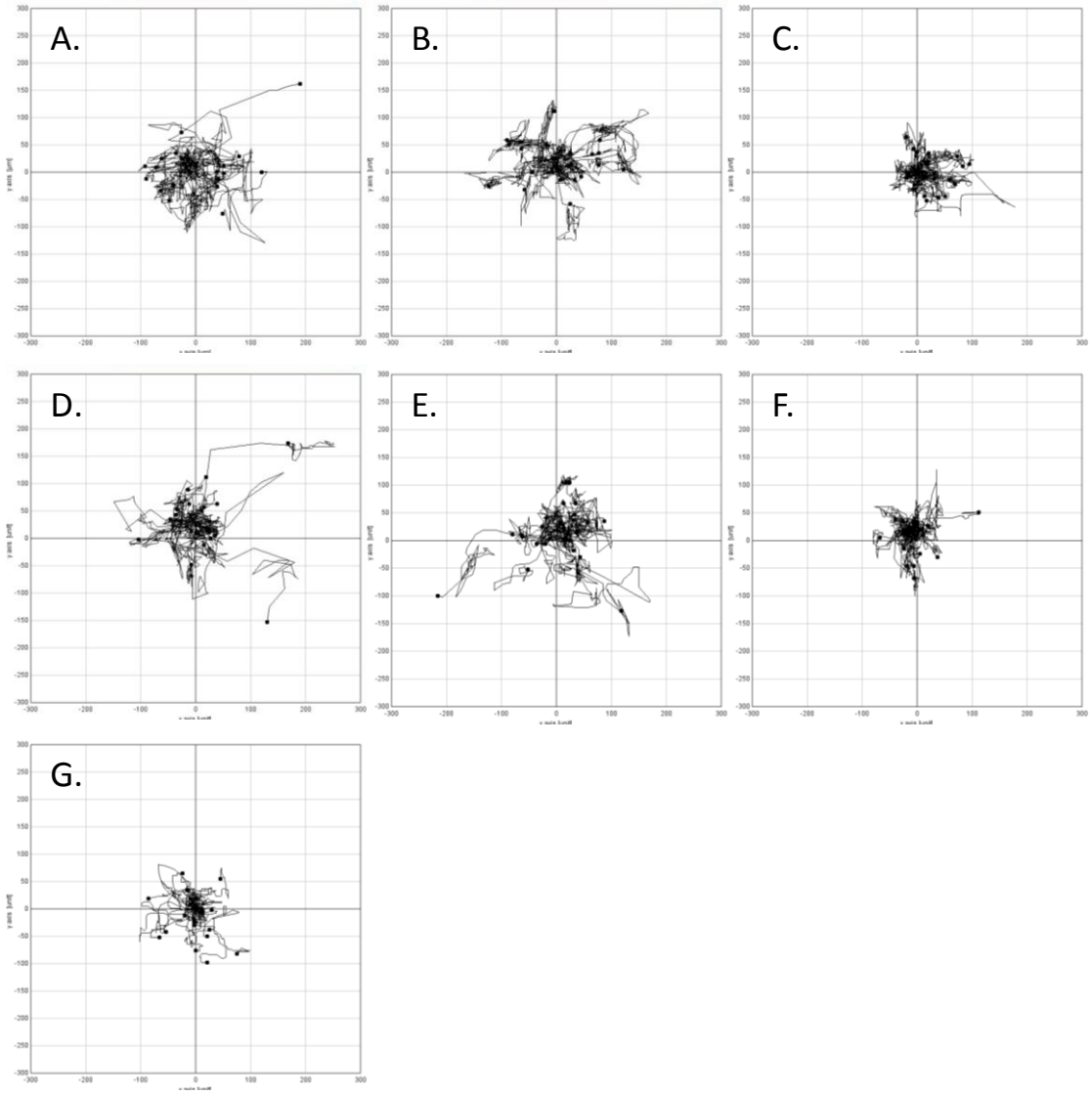

Figure 4.12 Migration plots of siMMP-10 transfected BMMs on fibronectin reflect migration velocity and distance. Cell trajectories were derived from time-lapse images of BMMs after 24 hours culture with (A) 10% fetal calf serum, or 10% fetal calf serum with either (B) 25 nM siScrambled, (C) 25 nM siMMP-10, (D) transfection vehicle control, (E) 15 nM siScrambled, (F) 15 nM siMMP-10 or (G) 10 ng/ml LPS were captured every 10 minutes over a 17 hour period. The migration of 25 cells per substrate was analyzed with ImageJ processing software.

4.3.4 Recombinant human MMP-10 protein can rescue the effects of siRNA driven MMP-10 repression on bone marrow-derived macrophage migration on fibronectin

Given that siMMP-10 is shown to significantly reduce BMM migration velocity, accumulated distance and Euclidean distance from start point it is important to further investigate whether this effect is a consequence of reduction in MMP-10 protein secretion. Approximate endogenous MMP-10 protein secretion from BMMs over 24 hours was estimated from previous western blots and human MMP-10 ELISA. Time lapse migration assays were performed as above, this time including siMMP-10 transfected BMMs cultured with 2.7 ng/ml recombinant human MMP-10 (rhMMP-10) for 6 hours before time lapse microscopy began. Again, there appears to be a change in gross morphology in cells treated with siMMP-10 or exposed to LPS. In this case the BMMs transfected with siMMP-10 alone appear the most morphologically different from their controls, with the majority of cells appeared rounded with large areas of lamellipodia (figure 4.13 D). The majority of BMMs transfected with siMMP-10 then cultured with rhMMP-10 also appear to have large areas of lamellipodia, as do those stimulated with LPS, however their difference in gross morphology is not as striking compared with control cells, or those seen in the previous experiment.

Confirming the previous results, both LPS-stimulation and transfection with siMMP-10 repressed migration velocity and accumulated distance of BMMs on 2D plasma fibronectin (figure 4.14 A, B). Importantly, the addition of rhMMP-10 to siMMP-10 transfected BMMs for 6 hours significantly reverses the effect of the RNA interference on velocity and accumulated distance, restoring their migratory phenotype to that of siScrambled treated cells. Interestingly, in this case (as opposed to figure 4.11) the effect of siMMP-10 appears to be stronger than that of LPS. This, however, is not statistically significant.

Corresponding migration plots showing the trajectories of 50 individual cells are shown in figure 4.15 A – E. These reflect the reduction in accumulated and Euclidean migration distance quantified for 15 nM siMMP-10 transfected macrophages (D) compared with their controls. Figure 4.15 E also reflects the trend for reduction in Euclidean distance migrated by the rhMMP-10 rescued BMMs and the perceived trend for increase in Euclidean distance migrated by LPS – stimulated cells. A montage of frame capture images for untreated, siMMP-10 transfected, LPS treated and rhMMP-10 rescued cells corroborates the quantitative results (figure 4.16), with both untreated and rhMMP-10 rescued BMMs migrating the greatest distance from their starting point. These results are representative of the outcome of assays performed with BMMs extracted from three different mice.

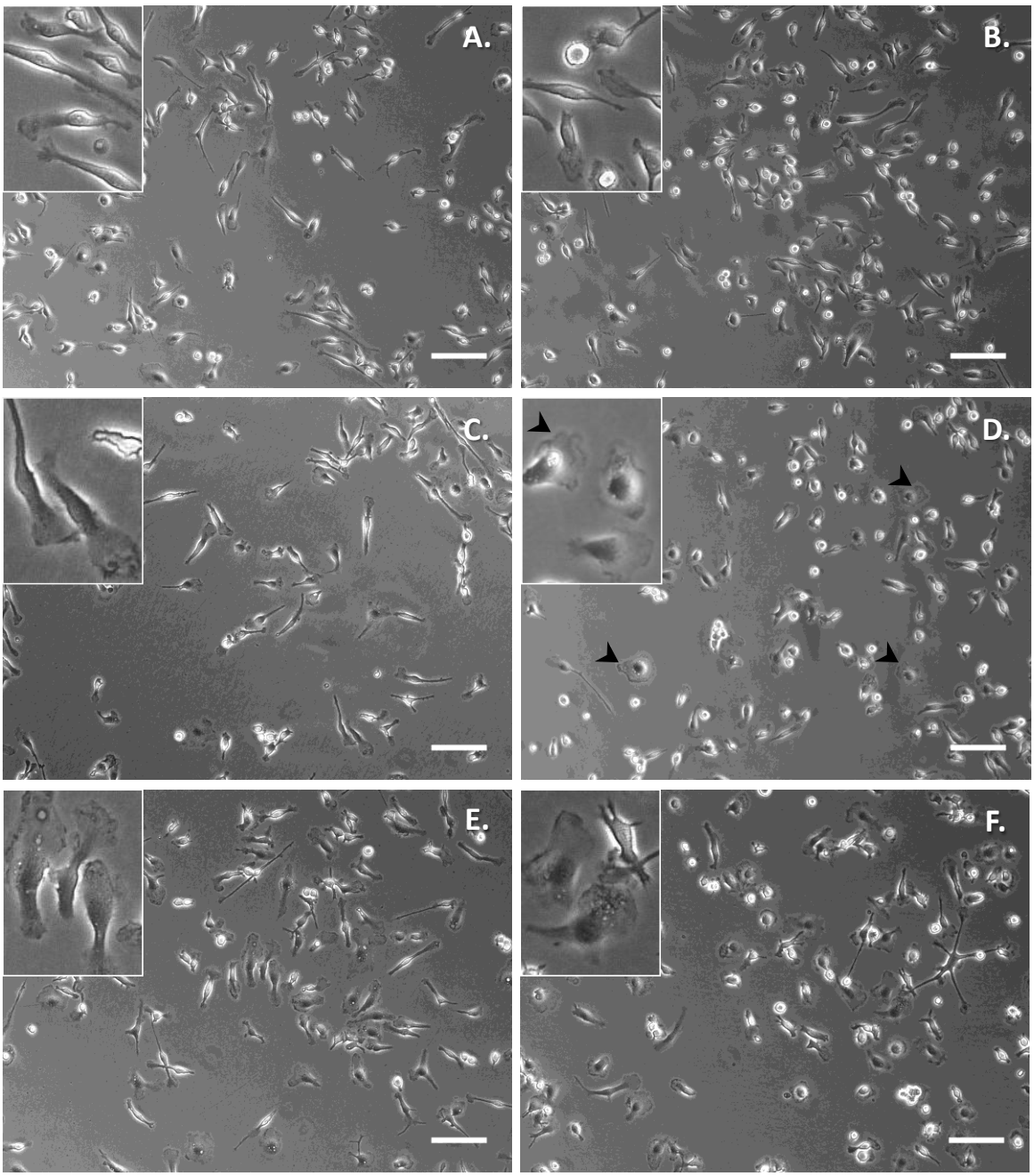

Figure 4.13 Phase contrast images of BMMs reveal changes in gross morphology in response to siMMP-10, LPS and rhMMP-10. Phase contrast images of BMMs on fibronectin after 24 hours culture with (A) 10% fetal calf serum, or 10% fetal calf serum with either (B) 15 nM siScrambled, (C) 15 nM siScrambled + 6 hours rhMMP-10, (D) 15 nM siMMP-10, (E) 15 nM siMMP-10 with 6 hours rhMMP-10, (F) 10 ng/ml LPS. Arrowheads indicate lamellipodia. Scale bar = 150 µm. Insets

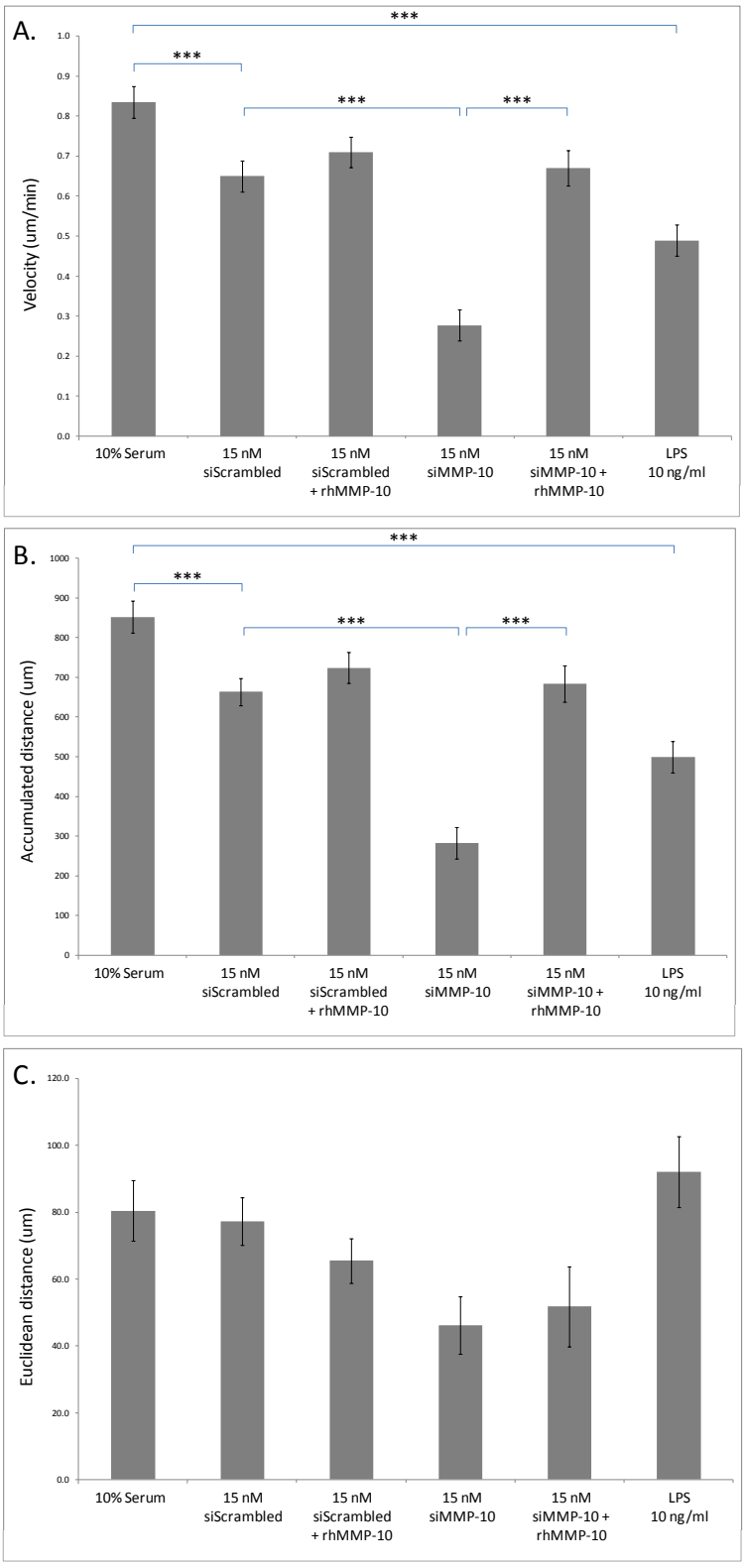

Figure 4.14 rhMMP-10 rescues siMMP-10 effect on BMM migratory phenotype. Time-lapse images were captured every 10 minutes over a 17 hour period of BMMs on plasma fibronectin 24 hours after transfection with siMMP-10 with 6 hours rhMMP-10. (A) Migration velocity, (B) accumulated distance and (C) Euclidean distance of BMMs were analyzed with ImageJ processing software. Each bar represents the mean of 50 cells ± SEM. Statistical significance was determined using the Student's t-test. *** $p \leq 0.001$.

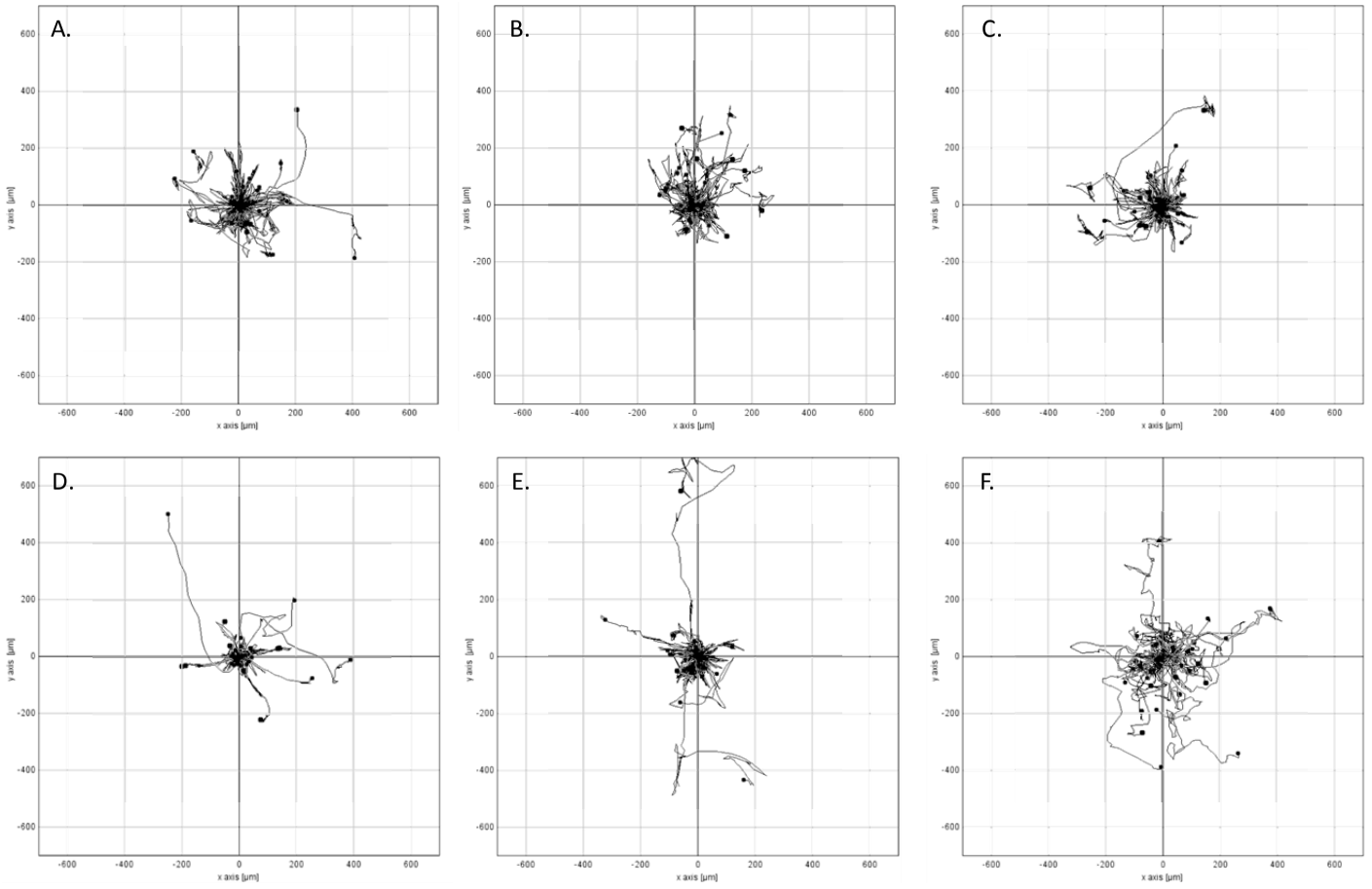

Figure 4.15 Migration plots of siMMP-10 transfected BMMs rescued with rhMMP-10 reflect migration velocity and distance on fibronectin. Time-lapse images of BMMs after 24 hours culture with (A) 10% fetal calf serum, or with 10% fetal calf serum and either (B) 15 nM siScrambled, (C) 15 nM siScrambled + 6 hours rhMMP-10, (D) 15 nM siMMP-10, (E) 15 nM siMMP-10 with 6 hours rhMMP-10, and (F) 10 ng/ml LPS were captured every 10 minutes over a 17 hour period. The migration of 50 cells per substrate was analyzed with ImageJ processing software.

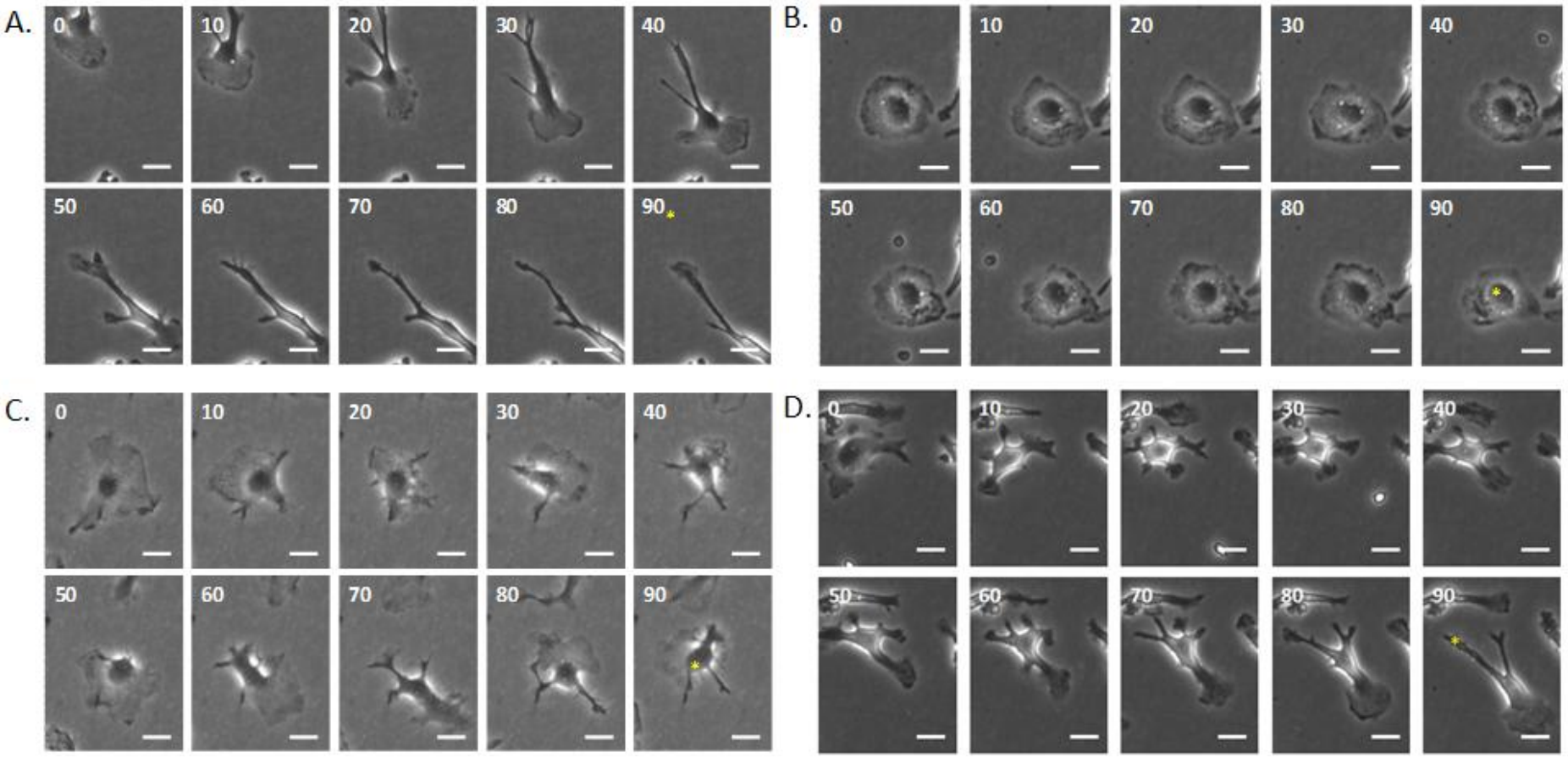

Figure 4.16 Frame capture montage demonstrates that rhMMP-10 rescues siMMP-10 effect on BMM migratory phenotype. Phase contrast time-lapse images were captured every 10 minutes over a 17 hour period of BMMs on plasma fibronectin. The position of one cell treated with (A) 10% fetal calf serum control, or 10% fetal calf serum with either (B) 15 nM siMMP-10, (C) 10 ng/ml LPS or (D) 15 nM siMMP-10 + 6 hrs rhMMP-10 is shown over 90 minutes. * indicates position of cell nucleus at start of 90 minutes. Scale bar = 30 µM

4.3.5 Antisense LNA oligonucleotide driven repression of microRNA-155 may alter the migratory phenotype of bone marrow-derived macrophages on fibronectin

A microarray analysis of 518 unique murine microRNAs was performed for RAW264.7 macrophages (see Appendix, figure 8.2). This confirmed a high basal level of miR-155 expression and a robust increase in expression 4 hours post-LPS (figure 4.17 A, B). Given that LPS-driven repression of MMP-10 mRNA can be reversed by inhibition of the NF-κB signalling pathway (Chapter 3, figure 3.19) and that MMP-10 is up-regulated in LPS-stimulated miR-155 knock-down monocytic cells (Ceppi et al., 2009), miR-155 expression was also analysed in response to the IκB kinase inhibitor BMS-345541. A trend for inhibition of LPS-driven miR-155 induction following simultaneous incubation with BMS-345541 was observed (figure 4.17), suggesting that MMP-10 and miR-155 are regulated by LPS via a similar signalling pathway.

The microarray analysis of RAW264.7 macrophages was performed once on single samples.

Antisense locked nucleic acid (LNA) oligonucleotides complementary to the miR-155 sequence (anti-miR-155) were utilised to further explore the role of this microRNA in macrophages. These oligonucleotides bind to their complimentary sequence and inhibit the action of the target miRNA. LNA technology limits nucleotide binding to the ideal conformation as determined by Watson-Crick base pairing rules, thus increasing the stability of the oligonucleotide binding. To determine whether transfection of anti-miR-155 in BMMs was successful expression of TNF-α mRNA was analysed. TNF-α transcript levels have been found to respond to changes in miR-155 expression in an NF-κB-dependent manner (Tili et al., 2007) thus providing an indirect method of quantifying miR-155 expression. A trend for repression of TNF-α mRNA expression was observed in BMMs exposed to anti-miR-155 for 24 hours (figure 3.20) thus suggesting the anti-miR was successfully repressing its target.

TNF-α mRNA analysis was performed once on single samples of anti-miR-155 transfected BMMs.

To investigate the potential function of miR-155 in macrophage migration BMMs from two mice were transfected with a range of anti-miR-155 concentrations before time-lapse migration assays on fibronectin were performed (figure 4.21). No effect on BMM velocity or accumulated distance was observed except for a minor repression caused by 10 nM Scramble-miR. Anti-miR-155 did however cause a statistically significant reduction (~40%) in Euclidean distance migrated (figure 4.21 C). This suggests macrophages were migrating in a less directional manner. These results are representative of migration assays performed once with BMMs extracted from two different mice.

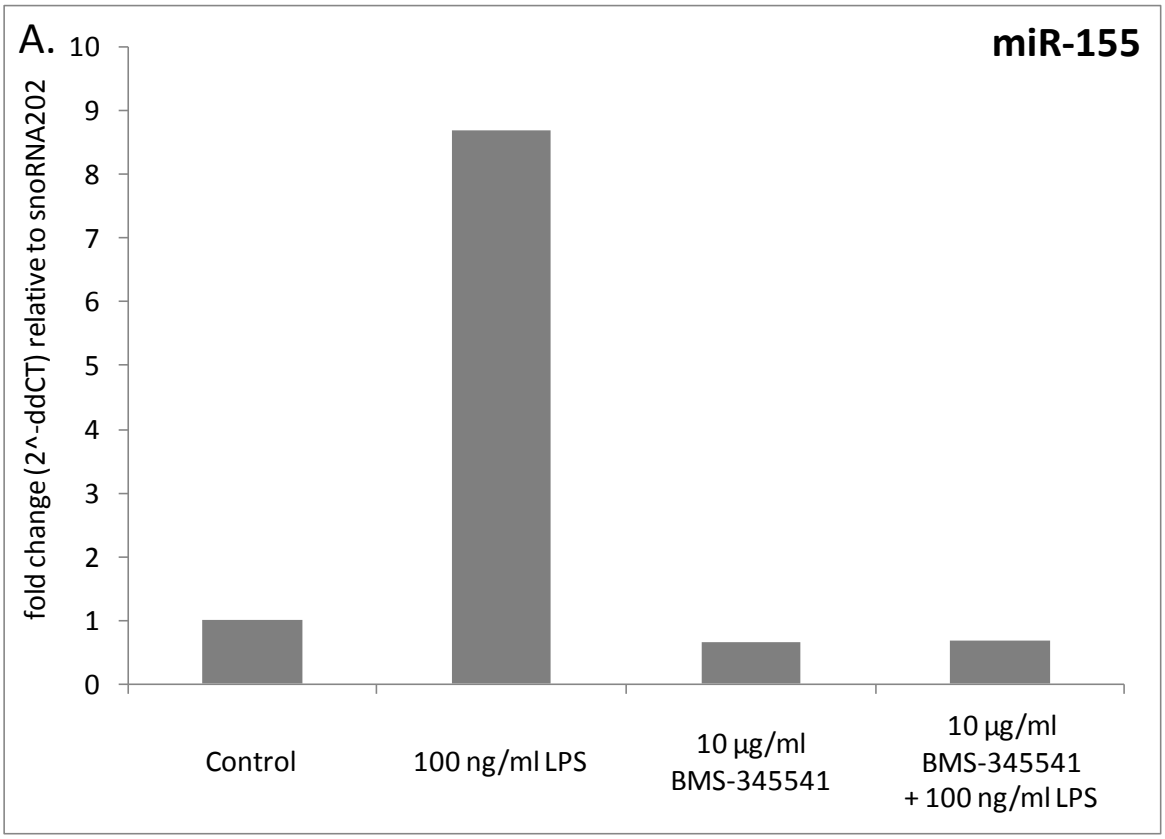

B.

Treatment	C_T value
Control	29.48
LPS 100 ng/ml	26.38
BMS-345541 10 µg/ml	29.97
BMS-345541 10 µg/ml + LPS 100 ng/ml	30.13

Figure 4.17 LPS induced expression of miR-155 in the RAW264.7 macrophage cell line is inhibited by the IκB kinase inhibitor BMS-345541. A Taqman low density array (TLDA) was performed on single samples of cDNA extracted from RAW264.7 4 hours post-LPS. (A) Data was analysed with the comparative C_T method (2^{ddCT}) for miR-155 normalised to snoRNA202. (B) Corresponding C_T values are shown.

A.

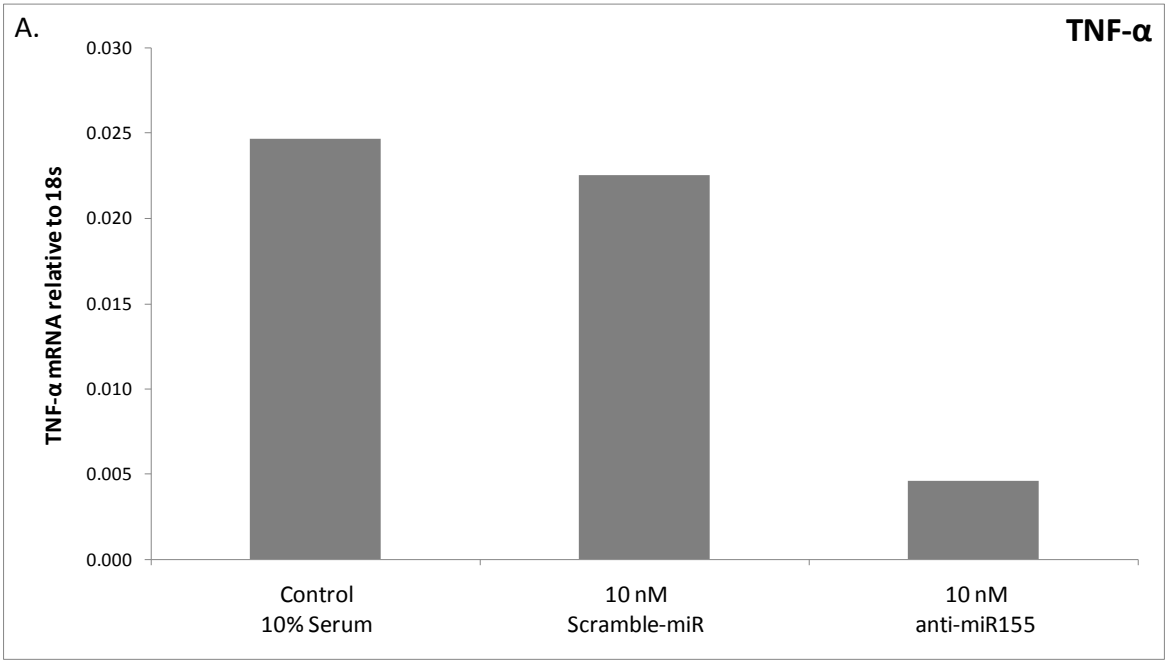

B.

Treatment	C_T value
Control	26.51
10 nM Scramble-miR	27.35
10 nM anti-miR155	29.9

Figure 4.18 Successful transfection of anti-miR155 leads to repression of TNF-α mRNA expression in BMMs. qRT-PCR was performed on single samples of cDNA extracted from BMMs 24 hours post-anti-miR-155 transfection. (A) Data was analysed by relative quantification for TNF-α and normalized to 18S. (B) Corresponding C_T values are shown.

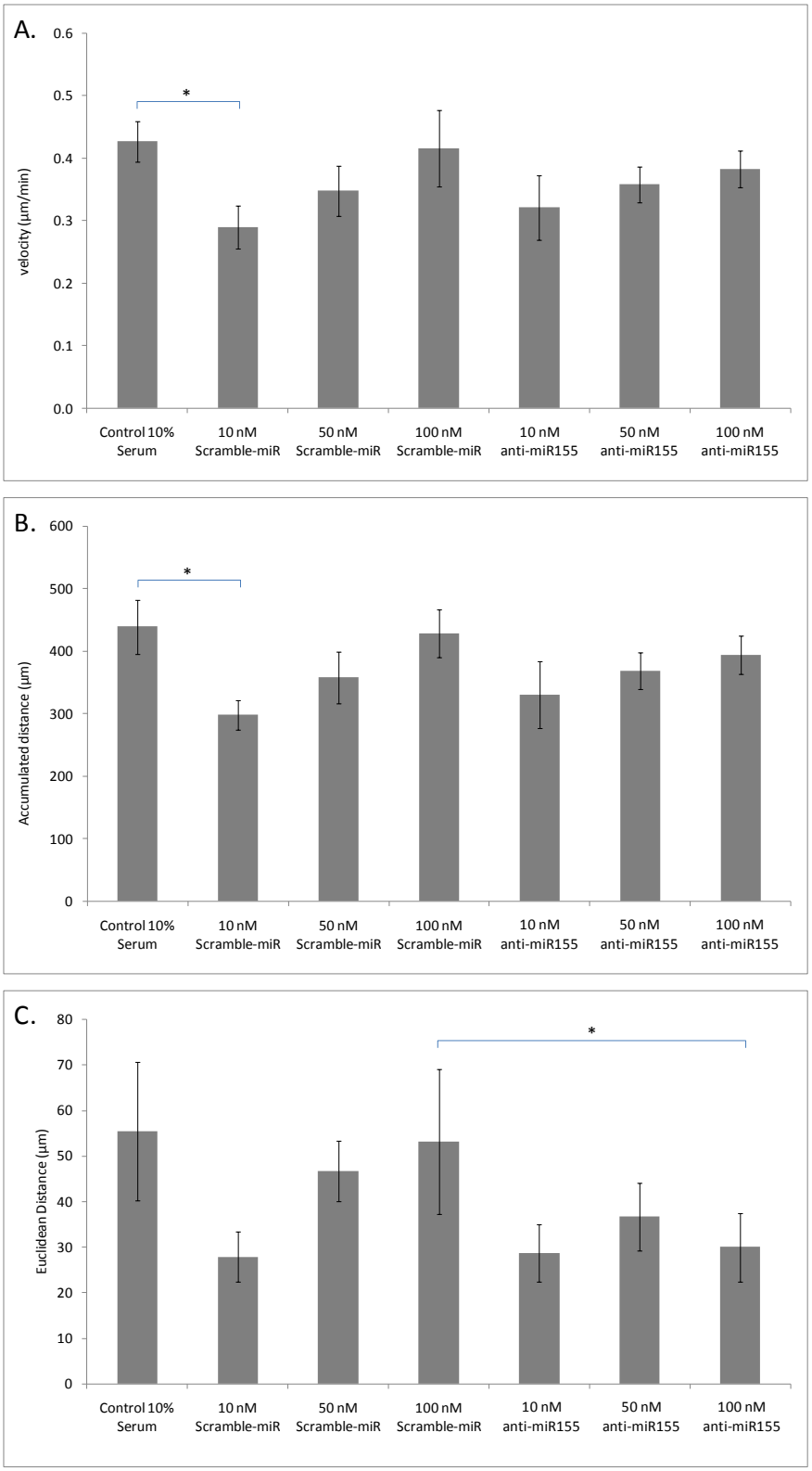

Figure 4.19 Anti-miR-155 has no effect on migration speed or velocity of BMM. Time-lapse images were captured every 10 minutes over a 17 hour period of BMMs on plasma fibronectin 24 hours after transfection with anti-miR-155. (A) Migration velocity, (B) accumulated distance and (C) Euclidean distance of BMMs were analyzed with ImageJ processing software. Each bar represents the mean of 25 cells ± SEM. Statistical significance was determined using the Student's t-test. * $p \leq 0.05$.

4.4 Discussion

The importance of cell migration for successful homeostatic processes in eukaryotes is well understood. Elucidation of the cellular mechanisms controlling migration is vital to our comprehension of its role in the development of various pathologies. The effect of deregulated macrophage migration is clearly seen in inflammatory disorders such as diabetic ulceration and atheromatous plaque formation. Throughout this chapter macrophage migration has been analysed, both with and without LPS pro-inflammatory stimulation. Investigation was focused on the functional effects of LPS-driven repression of MMP-10, following the results obtained in Chapter 3.

The gross morphology of BMMs on various 2D substrates *in vitro* reflects their potential interactions *in vivo* (figure 4.1). Fibronectin, for example, is present in the body in either a soluble or less soluble form (Wierzbicka-Patynowski and Schwarzbauer, 2003). Soluble plasma fibronectin is abundant in the blood whilst less soluble cell-associated fibronectin is a major component of the ECM and plays an important role in wound healing. BMMs displayed an active and migratory morphology with fibronectin as a substrate (figure 4.2 and 4.3). In contrast, 2D type 1 collagen induced an unusually rounded morphology in BMMs. This substrate is present in large blood vessels but is largely absent from sites of macrophage diapedesis, such as venules and capillaries where type IV collagen predominates the basement membrane (Bou-Gharios et al., 2004). Studies comparing macrophage adhesion to type 1 collagen with fibronectin revealed that macrophages on collagen only made contact with the substrate by the tips of cell processes, whereas on fibronectin adhesion was closely opposed to the substratum (Koyama et al., 2000). Novel methods of quantifying cell morphology, in terms of lamellipodia area and cell protrusions, have been described (Parker et al., 2002). Further work to apply this to BMMs could enable a hierarchy of substrate-induced morphological response to be established.

In light of these observations it is perhaps unsurprising that Euclidean distance migrated is significantly greater for BMMs on fibronectin than those on fibrinogen, type 1 collagen or with 0.2% fetal calf serum alone, despite no change in migration velocity (figure 4.2). Previous studies have revealed similar results, with a trend for increased directional persistence observed for BMMs on fibronectin compared to those on glass (Wheeler and Ridley, 2007). Two major cell adhesion molecules mediating macrophage adhesion to fibronectin are integrins αvβ3 and α5β1 (also known as VLA-5). When bound to α5β1, soluble plasma fibronectin dimers become activated

and cluster at specific sites on the cell surface (focal adhesions and fibrillar adhesions) forming an insoluble network of fibronectin fibrils (Wierzbicka-Patynowski and Schwarzbauer, 2003). This not only provides a rigid scaffold for BMM migration and intracellular interaction with the cytoskeleton but also instigates cell signalling pathways via the cytoplasmic integrin domain, such as the β1-dependent activation of RhoA in epithelial cells (Danen et al., 2002). α5β1 is also known to play a critical role in the up-regulation of MMP expression in macrophages cultured on fibronectin (Xie et al., 1998). Recently the RhoGEF Arhgef1 has been shown to participate in α5β1 mediated MMP expression in pulmonary macrophages with exaggerated expression of MMP-2 and -9 in Argef1-/- cells on fibronectin (Hartney et al., 2010). This provides a novel link between the RhoGTPase cycle and integrin-mediated MMP control. It is likely that the BMMs studied in this chapter express α5β1 in response to culture on fibronectin. It is also possible therefore that the interaction with fibronectin is affecting their MMP expression profile as well as their migratory capacity.

Like fibronectin, plasma fibrinogen is also a soluble blood protein with a role in wound healing. Following trauma to the blood vessel wall the 'coagulation cascade' is activated, resulting in the cleavage of fibrinogen to fibrin by the serine protease thrombin. Fibrin is then cross-linked to form the blood clot which acts as a scaffold for macrophages migrating to the site of injury. The relevance of this substrate to macrophage migration *in vivo* is clear, however *in vitro* we see no effect on accumulated or Euclidean distance migrated (figure 4.2 and 4.3). Macrophages are known to express integrin αMβ2, which binds immobilised fibrinogen with great avidity (Mosesson, 2005). The strength of this interaction however is increased in the presence of fibronectin, due to a direct interaction between the amino-terminal domains of each substrate (Blystone et al., 1991). It is possible that, on a more physiologically relevant combination of substrates, such as fibrinogen and fibronectin together, BMMs would show increased binding by αMβ2 and subsequently increased migration.

Type 1 collagen forms triple-helical fibrils that, as explained above, are widely expressed throughout the body though not necessarily in areas of macrophage function. Due to the rounded morphology observed for BMMs on type 1 collagen it follows that their migratory capacity may also be altered. Despite a trend for reduced velocity and accumulated distance, however, the Euclidean distance migrated by BMMs on 2D type 1 collagen varies little to that seen for untreated cells (figure 4.2 and 4.3). From what we know about the 'loose' adhesions formed by macrophages on type 1 collagen (Koyama et al., 2000) this suggests that macrophages may 'roll' along the

surface of the substrate rather than forming strong adhesions with the collagen fibrils. Integrins α1β1 and α2β1 bind type 1 collagen and studies have shown that α1 deficiency can lead to reduced macrophage migration, specifically in the advanced atherosclerotic plaques of $\alpha1^{-/-}$/$ApoE^{-/-}$ mice (Schapira et al., 2005). This indicates that macrophage migration in type 1 collagen is physiologically relevant. Recent work with human macrophages derived from human blood monocytes (MDMs) reflects results seen with BMMs; MDMs take on an amoeboid morphology on fibrillar type 1 collagen and show less directional migration than cells in gelled 3D type 1 collagen (Van et al., 2010). This suggests that BMMs would respond differently to type 1 collagen in a 3D formation and suggests that ECM structure and extracellular ligand spacing, as well as ECM composition, plays an important role in the migratory phenotype of macrophages. However, as type 1 collagen did not appear to be conducive for BMM migration in this model it was not pursued further here.

The relationship between macrophage migration and LPS stimulation is fairly well characterised. In terms of migration towards a gradient of LPS, macrophage recruitment has been shown to increase both *in vivo* and *in vitro*. For example, LPS increases macrophage infiltration into the lungs of mice in a CD44-dependent manner (Hollingsworth et al., 2007). CD44 is a cell surface adhesion molecule known to play a role in cell adhesion and cell migration. Similarly, RAW264.7 macrophages have shown increased migration across an uncoated membrane in response to LPS *in vitro* (Gu et al., 2010). This increased migratory capacity is, in part, due to LPS-induced changes in the macrophage cytoskeleton. For example, the indirect phosphorylation and co-localisation of cytoskeletal proteins Pyk2 and paxillin was observed in membrane ruffles of LPS treated macrophages (Williams and Ridley, 2000). In this chapter BMMs exposed to LPS certainly displayed greater areas of lamellipodia and numbers of filopodia, consistent with this finding (figure 4.2).

Despite the evidence for increased migration and macrophage activation in a gradient of LPS (Hollingsworth et al., 2007), a trend for reduced migration velocity and accumulated distance was observed for LPS treated BMMs in 0.2% serum and on fibrinogen, with a significant reduction seen on fibronectin (figure 4.3). Interestingly, the Euclidean distance migrated by LPS-stimulated BMMs on fibronectin did not vary from that of untreated cells and this is reflected in their migration plots (figure 4.4). This suggests that the more directional migration induced by culture on fibronectin cannot be further enhanced by LPS in BMMs.

To resolve this perceived discrepancy in LPS-induced macrophage migration it is important to consider the physiological relevance of this response. Whilst previous work has shown increased

migration towards an LPS gradient, mimicking the migration of macrophages towards sites of infection *in vivo*; these observations reveal a suppression of migration in a relatively high, yet uniform, concentration of LPS (100 ng/ml), perhaps mimicking macrophage arrest in tissues with elevated pathogen level. Simply put, these results suggest that velocity of macrophage migration may slow once cells have reached their site of action, i.e., maximum pathogen concentration. Again, the Rho GTPases appear to play a role in mediating the directionality of macrophage migration. Rac1, for example, controls random migration with a correlation between decreasing Rac1 activation and increased directionality (Allen et al., 1998a; Pankov et al., 2005). This would suggest that Rac1 may be down-regulated by LPS, however studies have shown that Rac1 activity is in fact induced by uniform concentrations of LPS over time (Kong and Ge, 2008). It is clear, therefore, that the mechanisms controlling LPS-induced macrophage migration are complex, and it would be of great interest to explore the activation of Rho GTPases in LPS-stimulated BMMs to further elucidate the signalling pathways involved.

It has recently become apparent that the MMPs play an intriguing role in cell migration downstream of Rho GTPase signalling in non-small cell lung cancer (NSCLC) cells (Frederick et al., 2008). Frederick et al have shown MMP-10 expression to be down-regulated by RNAi mediated knockdown of Rac1 or the Rac1 binding protein Par6α, whilst RNAi against MMP-10 itself decreases migration of NSCLC cells through Matrigel. This suggests a role for MMP-10 in responding to migrational cues. In this chapter siRNA mediated knockdown of MMP-10 induced a BMM morphology similar to that seen in LPS treated BMMs; cells appear less polarised, with larger areas of lamellipodia and less membrane protrusions (figure 4.10). Other MMP-deficient myeloid cells have shown a similar response, for example, osteoclasts derived from the bone marrow of MT1-MMP/MMP-$14^{-/-}$ mice display fewer membrane protrusions whilst also exhibiting reduced migration through endothelial monolayers (Gonzalo et al., 2010). Results in this chapter demonstrate a significantly reduced velocity and distance migrated by MMP-10-deficient BMMs on fibronectin with this clearly reflected in the corresponding migration plots (figure 4.11 and 4.12). Again, analysis of the Rho GTPases in these cells, specifically Rac1 activation, would be interesting.

Interestingly *in vivo* analysis of pneumonia induced by the gram-negative bacterium *P. aeruginosa* in MMP-10-null mice reveals increased levels of pulmonary inflammation (Kassim et al., 2007) supporting the hypothesis that MMP-10 is vital for proper control of immune cell migration, such as macrophages, in a physiologically relevant setting.

The effect of MMP-10 knockdown on BMM migratory phenotype is rescued with the addition of rhMMP-10 to culture medium; the velocity and accumulated distance migrated is restored to that of scrambled siRNA treated cells on fibronectin (figure 4.12). This suggests that the role of MMP-10 in BMM migration is extracellular, possibly acting on the fibronectin substrate. This hypothesis is further strengthened by the results of recent preliminary experiments with BMMs harvested from the *mmp10*$^{-/-}$ mouse. Analysis of random migration on fibronectin reveals a reduction in distance and velocity migrated by *mmp10*$^{-/-}$ BMMs compared to back-crossed wild-type control BMMs, which can also be rescued by the addition of rhMMP-10 (data not shown). Fibronectin is a known substrate of MMP-10 (Chin et al., 1985) and it is possible that the MMP-10 protein (either endogenously secreted by BMMs or exogenously applied) is able to cleave the 2D fibronectin. This could enhance migration either by creating a path for the macrophages through the substrate or releasing potentially pro-migratory fibronectin cleavage fragments. Previous work has shown that fibronectin fragments are capable of modulating monocyte migration. For example, monocytes incubated with fibronectin fragments obtained from post-infarction cardiac lymph fluids showed decreased expression of α5β1 and altered migration (Trial et al., 1999). Surprisingly however Trail et al revealed a clustering of monocytes and a decrease in migration in response to these fibronectin fragments, suggesting that this is not the mechanism at play in the BMMs studied in this chapter. Interestingly the reduction in Euclidean distance migrated was not restored by rhMMP-10, despite its effect on velocity, suggesting that the mechanisms controlling directional migration of BMMs are more complex and perhaps regulated intracellularly, as opposed to the result of extracellular substrate remodelling.

Repression of BMM miR-155 expression with LNA oligonucleotides had no effect on migration velocity or accumulated distance on fibronectin but did repress Euclidean distance at the highest concentration used (figure 4.19). This suggests that miR-155 may play a role in control of directionality of migration and supports what is already known about miR-155 targeting the Rho GTPase, RhoA, in epithelial cells (Kong et al., 2008). Constitutive over-expression of RhoA in macrophages has been found to repress their ability to polarise and migrate in response to a CSF-1 gradient (Allen et al., 1998b). One can speculate, therefore, that repression of miR-155 in BMMs may potentially de-repress RhoA activity and could result in reduced directionality. It would be vital, therefore, to analyse the expression and activation of the Rho GTPases in BMMs during migration and following miR-155 knock down to further understand the LPS-driven macrophage migratory response. Similarly, it would be important to analyse the effect of anti-miR-155 on LPS-driven repression of migration. MMP-10 has been found to increase in expression following miR-

155 knockdown in human monocyte-derived dendritic cells (Ceppi et al., 2009), hinting at a potential mechanism for MMP-10 repression in BMMs. Therefore, it can be hypothesised that anti-miR-155 treatment of LPS-stimulated BMMs may rescue the reduction in migration seen on fibronectin.

Chapter 5: **Metalloproteinase expression in wounded and healthy skin from diabetic and non-diabetic mice**

5.1 Introduction

5.1.1 The role of macrophages in the wound healing response

The wound healing response in healthy tissue (explained in detail in Chapter 1, 1.3.2,) comprises, in part, a cascade of pro-inflammatory cell recruitment events, commencing with an influx of neutrophils closely followed by the diapedesis of circulating monocytes that differentiate into tissue macrophages. The role of macrophages in wound healing is vital; macrophage depletion in wounds has been shown to dramatically delay resolution of tissue damage and wound closure (Maruyama et al., 2007; Mirza et al., 2009).

The function of the macrophage during wound healing is two-fold. Following the anti-microbial action of the invading neutrophils, macrophages are recruited in a classic phagocytic capacity to clear the wound of debris, such as degraded ECM components (including fibrin) and spent neutrophils (Leibovich and Ross, 1975). Macrophages also play an important role in triggering neovascularisation, angiogenesis and fibro-proliferation in wounds due to their ability to express numerous cytokines and growth factors (Martin and Leibovich, 2005).

In their role as phagocytes macrophages are responsible for the clearance of large numbers of apoptotic neutrophils that, if allowed to remain at the wound site, contribute to a build up of debris that can be detrimental to healing. It has recently been postulated however that this phagocytosis alone cannot entirely account for the reduction in neutrophil numbers at the wound site, but rather macrophages also secrete proteases that indirectly inhibit neutrophil recruitment through the cleavage of several chemokines, such as IL-8 (Dean et al., 2008). Simultaneously, hypoxic conditions at the wound site can trigger a pro-angiogenic/neovasculogenic macrophage phenotype capable of producing factors that stimulate the growth and migration of endothelial cells. For example, macrophages have been found to secrete basic fibroblast growth factor (bFGF), vascular endothelial growth factor (VEGF) and interleukin (IL)-8 (Sunderkotter et al., 1994) stimulating the growth of new blood vessels in wounded tissue. This process is clearly vital for the rapid resolution of wounding and to prevent further tissue damage.

5.1.2 Expression of matrix metalloproteinases during wound healing

MMP expression is vital for a timely and efficient wound healing response (Lund et al., 1999; Mirastschijski et al., 2002). The role of the MMPs in wound healing can be divided into two classes; those that mediate tissue remodelling by degradation of the extracellular matrix (ECM), and those that cleave and inactivate (and occasionally activate) chemokines. In the main, investigation into

the ability of MMPs to mediate tissue remodelling in wounds has focused on their ECM-degrading function. For example, in man MMP-1 is found localised to the basal keratinocyte layer of wounded skin, where it is shown to facilitate the migration of keratinocytes by cleaving the collagen-integrin contacts that form with the dermal matrix (Pilcher et al., 1997).

The ability of MMPs to degrade ECM is no longer considered to be their major function in this context, however, and focus has shifted to their role in fine-tuning the chemokine and growth factor response (reviewed in (Gill and Parks, 2008)). For example, macrophages control the clearance and recruitment of neutrophils in wounds by secreting a protease, namely MMP-12. Macrophage MMP-12 cleaves and inactivates potent pro-neutrophil chemokines CXCL-5 and -8, preventing further influx into wound tissue. Over time MMP-12 expressed by macrophages in the wound further contributes to the degradation of pro-monocyte/macrophage chemokines CCL2, 7, 8 and 13, to disrupt their own recruitment and bring about the resolution of inflammation (Dean et al., 2008). MMP-10 has also been proposed to play a role in wound healing and is seen expressed in similar patterns to MMP-1 in basal keratinocytes (Pilcher et al., 1997) but appears to be regulated in a spatiotemporal manner, peaking in expression at both day 1 and day 5 post wounding (Madlener et al., 1996). Over expression of MMP-10 in wounded epithelium disrupts cell migration at the wound edge, possibly triggered by increased keratinocyte apoptosis; reduces expression of laminin-5, important in cell adhesions; and triggers the aberrant expression of β1 integrins (Krampert et al., 2004). Interestingly MMP-10 has also been found to be expressed in intestinal wounds; specifically in the migrating enterocytes surrounding gastric ulcers (Salmela et al., 2004). Despite the clear necessity for tight regulation of MMP-10 expression during wound healing and recent work investigating inflammation in the MMP-10 null mouse (Kassim et al., 2007), the specific mode of action for this MMP in this context has not yet been elucidated.

5.1.3 Impaired wound healing in type II diabetes

Impaired wound healing has long been associated with type II diabetes, particularly in elderly patients (Liu et al., 2008). Factors that contribute to this are an abnormal inflammatory response and decreased angiogenesis due to a reduction in VEGF expression (Liu et al., 2008); both of which are partly influenced by the macrophage contingent of the wound healing response.

The type II diabetic Db/Db mouse can be used to model impaired wound healing *in vitro*. In healthy, non-diabetic mice studies have shown full thickness wounds of 2.25cm^2 to heal fully within 16 days. In Db/Db counterparts however wounds fail to heal even by 40 days post-wounding (Greenhalgh et al., 1990). Several growth factors have been implicated in wound healing

and studies of their induction post-wounding in Db/Db mice has revealed important discrepancies in expression: levels of insulin-like growth factor (IGF)-1 mRNA in non-diabetic wounds, for example, show a sharp increase at 3 days post wounding whilst IGF-1 mRNA levels in Db/Db fail to peak until 14 days post-wounding (Brown et al., 1997). Brown et al have also observed a similarly delayed response for IGF-1 protein levels in wounds. Unsurprisingly, knowledge of some of the triggers for delayed wound healing in Db/Db skin has led to studies attempting to rescue this phenotype with exogenous growth factors. Hepatocyte growth factor/scatter factor (HGF/SF), for example, has potent cell growth and motility properties during embryonic organ development and is thought to play a role in adult organ regeneration. Application of HGF/SF on Db/Db wounds has been shown to increase wound re-epithelialisation and neovascularisation, and stimulate greater numbers of neutrophils, macrophages, endothelial cells and mast cells to the diabetic wound (Bevan et al., 2004). Bevan et al hypothesise that this growth factor acts both directly and indirectly on macrophages, via either the stimulation of the macrophage c-Met receptor triggering migration and chemokine expression, or by triggering the expression of platelet activating factor (PAF) in macrophages that in turn contribute to angiogenesis.

The matrix metalloproteinases have also been implicated in impaired diabetic wound healing, both in the Db/Db model and in chronic diabetic foot ulcers in man. Expression of the gelatinases, pro-MMP-2 and pro-MMP-9, has been shown to be significantly reduced at 5 days post wounding in Db/Db skin compared to non-diabetic Db/+ skin. Pro-MMP-9 is also reduced in Db/Db wound fluid 5 days post-wounding and in the wound fluid from chronic human diabetic foot ulcers compared to acute control wounds (Wall et al., 2002). This highlights the importance of proteases in tissue remodelling, such as that which takes place during wound healing, and suggests that the role of certain MMPs during wound healing may be conserved between species.

5.2 Aims

In light of previous experiments that revealed differential MMP-10 expression in BMMs following LPS stimulation, the expression of MMP-10 mRNA in BMMs from the type II diabetic Db/Db and non-diabetic Db/+ mouse with and without LPS stimulation was determined.

To explore MMP-10 expression *in vivo*, specifically during wound healing, MMP-10 mRNA and protein expression in normal skin and full thickness wounds from Db/Db and Db/+ mice at both 5 and 7 days post-wounding was analysed.

5.3 Results

5.3.1 LPS treatment represses MMP-10 mRNA expression in bone marrow-derived macrophages from the Db/Db type II diabetic mouse and the Db/+ heterozygous counterpart

In order to investigate any potential variation in macrophage function key LPS-responsive macrophage MMPs identified in Chapter 3 were analysed in diabetic bone marrow-derived macrophages (BMMs). BMMs from type II diabetic (Db/Db), heterozygous control (Db/+) and wild type C57BL6 (WT) mice were exposed to 100 ng/ml lipopolysaccharide (LPS) for 24 hours before total RNA was extracted and quantitative RT-PCR (qRT-PCR) performed. The statistically significant repression of MMP-10 mRNA 24 hours post-LPS stimulation seen in WT BMMs was also observed in Db/Db and Db/+ BMMs (figure 5.1 A, B, C). The corresponding C_T values reveal similar levels of expression in all three macrophage genotypes (figure 5.1 D, E, F). To confirm that these results are not due to a universally repressive effect of LPS on MMP expression the levels of steady-state MMP-14 (MT1-MMP) mRNA was analysed. A significant induction of MMP-14 is also seen across all three BMM genotypes (figure 5.2 A, B, C). Again, C_T values reveal similar levels of expression in all three macrophage populations (figure 5.2 D, E, F). These results suggest that the diabetic phenotype does not affect BMM ability to respond to LPS in terms of MMP expression, at least *in vitro*.

These results are representative of two experiments with all experiments performed in triplicate.

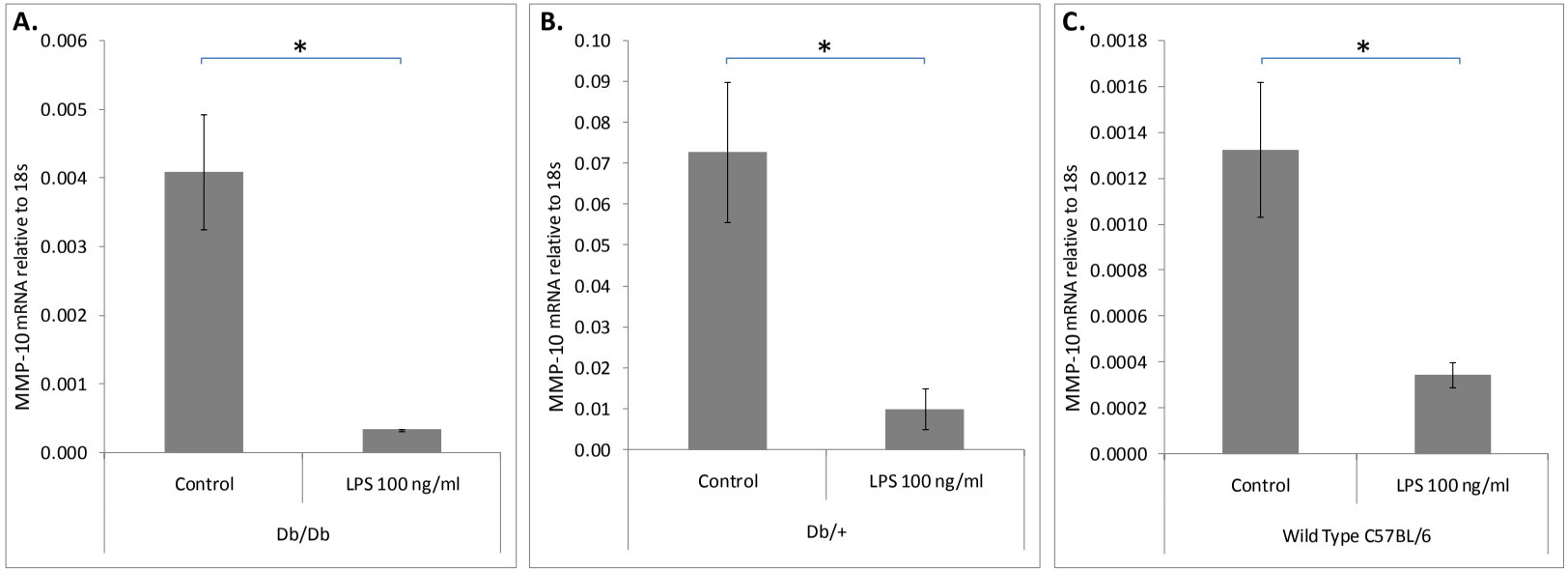

D.

	Treatment	C_T value 1	C_T value 2	C_T value 3
Db/Db	Control	33.2	32.9	33.1
	LPS 100 ng/ml	37.0	36.5	36.2

E.

	Treatment	C_T value 1	C_T value 2	C_T value 3
Db/+	Control	32.8	33.3	34.6
	LPS 100 ng/ml	37.6	38.8	35.8

F.

	Treatment	C_T value 1	C_T value 2	C_T value 3
WT	Control	33.3	33.5	32.8
	LPS 100 ng/ml	35.4	35.8	35.8

Figure 5.1 LPS represses relative expression of MMP-10 normalized to 18S in BMMs from Db/Db diabetic mice. qRT-PCR was performed on (A) Db/Db BMMs, (B) BMMs from the heterozygous Db/+ control and (C) wild type BMMs 24 hours post-LPS stimulation. Data was analysed by relative quantification and normalized to 18S. (D – F) Corresponding C_T values are shown. Each bar represents the mean of 3 samples ± SEM. Statistical significance was determined using the Student's t-test. * $p \leq 0.05$.

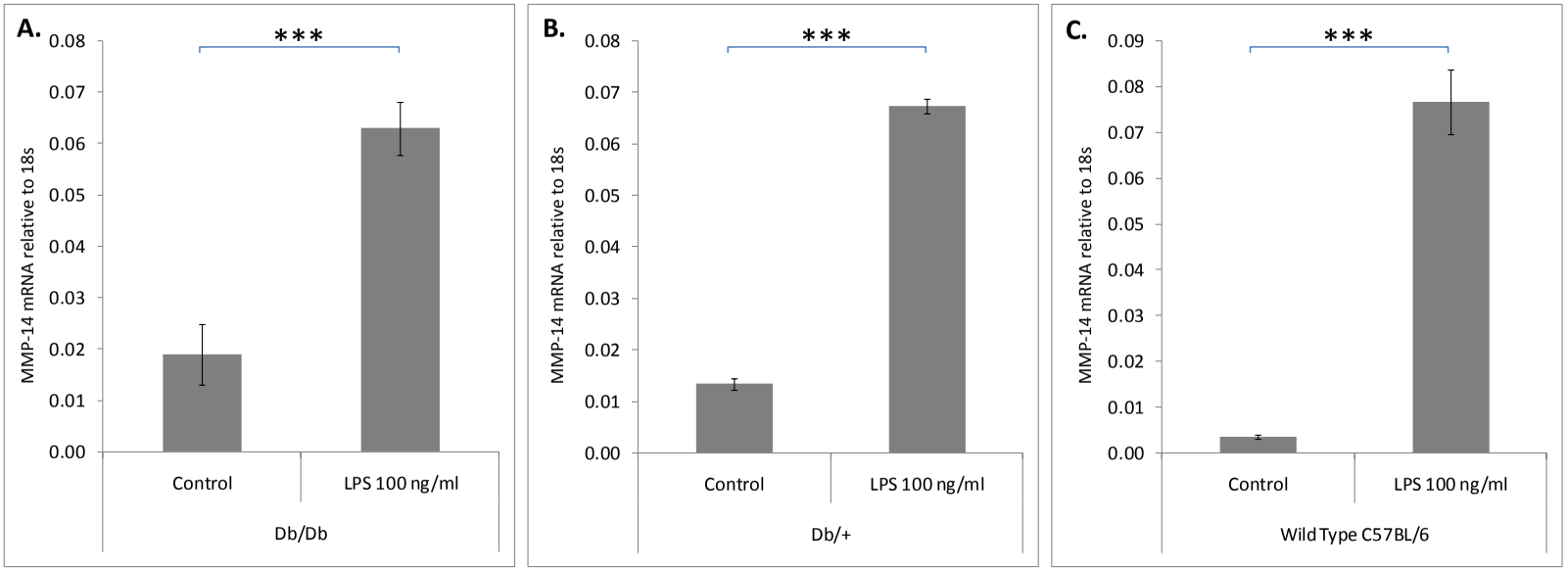

D.

	Treatment	C_T value 1	C_T value 2	C_T value 3
Db/Db	Control	33.0	33.7	33.6
	LPS 100 ng/ml	28.0	27.4	27.7

E.

	Treatment	C_T value 1	C_T value 2	C_T value 3
Db/+	Control	33.6	33.4	33.8
	LPS 100 ng/ml	27.4	27.2	27.3

F.

	Treatment	C_T value 1	C_T value 2	C_T value 3
WT	Control	35.7	35.0	35.1
	LPS 100 ng/ml	25.3	25.6	25.5

Figure 5.2 LPS enhances relative expression of MMP-14 normalized to 18S in BMMs from Db/Db diabetic mice. qRT-PCR was performed on (A) Db/Db BMMs, (B) BMMs from the heterozygous Db/+ control and (C) wild type BMMs 24 hours post -LPS stimulation. Data was analysed by relative quantification and normalized to 18S. (D – F) Corresponding CT values are shown. Each bar represents the mean of 3 samples ± SEM. Statistical significance was determined using the Student's t-test. *** $p \leq 0.001$.

5.3.2 The expression of MMP-10, TNF-α and the murine macrophage marker, F4/80, in normal and wounded skin suggest aberrant response to wounding in the type II diabetic Db/Db mouse

The wound healing response of the Db/Db mouse has been well characterised in terms of immune cell recruitment and some work has been performed studying expression of the gelatinases, MMP-2 and -9 (Wall et al., 2002; Bevan et al., 2004) and ADAMTS1 (Krampert et al., 2005). A comparison of gross wound morphology in Db/Db skin compared to Db/+ skin reveals a difference in wound size after 5 days (figure 5.3 C, D). The physiological difference between Db/Db and Db/+ mice, due to obesity of the type II diabetes model, means that only two biopsy wounds can be made in the dorsal flank of the Db/+ mouse compared with four on the Db/Db dorsal flank (figure 5.3 A, B). In subsequent mRNA analysis Db/+ controls have occasionally been omitted to conserve tissue for protein analysis.

A full list of mice used and wound number is included in the Appendix (table 8.3).

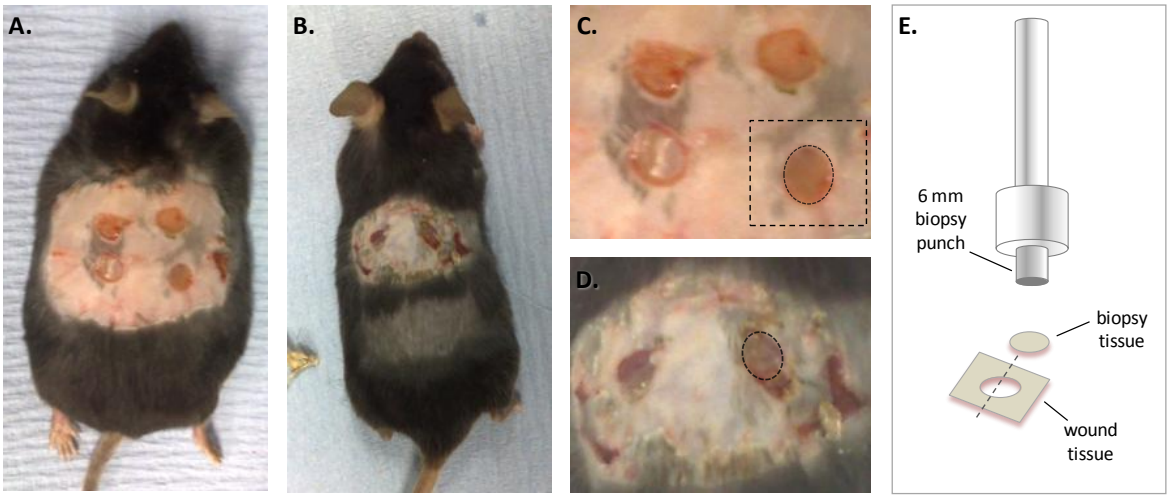

Figure 5.3 Gross morphology of full thickness skin wounds on the dorsal flank of Db/Db and Db/+ mice after 5 days. (A, C) Four full-thickness punch biopsies are made in the dorsal flank skin of the obese Db/Db mouse. Circular dotted line indicates wound edge and squared dotted line indicates tissue harvested. (B, D) The Db/+ heterozygous control can only sustain two punch biopsies due to its size. (E) Biopsy tissue is retained following wounding procedure and serves as a 'day 0' control whilst wound tissue is harvested after indicated healing time. One half of wound tissue is reserved for protein extraction and one half for RNA extraction.

Relative levels of MMP-10, TNF-α and F4/80 mRNA were examined in Db/Db and Db/+ normal skin and some preliminary wounded tissue (figure 5.4). At 5 days post-wounding the relative level of MMP-10 mRNA appears enhanced in Db/+ wound tissue (n = 1) compared with Db/+ normal skin (n = 3) and the corresponding C_T values reflect this. In Db/Db wounds (n = 2) the pattern of MMP-10 mRNA induction appears the same (figure 5.4 A, D). Relative levels of TNF-α mRNA expression also suggest an increase in wounded compared to normal skin, for both Db/+ and Db/Db (figure 5.4 B, E). Interestingly C_T values for F4/80 mRNA, a murine macrophage specific marker, are particularly high and out of the range considered to indicate expression in both Db/Db and Db/+ samples (figure 5.4 C, F).

The 'n' numbers given in figure 5.4 indicate the number of different mice analysed.

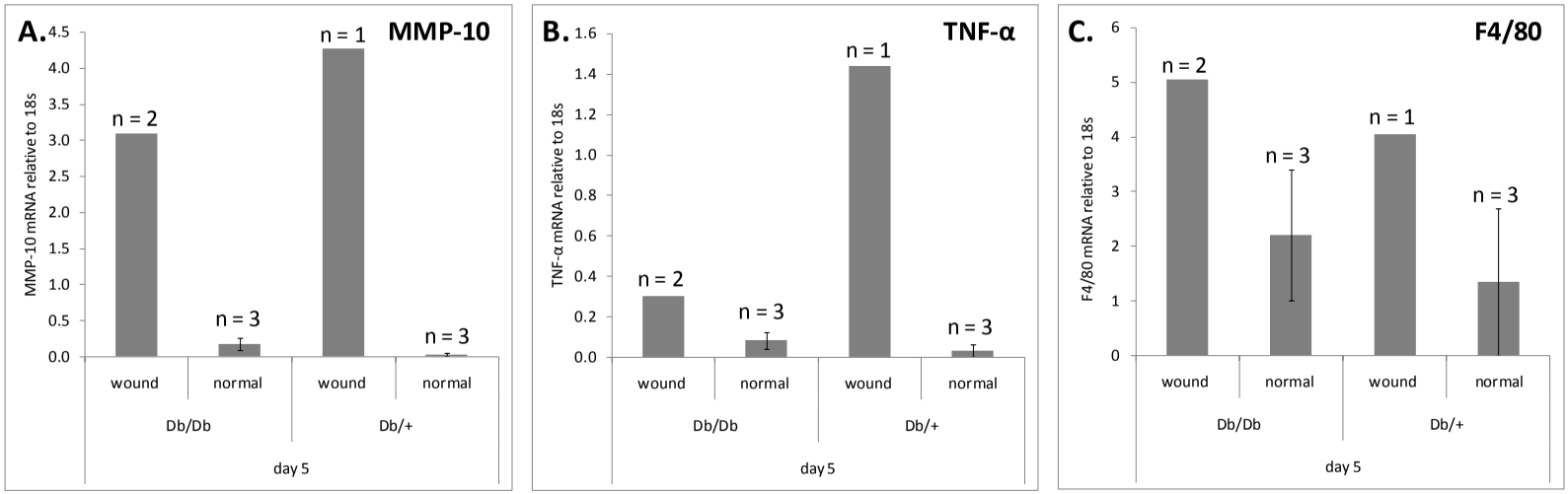

D.

Day	Genotype	Condition	C_T value Mouse 1	Mouse 2	Mouse 3
Day 5	Db/Db	wound	30.8	29.6	ND
		normal	35.9	35.3	36.3
	Db/+	wound	29.7	ND	ND
		normal	38.7	35.9	39.1

E.

Day	Genotype	Condition	C_T value Mouse 1	Mouse 2	Mouse 3
Day 5	Db/Db	wound	30.2	30.5	ND
		normal	32.0	32.4	29.8
	Db/+	wound	27.5	ND	ND
		normal	33.1	30.8	29.5

F.

Day	Genotype	Condition	C_T value Mouse 1	Mouse 2	Mouse 3
Day 5	Db/Db	wound	34.3	34.0	ND
		normal	35.1	37.1	36.2
	Db/+	wound	35.4	ND	ND
		normal	35.7	35.2	35.1

Figure 5.4 Comparing relative expression of MMP-10, TNF-α and F4/80 mRNA in Db/Db and Db/+ skin with preliminary 5 day wound samples. qRT-PCR for (A) MMP-10, (B) TNF-α and (C) F4/80 was performed on normal and wounded skin harvested 5 days post wounding from Db/Db and Db/+ mice. (D – F) Corresponding C_T values are shown. ND - not done. Each bar represents the relative mRNA in samples indicated in tables D – F with 'n' number displayed ± SEM.

The level of MMP-10 protein in wounded and normal Db/+ skin, revealed by Western blotting, seems to correspond with the mRNA levels described above (figure 5.5); after 5 days post-wounding the 57 KDa proMMP-10 form is increased compared to normal skin whilst the 47 KDa processed form is no longer expressed. This suggests either an increase in MMP-10 transcript translation or a decrease in proMMP-10 processing. In Db/Db tissue MMP-10 protein expression is more ambiguous as several bands are observed. In both wounds analyzed the level of processed MMP-10 appears to be raised compared with normal skin, whereas levels of the pro form do not appear to change.

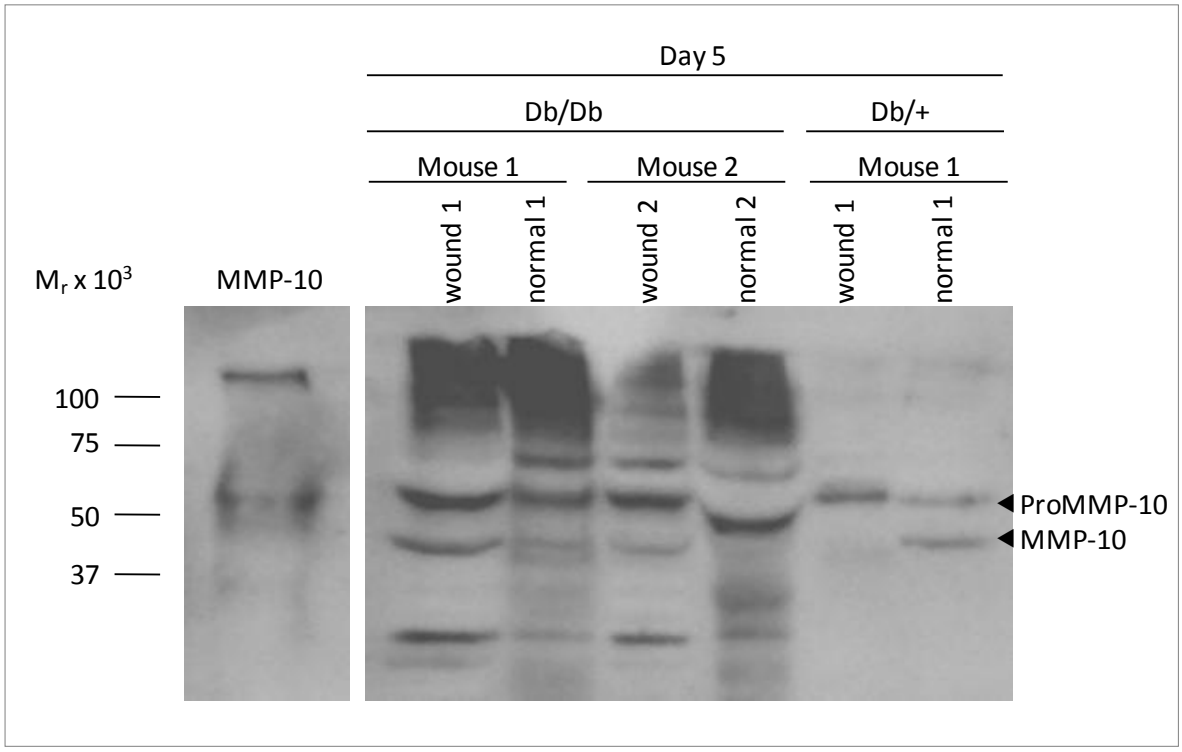

Figure 5.5 Western blot for MMP-10 protein expression in skin 5 days post-wounding. Wound tissue and normal skin was harvested 5 days post-wounding and snap frozen. Protein was extracted as described in Chapter 2 and equal concentrations were loaded into each well. 2.5 ng of rhMMP-10 was loaded as a positive control which runs at the slightly lower molecular weight of 54KDa. Position of BioRad Precision Plus protein standards are indicated.

To further investigate the aberrant expression of MMP-10 in Db/Db skin, wound tissue was harvested 7 days post-wounding (n = 3) for comparison with day 5 samples (n = 2) and day 0 unwounded tissue (n = 3). MMP-10 mRNA was undetectable in day 0 skin but shows a trend for enhanced expression at day 5 and significant increase by day 7, which is made clear by the associated C_T values (figure 5.6 A, D). Expression of TNF-α mRNA also shows a trend toward increase at day 5 and a significant increase at day 7 (figure 5.6 B, E). Expression of F4/80 mRNA appear to peak at day 5 in Db/Db wounded skin and is significantly greater by day 7 (figure 5.6 C, F). As observed previously however, C_T values for F4/80 mRNA expression are high (≥35). This perhaps reflects that fact that mRNA was extracted from whole tissue including epidermis, dermis and some subcutaneous tissue.

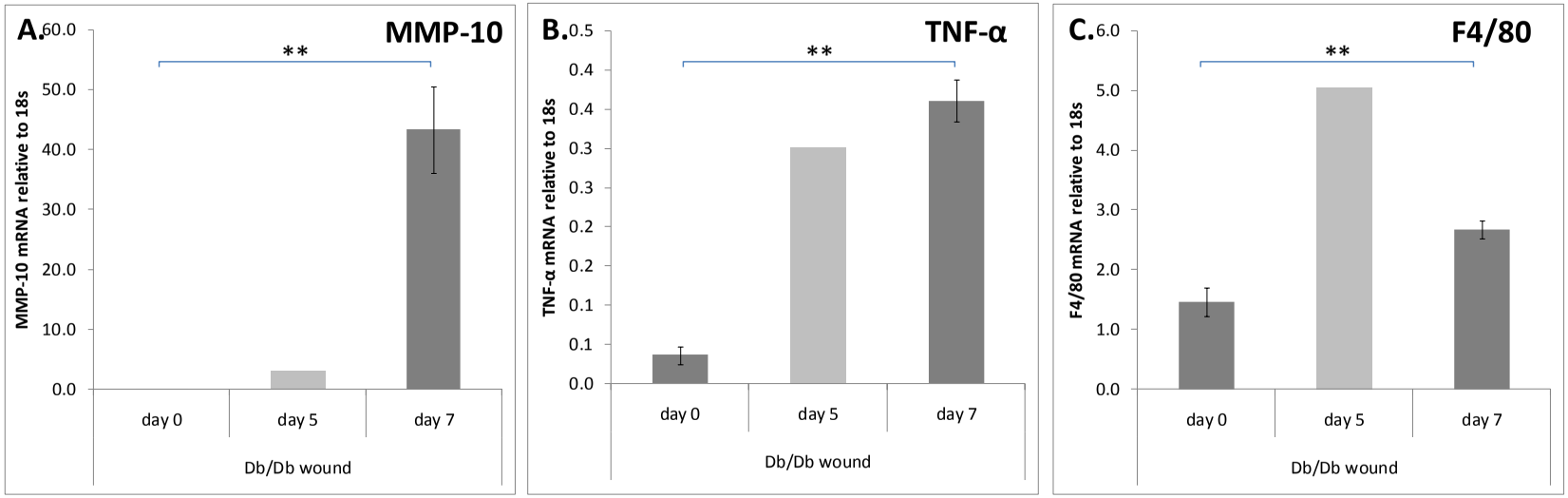

D.

Day	Genotype	Condition	C_T value		
0	Db/Db	wound	Mouse 1a	Mouse 2a	Mouse 3a
			40	40	40
5			Mouse 1	Mouse 2	-
			30.8	29.6	ND
7			Mouse 4	Mouse 5 (w6)	Mouse 5 (w7)
			24.3	25.3	24.2

E.

Day	Genotype	Condition	C_T value		
0	Db/Db	wound	Mouse 1a	Mouse 2a	Mouse 3a
			33.3	34.9	36.6
5			Mouse 1	Mouse 2	-
			30.2	30.5	ND
7			Mouse 4	Mouse 5 (w6)	Mouse 5 (w7)
			30.6	30.1	29.6

F.

Day	Genotype	Condition	C_T value		
0	Db/Db	wound	Mouse 1a	Mouse 2a	Mouse 3a
			39.6	40	39.3
5			Mouse 1	Mouse 2	-
			34.3	34.0	ND
7			Mouse 4	Mouse 5 (w6)	Mouse 5 (w7)
			36.8	37.1	36.3

Figure 5.6 Comparing relative expression of MMP-10, TNF-α and F4/80 mRNA in Db/Db unwounded (day 0) skin and at days 5 and 7 post wounding. qRT-PCR for (A) MMP-10, (B) TNF-α and (C) F4/80 was performed on day 0 normal skin and wounded skin harvested 5 or 7 days post wounding from Db/Db. (D – F) Corresponding C_T values are shown. Each bar represents the relative mRNA in samples indicated in tables D – F± SEM. Pale grey bar indicates day 5 data included for comparison (also shown in figure 5.4).. Statistical significance was determined using the Student's t-test. ** $p \leq 0.01$.

Again, MMP-10 protein levels in corresponding tissue samples were examined by Western blot revealing a possible increase in the 57 KDa proMMP-10 levels 7 days post wounding (figure 5.7). By day 7 the potential 47 KDa processed MMP-10 band has decreased, similar to the response seen at 5 days post wounding in Db/+ tissue (figure 5.5).

The qRT-PCR (figure 5.6) and Western blot (figure 5.7) comparison of MMP-10 expression in wounds harvested at different time points was performed once.

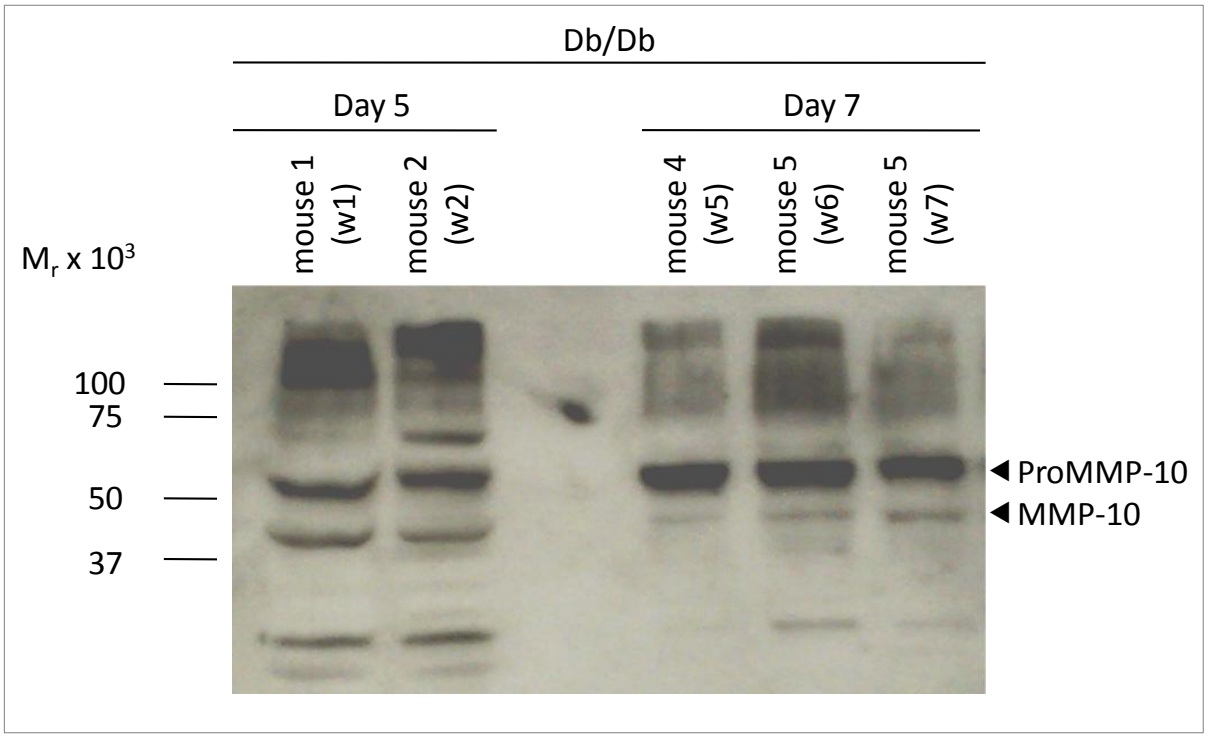

Figure 5.7 Western blot for MMP-10 protein expression in Db/Db skin 5 and 7 days post-wounding. Wound tissue and normal skin was harvested 5 or 7 days post-wounding and snap frozen. Protein was extracted as described in Chapter 2 and equal concentrations were loaded into each well. Position of BioRad Precision Plus protein standards are indicated.

5.3.3 Expression of MMP-10, TNF-α and the murine macrophage marker F4/80, in type II diabetic Db/Db mouse wound explants cultured with LPS

As a model system of *in vivo* infection wounded Db/Db and Db/+ skin tissue was harvested 7 days post-wounding and then cultured *ex vivo* with 100 ng/ml LPS for a further 24 hours. This enabled analysis of MMP-10, TNF-α and F4/80 in response to LPS in a more physiologically relevant environment. In terms of F4/80 expression this would reflect the presence of resident macrophages together with macrophages recruited in response to LPS.

No significant change in expression of MMP-10, TNF-α and F4/80 mRNA was observed in LPS-treated wound explants (see Appendix, figure 8.3). Corresponding MMP-10 protein levels in LPS-treated Db/Db and Db/+ wound explants were examined by Western blot along with unwounded Db/Db and Db/+ explants (figure 5.8). In unwounded tissue basal levels of MMP-10 are higher in Db/+ skin than Db/Db skin, but in both cases expression appears inhibited when cultured with 100 ng/ml LPS for 24 hours (figure 5.8 A). In wounded tissue explants there is little difference in basal Db/Db MMP-10 protein expression and MMP-10 protein in Db/Db samples cultured with LPS. In Db/+ wound explants, however, there appears to be an increased level of MMP-10 protein following LPS treatment (figure 5.8 B). This suggests that expression of MMP-10 in non-diabetic skin has further potential to be regulated by LPS *ex vivo*.

Table 5.1 shows a summary of relative MMP-10, TNF-α and F4/80 expression in wound tissue from both Db/Db and Db/+ mice.

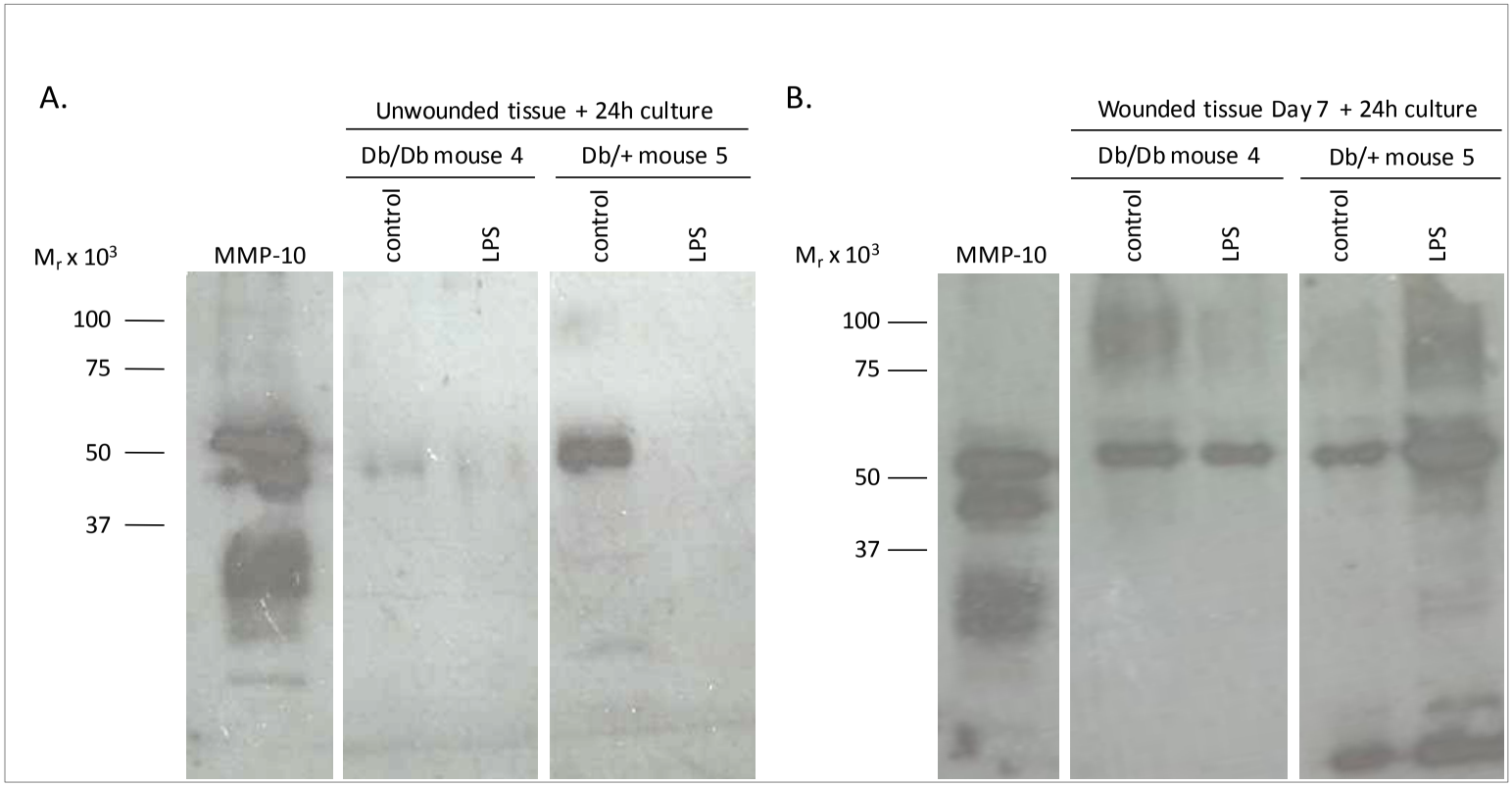

Figure 5.8 Western blot for MMP-10 protein expression in Db/Db and Db/+ unwounded skin, or 7 days post-wounding, after a further 24 hours *ex vivo* culture with LPS. (A) Wounded and (B) unwounded tissue was harvested 7 days post-wounding and cultured for a further 24 hours *ex vivo* with 100 ng/ml LPS in explant culture medium containing 5µM monensin sodium salt. Protein was extracted as described in Chapter 2 and equal concentrations were loaded into each well. 2.5 ng of rhMMP-10 was loaded as a positive control which runs at the slightly lower molecular weight of 54KDa. Position of BioRad Precision Plus protein standards are indicated.

Wound	Genotype	
	Db/Db	Db/+
Day 5	MMP-10 mRNA ProMMP-10 (57KDa) protein Processed MMP-10 (47 KDa) protein TNF-α mRNA F4/80 mRNA (≥ 34 C_T)	MMP-10 mRNA ProMMP-10 (57 KDa) protein Processed MMP-10 (47 KDa) protein TNF-α mRNA F4/80 mRNA (≥ 34 C_T)
Day 7	MMP-10 mRNA ProMMP-10 (57 KDa) protein Processed MMP-10 (47 KDa) protein TNF-α mRNA expression F4/80 mRNA (≥ 34 C_T)	
Day 7 + 24 hours LPS	MMP-10 mRNA TNF-α mRNA F4/80 mRNA (≥ 34 C_T) ProMMP-10 (57 KDa) protein	ProMMP-10 (57 KDa) protein (in wound) ProMMP-10 (57 KDa) protein (in unwounded tissue)

Table 5.1 A summary of MMP-10, TNF-α and F4/80 mRNA and protein expression in Db/Db and Db/+ skin in response to wounding or LPS treatment. Information compiled from figures 5.4 – 5.8 and Appendix, figure 8.3. For quick reference; **green** text indicates an increase in expression, **red** text indicates a decrease in expression and **black** text indicates no change.

5.3.4 Immunohistochemistry reveals localised expression of MMP-10 and F4/80 in wound tissue from the type II diabetic Db/Db mouse

Expression of MMP-10 has previously been analysed in wounds, showing localisation to basal keratinocytes at the base of the epidermal tongue (Krampert et al., 2004) and especially high expression in chronic diabetic ulcers (Rechardt et al., 2000). To address the question of whether MMP-10 is expressed in macrophage-rich regions in wounds, tissue was sectioned, fixed and stained for MMP-10 and F4/80.

Wound architecture was determined by haematoxylin staining normal and wounded Db/Db and Db/+ skin (figure 5.9). The most striking differences between Db/Db and Db/+ skin is the thick layer of adipose tissue present in Db/Db tissue due to obesity, and the impaired formation of granulation tissue (figure 5.9 B and D).

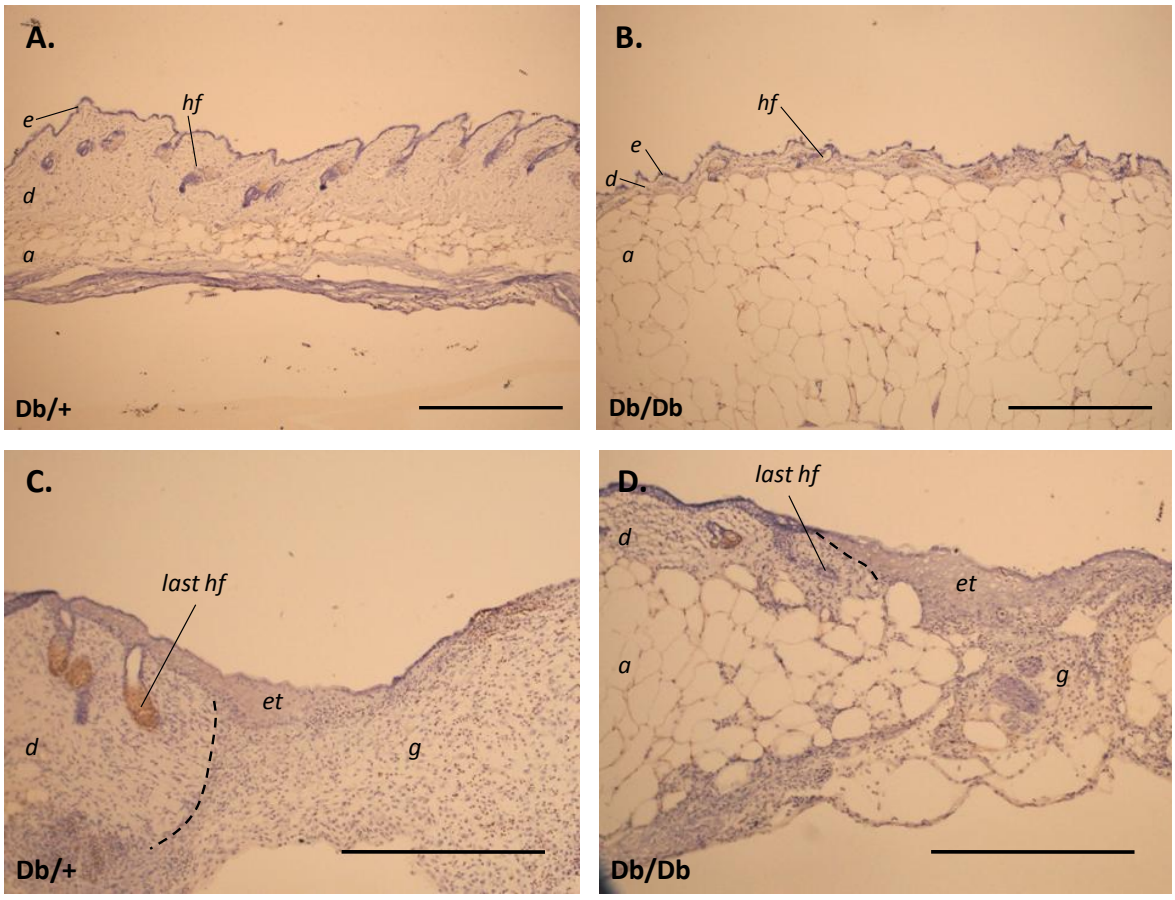

Figure 5.9 Architecture of normal skin and wound tissue harvested from the dorsal flank of Db/+ and Db/Db mice. 10 µm sections were fixed and stained with haematoxylin for comparison of (A, B) normal skin and (C, D) excisional wound architecture 7 days post wounding. Labels indicate: e – epidermis, et – epidermal tongue, d – dermis, a – adipose tissue, g – granulation tissue, hf – hair follicle. Dashed line represents wound edge. Scale bar = 200 µm.

In order to explore macrophage distribution in the skin immunofluorescent staining for F4/80 expression was performed. A scattered distribution of macrophages is observed throughout the dermis in both Db/Db and Db/+ unwounded skin (figure 5.10 A, C). A greater number of F4/80 positive cells are apparent in Db/Db tissue however, particularly localised to the bottom of the dermis and surrounding adipose tissue. F4/80 staining appears to be specific as indicated by the secondary only control (Appendix, figure 8.4 C) and may therefore be indicative of the pro-inflammatory state the diabetic phenotype imposes on all tissues of the body. Expression of MMP-10 in Db/+ and Db/Db normal skin is minimal and appears to be more diffuse than cell-specific (figure 5.10 B, D).

A non-fluorescent staining method known as ABC (avidin-biotin complex) DAB (diaminobenzidine) peroxidise staining (DAB staining) was also utilized to investigate the localisation of MMP-10 and F4/80 in Db/+ and Db/Db skin. DAB staining exploits the high degree of affinity and specificity between the biotinylated secondary antibody and an avidin/horseradish peroxidise conjugate. This not only results in a more permanent stain but also amplifies signal greatly. In combination with a haematoxylin counter-stain this enables the visualisation of both MMP-10 and F4/80 protein expression in wound histology more clearly.

DAB staining for F4/80 expression in normal skin reveals low levels of macrophages in Db/+ skin (figure 5.11 A) and suggests a greater number in Db/Db skin (figure 5.11 B). Secondary antibody-only controls suggest that staining of the adipose layer may be non-specific, particularly in Db/+ skin (figure 5.11 C, D). DAB staining for MMP-10 shows minimal expression in Db/+ skin and no expression in Db/Db tissue (figure 5.11 E, F), which was not unexpected (Madlener et al., 1996). Secondary only controls reveal non-specific staining in the adipose tissue and around the hair follicles (figure 5.11 G, H).

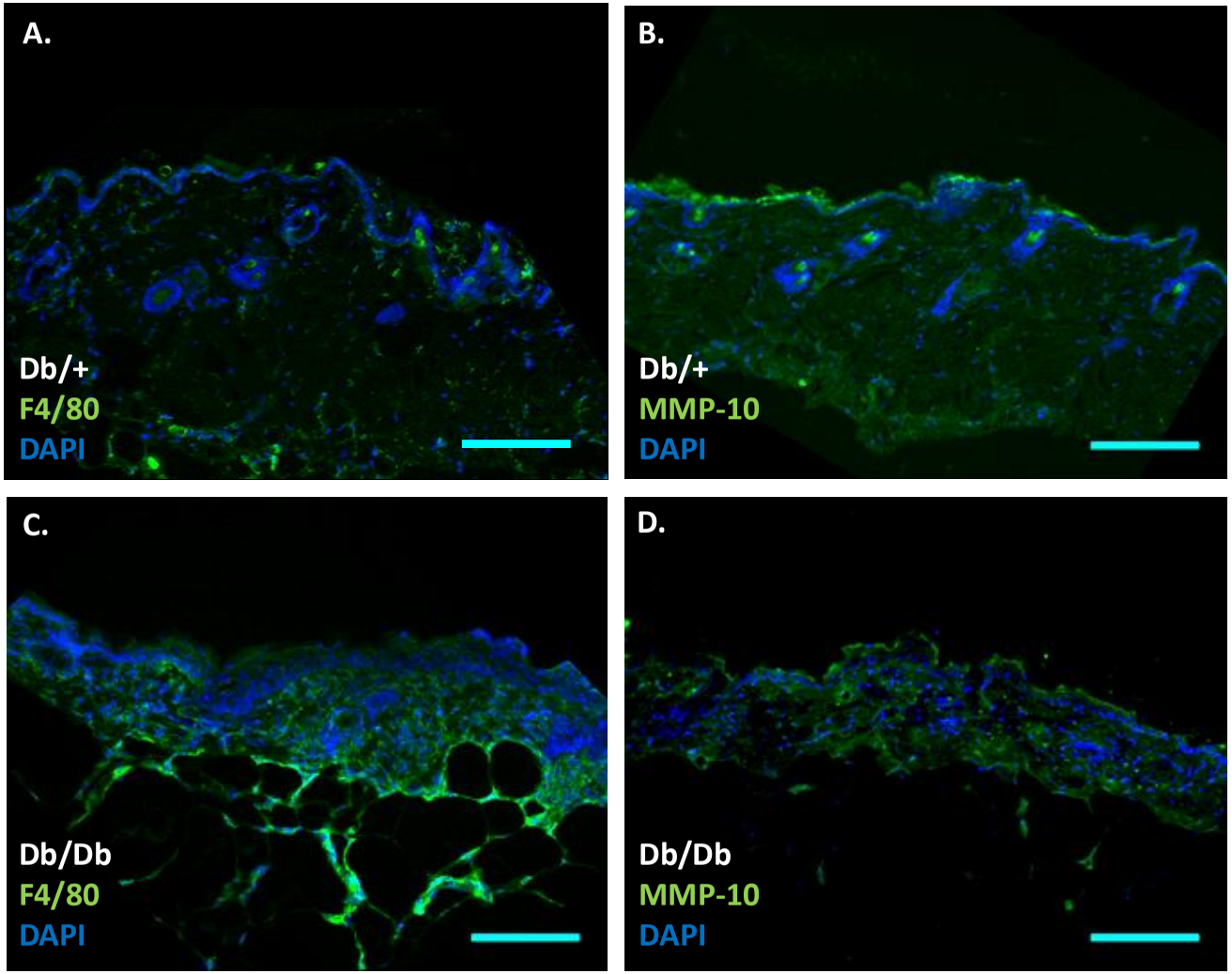

Figure 5.10 Immunofluorescent staining for F4/80 and MMP-10 expression in normal tissue from Db/Db and Db/+ mouse dorsal flank. 10 µm sections were fixed and stained for (A, C) F4/80, (B, D) MMP-10 and DAPI nuclear stain. For secondary antibody only controls see Appendix, Figure 8.4. Scale bar = 75 µm.

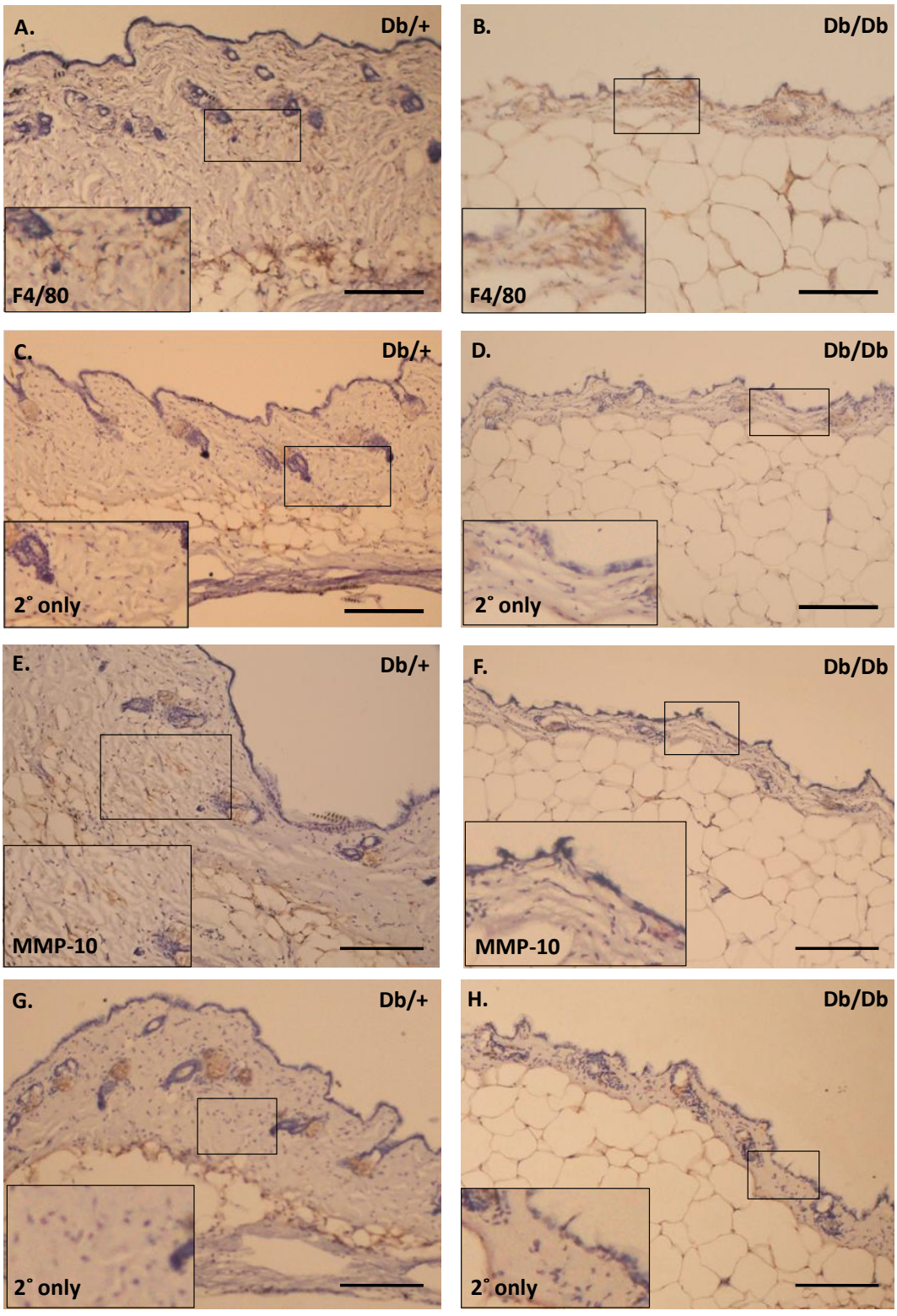

Figure 5.11 DAB staining for F4/80 and MMP-10 in normal tissue from Db/+ and Db/Db dorsal flank. 10 µm sections were fixed and stained for (A, B) F4/80, (E,F) MMP-10 or (C, D, G and H) treated with secondary only control. Tissue was counterstained with haematoxylin to emphasize skin architecture and appears blue whilst protein of interest is brown. Inserts show detail highlighted in black box. Scale bar = 200 µm.

As both DAB and immunofluorescent staining techniques have their own benefits both were utilised to further investigate F4/80 and MMP-10 expression in wounded tissue.

Immunofluorescent staining for F4/80 in Db/+ wound tissue reveals increased concentration of fluorescent F4/80 positive cells, chiefly in the granulation tissue (to the right of the wound edge, figure 5.12 A, C). In Db/Db tissue however there appear to be fewer F4/80 positive cells in the granulation tissue immediately next to the wound edge, but still a relatively large amount of staining further into the granulation tissue (figure 5.12 B, D).

DAB staining for F4/80 in wounded tissue from both Db/+ and Db/Db mice gives a clearer representation of macrophage distribution in wound tissue. In Db/+ wounds F4/80 staining is concentrated around the wound edge, on the border between dermis and granulation tissue and below the area covered by the epidermal tongue. F4/80 immunostaining is absent from the epidermis (figure 5.12 E). In Db/Db wound tissue there appears to be increased F4/80 immunostaining throughout the dermis and granulation tissue with no obvious area of increased concentration. There also appears to be some staining towards the tip of the epidermal tongue (figure 5.12 B). This is not visible in the Db/+ tissue, perhaps due to the advanced migration of the epidermal tongue.

Figure 5.12 Immunostaining for F4/80 expression in 5 day wounded tissue from Db/Db and Db/+ mouse dorsal flank. 10 µm sections were fixed and fluorescently stained for (A-D) F4/80 and DAPI or (E-H) DAB stained for F4/80. (A,C) F4/80 staining in Db/+ wound reveals an activated morphology at the wound edge. White box indicates field of view enlarged in image below. (B, D) F4/80 positive cells in Db/Db wound appear rounded at the wound edge. White box indicates field of view enlarged in image below. (E,F) DAB staining reveals more F4/80 positive cells at the wound edge in Db/+ skin compared to Db/Db skin. Black box indicates inset. (G,H) 2˚ antibody only control. (A,B) Scale bar = 75 µm, (C,D) Scale bar = 50 µm, (E-H) Scale bar = 400 µm.

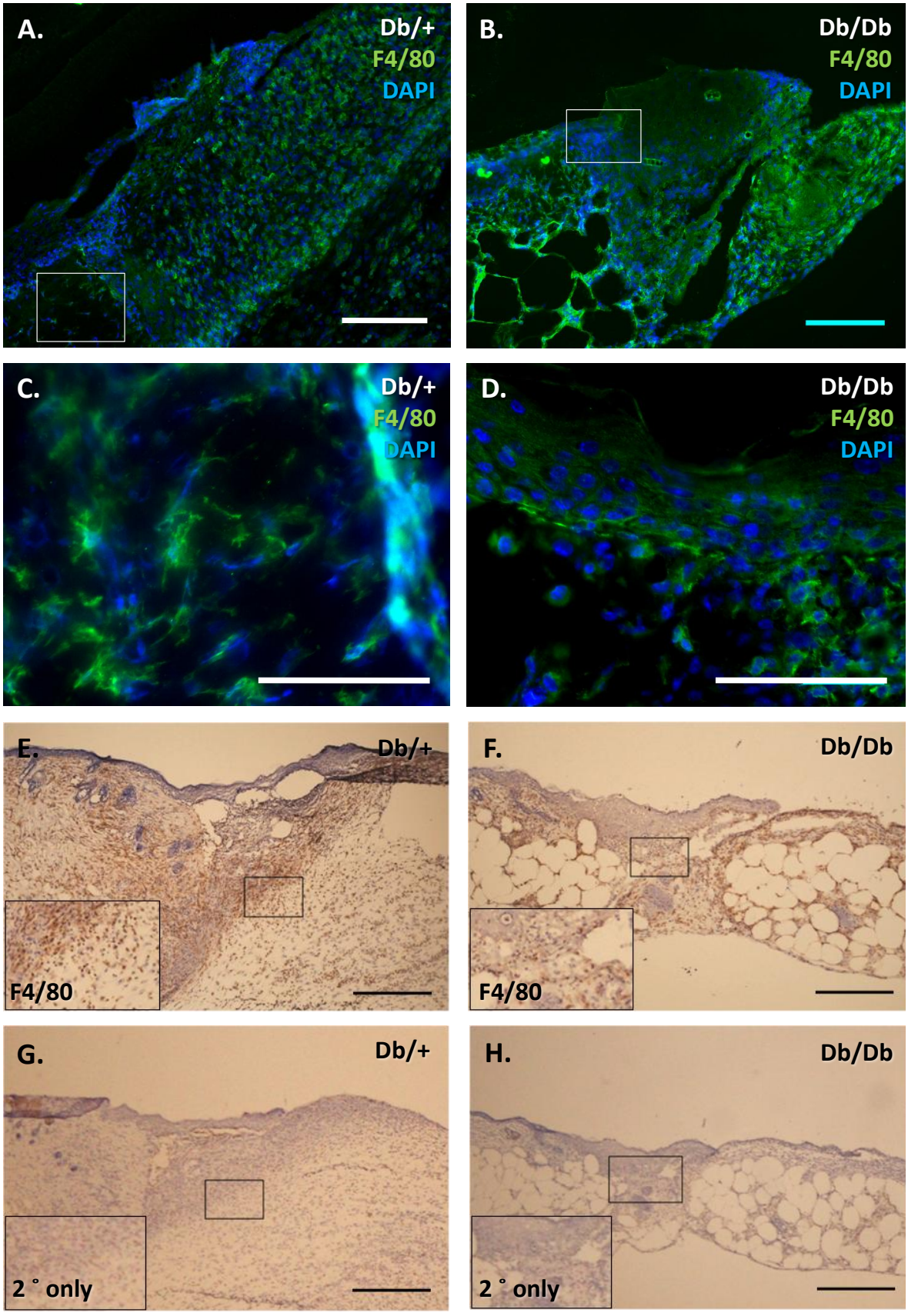
A.
Db/+
F4/80
DAPI
B.
Db/Db
F4/80
DAPI
C.
Db/+
F4/80
DAPI
D.
Db/Db
F4/80
DAPI
E.
Db/+
F4/80
F.
Db/Db
F4/80
G.
Db/+
2 ˚ only
H.
Db/Db
2 ˚ only

Immunolocalisation of MMP-10 in Db/+ and Db/Db wounds also reveals some difference in expression between the phenotypes (figure 5.13). In Db/+ wounded skin, for example, MMP-10 immunostaining appears fairly diffuse with a small area of positive staining at the base of the migrating epidermal tongue at the wound edge (figure 5.13 A, C). In equivalent Db/Db wounds this area of staining does not appear to be as clearly defined, if present at all (figure 5.13 B, D). The base of the epidermis is known to be populated with keratinocytes, known as basal keratinocytes, and this area has previously been shown to stain positively for MMP-10 (Krampert et al., 2004), suggesting this as the source of MMP-10 expression in this experiment. MMP-10 positive cells were also observed in the granulation tissue of Db/+ wounds (figure 5.14 A-C). No such specific staining was detected in Db/Db granulation tissue.

DAB staining for MMP-10 in Db/+ and Db/Db wounded tissue is less revealing than that of F4/80 (figure 5.13). In wounded tissue from the Db/+ mouse there appears to be a small area of cell associated staining at the border between epidermal tongue and granulation tissue (figure 5.13 E) however the section has split along this border making it difficult to determine the accuracy of these images. There also appears to be some faint brown staining in the secondary only control (figure 5.13 G, open arrowheads), which may indicate action of endogenous peroxidises. In Db/Db tissue positive MMP-10 staining is visible at the tip of the epidermal tongue (figure 5.13 F, arrowheads), which has been described previously (Madlener et al., 1996). This cannot be seen in Db/+ tissue as the epidermis has almost healed; indicative of the Db/Db delayed healing response. Interestingly this area of MMP-10 expression is in a similar vicinity to an area of F4/80 expression (sections < 160 µm apart; figure 5.14).

A summary of the immunohistochemical staining for MMP-10 and F4/80 in normal and wounded Db/Db and Db/+ skin is shown in Table 5.2.

Figure 5.13 Immunostaining for MMP-10 expression in 5 day wounded tissue from Db/Db and Db/+ mouse dorsal flank. 10 µm sections were fixed and fluorescently stained for (A-D) MMP-10 and DAPI or (E-H) DAB stained for MMP-10. (A,B) MMP-10 staining in Db/+ wound reveals a concentration at the wound edge and at the base of the epidermal tongue. White box indicates field of view enlarged in image below. (B, D) MMP-10 staining at the wound edge is reduced in Db/Db wound. White box indicates field of view enlarged in image below. (E,F) DAB staining for MMP-10 shows expression along the base of the epidermal tongue in Db/+ wound and in the tip of the epidermal tongue in Db/Db wound. Black box indicates inset. (G,H) 2˚ antibody only control. (A,B) Scale bar = 75 µm, (C,D) scale bar = 50 µm, (E-H) Scale bar = 400 µm.

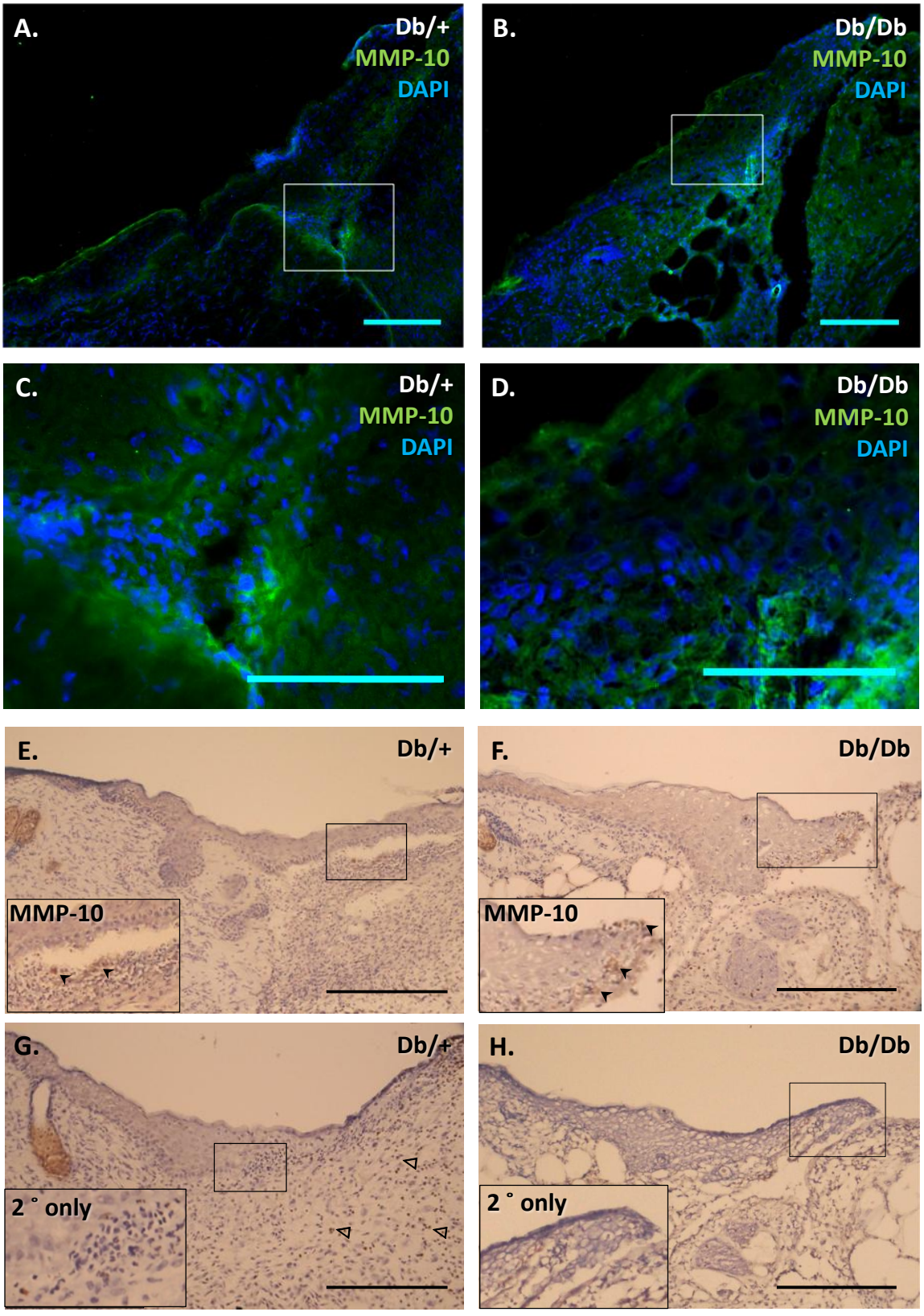
A.
Db/+
MMP-10
DAPI
B.
Db/Db
MMP-10
DAPI
C.
Db/+
MMP-10
DAPI
D.
Db/Db
MMP-10
DAPI
E.
Db/+
MMP-10
F.
Db/Db
MMP-10
G.
Db/+
2 ˚ only
H.
Db/Db
2 ˚ only

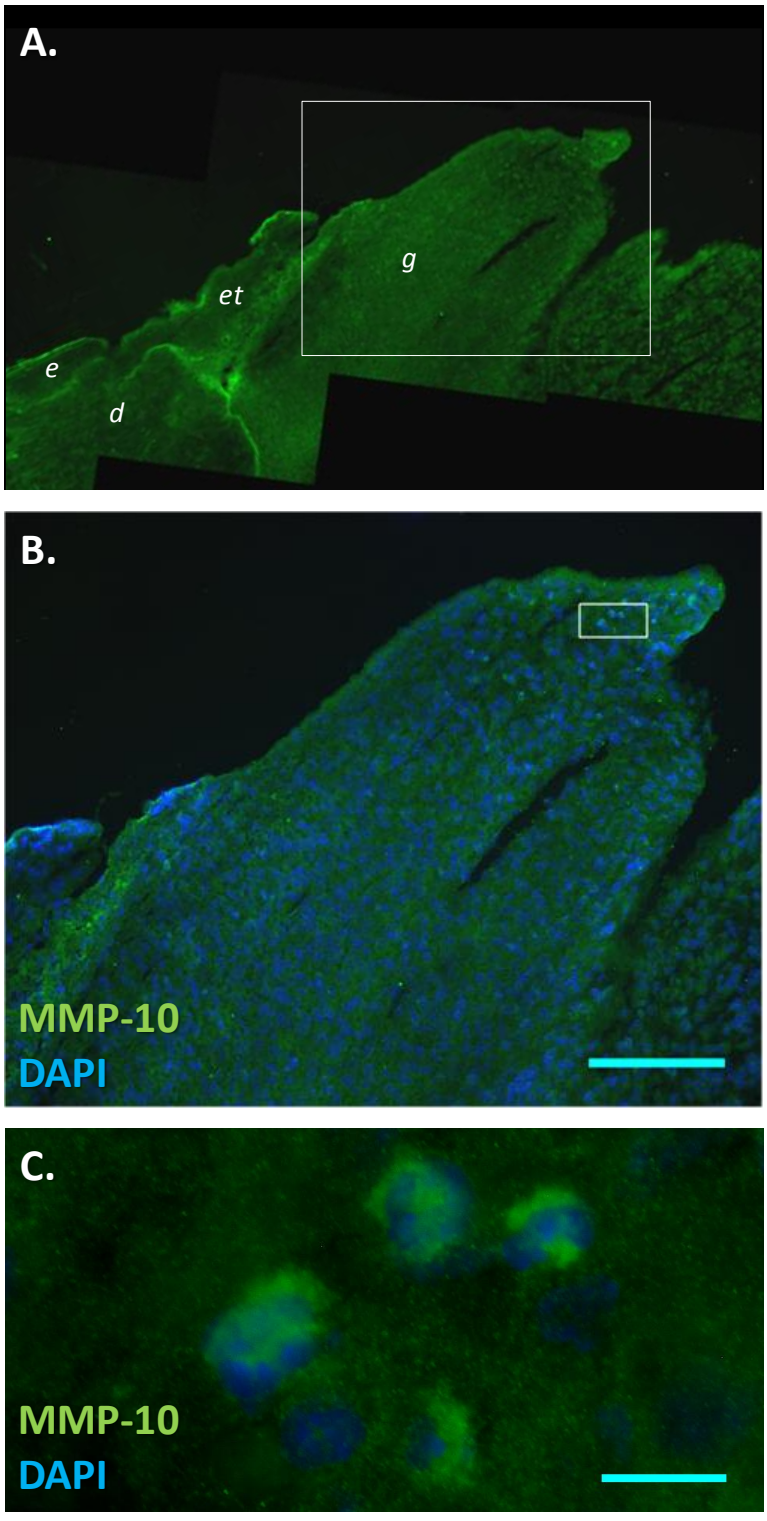

Figure 5.14 Immunofluorescent staining for MMP-10 expression reveals MMP-10 positive cells in Db/+ 5 day wound granulation tissue. 10 µm sections were fixed and stained for MMP-10 and DAPI. (A) Composition image of MMP-10 localisation at wound edge. (B) MMP-10 localisation and DAPI staining in granulation tissue. (C) Higher power image of MMP-10 positive cells in granulation tissue. *g* – granulation tissue, e – epidermis, d – dermis, et – epithelial tongue. White boxes indicate area shown in subsequent picture. (B) Scale bar = 75 µm, (D) scale bar = 10 µm.

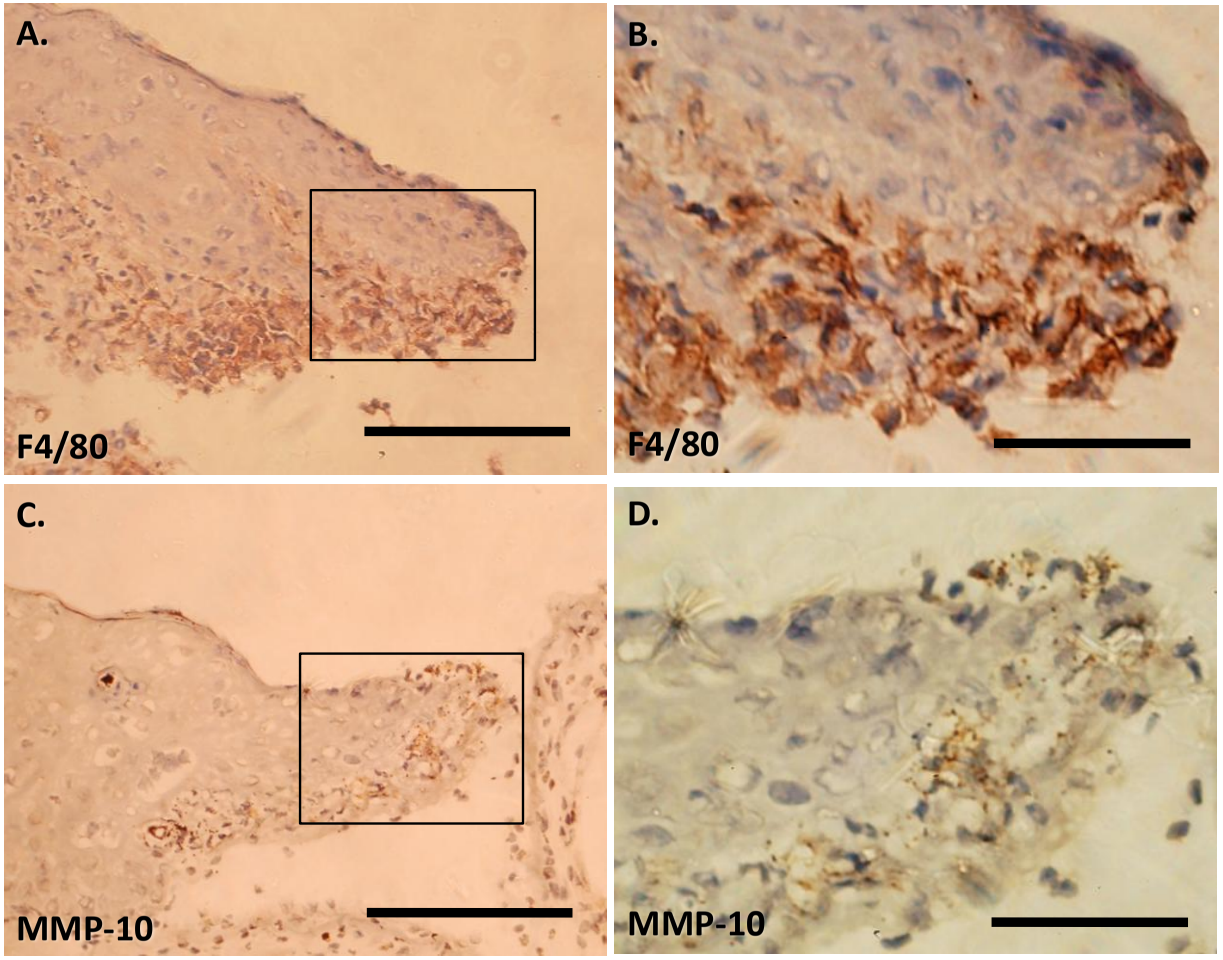

Figure 5.15 ABC DAB staining for MMP-10 and F4/80 at the tip of the epidermal tongue in 5 day wounded tissue from Db/Db dorsal flank. 10 µm sections cut from the same wound were fixed and stained for (A, B) F4/80 or (C, D) MMP-10. Tissue was counterstained with haematoxylin to emphasize skin architecture and appears blue whilst F4/80 and MMP-10 are brown. Black boxes indicate area shown adjacent picture. Scale bar = (A, C) 400 µm, (B, D) 200 µm.

Genotype	Normal Skin		Wounded Skin	
	F4/80	MMP-10	F4/80	MMP-10
Db/+	Minimal expression	Minimal expression	Increased expression in **granulation tissue** and at **wound edge**	Some increased expression at base of **epidermal tongue** and at **wound edge** Positive cells found in **granulation tissue**
Db/Db	Some diffuse expression	Some diffuse expression	Increased expression in **granulation tissue** and tip of **epidermal tongue** Does not reach intensity seen in Db/+	Positively stained cells at tip of **epidermal tongue**

Table 5.2 A summary of MMP-10 and F4/80 protein expression and localisation in Db/Db and Db/+ 5 day wound tissue and normal skin. Information compiled from figures 5.10 – 5.15.

5.4 Discussion

Understanding the significance of macrophage activity during the wound healing process is vital for the treatment of chronic wounds, prevalent in diseases such as type II diabetes. There is currently little treatment available for chronic wound healing other than prevention of infection and pain management (Campbell, 2009). As a common problem causing great discomfort in type II diabetic patients it is vital to understand the pathophysiology of the chronic wound in order to develop better treatments and prevent potentially serious consequences developing that place an immense strain on the health service in the UK.

In a healing wound there are likely to be two types of macrophage present; those that are recruited during the immune response and resident macrophages already present in the tissue before wounding. In this chapter we do not draw distinction between these two subsets. Similarly, the MMP-10 expression analysed throughout this chapter is not necessarily specific to macrophages but rather represents the level of expression throughout the skin and its potential for secretion from other cell types.

Having shown that LPS triggers differential expression of the MMPs in wild type BMMs, and given that infection with gram negative bacteria is a significant problem in the management of chronic wounds, it was important to establish the ability of BMMs from the Db/Db mouse to respond to LPS. Studies have shown Db/Db derived peritoneal macrophages to have a significantly different profile of cytokine and pro-inflammatory gene expression compared to Db/+ controls (Li et al., 2006), so it is perhaps surprising that the diabetic phenotype does not seem to affect BMM response to LPS in terms of expression of key LPS-responsive MMPs; MMP-10 and MMP-14 (figure 5.1 A and 5.2 A). One important difference between Db/Db BMMs used in this study and Db/Db derived peritoneal macrophages is the environment they differentiate in; either *in vitro* or *in vivo*, respectively. Macrophages that have endured the diabetic milieu during their differentiation *in vivo* are perhaps more likely to have a different expression profile of MMPs. It is important, therefore, to analyse both MMP expression and macrophage localisation *in vivo*, in a clinically relevant setting such as wound healing.

In both Db/Db and control Db/+ wound tissue a trend for increased expression of TNF-α mRNA 5 days post-wounding was observed in preliminary experiments compared to unwounded controls (figure 5.4 B, E). By day 7 in Db/Db skin this increase was significant but appeared to have

plateaued (figure 5.6 B, E). Enhanced TNF-α expression in wounded skin has been shown previously in the literature (Han et al., 2001; Goren et al., 2007). Formerly, adipocytes were considered to be the main source of TNF-α in skin however studies have shown that this is more likely to be bone marrow-derived adipose tissue macrophages, particularly in obese (Ob/Ob) mice where increased adipose mass triggers increased macrophage infiltration (Weisberg et al., 2003).

Ex vivo cultured 7 day Db/Db wound explants reveal no significant up-regulation of TNF-α mRNA in response to 24 hours exposure to LPS (see Appendix, figure 8.3). Initially, this result is surprising due to the substantial induction of TNF-α observed in wild type macrophages *in vitro* (see Chapter 3). Db/Db peritoneal macrophages have however been shown to have a repressed TNF-α expression profile *in vitro* in response to LPS (Zykova et al., 2000), so it is reasonable to assume this would translate into a deregulated response *in vivo*, perhaps also involving other TNF-α expressing cells such as neutrophils (Feiken et al., 1995). It is important, therefore, to confirm the functionality of LPS in this system by including Db/+ control tissue explants in repeat experiments.

The preliminary investigation into expression of MMP-10 mRNA in day 5 wounds reflects the trend seen for TNF-α; MMP-10 mRNA may be up-regulated in wounded compared to normal skin in both Db/Db and Db/+ tissue (figure 5.4 A, D). By day 7 the expression of MMP-10 mRNA is significantly increased compared with unwounded Db/Db skin (figure 5.6 A, D) and shows a clear trend to increase compared with day 5 tissue. Studies have shown that MMP-10 mRNA is induced in a biphasic pattern in whole wounds at day 1 and day 5 post wounding in healthy mice, with levels falling by day 7 (Madlener et al., 1996). This suggests that the MMP-10 response in Db/Db mice is delayed, at least at the message level. The increase in MMP-10 mRNA in Db/Db wounds 7 days post wounding is reflected at the protein level also (figure 5.7). Recent work studying the effect of MMP-10 over-expression in diabetic corneas implies that MMP-10 is responsible for alterations in the epithelial basement membrane that contribute to reduced rate of healing in this model (Saghizadeh et al., 2010). It is possible, therefore, that the deregulation of MMP-10 mRNA and protein in Db/Db dermal wounds could play a role in delayed healing in diabetic skin by affecting the epithelial basement membrane integrity.

In explants of Db/+ unwounded skin treated with LPS for 24 hours a dramatic reduction in basal MMP-10 protein expression was observed (figure 5.8 A), which potentially reflects the *in vitro* macrophage response to LPS. Conversely, MMP-10 produced in wounded Db/+ skin explants is further increased following exposure to LPS for 24 hours, an observation not replicated in Db/Db skin (figure 5.8 B). Studies have shown that MMPs are required *in vivo* for proper chemotaxis of

immune cells in response to LPS. For example, neutrophils require MMP-8 for chemotaxis in an LPS gradient due to its ability to cleave and activate various chemokines (Tester et al., 2007).

In explants of Db/Db unwounded skin there is little expression of MMP-10 protein and no regulation in response to 24 hours LPS (figure 5.8 A). In explants of Db/Db wounded skin basal expression of MMP-10 protein appears induced but again there is no response to LPS treatment (figure 5.8 B). It is tempting to speculate that there may be a lower level of the LPS receptor TLR4 expressed by Db/Db macrophages, explaining the reduction in response to LPS. Given the robust induction of TNF-α observed in preliminary experiments (figure 5.4B) this seems unlikely but further investigation would be beneficial. In future experiments it will also be vital to optimise the analysis of MMP-10 protein expression in skin by Western blots. Whilst Western blots provide the perfect platform for protein analysis in whole tissue lysate, for results to be of real, qualitative use the simultaneous application of a loading control will be necessary.

Asides from the macrophage population in wounded skin there is the potential for other MMP-10 and TNF-α expressing cells to be present in both the dermis and epidermis. It is important to remember this when drawing conclusions from these results with respect to macrophage response to LPS. Prior studies into the expression of the murine macrophage marker F4/80 in skin suggest that macrophages constitute approximately 60% of the total cells in the mouse dermis (Dupasquier et al., 2004). In normal skin from the Db/+ mouse immunofluorescence and DAB staining revealed a low level of expression of F4/80 throughout the dermis which is moderately enhanced in Db/Db skin (figure 5.10 A, C). This increased staining for F4/80 positive cells in Db/Db normal skin suggests that macrophages are deregulated in diabetic tissue even before wounding initiates an immune response.

The expression pattern of F4/80 in the day 5 Db/+ wound indicates a massive influx of macrophages to the wound edge (figure 5.12 A, E), echoing what is seen in the literature (Goren et al., 2003). In equivalent day 5 Db/Db wounded skin staining for F4/80 indicates enhanced expression compared to unwounded skin but not to the extent seen in Db/+ wounded skin, and is reminiscent of F4/80 DAB staining seen in the literature (Bevan et al., 2004). This suggests that macrophage recruitment to the Db/Db wound is impaired in our model and is consistent with the hypothesis that macrophages are a rate limiting factor in wound healing (Leibovich and Ross, 1975; Mirza et al., 2009). An interesting new role for F4/80-positive macrophages in lymphatic vessel formation during wound healing has been demonstrated recently, also using the Db/Db model (Maruyama et al., 2007). This study found macrophage integration into lymphatic vessels to

be impaired in Db/Db skin and corneal wounds. Stimulation of these wounds with IL-1β or the application of IL-1β-treated Db/Db macrophages onto wounds not only increased lymphatic vessel formation but also hastened the wound healing response. This implies an IL-1β deficiency in Db/Db skin (or perhaps an inability to cleave and activate it) and reveals a structural as well as immunomodulatory function for macrophages in wound repair.

Currently, most studies have focused on the expression of MMP-10 in the basal keratinocytes of the healing wound. Immunolocalisation of MMP-10 protein (Rechardt et al., 2000) and in situ hybridisation for MMP-10 mRNA (Madlener et al., 1996) have revealed spatiotemporal regulation of this protease with an increase observed 3 days post-wounding in the migrating basal keratinocytes at the edge of the wound. Once re-epithelialisation is complete Rechardt et al have also shown MMP-10 expression to be attenuated. Immunofluorescent staining for MMP-10 reveals little if any specific staining in unwounded Db/+ skin (figure 5.10 B), as expected from the literature (Madlener et al., 1996). In Db/Db unwounded skin MMP-10 protein expression seems slightly enhanced however (figure 5.10 D), reflecting increased F4/80 staining observed and possibly due to the pro-inflammatory diabetic phenotype.

Immunofluorescence and DAB staining for MMP-10 in Db/+ wound tissue does suggest some expression in the basal keratinocytes of the migrating epithelial tongue and at the wound edge as shown in the literature (Madlener et al., 1996; Rechardt et al., 2000; Krampert et al., 2004) (figure 5.13 A, C, E). The band-like expression pattern of MMP-10 between dermis and epidermis in Db/+ tissue seen in figure 5.13 A is also reminiscent of MMP-10 staining seen in human 7 day gingival wounds from healthy volunteers (Rechardt et al., 2000). Over-expression of MMP-10 in keratinocytes *in vivo* has been shown to result in excess processing of the ECM component laminin-5 and aberrant localisation of β1 integrins (Krampert et al., 2004). This reflects the potential role for MMP-10 in normal cell migration and for ECM structure and function. In Db/Db wounds MMP-10 protein expression seems less discrete with little positive staining in the basal keratinocytes either via immunofluorescence or DAB staining (figure 5.13 B, D, F). In the literature MMP-10 protein expression has also been used as a marker of diabetic retinopathy, being the only protease to show strong expression in epithelium and stroma from the corneas of diabetic patients (Saghizadeh et al., 2001). The authors speculate a role for MMP-10 in mediating the abnormal adhesive activities of corneal epithelium in diabetic patients by enhanced proteolysis of basement membrane. This also suggests a tissue specific level of regulation for MMP-10 however, be it in skin, cornea or the gingival of both healthy and diabetic patients.

In Db/Db wounds distinct MMP-10 positive regions are observed in the tip of the migrating epidermal tongue by DAB staining (figure 5.13 F and figure 5.15 C, D). This area of staining is not visible in Db/+ skin, probably because the epidermal tongue is less apparent due to advanced wound healing. There is some staining visible at the border between epidermis and dermis however (figure 5.13 E) and is possible that MMP-10 staining would be visible in Db/+ wounds at the tip of their epidermal tongue at an earlier stage of healing. DAB staining for F4/80 at the tip of the epidermal tongue in adjacent sections to those expressing MMP-10 show a strong correlation in areas of staining (figure 5.15 A, B). This implies the possibility that macrophages are expressing MMP-10 *in vivo*, at the tip of the migrating epidermal tongue, facilitating their functions in wound healing described above; be it by clearance of debris (Leibovich and Ross, 1975), cleavage of chemokines (Tester et al., 2007), integration into lymphatic vessels (Maruyama et al., 2007) or proteolysis of basement membrane proteins (Krampert et al., 2004). This parallel expression suggests that the role of MMP-10 in wound healing is, at least in part, mediated by its expression in macrophages.

Chapter 6: **The functional impact of apparent morphological differences between diabetic and non-diabetic macrophages.**

6.1 Introduction

6.1.1 Macrophage chemotaxis

The morphology of a cell is often a direct reflection of the cell's function in the body. Macrophage morphology is highly dynamic, therefore mirroring the varying environments and extracellular stimuli these cells must respond to during their diapedesis out of the blood vessels and towards sites of injury and infection. The ability of these cells to modify their morphology in response to external signals results in the acquisition of a polarised cell shape (see Chapter 1) allowing for chemotaxis towards gradients of pro-migratory and stimulatory factors.

The first stage in initiation of chemotaxis in all cell types is the binding of chemotactic factors to its receptor on the cell surface. There are two major families of transmembrane receptors at play during macrophage response to chemokines; the G-protein coupled receptors (GPCR) and the receptor tyrosine kinases (RTK) (reviewed in (Jones, 2000)), both of which trigger signalling via phosphatidylinoside-3-kinase (PI3-K). Numerous studies with PI3-K inhibitors have revealed the importance of PI3-K signalling to chemotaxis in macrophages and, perhaps most significantly, PI3-K family members have been found to accumulate at the leading edge of leukocytic cells (reviewed in (Curnock et al., 2002)). Different chemokines trigger different signalling events within the cell, and with a superfamily of over 40 members the potential for variation in response is huge. Ligand binding triggers association with and activation of G-proteins that further activate intracellular effector signalling molecules, such as Ras, MAPK and PI3-K as mentioned above.

Monocyte chemotactic protein (MCP)-1, also known as CCL2, is one of the key chemokines involved in the induction of macrophage migration. MCP-1 binds to its receptor CCR2 and whilst MCP-1 is widely expressed by a variety of cell types, expression of CCR2 is more discrete. Studies have shown expression of CCR2 to be up-regulated in macrophage-rich areas of human atherosclerotic plaques and to correlate with increased macrophage influx to these regions in mice (Boring et al., 1998). Importantly Boring et al have revealed a decrease in lesion formation in CCR2-null mice, suggesting that both CCR2 and MCP-1 have potential as drug targets. In population studies an activating polymorphism in the MCP-1 promoter region has been found to correlate with increased risk of developing coronary heart disease (Szalai et al., 2001), also highlighting its possible use as a biomarker for prevention of cardiovascular disease.

Colony stimulating factor (CSF)-1, or macrophage-CSF, is a widely expressed cytokine of key importance in the differentiation, survival and proliferation of mononuclear phagocytes, such as

macrophages. Much of what is known about CSF-1 has been achieved through studying the CSF-1 deficient osteopetrotic (op/op) mouse, characterised by severely decreased macrophage number in various organs and altered macrophage actin cytoskeleton (Chitu and Stanley, 2006). CSF-1 binds its receptor CSF-1R, triggering dimerisation and autophosphorylation, and further stimulating downstream signalling that regulates macrophage number, adhesion and motility (Pixley and Stanley, 2004). Activation of the RhoGTPases is vital for normal migratory response to CSF-1 in macrophages and studies have shown distinct roles for each. For example; whilst Rho and Rac are essential for macrophage locomotion in response to CSF-1, Cdc42 is required for response to the gradient by regulating cell polarity (Allen et al., 1998a). Despite not being classed as a chemokine CSF-1 does appear to exert some chemoattractant effects on macrophages. For example, murine macrophages have been shown to reorient and re-align themselves in a gradient of CSF-1 and migrate preferentially to its source, with a concentration of F-actin evident the cells' leading lamellae (Webb et al., 1996). Similarly primary macrophages have been stimulated to migrate across a membrane towards CSF-1, a process that depends on the activity of Wiskott-Aldrich Syndrome protein (WASp) family members through their regulation of F-actin-rich cell protrusions (Kheir et al., 2005).

Recently MCP-1 has been shown to promote monocyte adhesion to vascular smooth muscle cells (VSMCs) in high glucose conditions chosen to mimic the diabetic milieu (Meng et al., 2010). Given that macrophage response to pro-inflammatory stimuli is known to be deregulated in diabetes (Wall et al., 2002; Goren et al., 2007; Maruyama et al., 2007), the work described above suggests a role for MCP-1 and its receptor in diabetic pathologies. The concept of deregulated leukocyte migration in diabetic tissues is not new however. Several studies have explored increased macrophage migration as a key feature of diabetic pathology. For example, studies have shown that CSF-1-dependent macrophage infiltration into adipose tissue is increased in obese mice and humans (Weisberg et al., 2003). In turn, obesity and increased adipocyte volume strongly correlate with risk of type II diabetes. Similarly, type II diabetes raises the chance of suffering a cardiovascular disease, such as atherosclerosis. Macrophage adhesion to and infiltration of the vascular endothelium is a key feature of atherosclerosis and can be triggered by oxidised low density lipoprotein (oxLDL) inducing a shift in cell surface chemokine receptor expression (Barlic et al., 2006). Macrophage migration also plays a role in impaired wound healing in diabetic patients where it seems a delicate balance of macrophage infiltration and clearance must be achieved. For example, inactivation of macrophages in the ob/ob mouse restores diabetes-impaired wound healing by attenuating inflammation (Goren et al., 2007), however excessive reduction in

macrophage number can also impair healing by loss of macrophage contribution to lymphatic vessel formation (Maruyama et al., 2007).

6.1.2 The macrophage cytoskeleton

Components of the cell cytoskeleton are instrumental in the control of cell motility, including change in cell shape, interaction with substrates and other cells, and mediation of chemotaxis by augmenting cell polarity. There are two main types of filaments present in all eukaryotic cells that form this cellular 'scaffold'; microtubules, consisting of α- and β-tubulin subunits; and microfilaments, composed of actin polymers.

As a major component of the microtubule network, α-tubulin plays an important role in cell polarisation and rapid morphological response to stimulus. Along with β-tubulin, dimers of α-tubulin are able to rapidly assemble and disassemble microtubule proto-filaments in a process known as dynamic instability (Nogales, 2000). Microtubules have been shown to play an important role in immune cells, such as macrophages, by mediating swift morphological responses to pro-inflammatory factors LPS and interferon-γ (Binker et al., 2007). Binker et al found that increased macrophage cell spreading in response to LPS was, in part, driven by enhanced microtubule stability.

β-actin, a non-muscle actin subunit, forms the principle component of microfilaments within the cell under the control of the RhoGTPases and the Wiskott-Aldrich Syndrome protein (WASP) family (Kheir et al., 2005). The main role for actin in the migrating cell is to drive the protrusion of the leading edge by a process of polymerisation and de-polymerisation of the α- and β- subunits in response to extracellular signals (Vicente-Manzanares et al., 2005). These extracellular signals are mediated via the transmembrane cell adhesion molecules, integrins. As well as classical signal transduction via the integrins (indirect activation of Ras/MAPK phosphorylation pathways, for example) these receptors are also able to transmit information about the surrounding microenvironment and extracellular matrix (ECM) directly to the actin microfilaments via actin binding proteins talin, vinculin and paxillin, amongst others (Brakebusch and Fassler, 2003). For example, β1 integrin binding triggers F-actin stress fibre formation and paxillin integration to focal adhesions in epithelial cells in response to culture on fibronectin (Danen et al., 2002). Similarly, in mouse and human monocytes active phosphorylated paxillin has been observed in the lamellipodia and membrane ruffles formed after LPS stimulation (Williams and Ridley, 2000), again indicating reorganisation of the actin microfilaments potentially driven by integrin mediated activity. An interesting recent study into a novel family of integrin-related adhesion proteins, the

kindlins, has found the hematopoietic lineage-specific kindlin-3 to co-localise with vinculin in F-actin rich areas known as podosomes (Ussar et al., 2006). Whilst the integrin binding partners of kindlin-3 are not yet known kindlin-1 can interact with the cytoplasmic tail of β1 and β3 integrins.

In addition to filamentous proteins the cytoskeleton is also composed of numerous accessory proteins, like paxillin mentioned above, which aid its function. In polarised cells actin related protein (Arp)2/3 has been shown to concentrate at the leading edge where it is thought to mediate the branching of actin filaments (Ridley et al., 2003). Despite the mechanism of Arp2/3 function coming into some controversy recently it is clear that this protein does play an important role in the formation of actin microfilaments (Urban et al., 2010). In macrophages Arp2/3 appears to play a critical role in cell polarisation and migration via the formation of podosomes (Linder et al., 2000). Linder et al found that macrophages deficient in WASp, which plays a role in actin organisation via Arp2/3, are unable to polarise in a gradient of chemoattractant whilst also failing to form podosomes.

Non-muscle myosin II-A, also an actin accessory protein, plays an important role in cell polarisation and migration by acting as a motor protein. Myosin II mediates intracellular force by 'walking' along actin filaments, forming stress fibres. Whilst myosin II is typically considered to be involved in force generation during tail retraction of migrating cells (Uchida et al., 2003) there is also evidence to suggest it plays a role at the cell periphery and in lamellipodia disassembly. For example, when the phosphorylation and subsequent activation of myosin II is inhibited in fibroblasts the formation of peripheral actin stress fibres is disturbed and cells were no longer able to spread (Conti and Adelstein, 2008; Katoh et al., 2001). *In vivo* studies utilizing a myosin II inhibitor in a model of renal disease have shown a reduction in inflammation and tissue damage as a result of reduced migration and infiltration of immune cells, including macrophages (Si et al., 2010). This demonstrates the importance of actin accessory proteins in physiologically relevant cell migration within inflammatory disease states.

6.2 Aims

In this chapter chemotaxis is explored *in vitro*, in the type II diabetic Db/Db bone marrow-derived macrophage compared to Db/+ heterozygous counterparts. Time-lapse microscopy is utilized to quantify differences in migratory phenotype in response to MCP-1 and CSF-1. To further explore the role of morphology and potential mechanisms controlling cell motility in bone marrow-derived macrophages, immunocytochemical staining for cytoskeletal components α-tubulin, β-actin, myosin II and the Arp2 sub-unit was performed.

6.3 Results

6.3.1 Bone marrow-derived macrophages from the Db/Db type II diabetic mouse exhibit significantly longer cell protrusions than their Db/+ heterozygous control and wild-type counterparts

During routine culture of type II diabetic (Db/Db) bone marrow-derived macrophages (BMMs) a distinct morphological difference was observed when compared to their heterozygous (Db/+) control and wild type (WT) BMMs (figure 6.1). Specifically, Db/Db BMM appear to have longer cell protrusions than either Db/+ or WT BMM. In order to quantify this observation, fully differentiated cells were measured from the centre of the nucleus to the tip of the protrusion (figure 6.1 C and D). Comparison of WT, Db/+ and Db/Db BMM from three mice per phenotype reveals this difference in morphology to be significant, with average protrusion lengths of 24.9 µm ±11.04, 25.8 µm ±12.54 and 39.5 µm ±19.98, respectively (figure 6.2). It is interesting to note the range of protrusion lengths measured for each BMM phenotype highlighting the heterogeneity of BMM culture despite the significantly greater mean protrusion length observed for Db/Db BMMs.

These results represent combined data from three independent experiments comparing WT, Db/+ and Db/Db BMM protrusion length.

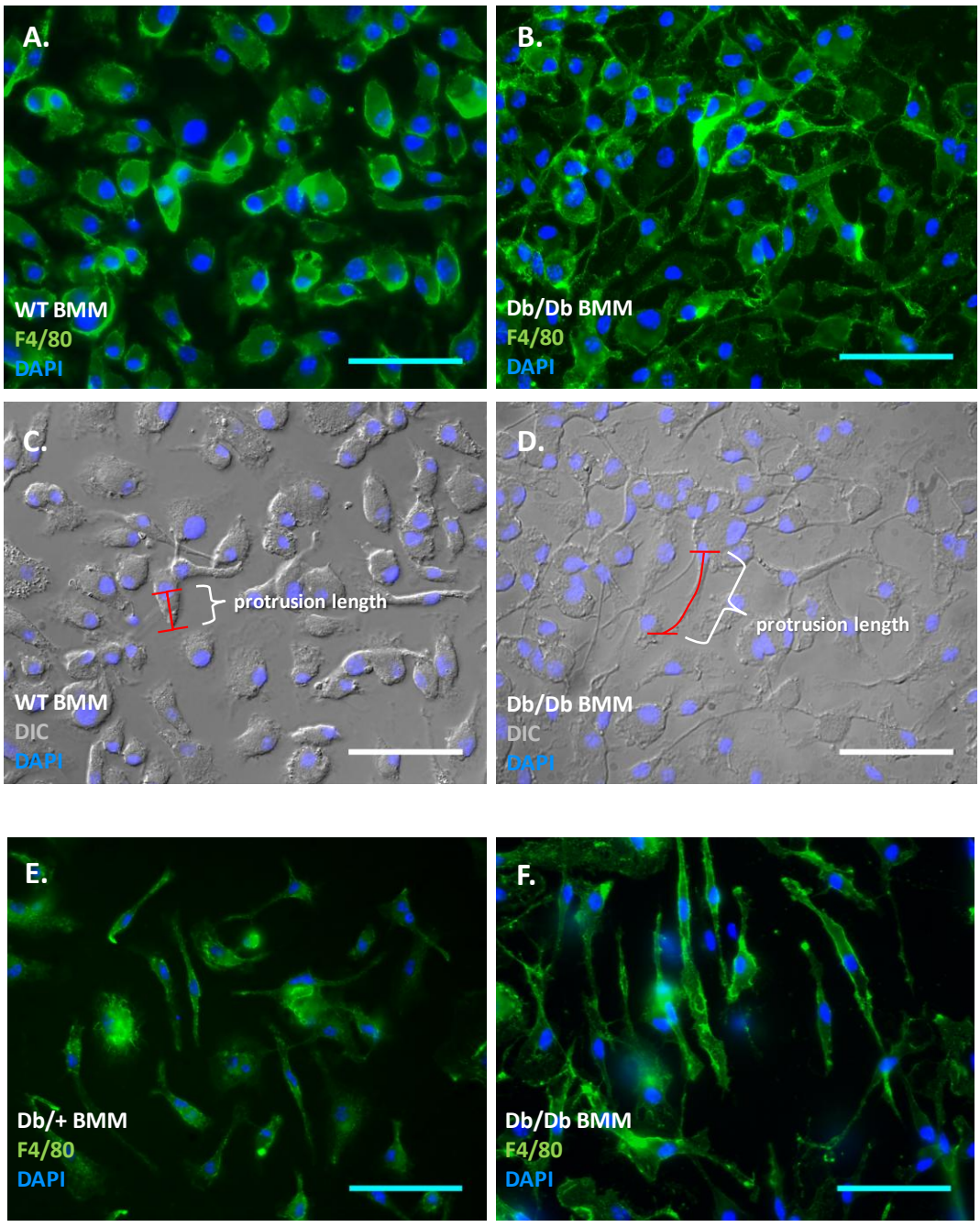

Figure 6.1 Routine culture reveals an apparent difference in morphology between type II diabetic Db/Db BMMs, heterozygous Db/+ BMMs and their wild-type BMM counterparts. (A, C) Fully differentiated wild-type and (B, D) Db/Db BMMs stained for the murine macrophage marker F4/80 and DAPI and imaged via DIC microscopy, display morphological differences that can be quantified by measuring protrusion length as shown. (E) Db/+ BMMs also appear morphologically distinct compared to (F) Db/Db BMM (images E and F taken of a region of lower cell density). Scale = 50 µm.

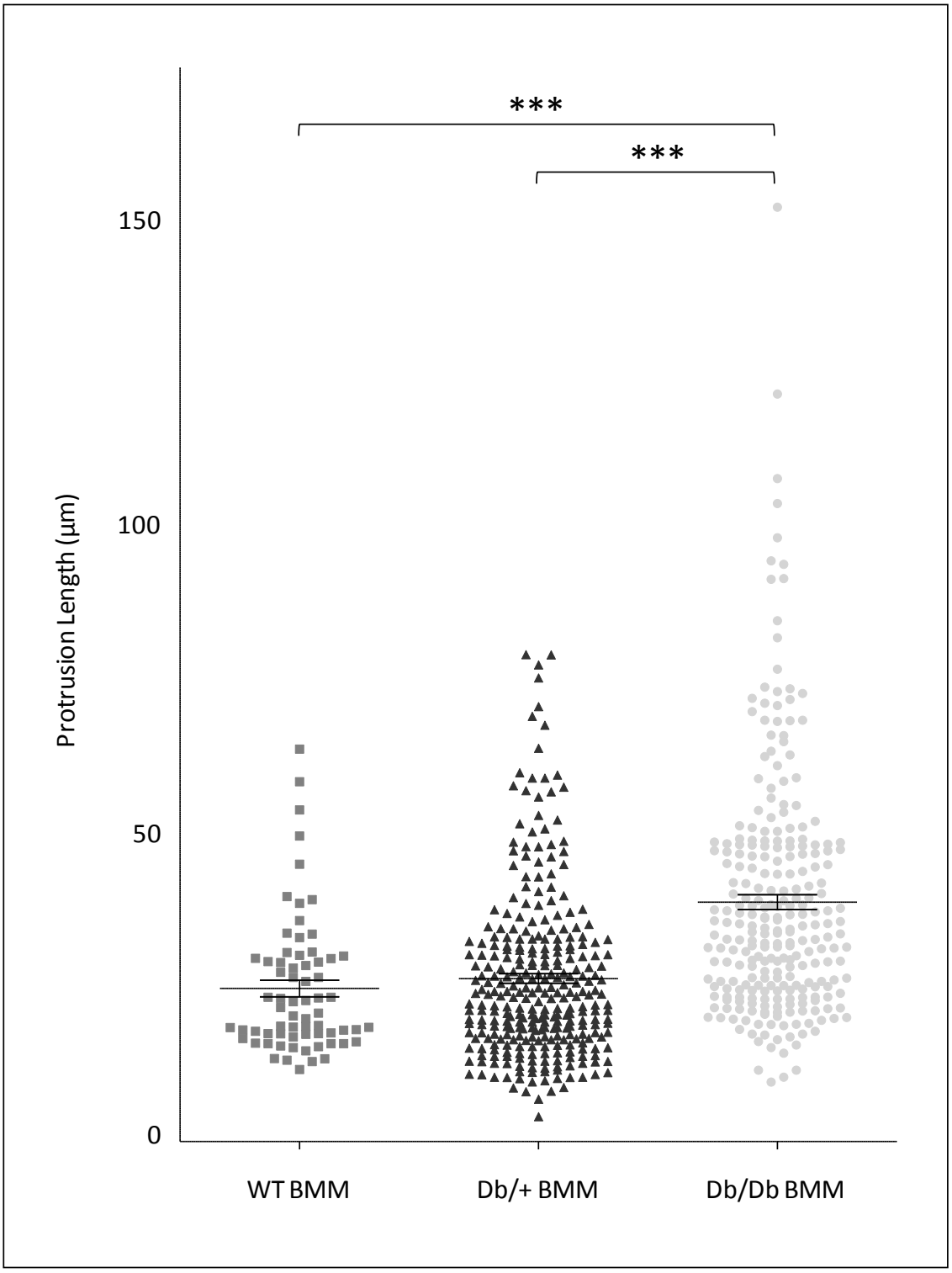

Figure 6.2 Range and average length of cell protrusions from type II diabetic Db/Db BMMs, heterozygous Db/+ BMMs and their wild-type BMM counterparts. Cell protrusions from fully differentiated wild-type (n = 68), Db/+ (n = 190) and Db/Db BMMs (n = 190) from 3 mice per phenotype were measured. Horizontal bar shows mean protrusion length of number of cells given ± SEM. Statistical significance was determined using the Student's t-test. *** $p \leq 0.001$.

6.3.2 Exposure to high levels of blood glucose does not appear to be the cause of increased protrusion length in type II diabetic Db/Db bone marrow derived macrophages

To determine the cause of altered Db/Db BMM morphology we considered the possibility of epigenetic regulation caused by exposure to high blood glucose levels in vivo. As with all cells, macrophages require glucose for survival but little is known about the effect of high glucose levels on macrophages long term, such as those experienced in the Db/Db mouse *in vivo*. Transient hyperglycemia is sufficient to cause epigenetic modification for up to 7 days in endothelial cells (Curnock et al., 2002) leading to the hypothesis that, once harvested, the Db/Db BMMs are likely to retain any glucose-induced epigenetic changes throughout the duration of these experiments. If increased protrusion length is due to Db/Db BMM exposure to higher concentrations of glucose *in vivo* it is possible that treating WT BMM with comparable levels of glucose will induce a similar morphology. Monitoring of blood glucose in Db/Db mice revealed a range from 17.4 - ≥33 mM (chapter 2, table 2.6), so to ensure hyperglycaemic levels were achieved *in vitro* WT BMM were cultured in 40 mM D-Glucose. Despite a small trend toward increased protrusion length however, exposure of WT BMM to 40 mM D-Glucose for 24 hours *in vitro* triggered no significant change in protrusion length or gross cell morphology (27.38 µm ±17.46 compared with 33.14 µm ±15.87, respectively; figure 6.3 A-E). D-Mannitol, a sugar that has the same osmotic properties as D-Glucose but is not metabolised, is used as a control. Interestingly this also appears to stimulate a trend for increased protrusion length with an average of 35.37 µm and, rather unexpectedly, appeared to trigger a more spread-out and dendritic phenotype in WT BMMs (figure 6.3 A, F, G).

This preliminary experiment was performed once and results represent cells harvested from one mouse per phenotype.

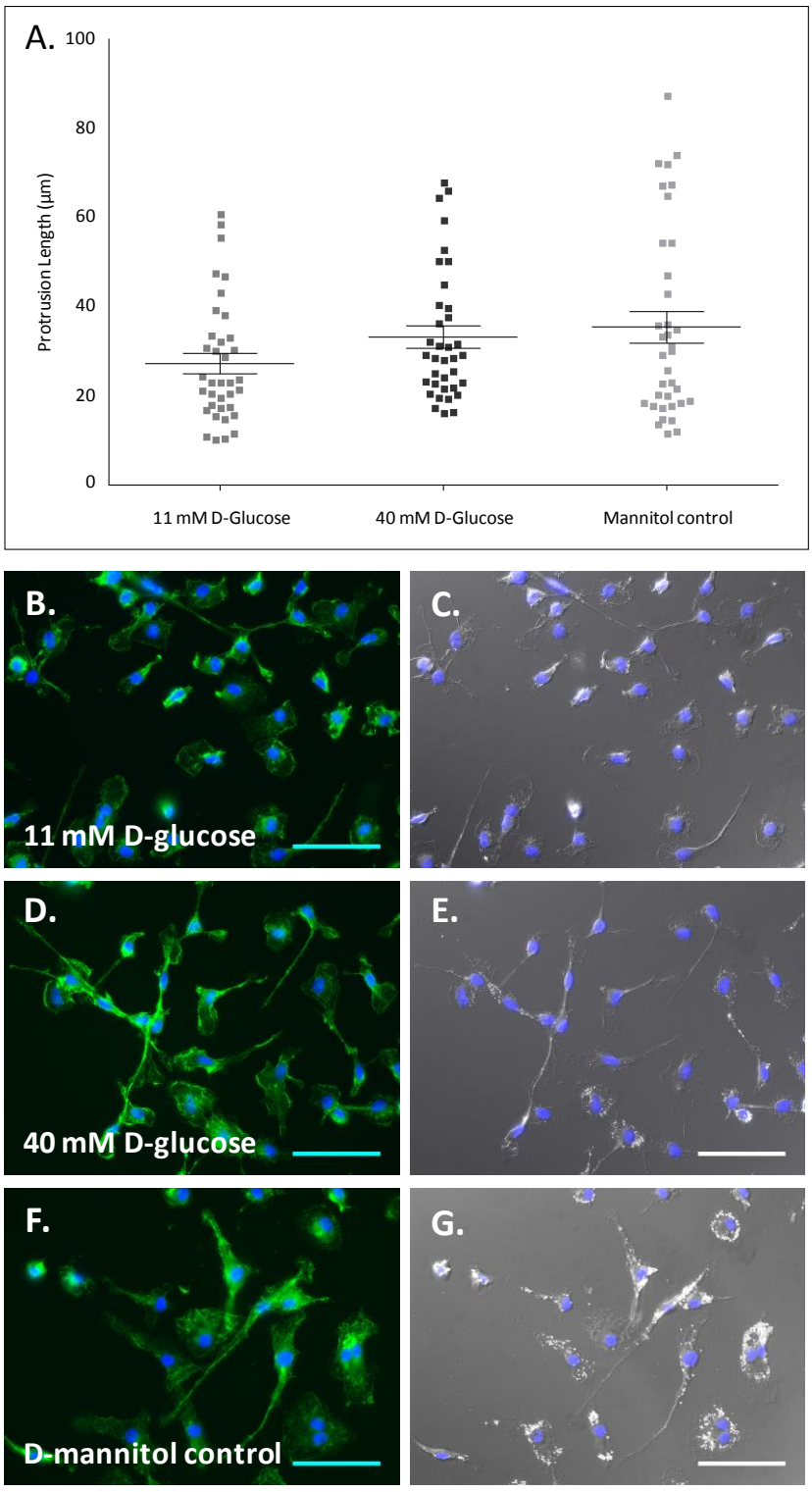

Figure 6.3 Range and average length of cell protrusions from WT BMMs cultured in normoglycemic and hyperglycaemic conditions for 24 hours. (A) Cell protrusions from wild-type BMMs (n = 36 cells per treatment) cultured in either 11mM (normoglycemic) or 40 mM (hyperglycaemic) D-glucose for 24 hours were measured. Cells were cultured in D-mannitol as a control. Horizontal bar shows mean protrusion length of 36 cells ± SEM. (B-G) WT BMM were fixed and stained for F4/80 murine macrophage marker and DAPI, or imaged via DIC microscopy, to further reveal any morphological differences. Scale bar = 50 µm.

6.3.4 Bone marrow-derived macrophages from the Db/Db type II diabetic mouse migrate significantly more slowly on two-dimensional fibronectin and fibrinogen than the Db/+ heterozygous counterparts

The morphological differences observed in Db/Db BMM (figure 6.1 - 6.2) could relate to a change in migratory phenotype and this can be analysed by time-lapse microscopy of BMM migration. *In vivo,* macrophage migration occurs commonly on matrices composed of fibronectin and fibrinogen. To this end functional studies of random cell migration on various 2D matrices were performed with Db/+ BMMs as a control.

There were no significant differences in velocity or distance migrated when comparing Db/Db and Db/+ BMMs in the presence of 0.2% serum alone with no 2D matrix (figure 6.4 A). On 2D coats of fibrinogen and fibronectin, however, both Db/Db and Db/+ BMMs showed significantly slower migration velocity and decreased accumulated distance migrated compared to those with only 0.2% serum (figure 6.4 A, B). Db/+ BMMs also showed a significant decrease in Euclidean distance migrated on fibrinogen compared to 0.2% serum (figure 6.4 C). Perhaps most interesting is the significant reduction in velocity and accumulated distance migrated observed in Db/Db BMM compared to Db/+ BMMs on both fibrinogen and fibronectin (figure 6.4 A, B). This is also reflected in the Euclidean distance migrated on fibronectin, despite not being statistically significant (figure 6.4 C).

Plots of Db/Db and Db/+ BMM trajectory on each substrate reflect the quantitative results described above (figure 6.5). The reduction in Db/Db BMM migration distance, both accumulated and Euclidean, is particularly evident on plasma fibronectin compared to Db/+ BMMs (figure 6.5 C, F). These results suggest that the increase in protrusion length observed on Db/Db BMMs has a functional effect on their ability to migrate.

This preliminary experiment was performed once and results represent cells harvested from one mouse per phenotype.

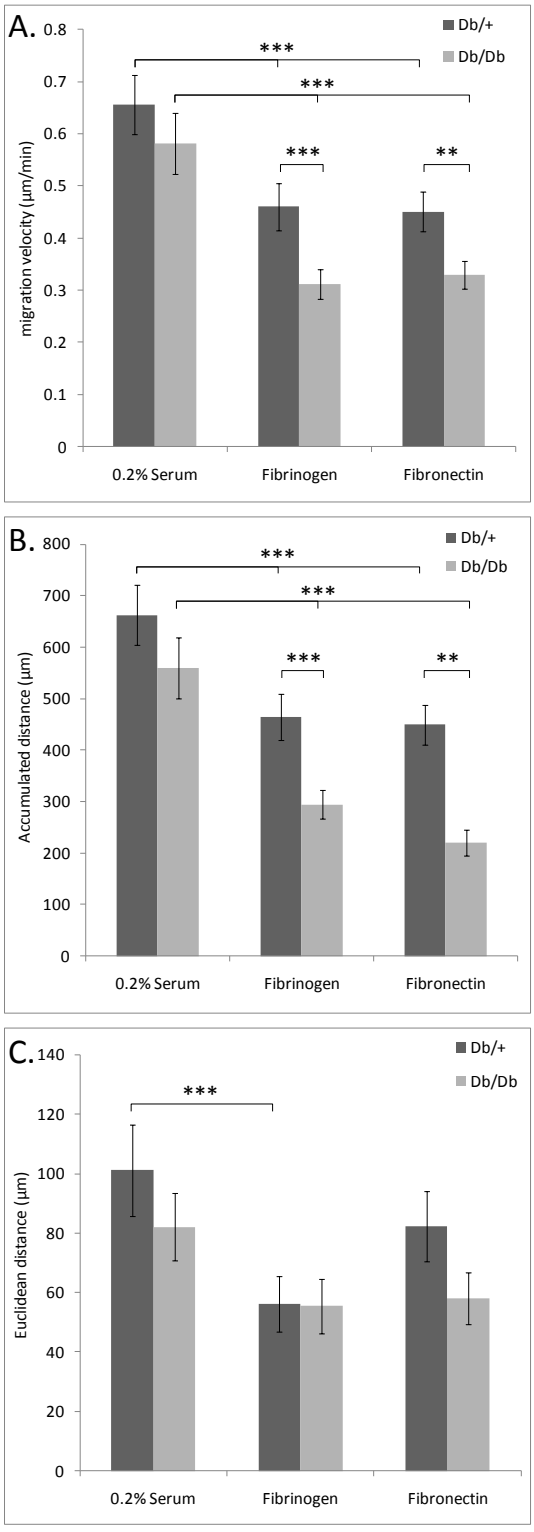

Figure 6.4 Type II diabetic Db/Db BMM migration velocity is significantly less than heterozygous Db/+ BMMs. Time-lapse images were captured every 10 minutes over a 17 hour period for Db/+ and Db/Db BMMs in 0.2% serum alone (n = 35 or n = 29 cells, respectively) or on plasma fibrinogen or plasma fibronectin (n = 39 or n = 35 cells, respectively). (A) Migration velocity, (B) accumulated distance and (C) Euclidean distance of BMMs were analyzed with ImageJ processing software. Each bar represents the mean of the number of calls given ± SEM. Statistical significance was determined using the Student's t-test. *** $p \leq 0.001$.

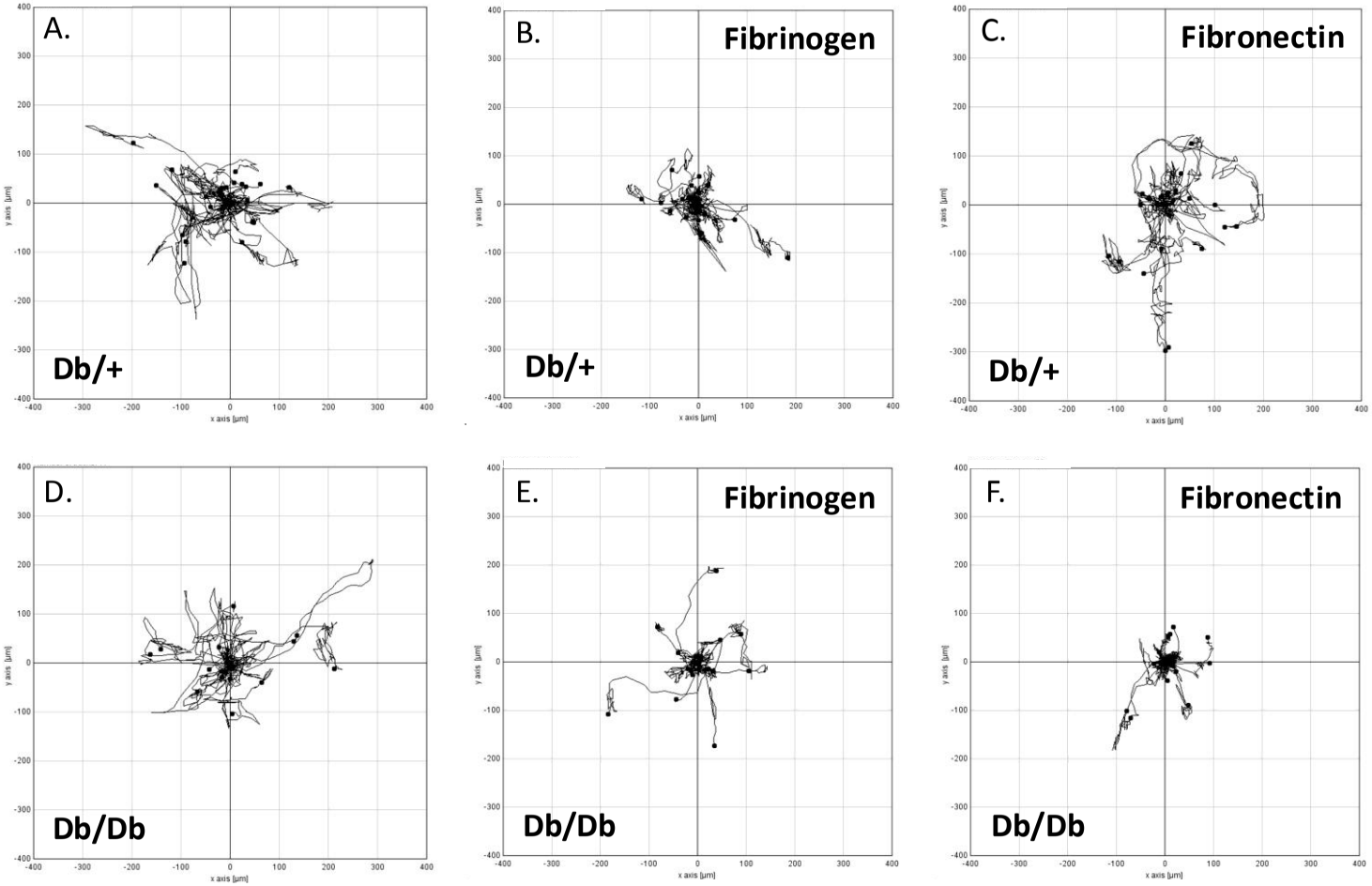

Figure 6.5 Plots of type II diabetic Db/Db BMM migration trajectory on ECM components reflect migration velocity and distance compared to heterozygous control. Cell trajectories were derived from time-lapse images of (A) Db/+ BMMs with 0.2% serum only, (B) plasma fibrinogen and (C) plasma fibronectin; and (D) Db/Db BMMs with 0.2% serum only, (E) plasma fibrinogen and (F) plasma fibronectin were captured every 10 minutes over a 17 hour period. Migration was analyzed with ImageJ processing software.

6.3.5 Wild-type bone marrow-derived macrophages migrate significantly more quickly in gradients of Colony Stimulating Factor-1 and Monocyte Chemotactic Protein-1

The data regarding random migration (figure 6.4 - 6.5) revealed intriguing differences between the migration of diabetic and non-diabetic-derived macrophages. It was important, however, to explore this in more detail by analysing directional migration.

It is well understood that monocyte chemotactic protein (MCP)-1 is responsible for mobilisation of several leukocyte subsets during inflammation (Dean et al., 2008), whilst colony stimulating factor (CSF)-1 has been shown to play an important role in the growth and survival of macrophages *in vivo* (Kleemann et al., 2008). In keeping with such observations, wild-type BMMs responded to gradients of recombinant murine (rm) MCP-1 and CSF-1 with increased migration *in vitro* (figure 6.6). This result is particularly interesting as the increased Euclidean distance migrated by WT BMMs in the rmMCP-1 gradient suggests a far greater directionality of migration compared to both the control treatment and the gradient of rmCSF-1, indicating that these factors stimulate chemotaxis in WT BMMs (figure 6.6 C). This is clearly reflected in plots of WT BMM trajectory (figure 6.7). WT BMM in 10% serum only show no clear uniformity of migration; despite a number of cells moving into the lower sector of the plot (red trajectories) there are also a number of cells migrating into the upper sector (black trajectories) (figure 6.7 A).

To further analyse data from directional migration it is possible to investigate directional bias or cell migration. Rose diagrams represent the number of times a cell passes through each 10° sector and correspond to plots of cell trajectory. For WT BMMs the Rose diagram clearly shows no bias for directionality (figure 6.7 B). The result of a Rayleigh test for uniformity of migration also reveals no significant directionality ($p = 0.55$). WT BMMs appear to show a strong trend for migration towards an rmCSF-1 gradient (figure 6.7 C), with several cells moving into the bottom sector. The corresponding Rose diagram also suggests a trend toward chemotaxis however the Rayleigh test reveals that this is not significant ($p = 0.33$) (figure 6.7 D). The response of WT BMMs to rmMCP-1, however, is far more robust. The plot of cell trajectories in this chemokine gradient show the majority of cells analysed migrating well into the bottom sector (figure 6.7 E). This is echoed by the corresponding Rose diagram showing a clear directional bias of cells moving towards the rmMCP-1 gradient and a significant result for the Rayleigh test for uniformity ($p \leq 0.05$).

This data is representative of the results of two experiments, harvesting BMMs from one mouse per experiment.

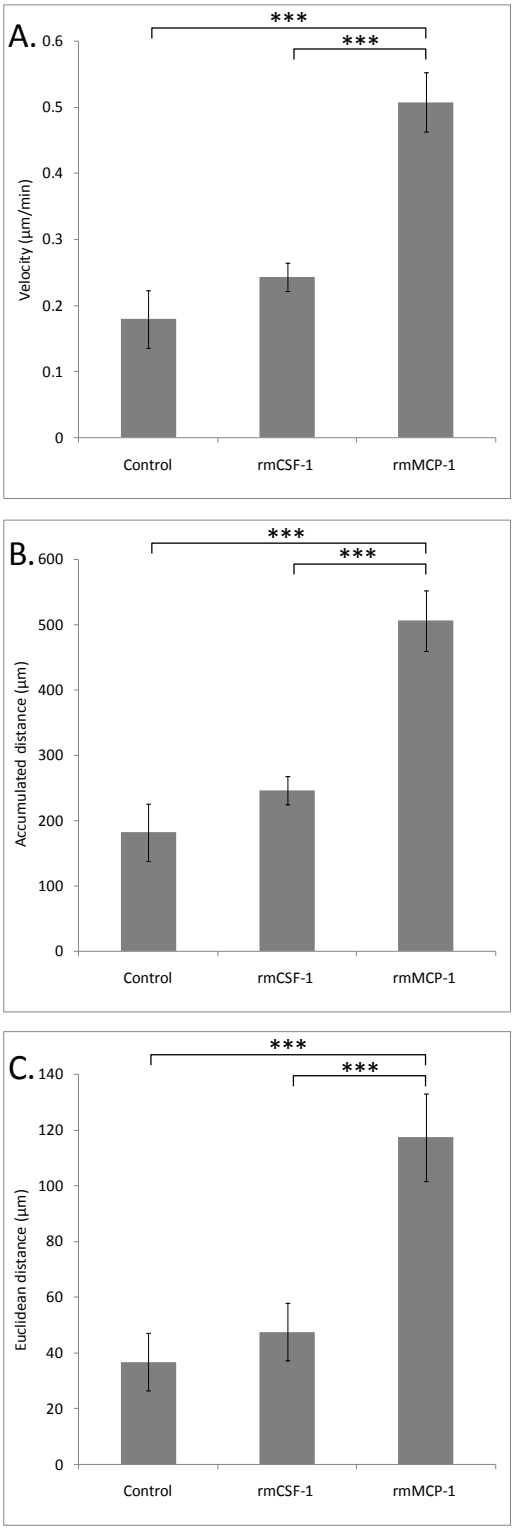

Figure 6.6 WT BMM migration velocity and Euclidean distance is significantly greater is gradients of rmCSF-1 and rmMCP-1. Time-lapse images were captured every 10 minutes over a 17 hour period of WT BMMs in either 10% serum (control; n = 16 cells), or a gradient of 200 ng/ml rmCSF-1 (n = 31 cells) or rmMCP-1 (n = 30 cells). (A) Migration velocity, (B) accumulated distance and (C) Euclidean distance of WT BMMs were analyzed with ImageJ processing software. Each bar represents the mean of the number of cells given ± SEM. Statistical significance was determined using the Student's t-test. *** $p \leq 0.001$.

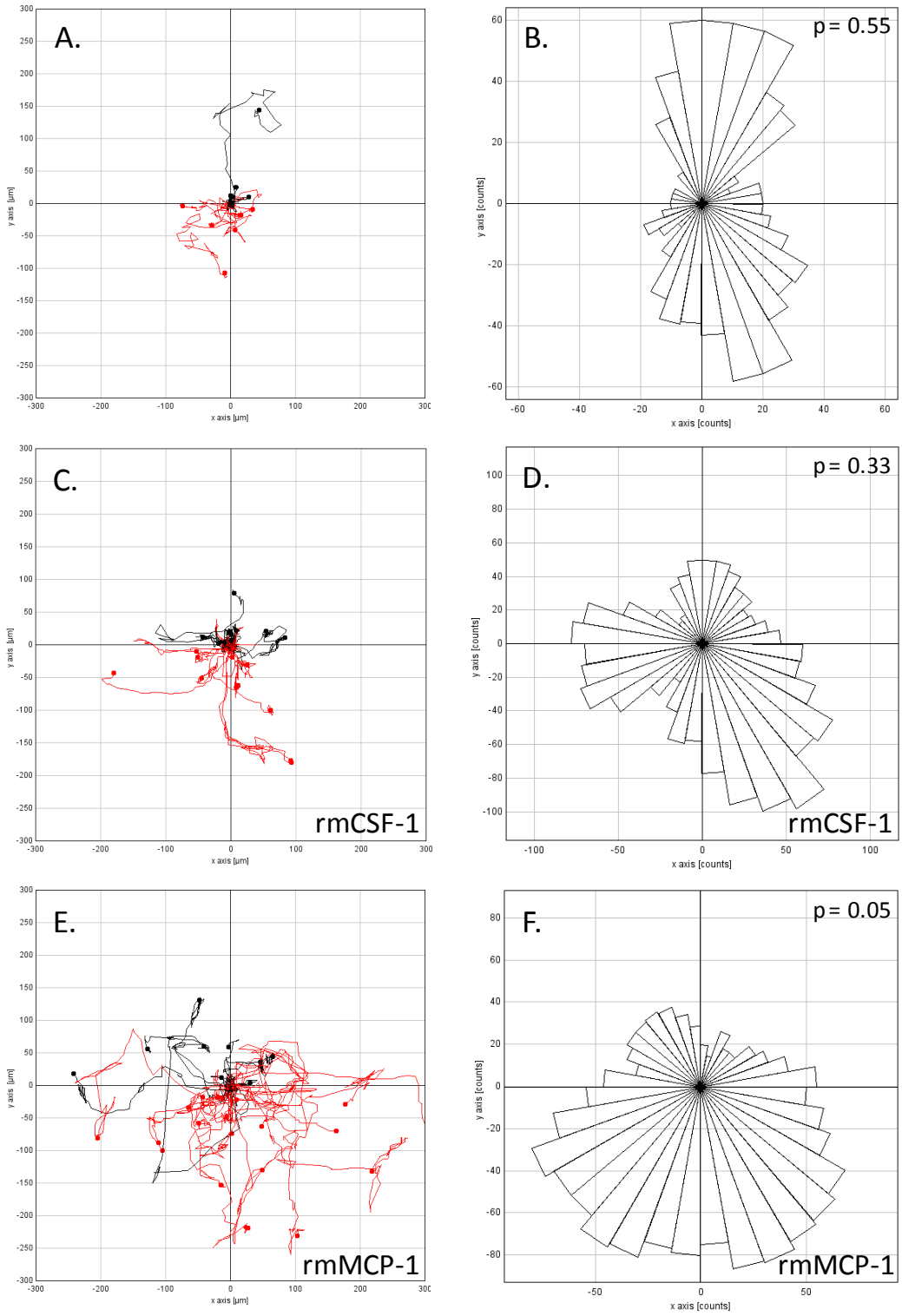

Figure 6.7 Plots of WT BMM migration trajectory in gradients of rmCSF-1 and rmMCP-1. Cell trajectories were derived from time-lapse images captured every 10 minutes over a 17 hour period of WT BMMs in (A) 10% serum only, (C) 200 ng/ml rmCSF-1 gradient and (E) 200 ng/ml rmMCP-1. (B, D, F) Corresponding 'Rose diagram' and result of Rayleigh test for uniformity are shown. The source of chemokines is at the bottom of each diagram whilst red trajectory indicates cells with an overall migration towards gradient. Migration was analyzed and Rayleigh test calculated with ImageJ processing software.

6.3.6 Bone marrow-derived macrophages from the Db/Db type II diabetic mouse are less responsive to a gradient of monocyte chemotactic protein-1 than their Db/+ heterozygous or wild-type controls

As a gradient of rmMCP-1 elicited the greatest migratory response in WT BMMs (figure 6.6) this chemokine was utilised to stimulate migration of Db/Db and Db/+ BMMs enabling further elucidation of the functional repercussions of greater protrusion length in Db/Db BMMs. When comparing WT, Db/+ and Db/Db BMM migration velocity and accumulated distance a significantly slower migratory phenotype was observed in the Db/Db macrophages (figure 6.8 A, B). A small trend for decreased Euclidean distance migrated was also observed for Db/Db BMMs (figure 6.8 C). Plots of BMM trajectory contribute additional information allowing application of these quantitative results to directional chemotaxis. For example, in addition to migrating significantly more slowly, the Db/Db BMM plot displays a number of cell trajectories in the upper sector and a Rose diagram that suggests little directional bias towards the source of rmMCP-1 (figure 6.9 E, F). The Db/+ BMM migration plot is less revealing, with a several cell trajectories remaining in the in the upper sector (figure 6.8 C) despite their migrating significantly more quickly and a greater accumulated distance than Db/Db BMMs. The Db/+ BMM Rose diagram does however reflect the directional bias towards the source of rmMCP-1 (figure 6.9 D). The WT BMM plot of cell trajectory and Rose diagram more clearly reflect the migration of macrophages towards to source of rmMCP-1 (figure 6.9 A, B). Perhaps surprisingly the Rayleigh test for uniformity shows no significant directional bias of migration by WT ($p = 0.16$), Db/+ ($p = 0.44$) or Db/Db ($p = 0.12$).

This experiment was performed twice and combined data is presented from two mice per phenotype.

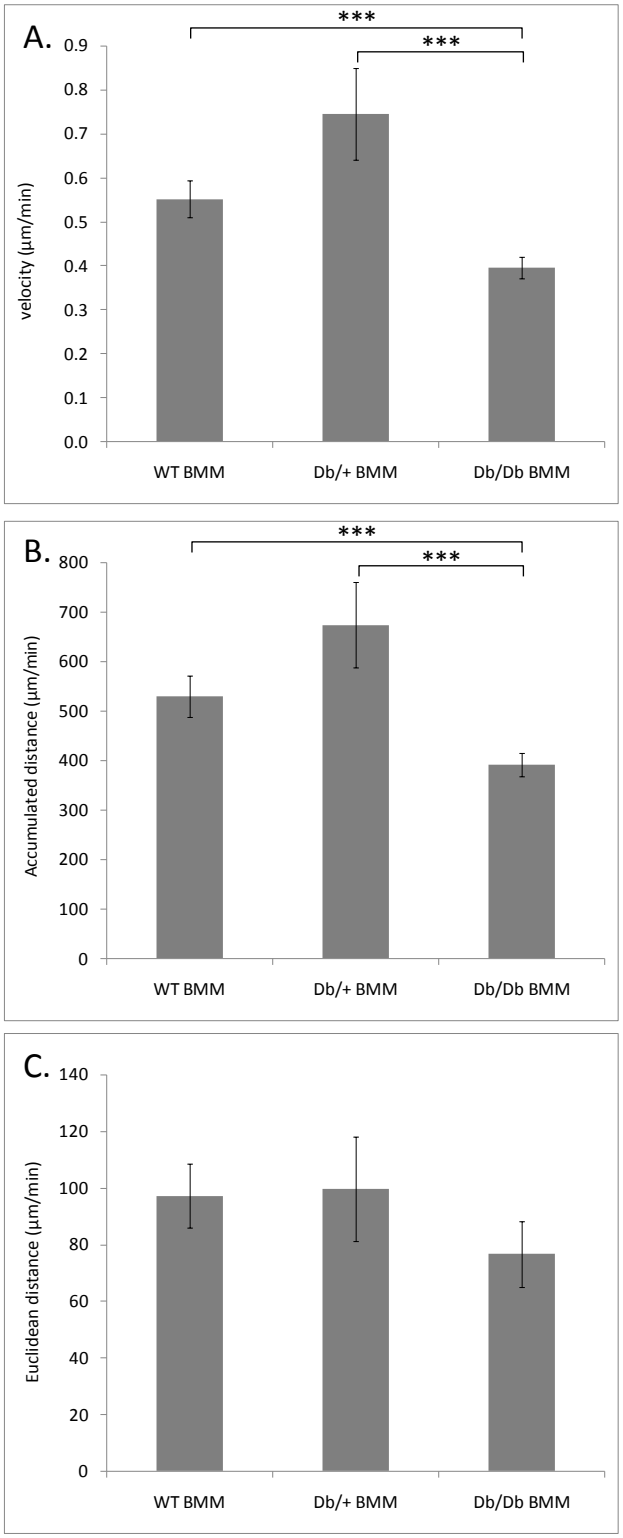

Figure 6.8 Comparing WT, Db/+ and Db/Db BMM migration in gradients of rmMCP-1. Time-lapse images were captured every 10 minutes over a 17 hour period of WT (n = 50 cells), Db/+ (n = 45 cells) and Db/Db BMMs (n = 47 cells) in a gradient of 200 ng/ml rmMCP-1. (A) Migration velocity, (B) accumulated distance and (C) Euclidean distance of each genotype of BMM was analyzed with ImageJ processing software. Each bar represents the mean of the number of cells given ± SEM. Statistical significance was determined using the Student's t-test. *** $p \leq 0.001$.

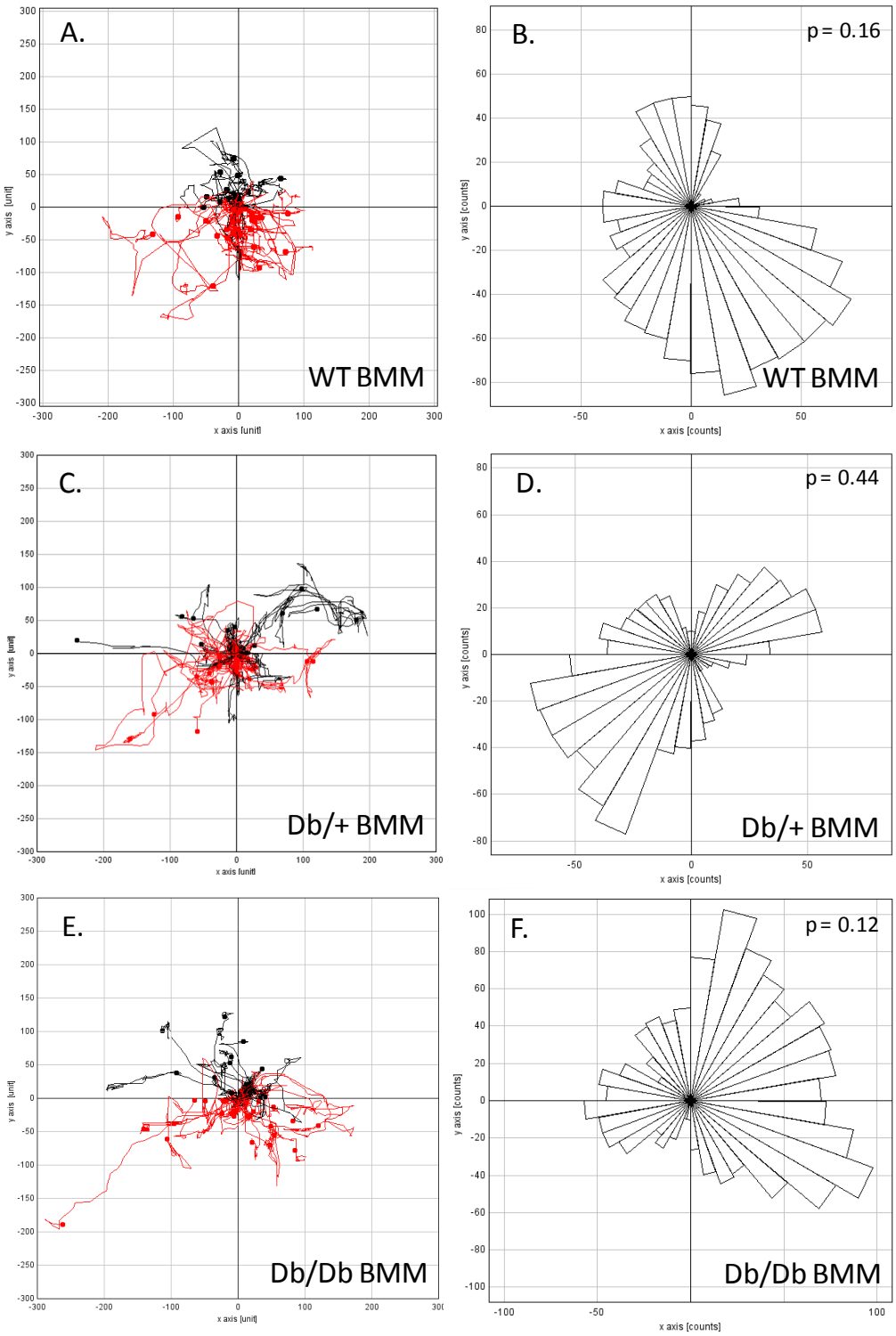

Figure 6.9 Plots of WT, Db/+ and Db/Db BMM migration trajectory in a gradients of rmMCP-1. Cell trajectories were derived from time-lapse images captured every 10 minutes over a 17 hour period of (A) WT BMMs, (C) Db/+ BMMs and (E) Db/Db BMMs in 200 ng/ml rmMCP-1. (B, D, F) Corresponding 'Rose diagram' and result of Rayleigh test for uniformity are shown. The source of chemokines is at the bottom of each diagram whilst red trajectory indicates cells with an overall migration towards gradient. Migration was analyzed and Rayleigh test calculated with ImageJ processing software.

6.3.7 Comparing cytoskeletal components in type II diabetic Db/Db bone marrow derived macrophages and their Db/+ heterozygous controls

The cytoskeleton is instrumental in the control of cell motility, including change in cell shape, interaction with substrates and other cells, and mediating chemotaxis. Following observations of enhanced protrusion length (figure 6.1 - 6.2) and decreased migratory phenotype in Db/Db compared to Db/+ BMMs (figure 6.8) an immunocytochemical approach was taken to explore potential differences in cytoskeleton. Immunocytochemical staining of four major components of the cytoskeleton; α-tubulin, β-actin, non-muscle myosin II-A and actin related protein (Arp) 2/3, was performed.

As a major component of the microtubule network, α-tubulin plays an important role in cell polarisation and rapid morphological response to stimulus. In Db/+ BMMs immunocytochemical staining of α-tubulin revealed relatively distinct networks of microtubules (figure 6.10 A). In certain cases these appear to emanate in an array from one distinct point adjacent to the nucleus, probably the microtubule organising centre (MTOC) (figure 6.11 A, C). In Db/Db BMMs this radial array of microtubules is not apparent, possibly due to lack of centrosomal focus (figure 6.10 B and 6.11 B, D).

β-actin, a non-muscle actin subunit, plays an important role in cell migration by polymerising to form actin filaments, although in macrophages the formation of classic 'stress fibres' is not observed. Immunocytochemical staining for β-actin in Db/+ and Db/Db BMM served to further highlight the morphological difference between the two macrophage phenotypes (figure 6.12). As well as the longer cell protrusions observed for Db/Db BMM there also appeared to be a possible increase in total cell area with increased lamellipodia and filopodia staining positive for β-actin (figure 6.12 B). As expected, filamentous actin stress fibres are not present in either phenotype and instead pools of β-actin are apparent.

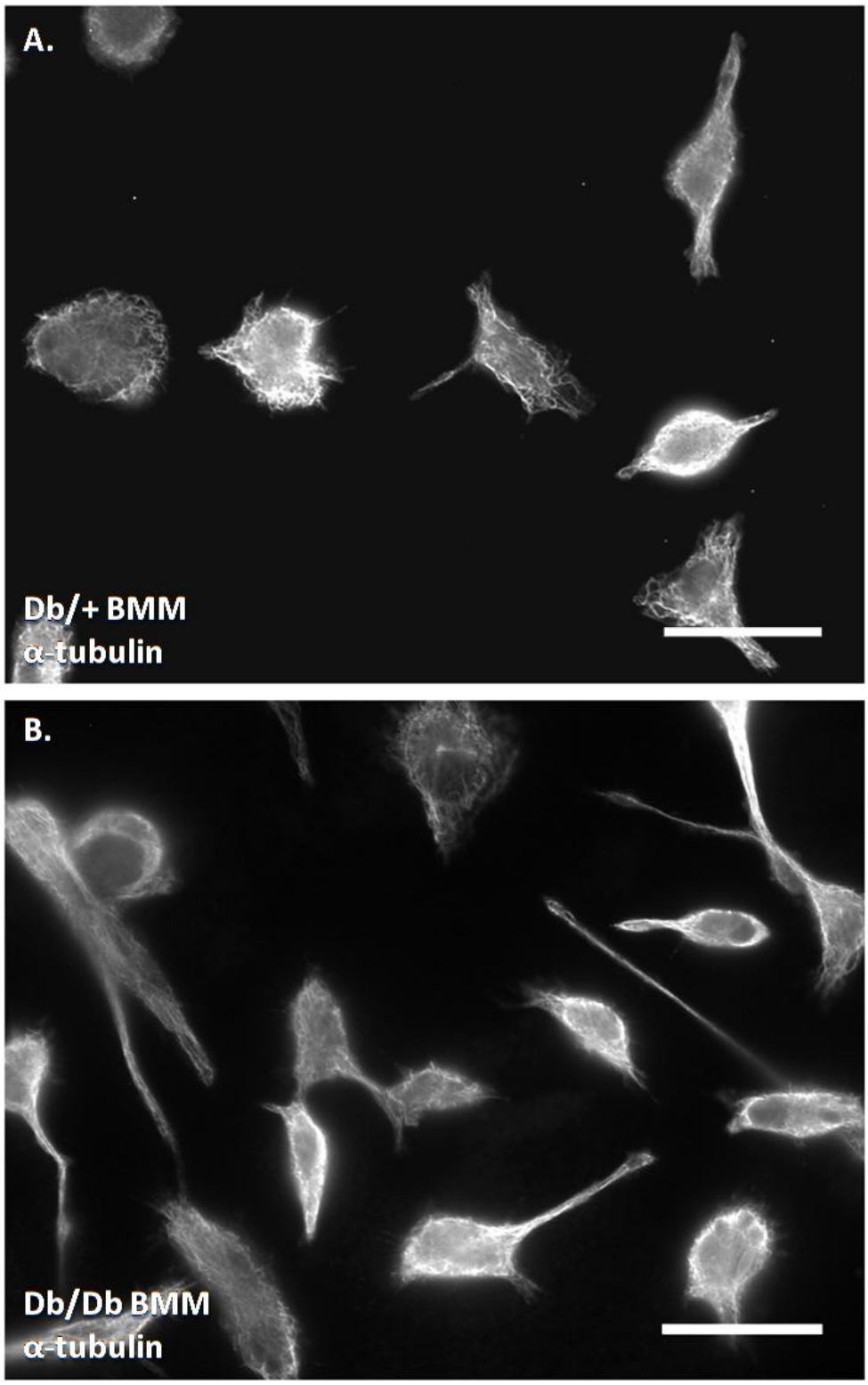

Figure 6.10 Immunocytochemical staining for α-tubulin in Db/+ and Db/Db BMMs. (A) Db/+ BMMs and (B) Db/Db BMMs were cultured on glass cover-slips for 24 hours before fixing and staining for α-tubulin. Scale bar = 25 µM

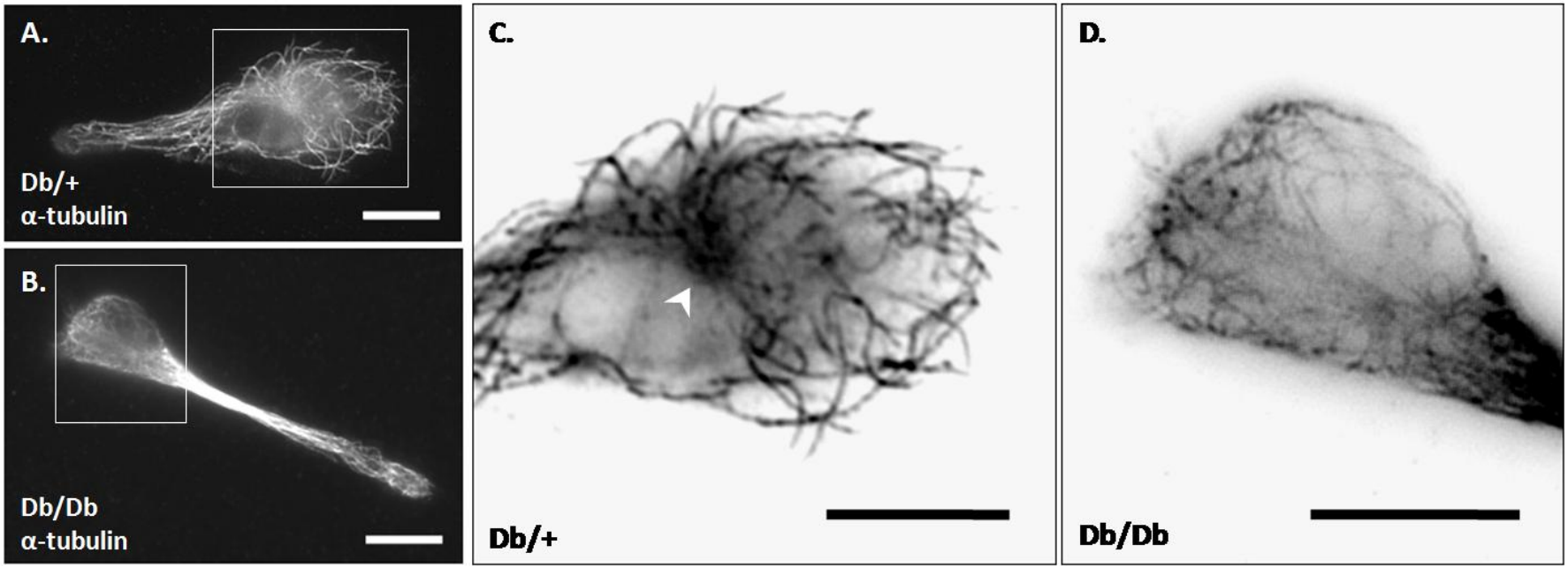

Figure 6.11 Immunocytochemical staining for α-tubulin in Db/+ and Db/Db BMMs: Detail. (A) Db/+ BMMs and (B) Db/Db BMMs were cultured on glass cover-slips for 24 hours before fixing and staining for α-tubulin. White boxes indicate areas highlighted in (C, D) inverted for clarity. Arrowhead indicates possible MTOC. Scale bar = 10 µM

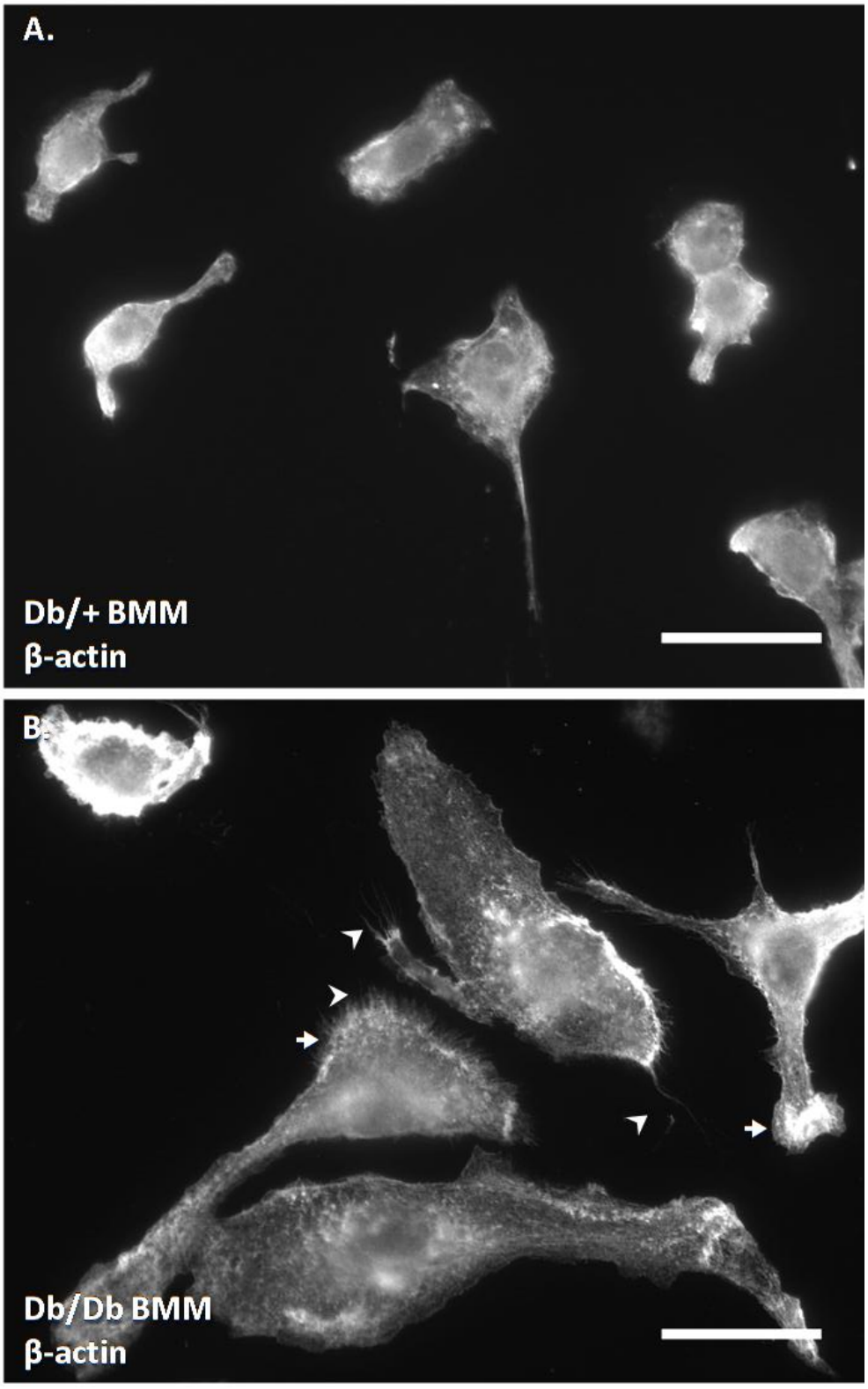

Figure 6.12 Immunocytochemical staining for β-actin in Db/+ and Db/Db BMMs. (A) Db/+ BMMs and (B) Db/Db BMMs were cultured on glass cover-slips for 24 hours before fixing and staining for β-actin. Arrows indicate areas of lamellipodia. Arrowheads indicate filopodia. Scale bar = 25 μM

Non-muscle myosin II-A (myosin II) also plays important roles in cell migration, polarisation and cell-cell interaction. This is achieved via its action as a motor protein that can mediate force by moving along actin filaments. Again, immunocytochemical staining for myosin II in both Db/+ and Db/Db BMMs highlights the increased protrusion length and total cell area of Db/Db macrophages (figure 6.13) and is reflective of the β-actin staining. Staining appeared to be more distinctly punctate in Db/Db BMMs than Db/+ BMMs, particularly along the cell membrane (figure 6.13 B). Interestingly, despite its proposed role in tail retraction, there did not appear to be any obvious polarisation of myosin II in either macrophage phenotype.

As the pattern of β-actin and myosin II expression appear similar in both phenotypes, double staining for these proteins was performed in Db/Db and Db/+ BMMs (figure 6.14). There appeared to be some co-localisation along the cell periphery and in small areas of lamellipodia in both Db/+ and Db/Db BMMs (figure 6.14 A, D).

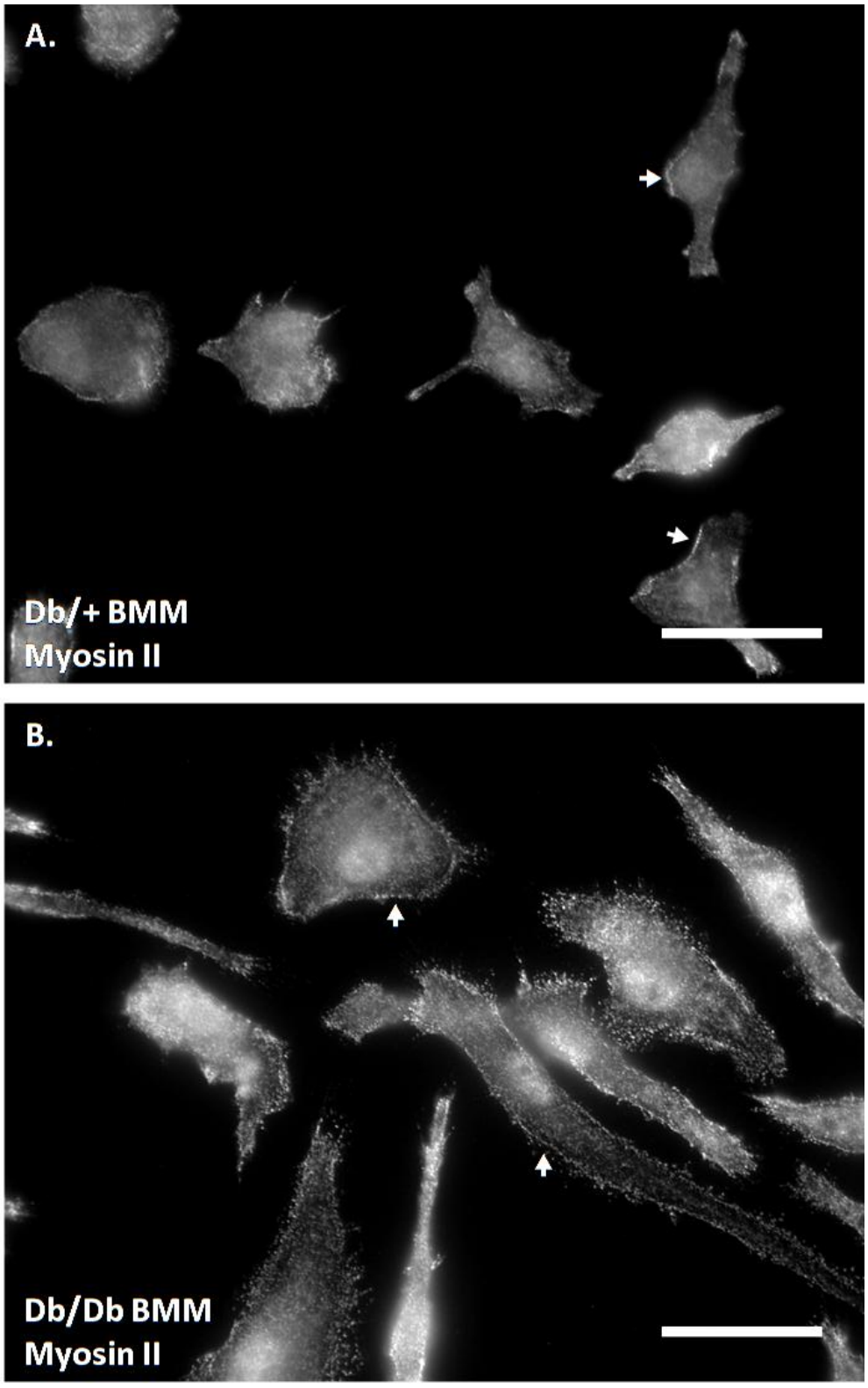

Figure 6.13 Immunocytochemical staining for non-muscle Myosin II in Db/+ and Db/Db BMMs. (A) Db/+ BMMs and (B) Db/Db BMMs were cultured on glass cover-slips for 24 hours before fixing and staining for non-muscle Myosin II. Arrows indicate concentration at cell membrane. Scale bar = 25 μM

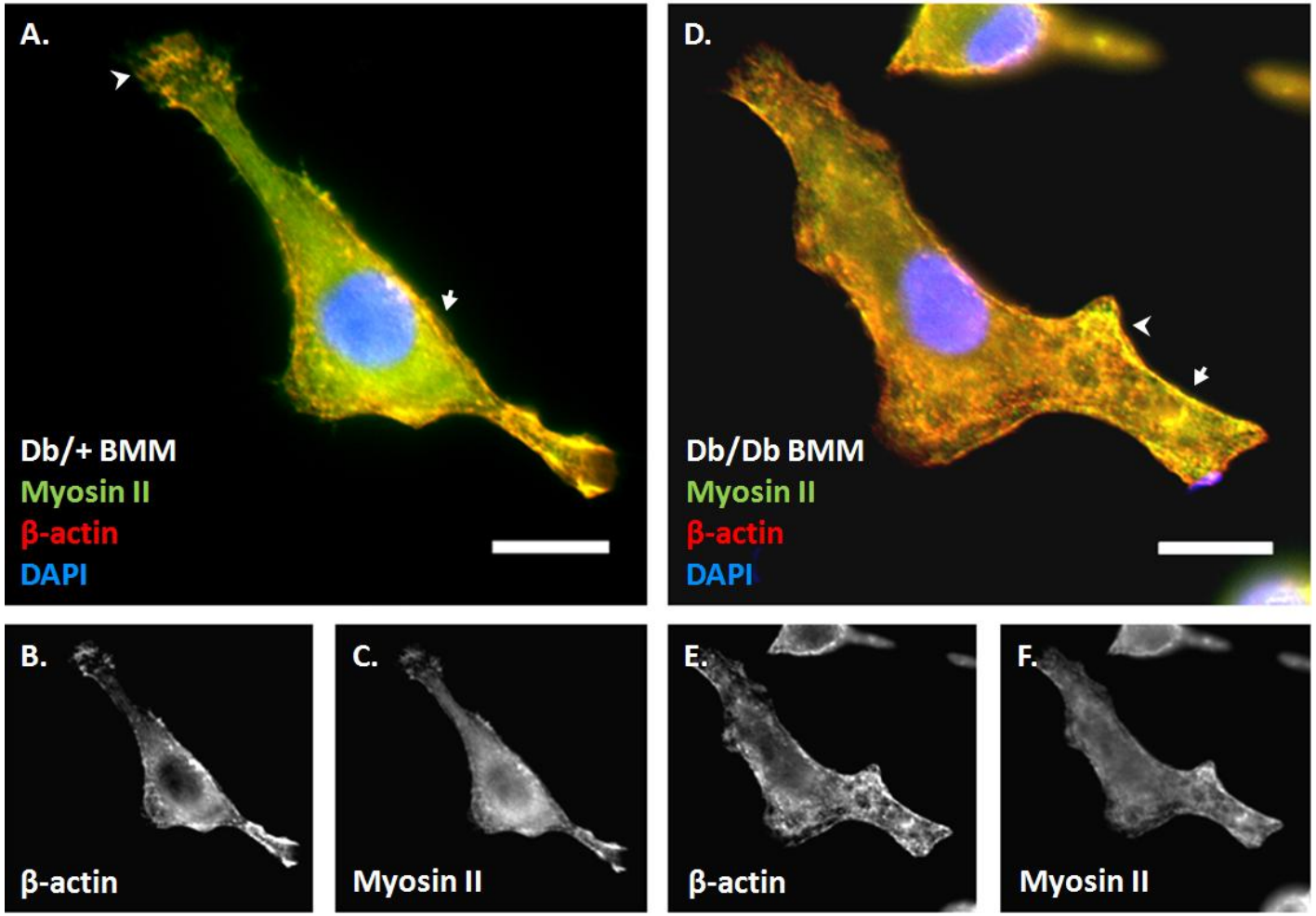

Figure 6.14 Double Immunocytochemical staining for β-actin and non-muscle Myosin II in Db/+ and Db/Db BMMs. (A) Db/+ BMMs and (B) Db/Db BMMs were cultured on glass cover-slips for 24 hours before fixing and sequentially staining for β-actin and non-muscle Myosin II. Arrow indicates co-localisation at cell membrane. Arrowhead indicates co-localisation in lamellipodia. Scale bar = 10 µM

To further investigate polarisation, Db/+ and Db/Db BMMs were immunocytochemically stained for Arp2 localisation. In polarised cells the Arp2/3 complex has been shown to concentrate at the leading edge where it is thought to mediate development of the actin filament network. In Db/+ and Db/Db BMMs Arp2 staining is diffuse throughout the cell (figure 6.15 A, B). As with myosin II, there does not appear to be an obvious polarity of Arp2 expression.

Double staining for myosin II and Arp2 in both Db/+ and Db/Db BMMs revealed discrete areas of protein expression within the cell (figure 6.16). In Db/+ and Db/Db BMMs there is a clear concentration of myosin II at what appears to be the leading edge of the cell pictured (figure 6.16 A-D and I-L, respectively), although staining was also apparent at the trailing edge of the cell. The expression of Arp2 was fairly distinct from the expression pattern of myosin II in Db/+ BMMs (figure 6.16 C, D and G, H), however in the Db/Db BMM the boundary of expression was less clear (figure 6.16 K, L and O, P). Again, neither myosin II nor the Arp2 complex showed absolute polarisation despite their proposed roles in migration.

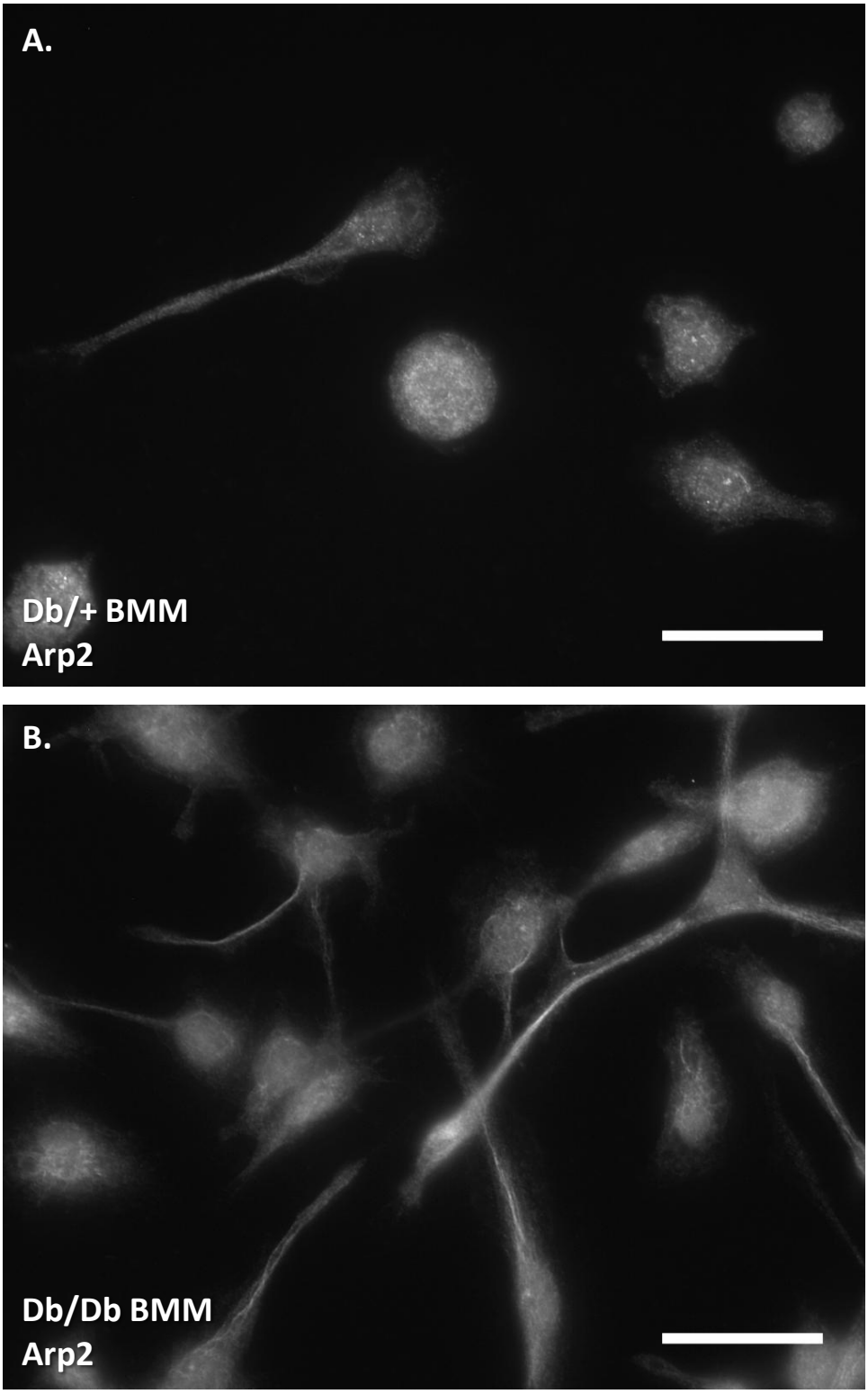

Figure 6.15 Immunocytochemical staining for Arp2 in Db/+ and Db/Db BMMs. (A) Db/+ BMMs and (B) Db/Db BMMs were cultured on glass cover-slips for 24 hours before fixing and staining for Arp2. Scale bar = 25 µM

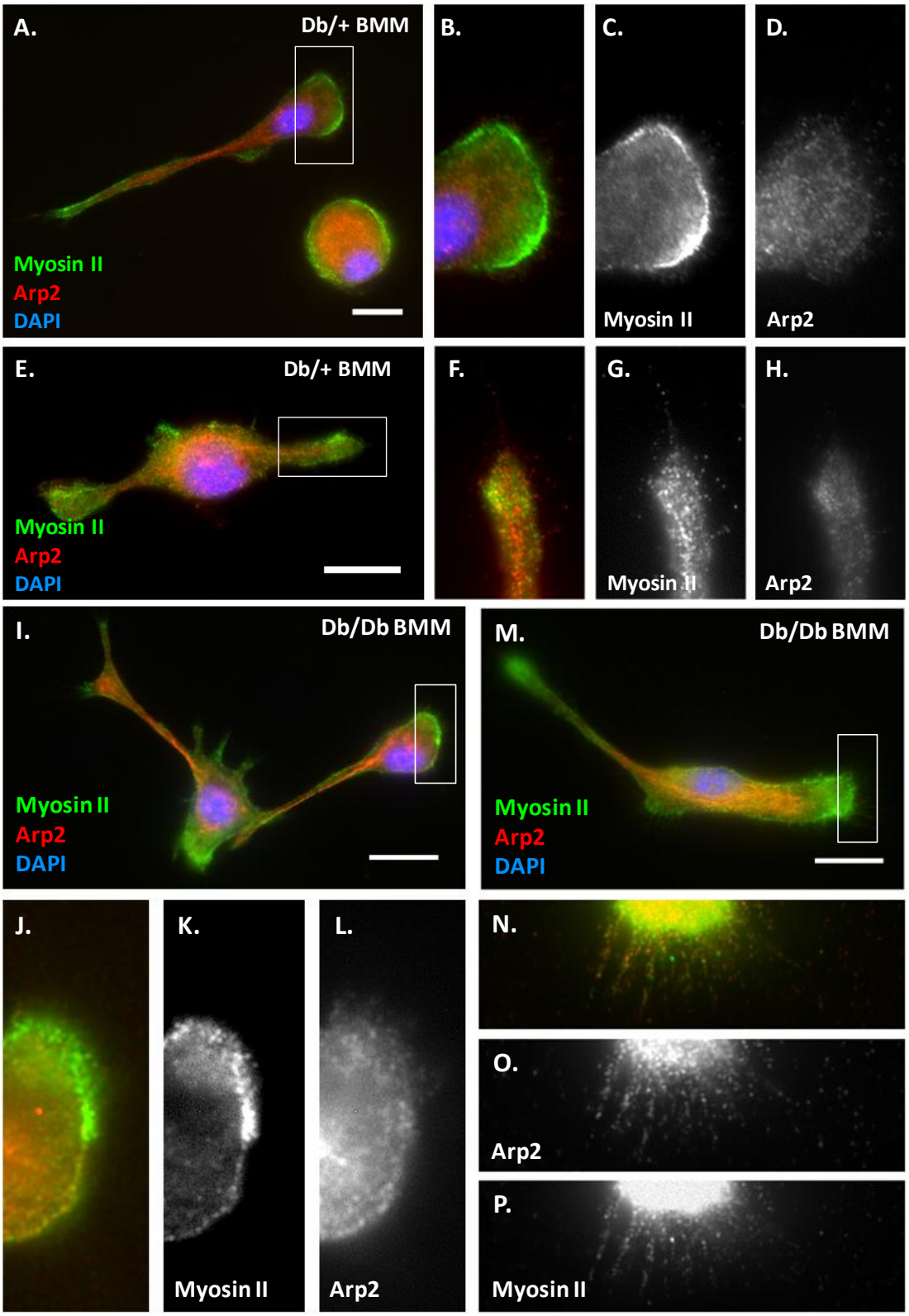

Figure 6.16 Double Immunocytochemical staining for Arp2 and non-muscle Myosin II in Db/+ and Db/Db BMMs. (A-H) Db/+ BMMs and (I-M) Db/Db BMMs were cultured on glass cover-slips for 24 hours before fixing and sequentially staining for Arp2 and non-muscle Myosin II. White boxes in (A), (E), (I) and (M) indicate area highlighted in (B-D), (F-H), (J-L) and (N-P), respectively. Scale bar = 10 µM

6.4 Discussion

Striking differences were observed in Db/Db BMM morphology compared to Db/+ morphology that, when quantified, reveal a significant increase in the length of cell protrusions from the Db/Db BMMs compared to the Db/+ heterozygous counterpart (figure 6.1 - 6.2). Variation in morphology between Db/Db and Db/+ macrophages has been observed previously, albeit in resident peritoneal macrophages (Zykova et al., 2000). In contrast to the results in this chapter Zykova et al observed Db/Db macrophages to be more rounded compared with their Db/+ counterparts, with less areas of cell spreading and what they describe as numerous cytoplasmic extensions. These observations have not been quantified however and the potential mechanism behind this observation is not explored. Interestingly this study makes no mention of CSF-1 in the macrophage medium so it seems that their culture conditions may vary from that of the BMMs, perhaps contributing to these conflicting results. In other studies wild type BMMs have shown an altered morphology in response to a loss of expression of Rac isoforms 1 and 2 (Wheeler et al., 2006); $Rac2^{-/-}$ and $Rac1/2^{-/-}$ macrophages display a significantly greater elongation that correlates with increased protrusion length in these cells. This suggests a possible Rac-driven mechanism controlling morphology of Db/Db BMMs and highlights the importance of future analysis of Rac activity in Db/Db BMMs.

Hyperglycaemia is a hallmark of the diabetic milieu and contributes to the formation of advanced glycation endproducts (AGEs) and oxidised low density lipoprotein (oxLDLs). In turn these molecules can influence macrophage behaviour and contribute to atherosclerotic plaque formation (Takahashi et al., 2002). *In vivo,* hyperglycaemia is associated with increased chemokine production (Shanmugam et al., 2003), increased superoxide, and altered cell surface topology in monocytes (Hayashi et al., 2007). Importantly high levels of glucose have also been shown to increase the adhesiveness of leukocytes to endothelial cells (Esposito et al., 2001; Meng et al., 2010) contributing to plaque formation. As there is a clear precedent for increased glucose affecting macrophage phenotype and activity we hypothesised that the significant difference in Db/Db BMM morphology observed could be due to exposure to hyperglycaemia *in vivo*, and that it may be possible to induce the diabetic macrophage phenotype in WT BMM by exposure to increased glucose. Wild type BMMs cultured in high glucose levels did not develop the phenotype observed in the Db/Db BMMs however; and despite a trend for increased protrusion length this was not significant (figure 6.3). Despite these results hyperglycaemia may still be a contributory factor to altered Db/Db BMM morphology, but it is possible that short term culture of wild type

cells is not enough to exert this effect. It is likely that the cause of increased protrusion length observed in Db/Db BMMs is multifactoral, combining the effects of the diabetic microenvironment with the epigenetic changes this drives.

One unexpected outcome of this experiment was the observation of a trend for increased protrusion length in the wild type BMMs exposed to the D-Mannitol control (figure 6.3 F, G). D-Mannitol, a sugar alcohol, is used as a control as it has the same effect on culture medium osmolarity as D-Glucose but is not metabolised by cells, and does not trigger hyperinsulinaemia *in vivo* (Song and Vieille, 2009). D-Mannitol can however be oxidised to form the sugar Mannose. Mannose is known to bind to a class of receptor on the macrophage cell surface know as pattern recognition receptors (PRRs) which trigger pro-inflammatory responses similar to LPS binding TLR4 (Stahl and Ezekowitz, 1998). It is likely therefore that D-Mannitol was able to be oxidised to Mannose in culture, thus triggering a pro-inflammatory response and a more activated phenotype in control BMM, and therefore inadvertently modulating the results.

To further investigate the morphological differences between Db/Db and Db/+ BMMs it may be useful to implement a more comprehensive 'scoring' system, alongside the quantification of protrusion length. For example, analysing the relative adhesive area and elongation ratio (longest:shortest axes) of BMMs would allow quantification of cell spreading and cell size, as applied to the analysis of $Rac1^{-/-}$ (Wells et al., 2003) and $RhoB^{-/-}$ BMMs (Wheeler et al., 2007).

In this chapter we have shown that Db/Db BMM migrate at a lower velocity than their Db/+ counterparts on both 2D plasma fibronectin and plasma fibrinogen (figure 6.4). Fibronectin also appears to induce a trend for decreased directionality of migration in Db/Db BMMs that becomes particularly apparent in plots of their migration trajectory (figure 6.5 F). Studies have shown monocyte adhesion in Db/Db mice to be mediated primarily through integrin α4β1 expression on monocytes interacting with VCAM-1 and fibronectin on the endothelium, and that monocyte-endothelium adhesion is amplified in Db/Db mice (Hatley et al., 2003). This suggests that increased adhesion to fibronectin may be the cause of reduced migration observed in this chapter.

Of the two key macrophage stimulatory factors tested we found that wild type BMMs demonstrated a more robust response to MCP-1 than to CSF-1 (figure 6.6 and 6.7). For this reason Db/Db and Db/+ BMM migration was analysed in response to a gradient of MCP-1, revealing a significant reduction in velocity and accumulated distance migrated by Db/Db BMMs (figure 6.8 and 6.9). A small but expanding body of work exists on the effect of diabetes on macrophage

chemotaxis. An important recent study revealed increased chemotaxis of wild type monocytes towards medium conditioned by adipocytes, rich in saturated fatty acids and increased glucose levels (Yeop et al., 2010). The chemoattractive properties of adipose tissue to leukocytic cells are relatively well characterised; however, the ability of diabetic macrophages to respond to chemokines once the diabetic milieu had been established is less well understood. A study of the developmental signalling protein, Sonic Hedgehog (Shh), revealed potent chemoattractive properties for healthy monocytes, which is impaired in monocytes isolated from the blood of type II diabetic patients with coronary artery disease (Dunaeva et al., 2010). Dunaeva et al suggest this is due to increased levels of the Shh receptor Patched on the surface of the monocytes triggered by the constant low level of inflammation experienced by diabetic patients. An impaired chemotactic response to MCP-1 in monocytes from type 1 diabetic patients was observed and associated with increased adhesion and expression of receptors CCR1, CXCR4 and CCR7 (Bouma et al., 2005). It is possible therefore that the Db/Db BMMs analysed in this chapter express greater levels of the MCP-1 receptor, CCR2, or other chemokine receptors, triggering increased adhesion and therefore reducing migration. There is also evidence to suggest that the Db/Db BMMs expressed a *reduced* level of CCR2 however, as human macrophages differentiated in the presence of oxLDLs show a switch from expression of CCR2 to CX3CR1, the fraktalkine receptor (Barlic et al., 2006). It is clear that further analysis of chemokine receptors expressed on the surface of the Db/Db and Db/+ BMMs is necessary to fully appreciate the different migratory phenotypes.

Analysis and comparison of the cytoskeletal components of Db/Db and Db/+ BMMs serves to highlight the morphological differences observed between the two phenotypes rather than revealing any striking differences in cytoskeletal protein localisation. The localisation of α-tubulin, for example, shows distinct networks of microtubules in both phenotypes although the potential site of the microtubule organising centre (MTOC) or centrosome is less clear in most Db/Db cells (figure 6.10 and 6.11). Staining in both cell types is reminiscent of that seen in wild type murine macrophages seen previously (Robinson and Vandre, 1995). The importance of microtubules in macrophage migration *in vivo* is elegantly demonstrated in studies performed in Zebrafish (Redd et al., 2006). By disrupting microtubule stability with the anti-mitotic agent nocodazole, Redd et al found that macrophages lost the ability to migrate towards a wound site in the Zebrafish embryo. It is possible, therefore, that the apparent interruption in Db/Db microtubule centrosomal focus may be related to the altered migratory phenotype of the Db/DB BMMs.

β-actin and myosin II are co-localised in certain areas of both Db/Db and Db/+ BMMs, suggesting active rearrangement of actin filaments, particularly along the cell periphery and in lamellipodia (figure 6.14). In single staining for both proteins extensive filopodia are also clearly visible (figure 6.12 and 6.13), serving as further indication of enhanced cell spreading and increased interaction with serum proteins present. A study of actin-myosin co-localisation in human monocytes revealed a similar pattern of expression to that observed in Db/+ and Db/Db BMMs, with both proteins being expressed at the periphery but myosin II also showing expression throughout the cytoplasm (Meconi et al., 1998). A trend for Db/Db BMM increased cell area is particularly evident in both β-actin and myosin II single staining (figure 6.12 and 6.13). It is possible, therefore, that the expression of these proteins contributes to the migratory phenotype of the Db/Db BMMs.

Double staining for myosin II and Arp2 shows no co-localisation of these two proteins in either phenotype BMM. Arp2/3 is known to play a role in actin branching and polymerisation so we would expect to see concentration at the leading edge of areas of lamellipodia. In both Db/Db and Db/+ BMMs however Arp2 appears to concentrate in filaments along cytoplasmic protrusions (figure 6.16). It is likely that these filaments are actin; however an extensive search revealed no evidence of similar staining in the literature. Expression of Arp2 along filopodia-like protrusions is also apparent, particularly in Db/Db BMMs (figure 6.16 M, N, O). This is reminiscent of staining patterns observed in fibroblast filopodia that are thought to be a precursor to lamellipodial expansion (Johnston et al., 2008). In both phenotypes myosin II also appears to be present in these filopodia-like protrusions in a similar pattern to that observed for Arp2, though not co-localised (figure 6.16 E-H and M-P).

Myosin II is typically considered to play a role in tail retraction in migrating cells but more recently has been found to be expressed in lamellipodia during their disassembly (Conti and Adelstein, 2008), which may explain why a strong band of expression is visible at the apparent leading edge of both Db/Db and Db/+ BMMs whilst also at the trailing edge (figure 6.16 A-D and I-L). Without the presence of a chemoattractant the nuclei of BMMs were observed to translocate up and down the cell body before the cell would commit to migration in one direction (as observed in time-lapse microscopy). This suggests that polarisation is occurring rapidly, again contributing to the presence of myosin II at either end of the cell. Despite there being a low level of L-cell derived CSF-1 present during cell culture before being fixed and stained, there is no gradient of chemoattractant present to trigger polarisation of either phenotype BMM. It is likely that there would be a clearer pattern of Arp2 and myosin II polarisation in the presence of a chemoattractant

and staining for these proteins in such an environment may reveal more about the mechanisms involved in the Db/Db BMMs repressed migration in response to a gradient of MCP-1.

Chapter 7: **Discussion**

7.1 Discussion

Given what is known about the role of the metalloproteinases in migration and invasion it is perhaps unsurprising that macrophages express high levels of these enzymes in response to pro-inflammatory stimuli and throughout the wound healing process. Data from this thesis proposes a novel function for MMP-10 during macrophage migration in response to pro-inflammatory stimuli and investigates a possible role for MMP-10 in diabetic wound healing.

7.1.1 A potential mechanism for LPS-driven temporal regulation of MMP-10 expression in macrophages

The initial profile of the metalloproteinases in primary bone marrow-derived macrophages (BMMs) performed in this thesis revealed a pattern of differential expression in response to lipopolysaccharide (LPS). These LPS-induced changes in proteinase expression were both time- and dose-dependent. Of particular interest was the secreted matrix metalloproteinase MMP-10. Previous reports of MMP-10 in macrophages have revealed increased expression in response to LPS at 3 hours post-stimulation (Ho et al., 2008). Data in this thesis confirm this early induction of MMP-10 mRNA in BMMs following LPS stimulation and demonstrate a return to basal levels between 8-16 hours after stimulation. Interestingly, a novel down-regulation of both MMP-10 mRNA and protein expression significantly below basal levels was observed 24 hours post-LPS treatment. Recent studies have shown that LPS-induced MMP-10 expression in macrophages is inhibited by siRNA targeting the NADPH oxidase Nox2 (Kim et al., 2010), which is crucial for the macrophage oxidative burst following phagocytosis and during the NF-κB-mediated pro-inflammatory response. Use of an NF-κB pathway inhibitor in this thesis revealed a role for this transcription factor in both the early induction and the late repression of MMP-10 mRNA by LPS. There is no evidence however that NF-κB binds the MMP-10 promoter directly in human cells although there is evidence of a putative binding site in murine cells ('MatInspector' algorithm (Cartharius et al., 2005)). This, coupled with the fact that NF-κB signalling is still implicated at 24 hours post-LPS, suggests that an intermediate factor may be involved in the regulation of MMP-10 repression. It is, in fact, unlikely that the LPS in the medium will have a long enough half-life to retain activity and be directly responsible for NF-κB signalling at later time-points (Kato et al., 2004).

Several reports in the literature point towards class II histone deacetylases (HDACs) as potential intermediates in the regulation of MMP-10. Experiments in this thesis, however, were unable to reproduce the induction of HDAC4, 5 and 7 mRNA 24 hours post-LPS stimulation observed previously in BMMs ((Aung et al., 2006) see Chapter 3). HDAC7 has been found to regulate expression of MMP-10 by binding to and inhibiting the LPS-inducible transcription factor myocyte enhancer factor (MEF)2, thus preventing MEF2 binding to promoter regions on the MMP-10 gene (illustrated in figure 7.1). Despite their being no regulation of HDAC7 mRNA in BMMs in response to LPS, there is evidence in the literature of a mechanism for the regulation of HDAC7 protein activity that offers encouragement for further research into the HDAC7/MMP-10 relationship in BMMs. Previous studies found HDAC7 protein to be sequestered within promyelocytic leukemia protein (PML) nuclear bodies (NBs) in epithelial and endothelial cells (Gao et al., 2008). PML NBs are sub-nuclear compartments known to play a role in transcriptional regulation. Gao et al have shown increased formation of PML NBs, and their co-localisation with HDAC7, following TNF-α and LPS stimulation in endothelial cells. Once HDAC7 is sequestered in these sub-nuclear compartments MEF2 is free to activate MMP-10 transcription. It is reasonable to assume that HDAC7 will eventually disassociate from PML NBs as the levels pro-inflammatory stimuli falls, allowing HDAC7 to bind to and inhibit MEF2 once more. This hypothesis (illustrated in figure 7.1) suggests a mechanism by which LPS can quickly induce MMP-10 transcription due to HDAC7 protein sequestration, but also drive its repression as levels of stimuli fall without effecting HDAC7 mRNA. Despite recent data confirming a role for HDAC4, 5 and 7 in the repression of MMP-10 via MEF2 inhibition in epithelial cells (Ishikawa et al., 2010a) there are, as yet, no publications implicating this relationship in macrophages.

This potential relationship between HDAC protein levels and MMP-10 transcription serves to highlight the importance of confirming the regulation of MMP-10 mRNA at the protein level. Although intriguing, LPS-induced MMP-10 mRNA modulation is of little physiological relevance unless this is translated into a change in MMP-10 protein activity.

Post-transcriptional regulation of MMP-10 driven by microRNAs may provide a further potential level of LPS-induced repression. Recent work has hinted at miR-155-driven regulation of several MMPs in LPS-stimulated human peripheral blood-derived dendritic cells, including MMP-10 (Ceppi et al., 2009). Ceppi et al found MMP-10 expression to be up-regulated in dendritic cells stimulated with LPS for 24 hours following transfection with anti-miR-155, suggesting that miR-155 (either directly or indirectly) represses MMP-10 mRNA. Various algorithms fail to predict a putative miR-

155 target sequence in the MMP-10 3' UTR (miRbase (Griffiths-Jones et al., 2008), TargetScan (Friedman et al., 2009)), again implicating an intermediate factor. It is unclear how, or if, this proposed mechanism of MMP-10 regulation could interact with the 'HDAC hypothesis' detailed above as published data concerning both miRNAs and HDACs is only recently emerging. Algorithms do predict a putative target site for miR-155 in the 3' UTR of the human MEF2A gene (TargetScan (Friedman et al., 2009)). Figure 7.1 suggests some possible mechanisms of LPS-driven MMP-10 regulation, including roles for HDAC7 and miR-155.

Figure 7.1 An hypothesis for the signalling mechanisms controlling LPS-driven early and late MMP-10 expression in BMM. *Early:* within 3-4 hours of LPS-TLR4 binding there is an NF-κB dependent induction of TNF-α and MMP-10 mRNA. LPS can increase activation of transcription factor MEF2 through p38-catalysed phosphorylation (Han et al., 1997). TNF-α is also known to bind its receptor and signal via the p38 MAPK pathway. Both LPS and TNF-α can trigger dissociation of MEF2 from HDAC7 in the nucleus via p38 MAPK. This frees MEF2 to bind to the MMP-10 promoter and sequesters HDAC7 in PML nuclear bodies (Aung et al., 2006; Chang et al., 2006; Gao et al., 2008). Studies have shown that Nox-2 also mediates LPS-driven MMP-10 mRNA expression, via NF-κB, presumably feeding in to this pathway (Kim et al., 2010). Expression of miR-155 is induced by LPS and is dependent on NF-κB signalling. At this stage it does not appear to have an inhibitory effect on MMP-10. *Late:* As LPS levels fall NF-κB-dependent induction of TNF-α mRNA returns to basal levels and by 24 hours MMP-10 mRNA is repressed. Without excessive p38 MAPK signalling to trigger sequestration of HDAC7 protein in nuclear bodies, HDAC7 is free to bind MEF2 in the nucleus and prevent its interaction with the MMP-10 promoter. Expression of MMP-10 is repressed. Throughout this process neither HDAC7 transcription nor total HDAC7 protein levels change. LPS-induced miR-155 expression continues to increase. Inhibition of miR-155 at 24 hours leads to an increase in MMP-10 expression (Ceppi et al., 2009). Relevant miR-155 targets are unclear but may include MEF2. IκB – Inhibitor of κB, IKK – IκB kinase, MAPK – mitogen activated protein kinase, MKK – MAPK kinase, MEKK – MKK kinase, protein, MyD88 - Myeloid differentiation primary response gene 88, TLR4 - Toll-like receptor-4, TNF-R – TNF-α receptor. Dashed arrows indicate hypothetical mechanisms.

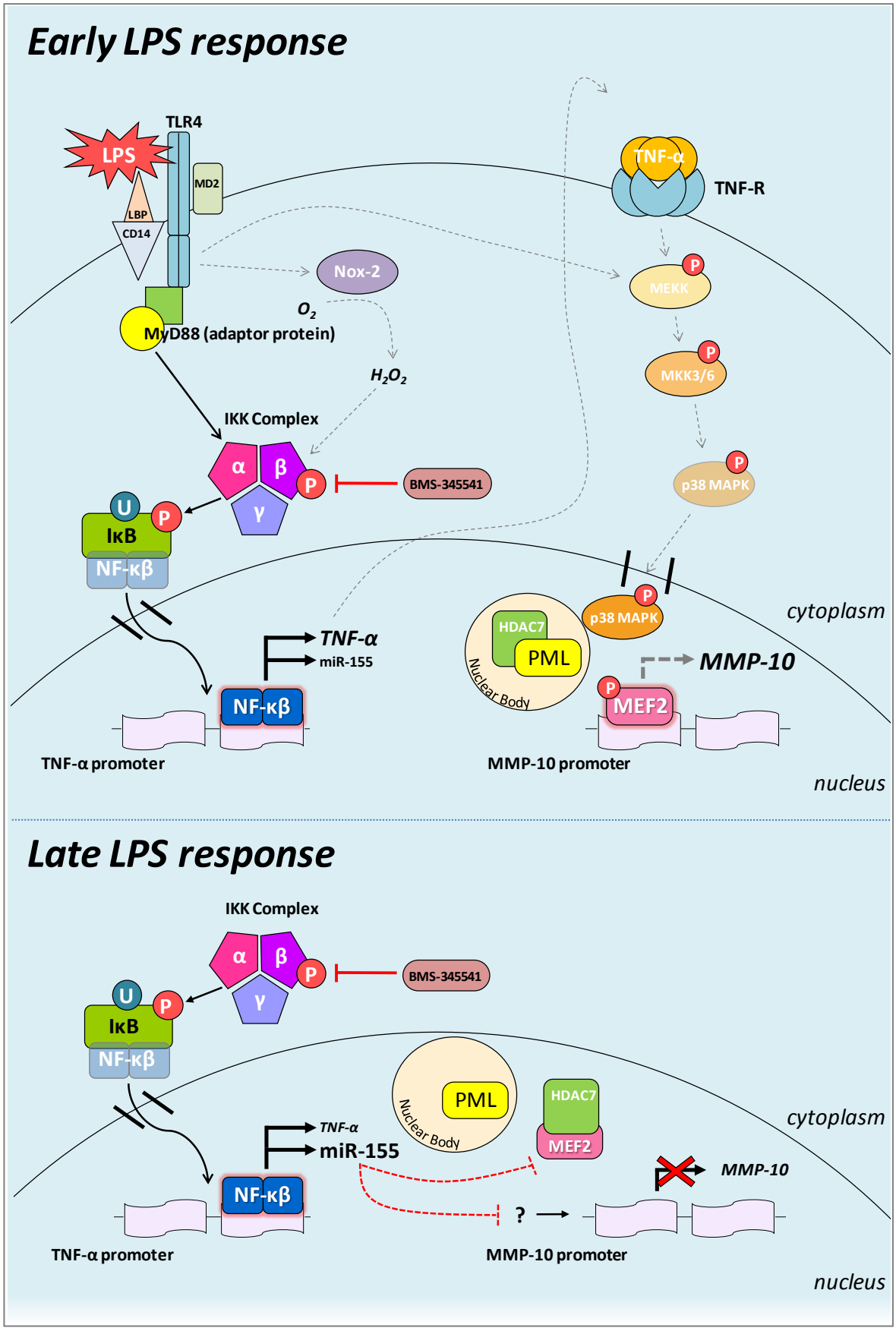
Early LPS response
TLR4
LPS
MD2
LBP
CD14
MyD88 (adaptor protein)
Nox-2
O_2
H_2O_2
IKK Complex
α
β
γ
P
BMS-345541
U
IκB
NF-κβ
TNF-α
TNF-R
MEKK
MKK3/6
p38 MAPK
cytoplasm
TNF-α
miR-155
HDAC7
PML
Nuclear Body
MMP-10
MEF2
TNF-α promoter
MMP-10 promoter
nucleus
Late LPS response
IKK Complex
BMS-345541
IκB
NF-κβ
PML
Nuclear Body
HDAC7
MEF2
cytoplasm
TNF-α
miR-155
MMP-10
?
TNF-α promoter
MMP-10 promoter
nucleus

7.1.2 The functional implications of LPS-driven MMP-10 expression on macrophage migration

Migration analysis was performed to further investigate the novel regulation of macrophage MMP-10 in response to LPS in terms of its potential functional repercussions. In this thesis analysis of 2D BMM migration on thin coatings of fibronectin, an MMP-10 substrate (Chin et al., 1985), demonstrated a reduction in macrophage migration velocity in response LPS, from 24 hours post-stimulation. In itself this was an intriguing result as previous studies have found LPS to induce 3D macrophage migration *in vitro* and *in vivo* (Tester et al., 2007; Hollingsworth et al., 2007). For example, Hollingsworth et al found increased macrophage migration into lung tissue in response to LPS aerosol challenge and also enhanced migration through a Transwell membrane towards bronchiolar lavage supernatants from LPS treated mice. Mice were exposed to an aerosol of 1 µg/ml LPS; however Hollingsworth et al did not determine the level of LPS activity in the lavage fluid.

Targeting the MMP-10 transcript with siRNA mimicked the repressive effect of 24 hour LPS-stimulation on BMM migration and could be rescued by addition of recombinant MMP-10 to the medium. This strongly implies that the loss of MMP-10 protein function is responsible for the reduction in migration velocity, rather than another LPS-inducible factor. This also suggests that MMP-10 cleavage of fibronectin or degradation of a fibronectin-associated motogenic factor may play a role in BMM migration. These results are strengthened by recent preliminary results revealing decreased motility of BMMs harvested from the *mmp10*$^{-/-}$ mouse (data not shown).

MMP-10 has previously been implicated in cell migration, albeit in the migration of lung carcinoma cells (Frederick et al., 2008). Frederick et al found siRNA targeting MMP-10 to repress the invasion of tumour cells through a matrigel plug *in vitro*; however they do not speculate on potential substrates or mechanisms of cell migration and matrigel is not known to contain any fibronectin. Interestingly another study into MMP-10 expression in lung carcinomas suggests a role for MMP-10 in the expansion of the tumour cell mass rather than the initial invasion of cells and progression to metastasis, and shows increased MMP-10 expression in the tumour itself rather than the surrounding stroma (Gill et al., 2004).

The basal level of MMP-10 expression in BMMs may be mediated by their interaction with fibronectin. As well as the fibronectin specifically applied in 2D coatings, there will also be a small amount present (0.2% serum ≈ 600 ng fibronectin) on uncoated plates due to estimated serum present in tissue culture medium extrapolated from known plasma fibronectin concentrations (Perttila et al., 1990). Macrophage adhesion to and migration on fibronectin is mediated by

integrins and this relationship is well-established. Macrophage-fibronectin binding is mainly mediated by integrins αVβ3, α4β1 and α5β1, which are also necessary during macrophage differentiation (Danen et al., 2002; Roldan et al., 1992; Xie et al., 1998). Integrin α4β1 however only binds to the variable region of fibronectin that is not present in the plasma fibronectin splice variant (Pankov and Yamada, 2002). Integrin binding is also associated with macrophage motility and polarity, for example, fibroblasts adhering to fibronectin experience a transient down-regulation in expression of the RhoGTPase RhoA followed by a prolonged increase in its expression (Ren et al., 1999). Later studies have shown that this is mediated by the extracellular integrin β1 domain (Danen et al., 2002).

Activation of the RhoGTPase Rac1 is also likely to be of importance to the migratory capacity of the BMMs studied in this thesis. For example, published data suggests an inverse correlation between levels of Rac1 and directionality of migration of macrophages and fibroblasts, i.e., more directionally persistent cells exhibit lower levels of Rac1 activation (Allen et al., 1998a; Pankov et al., 2005). LPS has been shown to enhance Rac1 activity in macrophages at early time-points (Kong and Ge, 2008) whilst fibronectin binding has been shown to quickly enhance Rac1 activation in epithelial cells, increasing F-actin expression and the formation of focal adhesions (Kimura et al., 2006). Rac1-null macrophages do not lose their ability to migrate however their morphology and mode of migration is altered (Wheeler et al., 2006). A relationship has also been proposed linking Rac1 activity to MMP-10 expression in lung carcinoma cells (Frederick et al., 2008). More specifically, activation of protein kinase C (PKC)-ι activates Rac1 through the adaptor protein Par6α and stimulates MMP-10 expression in carcinoma cells. Frederick et al do not propose a mechanism by which Rac1 is responsible for MMP-10 activation, however. These potential roles for Rac1 activation in the regulation of MMP-10 during macrophage migration are outlined in figure 7.3.

There is also evidence of direct integrin-MMP interactions that contribute to leukocyte and cancer cell motility. MMPs have been shown to activate integrins on the cell surface via proteolytic cleavage, whilst there is also evidence of integrin-mediated MMP activation via C-terminal domain binding. Integrin αVβ3, for example, can be activated by MMP-14-mediated proteolytic cleavage in endothelial cells (Galvez et al., 2002) whilst the interaction between MMP-14 and αVβ3 can, in turn, promote MMP-2 activation in breast cancer cells (Deryugina et al., 2001). Evidence of integrin-mediated MMP-10 expression can be found in studies of thymic lymphoma: T lymphocytes are shown to express increased levels of MMP-10 following binding to endothelial cells that is dependent on ICAM-1/αLβ2 integrin interaction (Van et al., 2004). However, there

does not appear to be any physical interaction between MMP-10 and αLβ2. Interesting *in vivo* data has shown abnormal β1 integrin expression in the wounds of mice that constitutively express MMP-10 in their keratinocytes (Krampert et al., 2004). Again, however, no direct interaction between MMP-10 and integrins is proposed.

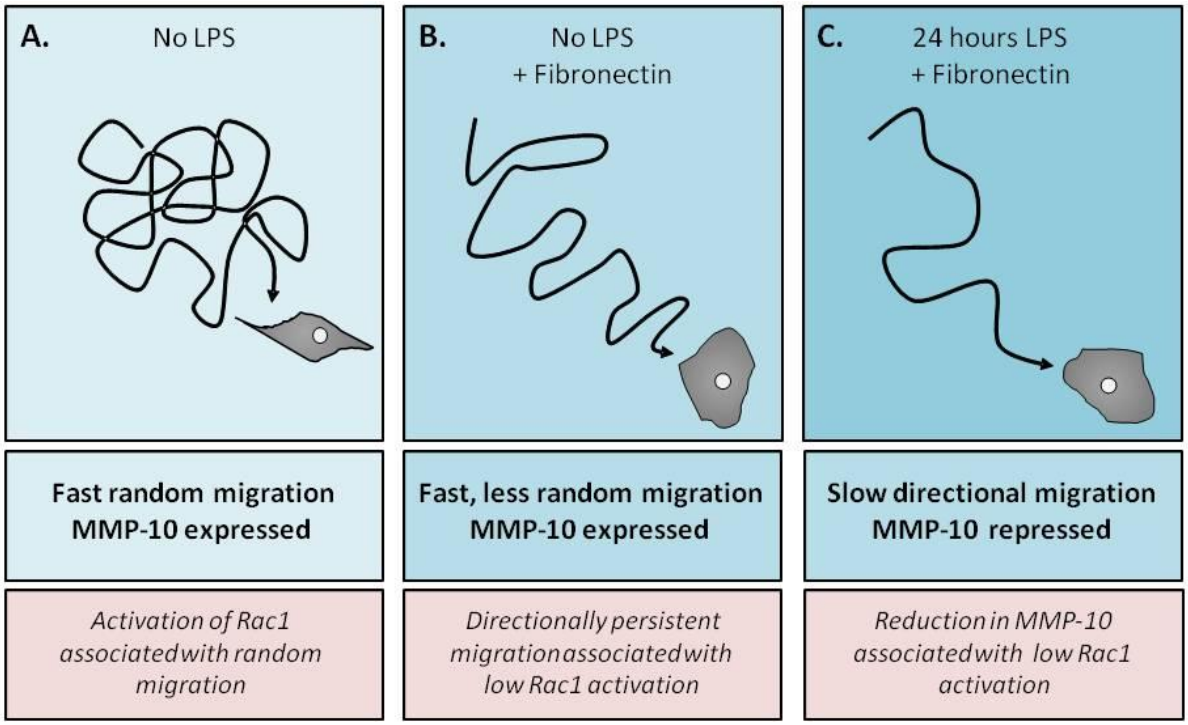

Figure 7.2 A potential role for the RhoGTPase Rac1 in LPS-driven macrophage migration and MMP-10 expression. *Results from this thesis shown in blue, speculations based on published data shown in pink.* (A) Macrophage migration is relatively fast but has little directionality when cultured without LPS or fibronectin. MMP-10 is expressed at basal levels. Increased Rac1 activation has been linked to random migration in epithelial cells and fibroblasts (Pankov et al., 2005) so it is not unreasonable to suppose levels of Rac1 may be high during random migration of macrophages. (B) On thin 2D coatings of fibronectin macrophages migrate less randomly and at a greater velocity. Rac1 activation is down-regulated in more directionally persistent cells (Pankov et al., 2005). (C) On fibronectin macrophages stimulated with LPS demonstrate a dramatic reduction in migration velocity concurrent with slightly increased directionality and repression of MMP-10 below basal levels. Repression of MMP-10 can occur downstream of reduced Rac1 activation, albeit in lung carcinoma cells (Frederick et al., 2008). This suggests a mechanism by which the Rac1 may regulate macrophage migration and also modulate the expression of MMP-10.

7.1.3 A possible role for miR-155 in post-transcriptional regulation of macrophage migration

Several previous studies have shown that LPS can induce the differential expression of macrophage miRNAs, particularly miR-155 (Taganov et al., 2006; Tili et al., 2007; O'Connell et al., 2008; Ceppi et al., 2009). Preliminary microarray data in this thesis corroborates this, showing miR-155 to be induced in the RAW264.7 macrophage cell-line in an NF-κB-dependent manner following 4 hours LPS-stimulation. MiR-155 is considered to be a critical regulator of immune function, contributing to the differentiation process of several haematopoietic lineages (Shivdasani, 2006; Rodriguez et al., 2007). Studies are emerging, however, suggesting this miRNA also plays a role in other processes, such as control of cell migration.

Given the data in this thesis outlining a role for MMP-10 in the migration of LPS-stimulated macrophages one could hypothesise that miR-155 is indirectly responsible for the repression of migration through inhibition of MMP-10 transcription. The migration velocity of BMMs did not change following transfection with anti-miR-155 oligonucleotides; however a significant down-regulation of Euclidean distance migrated was observed. This hints at a miR-155-driven regulation of factors associated with directional migration, such as the RhoGTPases. For example, both 2D and 3D epithelial cell migration can be induced by miR-155 over-expression due to the post-transcriptional targeting of RhoA mRNA (Kong et al., 2008). In macrophages a constitutive over-expression of RhoA has been found to inhibit the cells' ability to migrate and polarise in response to CSF-1 (Allen et al., 1998b). Due to this wealth of evidence suggesting a mechanism of post-transcriptional control of macrophage migration it would be important to further pursue the preliminary results obtained in anti-miR-155 transfected BMMs.

7.1.4 The physiological relevance of MMP-10 expression in macrophages

It is important to apply the potentially novel MMP-10-driven mechanism of macrophage migration to physiologically relevant situations *in vivo*, for example, the wound healing response. During wound healing and the multi-step pro-inflammatory cascade macrophages respond quickly to a barrage of chemotactic signals that ultimately trigger their migration towards the site of injury and infection. Convention no-longer dictates that the MMPs act solely as 'molecular scissors' implementing the degradation of matrix barriers, although this mode of action may well be important in the wound healing situation. The ability of MMPs to cleave and activate cryptic chemotactic molecules from the extracellular matrix is equally, if not more relevant in the mediation of macrophage migration *in vivo.* Novel high-throughput 'scanning' techniques have

revealed numerous chemokine substrates for MMPs (Overall et al., 2002). Specifically, MMP-12, also known as macrophage metalloelastase, has been found to cleave and inactivate IL-8 during the early pro-inflammatory response, aiding neutrophil clearance. At later stages MMP-12 cleaves macrophage chemotactic proteins (MCP)-1 – -4 at critical receptor binding motifs triggering macrophage clearance from inflamed tissue (Dean et al., 2008). Dean et al hypothesise that the synchronous expression of MMPs by macrophages aids both the pro- and anti-inflammatory response. The differential expression of macrophage MMP-10 observed in this thesis follows this premise.

Temporal changes in MMP expression have been studied in the context of inflammation and wound healing previously. For example, an analysis of cutaneous burn healing in mice showed early down regulation of MMP-9 and -13 followed by a rebound over-expression from 3 days up to two weeks after initial wounding (Feezor et al., 2004). These studies make no mention of MMP-10 expression however and do not speculate on the function of the changing MMP expression patterns. Interestingly however, research into Pyoderma gangrenosum, a non-infectious chronic ulcer of the skin driven by autoimmune response, has revealed an increase in expression of MMP-10 in the ulcer margin (Bister et al., 2007). Bister et al suggest this may contribute to excessive degradation of collagen IV and fibronectin in the wound thus impairing healing.

7.1.5 MMP-10 expression in diabetic wound tissue

The leptin receptor-deficient Db/Db mouse, a model of impaired wound healing and type II diabetes, was utilized to further elucidate a role for MMP-10 *in vivo*. Analysis of MMP-10 protein expression in full thickness dermal wounds from the Db/Db mouse and its non-diabetic (Db/+) counterpart suggest that the normal regulation of MMP-10 protein is delayed in diabetic wounds. It is tempting to speculate that levels of MMP-10 are due to the influx of macrophages to the wound tissue alone, known to be delayed in Db/Db mice (Tsuboi and Rifkin, 1990), however other cell types present in wounds have been found to express MMP-10, for example the basal keratinocytes (Rechardt et al., 2000; Krampert et al., 2004; Madlener et al., 1996). It is not possible to make any definitive conclusions about macrophage expression of MMP-10 *in vivo* until co-localisation studies are performed.

Overall there appeared to be a trend toward reduced MMP-10 protein induction in Db/Db skin explants exposed to LPS compared with Db/+ skin explants. These findings need to be further substantiated but suggest that LPS-induced MMP-10 expression is deregulated in diabetic wounds.

A brief mention of the aberrant kinetics of MMP-10 expression in Db/Db wounds can be found in a publication that focuses mainly on an alternative model of impaired wound healing (Madlener et al., 1996). Madlener et al state that MMP-10 induction was initially delayed in Db/Db wounds, but the subsequent expression was prolonged (their unpublished data). This suggests there would be merit to further investigation of this finding. There is also evidence to suggest role for integrins in diabetic wound healing. For example, in diabetic corneal wound tissue enhanced MMP-10 expression correlates with areas of weak and disorganised β1 integrin and impaired healing (Kabosova et al., 2003). This would also offer further explanation for the impaired migration of macrophages into diabetic wound tissue as well as delayed re-epithelialisation of the open wound.

7.1.6 Diabetic macrophages have an impaired response to chemoattractants

Despite the well-characterised delay in macrophage influx to diabetic wounds it is clear that diabetic macrophages do not completely lack the ability to be recruited *in vivo*. It was important, therefore, to examine any potential mechanism by which Db/Db macrophage migratory response is impeded. Data in this thesis show that Db/Db macrophages have a significantly altered morphology compared to their Db/+ counterparts, displaying longer protrusions and an appearance of increased cell size. Db/Db BMMs were also found to migrate more slowly on fibronectin or with MCP-1 stimulation, despite expressing similar levels of MMP-10 mRNA to Db/+ BMMs. This indicated an MMP-10-independent mechanism controlling macrophage migration.

The possibility that exposure to high blood glucose *in vivo* was responsible for variable macrophage morphology was investigated. Whilst exposure to high levels of glucose did not induce a Db/Db-like morphology in wild-type BMMs further examination of the literature suggests that macrophages can respond to glucose concentration by augmenting their adhesion and migration. For example, peripheral blood mononuclear cells (PBMCs) demonstrate significantly greater adhesion to monolayers of primary human aortic endothelial cells cultured in high glucose medium in a process that appears to be dependent on expression of vascular cell adhesion molecule (VCAM)-1 (Esposito et al., 2001). It is possible, therefore, that the diabetic microenvironment Db/Db BMMs are exposed to *in vivo* (before harvest and differentiation *in vitro*) triggers an increase in innate adhesiveness. Assuming the biphasic relationship between adhesion and migration applies this may contribute to the decreased migration speed and distance observed on fibronectin in this thesis. In another similar study monolayer cultures of vascular smooth muscle cells (VSMC) and endothelium-denuded aortic explants from Db/Db mice

induced increased binding of a non-diabetic monocytic cell line compared to VSMC from their Db/+ counterparts (Meng et al., 2010). Meng et al suggest this is due to an increased level of fraktalkine (CX3CL1) expressed by the diabetic VSMC. Results from Db/Db BMM migration studies in this thesis may be consistent with Meng et al's observations since the slower migration observed could be due to enhanced adhesion to the substrate. It would be interesting therefore to explore cell-cell interactions between diabetic macrophages and non-diabetic endothelial cells.

The hypothesis that enhanced macrophage adhesion is responsible for atherosclerosis is well accepted (Galkina and Ley, 2007) however there are some discrepancies when considering how this affects wound healing and resolution of inflammation (reviewed in (Duffield, 2003)). Despite the absolute necessity for macrophages during wound healing (Leibovich and Ross, 1975; Mirza et al., 2009) it seems that in type II diabetes inhibition of macrophage activity can actually be beneficial. For example, wound healing in the obese and diabetic Ob/Ob mouse was enhanced by the application of anti-TNF-α and anti-F4/80 neutralising monoclonal antibodies (Goren et al., 2007). In contrast, a study of corneal wound healing in Db/Db mice found macrophages to be a rate limiting factor for wound closure (Maruyama et al., 2007). Maruyama et al found that the application of IL-1β pre-treated Db/Db BMMs onto Db/Db wounds rescued impaired wound healing suggesting an inherent deregulation of cytokines in Db/Db tissues. This corroborates with the data in this thesis and suggests that macrophage inability to migrate properly in response to pro-inflammatory stimuli may contribute to impaired wound healing.

In conclusion, data in this thesis explore the expression of MMP-10, both in LPS-treated BMMs *in vitro* and in response to wound healing *in vivo*. Whilst LPS-driven induction and repression of MMP-10 mRNA in macrophages seems reliant on the NF-κB signalling pathway it is likely that an intermediate factor is more directly responsible for MMP-10 repression. The results presented here also suggest that MMP-10 plays a role in the migration of macrophages on fibronectin *in vitro* and may be implicated in the impaired wound healing observed in diabetic wounds. Finally Db/Db BMMs were found to have reduced ability to respond to chemoattractant signals, hinting at an MMP-10-independent mechanism behind the delayed macrophage influx in diabetic wounds and potentially reflecting their increased adhesion *in vivo*. This work has laid solid foundations for future experiments into the role of macrophage MMP-10 in inflammation as well as MMP-10-independent macrophage migration in diabetes.

7.2 Future Work

MMP-10 and cell migration: To further strengthen the hypothesis that MMP-10 is necessary for optimal macrophage migration on fibronectin the migration of BMMs derived from the MMP-10 null mouse could be investigated. As well as quantifying their migratory capacity in unstimulated conditions, it would be important to study their response to LPS and MCP-1. A complete MMP profile of these cells would also be useful in order to reveal any potential compensation mechanisms for MMP-10 redundancy. In addition it would be necessary to examine the degradation products of the plasma fibronectin used in these experiments by MMP-10. Mass spectrometry could be utilized to determine the fragments of fibronectin produced and also the potential release of any cryptic fibronectin-associated motogens.

Integrin expression: In order to build a more comprehensive understanding of BMM interaction with fibronectin and subsequent macrophage migratory capacity it would be interesting to profile BMM integrin expression. Adhesion assays utilizing integrin blocking antibodies would reveal specific interactions with the fibronectin matrix, both with and without LPS. Integrin blocking antibodies could also be used during migration analysis and would reveal the effect of specific integrins on velocity and directionality of BMM migration.

Deregulation of MMP-10 expression: Due to the wealth of published data suggesting a role for HDAC4, 5 and 7 in the control of MMP-10 transcription it will be vital to follow up this relationship in our model. The hypothesis that sub-cellular localisation of HDAC7 may vary following LPS stimulation should be pursued, either by immunocytochemistry or by cell fractionation and investigation of proteins present. It may also be possible to perform chromatin immunoprecipitation (ChIP) analysis to explore interaction of HDAC7, MEF2 and MMP-10 in BMMs at different time-points following LPS-stimulation. ChIP allows the investigation of protein-DNA interactions and could therefore indicate protein binding at the MMP-10 promoter region. Similarly co-immunoprecipitation (Co-IP) could be utilised to study protein-protein interaction, such as that between HDAC7 and MEF2.

Diabetic macrophages: A comparison of Db/+ and Db/Db BMM integrin profile may also aid understanding of the reduced velocity of migration observed in Db/Db cells. Analysis of RhoGTPase activity in BMMs during migration on fibronectin may also reveal a mechanism for regulation of macrophage motility. Specifically Rac1 could be analysed using PAK1 pull-down assays. PAK1 binds specifically to Rac1 in its active form, i.e., GTP-bound. Immunocytochemical

analysis of Rac1 distribution in polarized cells could also be performed potentially revealing a role for this RhoGTPase in Db/Db macrophage morphology.

It would be interesting to investigate both wild-type and Db/Db BMM migration in a 3D environment, either through 3D matrices in an invasion assay or on an undulating 3D surface such as a cell-derived matrix (as described in (Beacham et al., 2007)). Potentially, the investigation of macrophage migration and response to LPS *in vivo,* in wild-type, Db/Db and MMP-10 null mice, would provide more physiologically relevant data. For example, topical administration of LPS onto wounds would allow for analysis of MMP-10 expression in response to LPS *in vivo*.

Patient studies: Ultimately, however, it will be crucial to apply any findings to human studies. For example, obtaining blood samples from healthy and diabetic patients would enable me to profile MMP-10 expression at basal levels in the blood. Any potential correlation of MMP-10 expression and migratory behaviour of macrophages derived from patient blood samples would be explored. Similarly, obtaining diabetic skin samples, including that of chronic ulcers, would enable these initial investigations of MMP-10 expression to be repeated in a clinically relevant setting. It would also be important to study the potential co-localisation of MMP-10 expression with macrophages in human tissue to allow us to state definitively whether or not macrophages MMP-10 plays a role in the wound healing response. Investigating the expression of MCP-1 and its receptor in human diabetic tissues may also illuminate the relevance of impaired migration of Db/Db BMM in a physiological setting.

Appendix

Phenotype	Quantity	Cell Number x 10^6			
		Day 0 bone marrow flush	Day 3 non-adherent population	Day 10 bone marrow-derived macrophages	Average bone marrow-derived macrophages per mouse
WT C57Bl/6	2	45.22	15.75	2.94	1.47
	3	41.52	24.31	11.32	3.77
	3	37.94	25.92	10.05	3.35
	3	53.82	24.60	8.80	2.93
	1	53.82	26.78	4.20	4.20
Db/+	1	49.60	30.40	3.18	3.18
	1	20.80	16.50	3.48	3.48
	1	10.08	1.82	1.69	1.69
	1	11.01	3.60	5.07	5.07
	1	23.60	30.40	3.18	3.18
Db/Db	1	46.80	26.80	2.96	2.96
	1	22.00	16.92	5.30	5.30
	1	25.40	7.98	3.80	3.80
	1	15.22	10.02	3.69	3.69
	1	21.50	14.40	2.35	2.35

Table 8.1 Example bone marrow-derived macrophage yields. Bone marrow flush is harvested from mice on day 0 and counted. 10 x 10^6 cells were plated onto 100 mm diameter Bacteriological Petri Dishes (BD Falcon). At day 3 non-adherent cells were aspirated and counted again, then re-plated in fresh medium at the same density. At day 10 fully differentiated adherent bone marrow-derived macrophages were removed by scraping and counted before use in experiments.

Table 8.2 Primer and probe sequences for genes studied by qRT-PCR. Primer and probers for all the TIMPs, MMPs, ADAMs, ADAMTSs and for TNF-α were designed using Primer Express® software (Applied Biosystems) by Dr. Caroline Pennington. Primers and probe for F4/80 were designed, also using Primer Express® software, by Dr. Damon Bevan. Primers for HDAC4, 5 and 7 were purchased from Roche Universal ProbeLibrary system.

Gene		Primer and Probe Sequences
***Timp* 1**	Forward Primer:	5'-CATGGAAAGCCTCTGTGGATATG-3'
	Reverse Primer:	5'-AAGCTGCAGGCACTGATGTG-3'
	Probe:	5'-FAM-CTCATCACGGGCCGCCTAAGGAAC-TAMRA-3'
***Timp* 2**	Forward Primer:	5'-CCAGAAGAAGAGCCTGAACCA-3'
	Reverse Primer:	5'-GTCCATCCAGAGGCACTCATC-3'
	Probe:	5'-FAM-ACTCGCTGTCCCATGATCCCTTGC-TAMRA-3'
***Timp* 3**	Forward Primer:	5'-GGCCTCAATTACCGCTACCA-3'
	Reverse Primer:	5'-CTGATAGCCAGGGTACCCAAAA-3'
	Probe:	5'-FAM-TGCTACTACTTGCCTTGTTTTGTGACCTCCA-TAMRA-3'
***Timp* 4**	Forward Primer:	5'-TGCAGAGGGAGAGCCTGAA-3'
	Reverse Primer:	5'-GGTACATGGCACTGCATAGCA-3'
	Probe:	5'-FAM-CCACCAGAACTGTGGCTGCCAAATC-TAMRA-3'
MMP-1	Forward Primer:	5'- CGTGGACCAACAGCAGTGAA -3'
	Reverse Primer:	5'- GAGTGAGCCCAAGGGAGTGA -3'
	Probe:	5'- FAM-TCAACTTGTTCTATGTTACGGCTCATGAACTGG -TAMRA-3'
MMP-2	Forward Primer:	5'-AACTACGATGATGACCGGAAGTG -3'
	Reverse Primer:	5'-TGGCATGGCCGAACTCA -3'
	Probe:	5'- FAM-TCTGTCCTGACCAAGGATATAGCCTATTCCTCG -TAMRA-3'
MMP-3	Forward Primer:	5'-GGAAATCAGTTCTGGGCTATACGA -3'
	Reverse Primer:	5'-TAGAAATGGCAGCATCGATCTTC -3'
	Probe:	5'- FAM- AGGTTATCCTAAAAGCATTCACACCCTGGGTCT-TAMRA-3'
MMP-7	Forward Primer:	5'- GCAGAATACTCACTAATGCCAAACA -3'
	Reverse Primer:	5'- CCGAGGTAAGTCTGAAGTATAGGATACA -3'
	Probe:	5'- FAM- CCAAAATGGCATTCCAGAATTGTCACCTAC -3'
MMP-8	Forward Primer:	5'- GATTCAGAAGAAACGTGGACTCAA -3'
	Reverse Primer:	5'- CATCAAGGCACCAGGATCAGT -3'
	Probe:	5'- FAM-CATGAATTTGGACATTCTTTGGGACTCTCTCAC-TAMRA -3'
MMP-9	Forward Primer:	5'-CGAACTTCGACACTGACAAGAAGT -3'
	Reverse Primer:	5'- GCACGCTGGAATGATCTAAGC-3'
	Probe:	5'- FAM-TCTGTCCAGACCAAGGGTACAGCCTGTTC-TAMRA -3'
MMP-10	Forward Primer:	5'-CCTGCTTTGTCCTTTGATTCAGT-3'
	Reverse Primer:	5'-CGGGAT TCCAATGGGATCT-3'
	Probe:	5'- FAM-TCCTATTCTTTAAAGACAGGTACTTCTGGCGCA-TAMRA -3'
MMP-11	Forward Primer:	5'- ATTGATGCTGCCTTCCAGGAT -3'
	Reverse Primer:	5'- GGGCGAGGAAAGCCTTCTAG -3'
	Probe:	5'- FAM-TCCTTCGTGGCCATCTCTACTGGAAGTTTG-TAMRA -3'
MMP-12	Forward Primer:	5'- GAAACCCCCATCCTTGACAA -3'
	Reverse Primer:	5'- TTCCACCAGAAGAACCAGTCTTTAA -3'
	Probe:	5'- FAM-AGTCCACCATCAACTTTCTGTCACCAAAGC-TAMRA -3'
MMP-13	Forward Primer:	5'-GGGCTCTGAATGGTTATGACATTC -3'
	Reverse Primer:	5'-AGCGCTCAGTCTCTTCACCTCTT -3'
	Probe:	5'- FAM-AAGGTTATCCCAGAAAAATATCTGACCTGGGATTC-TAMRA -3'

Gene		Primer and Probe Sequences
MMP-14	Forward Primer:	5'- AGGAGACAGAGGTGATCATCATTG -3'
	Reverse Primer:	5'- GTCCCATGGCGTCTGAAGA -3'
	Probe:	5'- FAM-CCTGCCGGTACTACTGCTGCTCCTG-TAMRA -3'
MMP-15	Forward Primer:	5'- ATCCCCTATGACCGCATTGAC -3'
	Reverse Primer:	5'- CCCCTGCCAGACACTGATG -3'
	Probe:	5'- FAM-ACACAGCATGGAGACCCTGGCTACCC-TAMRA -3'
MMP-16	Forward Primer:	5'- GGCTACCTTCCACCGACTGA -3'
	Reverse Primer:	5'- CTTCATCCAGTCGATTGTGTTTCT -3'
	Probe:	5'- FAM- CTGCAGAGACCATGCAGTCAGCTCTAGCT-TAMRA -3'
MMP-17	Forward Primer:	5'-GGCAGTATGTTCCTGCACTTCA-3'
	Reverse Primer:	5'- GCTAGCACTGCCCTCAGGAT -3'
	Probe:	5'- FAM-CCTGTGGACCTCAGTCTCTGCCAAGG-TAMRA -3'
MMP-19	Forward Primer:	5'- GCCCATTTCCGGTCAGATG -3'
	Reverse Primer:	5'- AGGGATCCTCCAGACCACAAC -3'
	Probe:	5'- FAM- CCACAAGGGCCCGTATGAAGCAGC-TAMRA -3'
MMP-20	Forward Primer:	5'-GATCAGGAGGATTAAGGAGCTACAAA -3'
	Reverse Primer:	5'- GGCGGTAGTTAGCCACATCAG -3'
	Probe:	5'- FAM- CCAGAATACAATGAATGTGATCAAGAAGCCTCG-TAMRA -3'
MMP-21	Forward Primer:	5'-TCCAAAGAAGATGAGCCAAGTG -3'
	Reverse Primer:	5'-ACGCTGAATCGAGGTTTCTG -3'
	Probe:	5'- FAM-TTCCAGCAATAATGCCTCAAAACCACCC-TAMRA -3'
MMP-23	Forward Primer:	5'- CAGACTGTTGACCATGTCGGTAA -3'
	Reverse Primer:	5'- GAAGGAAAGAACTCTGTATGTGAGGTT -3'
	Probe:	5'- FAM- CCGCTACACGCTGACACCGGC-TAMRA -3'
MMP-24	Forward Primer:	5'- TATCATGGCTCCCTTCTACCAATAC -3'
	Reverse Primer:	5'- CTGCGGACCGGGAGTGT -3'
	Probe:	5'- FAM-CCAGCTGAGCCCTCTGGAGCCA-TAMRA -3'
MMP-25	Forward Primer:	5'- TGGCTGTCTGGGCTACTGAA -3'
	Reverse Primer:	5'- GGTAGGCCCGAGCAAAGTG -3'
	Probe:	5'- FAM-AATTCTCAGTACCAGGAGCCTGACATCATTATCC-TAMRA -3'
MMP-27	Forward Primer:	5'-AGGATAATAAAGTGCTTCCCAGGA-3'
	Reverse Primer:	5'-AAGAAATAGAGGAATCCATTATGTTGG-3'
	Probe:	5'- FAM-TCGCCTCCGTGTGGATGCTGTC-TAMRA -3'
MMP-28	Forward Primer:	5'- CCACTTGGACAGAGAGGATCAGT -3'
	Reverse Primer:	5'- AAGCGTTTCTTACGCCTCATTT -3'
	Probe:	5'- FAM- CTGCTTGCTGGACACCGAGCCAA-TAMRA -3'
ADAM8	Forward Primer:	5'-CCGAAAGGCTCCGAGACAA-3'
	Reverse Primer:	5'-GAAGGGTCTGGAGGCCTGTT-3'
	Probe:	5'-FAM-AGGAGTGTGGCACCCAAGCCTATCTCG-TAMRA-3
ADAM10	Forward Primer:	5'- GTGCCAGTACAGGCTCTTTGC -3'
	Reverse Primer:	5'- CACAGTAGCCTCTGAAGTCATTACATG -3'
	Probe:	5'- FAM-ACTATCACTCTGCAGCCGGGCTCTCC-TAMRA -3'

Gene		Primer and Probe Sequences
ADAM17	Forward Primer:	5'-AAGTGCAAGGCTGGGAAATG -3'
	Reverse Primer:	5'-CACACGGGCCAGAAAGGTT -3'
	Probe:	5'- FAM-CCTGCGCATGCATTGACACTGACAAC-TAMRA -3'
ADAM19	Forward Primer:	5'-CGGGCCCACCTCGAA-3'
	Reverse Primer:	5'-CCGTTTCATTCTGCGAGGTT-3'
	Probe:	5'- FAM-TGGGCCCTTCAGTTTACACATCAGACCA-TAMRA -3'
ADAM28	Forward Primer:	5'-TACTGCTTGAAGGGCAAATGTC -3'
	Reverse Primer:	5'-TGTCCCACCTTCATTCTGCTT -3'
	Probe:	5'- FAM-TCCAGGAACCAAGGTTGCAAATACATCATGTTAC-TAMRA -3'
ADAM33	Forward Primer:	5'-CAGGCACTGTCAGAATGCTACCT-3'
	Reverse Primer:	5'-CTATTGCAAACCCCACCGTTA-3'
	Probe:	5'- FAM-TGGAACGTTGCTTGACTGCCTGCC-TAMRA -3'
Adamts1	Forward Primer:	5'-CCAGAACACCCGGAACCA-3'
	Reverse Primer:	5'-CACAAATCGCTTCTTCCTTATGC-3'
	Probe:	5'- FAM-ACGCGGGAAAGCCATCAGGACC-TAMRA -3'
Adamts4	Forward Primer:	5'- TCAACACCCCTAACGACTCAGA -3'
	Reverse Primer:	5'- CAGCTCCTAGCTGGATCACACA -3'
	Probe:	5'- FAM- CTGACCACTTTGACACAGCCATTCTGTTCA -TAMRA -3'
Adamts8	Forward Primer:	5'-AGAGGACAGGAAGCAGGACAA-3'
	Reverse Primer:	5'-GGACACAAACCTCTTGCTTCTAGTT-3'
	Probe:	5'- FAM-AAGTGCCACCACCCTTCGGATCC-TAMRA -3'
Adamts15	Forward Primer:	5'-GCTCATCTGCCGAGCCAAT -3'
	Reverse Primer:	5'-CAGCCAGCCTTGATGCACTT -3'
	Probe:	5'- FAM-CCTGACTCCACCTCGGTCTGTGTCCA -TAMRA -3'
Adamts16	Forward Primer:	5'- AACTCAGACTGTGTCACGCATAGAG -3'
	Reverse Primer:	5'- GGAGGTAGAGATGTTTGTTTCGTAGA -3'
	Probe:	5'- FAM- TAAGCACCATTCCACCAACCAGTACTACCACA -TAMRA -3'
TNFa	Forward Primer:	5' – AGACCCTCACACTCAGATCATCTTC – 3'
	Reverse Primer:	5' – CCACTTGGTGGTTTGCTACGA – 3'
	Probe:	5'- FAM- CAAAATTCGAGTGACAAGCCTGTAGCCCA-TAMRA -3'
F4/80	Forward Primer:	5' – CCTGGACGAATCCTGTGAAG – 3'
	Reverse Primer:	5' – GGTGGGACCACAGAGAGTTG – 3'
	Probe:	Universal # 1
HDAC4	Forward Primer:	5' – AATCCTGCCCGTGTGAAC – 3'
	Reverse Primer:	5' – GTAGGGGCCACTTGCAGA – 3'
	Probe:	Universal #71
HDAC5	Forward Primer:	5' – GAGTCCAGTGCTGGTTACAAAA – 3'
	Reverse Primer:	5' – TACACCTGGAGGGGCTGTAA – 3'
	Probe:	Universal #71
HDAC7	Forward Primer:	5' – CCATGGGGGATCCTGAGT – 3'
	Reverse Primer:	5' – GCAAACTCTGGGCAATG – 3'
	Probe:	Universal # 71

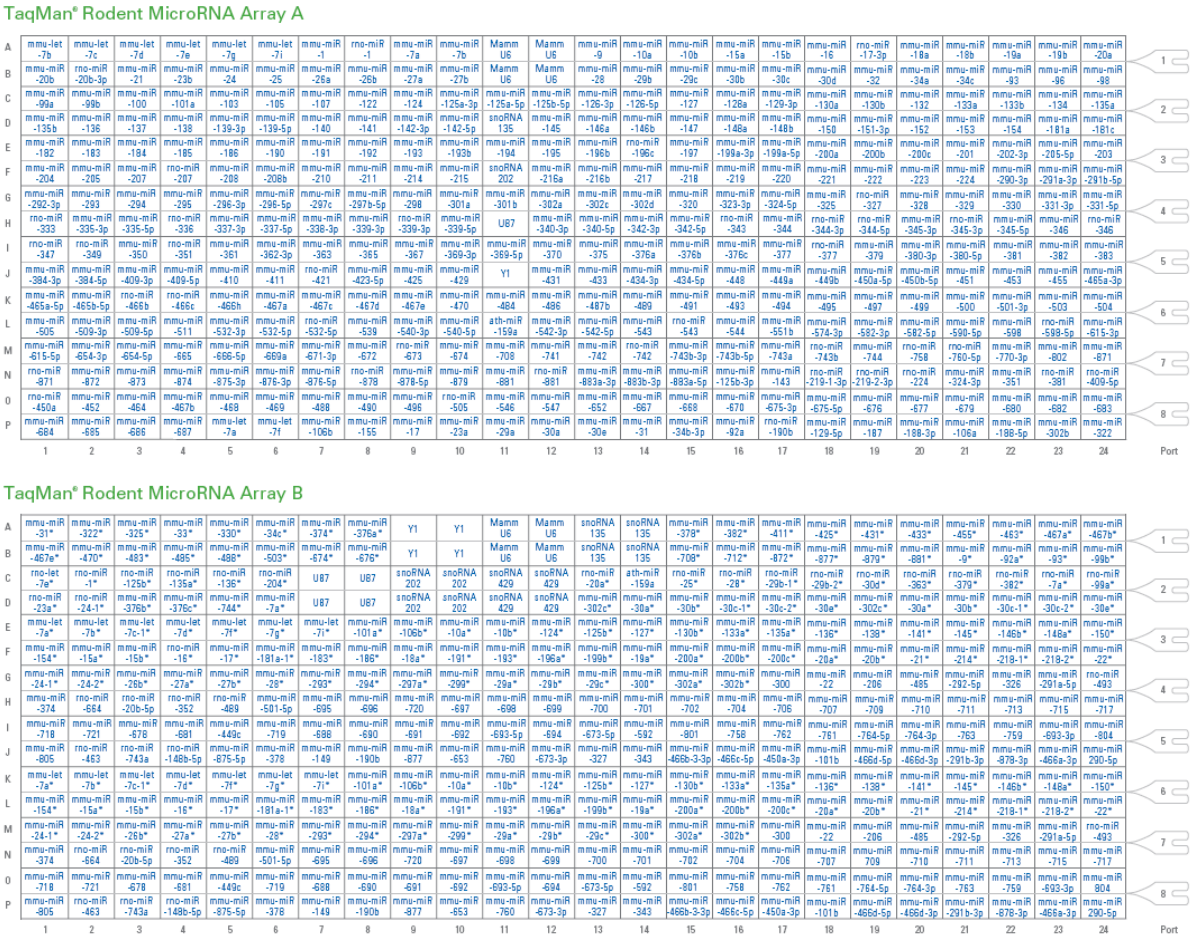

Figure 8.1 TaqMan® Array Rodent MicroRNA Card Set v2.0 (Applied Biosystems). A two card set containing a total of 364 TaqMan® MicroRNA Assays per card. Enables quantitation of 518 and 303 unique microRNAs for mouse and rat respectively. Three endogenous controls for each species are included on each card for data normalization and one unrelated to rodent as a negative control.

Figure 8.2 Microarray analysis of 518 unique murine microRNAs performed for RAW264.7 macrophages treated with LPS, the IκK kinase inhibitor BMS-345541 or LPS and BMS 345541 combined. Taqman low density array (TLDA) was performed on cDNA extracted from RAW264.7 4 hours post-treatment. C_T values were converted to a representative colour, black indicating no expression (≥ 35) and green indicating very high expression (≤ 20) as shown in key. MicroRNAs are ordered according to their basal level of expression (control). Red arrow indicates miR-155 whilst highlighted microRNAs indicate those that have been shown to respond to LPS previously: miR-9 (Bazzoni et al., 2009), miR-147a/b (Taganov et al., 2006), miR-155 (O'Connell et al., 2007; Tili et al., 2007).


RAW264.7
microRNA
control
LPS
BMS 345541
BMS 345541 + LPS
mmu-miR-24
mmu-miR-146a
mmu-miR-19b
mmu-miR-16
mmu-miR-17
mmu-miR-191
mmu-miR-21
mmu-miR-222
mmu-miR-29a
mmu-miR-20a
mmu-miR-142-3p
mmu-miR-484
mmu-miR-106a
mmu-miR-19a
mmu-miR-93
mmu-miR-223
mmu-miR-29c
mmu-miR-30c
mmu-miR-221
mmu-let-7g
mmu-let-7i
mmu-miR-652
mmu-miR-26b
mmu-miR-27b
mmu-miR-99b
mmu-miR-30b
mmu-miR-15b
mmu-miR-140
mmu-miR-467a
mmu-miR-146b
mmu-miR-301a
mmu-miR-92a
mmu-let-7e
mmu-miR-30e
mmu-miR-30a
mmu-let-7c
mmu-miR-425
mmu-miR-125a-5p
mmu-miR-532-5p
mmu-miR-26a
mmu-miR-27a
mmu-miR-15a
mmu-miR-106b
mmu-miR-30d
mmu-miR-186
mmu-let-7d
mmu-miR-103
mmu-miR-139-5p
mmu-miR-301b
mmu-miR-195
mmu-miR-10a
rno-miR-532-5p
mmu-miR-328
mmu-miR-100
mmu-miR-669a
mmu-miR-467c
mmu-miR-138
mmu-miR-148a
mmu-let-7b
mmu-miR-99a
mmu-miR-486
mmu-miR-23a
mmu-miR-23b
mmu-miR-467b
mmu-let-7a
mmu-miR-320
mmu-miR-210
mmu-miR-18a
mmu-let-7f
mmu-miR-324-3p
mmu-miR-322
mmu-miR-9
mmu-miR-155
mmu-miR-151-3p
mmu-miR-340-5p
mmu-miR-501-3p
mmu-miR-574-3p
mmu-miR-331-3p
mmu-miR-324-5p
mmu-miR-503
mmu-miR-539
mmu-miR-125b-5p
mmu-miR-339-3p
mmu-miR-687
mmu-miR-708
rno-miR-351
mmu-miR-200c
mmu-miR-182
mmu-miR-467e
mmu-miR-532-3p
mmu-miR-25
mmu-miR-351
mmu-miR-379
mmu-miR-28
mmu-miR-744
mmu-miR-192
mmu-miR-509-3p
mmu-miR-340-3p
mmu-miR-494
mmu-miR-152
mmu-miR-449b
mmu-miR-674
mmu-miR-350
mmu-miR-29b
mmu-miR-547
mmu-miR-467d
RAW264.7
microRNA
control
LPS
BMS 345541
BMS 345541 + LPS
mmu-miR-615-3p
mmu-miR-101a
rno-miR-333
mmu-miR-200b
mmu-miR-181a
mmu-miR-132
mmu-miR-676
mmu-miR-10b
mmu-miR-98
mmu-miR-185
mmu-miR-497
mmu-miR-365
mmu-miR-20b
mmu-miR-429
mmu-miR-142-5p
mmu-miR-544
mmu-miR-500
mmu-miR-342-3p
mmu-miR-34a
mmu-miR-124
mmu-miR-339-5p
mmu-miR-126-3p
mmu-miR-433
mmu-miR-7a
mmu-miR-449a
mmu-miR-188-5p
mmu-miR-7b
mmu-miR-107
mmu-miR-203
mmu-miR-872
mmu-miR-197
mmu-miR-139-3p
mmu-miR-685
mmu-miR-682
mmu-miR-423-5p
mmu-miR-200a
mmu-miR-667
mmu-miR-345-5p
rno-miR-196c
rno-miR-339-3p
mmu-miR-362-3p
mmu-miR-148b
mmu-miR-680
mmu-miR-128a
mmu-miR-361-
mmu-miR-465b-5p
mmu-miR-215
mmu-miR-499
rno-miR-345-3p
mmu-miR-208b
mmu-miR-491
mmu-miR-330
mmu-miR-193b
mmu-miR-331-5p
mmu-miR-181c
mmu-miR-671-3p
mmu-miR-194
mmu-miR-489
rno-miR-207
mmu-miR-196b
mmu-miR-130b
mmu-miR-190
mmu-miR-184
mmu-miR-126-5p
mmu-miR-150
mmu-miR-125a-3p
mmu-miR-297b-5p
mmu-miR-32
mmu-miR-193
mmu-miR-546
mmu-miR-672
mmu-miR-450a-5p
mmu-miR-183
mmu-miR-451
mmu-miR-542-3p
mmu-miR-338-3p
mmu-miR-294
mmu-miR-34b-3p
mmu-miR-542-5p
rno-miR-377
rno-miR-190b
mmu-miR-383
mmu-miR-590-5p
rno-miR-450a
mmu-miR-375
mmu-miR-677
mmu-miR-31
mmu-miR-582-5p
mmu-miR-363
mmu-miR-295
mmu-miR-224
mmu-miR-96
mmu-miR-434-3p
mmu-miR-141
mmu-miR-202-3p
mmu-miR-410
mmu-miR-741
rno-miR-347
mmu-miR-384-5p
mmu-miR-199a-3p
mmu-miR-297c
mmu-miR-376c
mmu-miR-466h
rno-miR-224
rno-miR-381
rno-miR-421
C_T
≤ 20
21-22
23-24
25-26
27-28
29-30
31-32
33-34
≥ 35

Tissue		Db/Db			Db/+			
Day 0 Unwounded	Mouse	1a	2a	3a	Mouse	-	-	-
	Sample	1a	2a	3a	Sample	-	-	-
Day 5 Wound	Mouse	1	2	3	Mouse	1	2	3
	Sample	n1 (normal) w1 (wound)	n2 (normal) w2 (wound)	n3 (normal)	Sample	n1 (normal) w1 (wound)	n2 (normal)	n3 (normal)
Day 7 Wound	Mouse	4	5	-	Mouse	4	5	-
	Sample	w5 (wound)	w6 (wound) w7 (wound)	-	Sample	n4 (normal) w4 (wound)	n5 (normal) w5 (wound)	-

Table 8.3 Mice used in wounding studies in Chapter 5. Mouse number correlates to numbers given in chapter 5, figures 5.4-5.8.

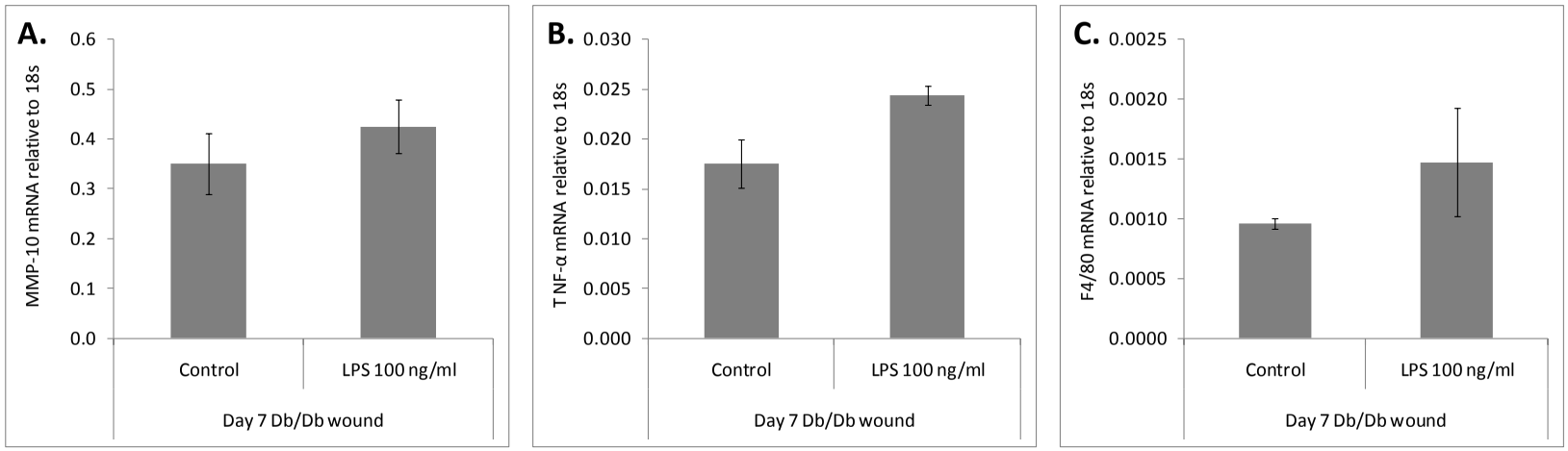

D.

	Treatment	C_T value 1	C_T value 2	C_T value 3
Db/Db wound	Control	24.74	24.08	26.16
	LPS 100 ng/ml	23.29	24.43	24.62

E.

	Treatment	C_T value 1	C_T value 2	C_T value 3
Db/Db wound	Control	26.66	26.47	25.84
	LPS 100 ng/ml	25.84	25.75	25.57

F.

	Treatment	C_T value 1	C_T value 2	C_T value 3
Db/Db wound	Control	35.71	35.37	35.53
	LPS 100 ng/ml	36.62	34.09	33.05

Figure 8.3 Comparing relative expression of MMP-10, TNF-α and F4/80 mRNA in Db/Db skin 7 days post wounding after a further 24 hours *ex vivo* culture with LPS. qRT-PCR for (A) MMP-10, (B) TNF-α and (C) F4/80 was performed on day 7 Db/Db wounds after 24 hours *ex vivo* culture with 100 ng/ml LPS in explant culture medium. (D-F) Corresponding C_T values are shown. Each bar represents the mean of 3 samples ± SEM

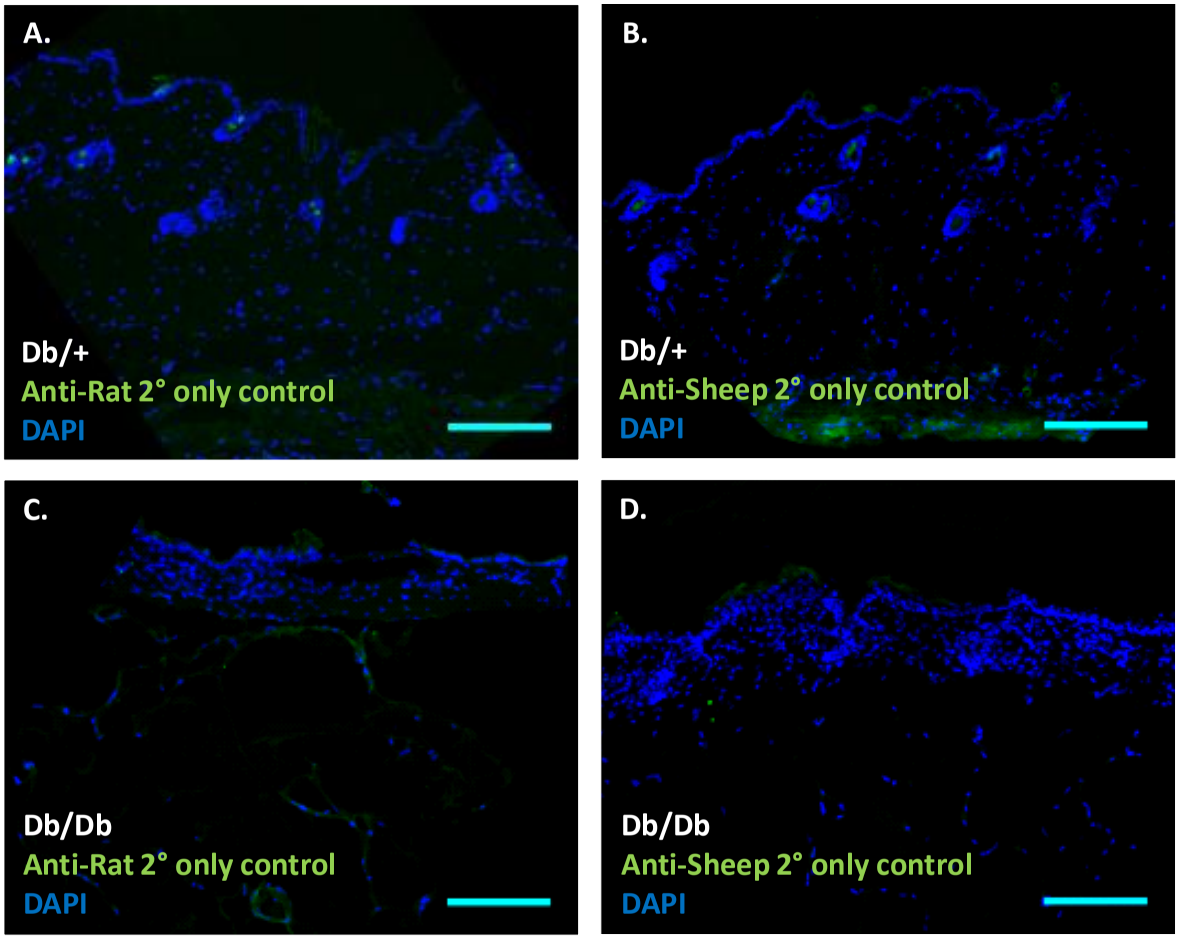

Table 8.4 Secondary antibody only controls for immunofluorescent staining of Db/Db and Db/+ mouse dorsal flank shown in Figure 5.10. 10 µm sections were fixed and incubated with DAPI nuclear stain and secondary antibodies only to check for non-specific binding and fluorescence. Sections were taken from within 160 µm of their primary antibody treated counterparts. Scale bar = 75 µm

References

Agrawal,S., Anderson,P., Durbeej,M., van,R.N., Ivars,F., Opdenakker,G., and Sorokin,L.M. (2006). Dystroglycan is selectively cleaved at the parenchymal basement membrane at sites of leukocyte extravasation in experimental autoimmune encephalomyelitis. J. Exp. Med. *203*, 1007-1019.

Akiyama,S.K., Olden,K., and Yamada,K.M. (1995). Fibronectin and integrins in invasion and metastasis. Cancer Metastasis Rev. *14*, 173-189.

Allen,W.E., Zicha,D., Ridley,A.J., and Jones,G.E. (1998a). A role for Cdc42 in macrophage chemotaxis. J. Cell Biol. *141*, 1147-1157.

Alon, R., Feigelson, S.W., Manevich, E., Rose, D.M., Schmitz, J., Overby, D.R., Winter, E., Grabovsky, V., Shinder, V., Matthews, B.D., Sokolovsky-Eisenberg, M., Ingber, D.E., Benoit, M., Ginsberg, M.H. (2005). Alpha4beta1-dependent adhesion strengthening under mechanical strain is regulated by paxillin association with the alpha4-cytoplasmic domain. J Cell Biol. *171*, 1073-84.

Askari,J.A., Buckley,P.A., Mould,A.P., and Humphries,M.J. (2009). Linking integrin conformation to function. J. Cell Sci. *122*, 165-170.

Aung,H.T., Schroder,K., Himes,S.R., Brion,K., van Zuylen,W., Trieu,A., Suzuki,H., Hayashizaki,Y., Hume,D.A., Sweet,M.J., and Ravasi,T. (2006). LPS regulates proinflammatory gene expression in macrophages by altering histone deacetylase expression. FASEB J. *20*, 1315-1327.

Bar-Or,A., Nuttall,R.K., Duddy,M., Alter,A., Kim,H.J., Ifergan,I., Pennington,C.J., Bourgoin,P., Edwards,D.R., and Yong,V.W. (2003). Analyses of all matrix metalloproteinase members in leukocytes emphasize monocytes as major inflammatory mediators in multiple sclerosis. Brain *126*, 2738-2749.

Barczyk,M., Carracedo,S., and Gullberg,D. (2010). Integrins. Cell Tissue Res. *339*, 269-280.

Barksby,H.E., Milner,J.M., Patterson,A.M., Peake,N.J., Hui,W., Robson,T., Lakey,R., Middleton,J., Cawston,T.E., Richards,C.D., and Rowan,A.D. (2006). Matrix metalloproteinase 10 promotion of collagenolysis via procollagenase activation: implications for cartilage degradation in arthritis. Arthritis Rheum. *54*, 3244-3253.

Barlic,J., Zhang,Y., Foley,J.F., and Murphy,P.M. (2006). Oxidized lipid-driven chemokine receptor switch, CCR2 to CX3CR1, mediates adhesion of human macrophages to coronary artery smooth muscle cells through a peroxisome proliferator-activated receptor gamma-dependent pathway. Circulation. *114*, 807-819.

Bazzoni,F., Rossato,M., Fabbri,M., Gaudiosi,D., Mirolo,M., Mori,L., Tamassia,N., Mantovani,A., Cassatella,M.A., and Locati,M. (2009). Induction and regulatory function of miR-9 in human monocytes and neutrophils exposed to proinflammatory signals. Proc. Natl. Acad. Sci. U. S. A *106*, 5282-5287.

Beacham,D.A., Amatangelo,M.D., and Cukierman,E. (2007). Preparation of extracellular matrices produced by cultured and primary fibroblasts. Curr. Protoc. Cell Biol. *Chapter 10*, Unit.

Bevan,D., Gherardi,E., Fan,T.P., Edwards,D., and Warn,R. (2004). Diverse and potent activities of HGF/SF in skin wound repair. J. Pathol. *203*, 831-838.

Binker,M.G., Zhao,D.Y., Pang,S.J., and Harrison,R.E. (2007). Cytoplasmic linker protein-170 enhances spreading and phagocytosis in activated macrophages by stabilizing microtubules. J. Immunol. *179*, 3780-3791.

Bister,V., Makitalo,L., Jeskanen,L., and Saarialho-Kere,U. (2007). Expression of MMP-9, MMP-10 and TNF-alpha and lack of epithelial MMP-1 and MMP-26 characterize pyoderma gangrenosum. J. Cutan. Pathol. *34*, 889-898.

Black,R.A., Rauch,C.T., Kozlosky,C.J., Peschon,J.J., Slack,J.L., Wolfson,M.F., Castner,B.J., Stocking,K.L., Reddy,P., Srinivasan,S., Nelson,N., Boiani,N., Schooley,K.A., Gerhart,M., Davis,R., Fitzner,J.N., Johnson,R.S., Paxton,R.J., March,C.J., and Cerretti,D.P. (1997). A metalloproteinase disintegrin that releases tumour-necrosis factor-alpha from cells. Nature *385*, 729-733.

Blander,J.M. and Medzhitov,R. (2006). On regulation of phagosome maturation and antigen presentation. Nat. Immunol. *7*, 1029-1035.

Blystone,S.D., Weston,L.K., and Kaplan,J.E. (1991). Fibronectin dependent macrophage fibrin binding. Blood. *78*, 2900-2907.

Bokoch,G.M. (2005). Regulation of innate immunity by Rho GTPases. Trends Cell Biol. *15*, 163-171.

Bord,S., Horner,A., Hembry,R.M., and Compston,J.E. (1998). Stromelysin-1 (MMP-3) and stromelysin-2 (MMP-10) expression in developing human bone: potential roles in skeletal development. Bone. *23*, 7-12.

Boring,L., Gosling,J., Cleary,M., and Charo,I.F. (1998). Decreased lesion formation in CCR2-/- mice reveals a role for chemokines in the initiation of atherosclerosis. Nature. *394*, 894-897.

Borzillo,G.V., Ashmun,R.A., and Sherr,C.J. (1990). Macrophage lineage switching of murine early pre-B lymphoid cells expressing transduced fms genes. Mol. Cell Biol. *10*, 2703-2714.

Bou-Gharios,G., Ponticos,M., Rajkumar,V., and Abraham,D. (2004). Extra-cellular matrix in vascular networks. Cell Prolif. *37*, 207-220.

Bouma,G., Coppens,J.M., Lam-Tse,W.K., Luini,W., Sintnicolaas,K., Levering,W.H., Sozzani,S., Drexhage,H.A., and Versnel,M.A. (2005). An increased MRP8/14 expression and adhesion, but a decreased migration towards proinflammatory chemokines of type 1 diabetes monocytes. Clin. Exp. Immunol. *141*, 509-517.

Brakebusch,C. and Fassler,R. (2003). The integrin-actin connection, an eternal love affair. EMBO J. *22*, 2324-2333.

Breitkreutz,D., Mirancea,N., and Nischt,R. (2009). Basement membranes in skin: unique matrix structures with diverse functions? Histochem. Cell Biol. *132*, 1-10.

Brew,K. and Nagase,H. (2010). The tissue inhibitors of metalloproteinases (TIMPs): an ancient family with structural and functional diversity. Biochim. Biophys. Acta. *1803*, 55-71.

Bridges,L.C., Tani,P.H., Hanson,K.R., Roberts,C.M., Judkins,M.B., and Bowditch,R.D. (2002). The lymphocyte metalloprotease MDC-L (ADAM 28) is a ligand for the integrin alpha4beta1. J. Biol. Chem. *277*, 3784-3792.

Brown,D.L., Kane,C.D., Chernausek,S.D., and Greenhalgh,D.G. (1997). Differential expression and localization of insulin-like growth factors I and II in cutaneous wounds of diabetic and nondiabetic mice. Am. J. Pathol. *151*, 715-724.

Burke,J.R., Pattoli,M.A., Gregor,K.R., Brassil,P.J., MacMaster,J.F., McIntyre,K.W., Yang,X., Iotzova,V.S., Clarke,W., Strnad,J., Qiu,Y., and Zusi,F.C. (2003). BMS-345541 is a highly selective inhibitor of I kappa B kinase that binds at an allosteric site of the enzyme and blocks NF-kappa B-dependent transcription in mice. J. Biol. Chem. *278*, 1450-1456.

Busiek,D.F., Ross,F.P., McDonnell,S., Murphy,G., Matrisian,L.M., and Welgus,H.G. (1992). The matrix metalloprotease matrilysin (PUMP) is expressed in developing human mononuclear phagocytes. J. Biol. Chem. *267*, 9087-9092.

Campbell,R.K. (2009). Type 2 diabetes: where we are today: an overview of disease burden, current treatments, and treatment strategies. J. Am. Pharm. Assoc. (2003.). *49 Suppl 1:S3-9.*, S3-S9.

Cao,J., Kozarekar,P., Pavlaki,M., Chiarelli,C., Bahou,W.F., and Zucker,S. (2004). Distinct roles for the catalytic and hemopexin domains of membrane type 1-matrix metalloproteinase in substrate degradation and cell migration. J. Biol. Chem. *279*, 14129-14139.

Cartharius,K., Frech,K., Grote,K., Klocke,B., Haltmeier,M., Klingenhoff,A., Frisch,M., Bayerlein,M., and Werner,T. (2005). MatInspector and beyond: promoter analysis based on transcription factor binding sites. Bioinformatics. *21*, 2933-2942.

Cawston,T.E. (1995). Proteinases and inhibitors. Br. Med. Bull. *51*, 385-401.

Ceppi,M., Pereira,P.M., Dunand-Sauthier,I., Barras,E., Reith,W., Santos,M.A., and Pierre,P. (2009). MicroRNA-155 modulates the interleukin-1 signaling pathway in activated human monocyte-derived dendritic cells. Proc. Natl. Acad. Sci. U. S. A. *106*, 2735-2740.

Chakraborti,S., Mandal,M., Das,S., Mandal,A., and Chakraborti,T. (2003). Regulation of matrix metalloproteinases: an overview. Mol. Cell Biochem. *253*, 269-285.

Chang,S., Young,B.D., Li,S., Qi,X., Richardson,J.A., and Olson,E.N. (2006). Histone deacetylase 7 maintains vascular integrity by repressing matrix metalloproteinase 10. Cell. *126*, 321-334.

Chaplin,D.D. (2010). Overview of the immune response. J. Allergy Clin. Immunol. *125*, S3-23.

Chen,H., Charlat,O., Tartaglia,L.A., Woolf,E.A., Weng,X., Ellis,S.J., Lakey,N.D., Culpepper,J., Moore,K.J., Breitbart,R.E., Duyk,G.M., Tepper,R.I., and Morgenstern,J.P. (1996). Evidence that the diabetes gene encodes the leptin receptor: identification of a mutation in the leptin receptor gene in db/db mice. Cell *84*, 491-495.

Cheng,L., Mantile,G., Pauly,R., Nater,C., Felici,A., Monticone,R., Bilato,C., Gluzband,Y.A., Crow,M.T., Stetler-Stevenson,W., and Capogrossi,M.C. (1998). Adenovirus-mediated gene transfer of the human tissue inhibitor of metalloproteinase-2 blocks vascular smooth muscle cell invasiveness in vitro and modulates neointimal development in vivo. Circulation. *98*, 2195-2201.

Chin,J.R., Murphy,G., and Werb,Z. (1985). Stromelysin, a connective tissue-degrading metalloendopeptidase secreted by stimulated rabbit synovial fibroblasts in parallel with collagenase. Biosynthesis, isolation, characterization, and substrates. J. Biol. Chem. *260*, 12367-12376.

Chitu,V. and Stanley,E.R. (2006). Colony-stimulating factor-1 in immunity and inflammation. Curr. Opin. Immunol. *18*, 39-48.

Conti,M.A. and Adelstein,R.S. (2008). Nonmuscle myosin II moves in new directions. J. Cell Sci. *121*, 11-18.

Cox,D., Chang,P., Zhang,Q., Reddy,P.G., Bokoch,G.M., and Greenberg,S. (1997). Requirements for both Rac1 and Cdc42 in membrane ruffling and phagocytosis in leukocytes. J. Exp. Med. *186*, 1487-1494.

Curnock,A.P., Logan,M.K., and Ward,S.G. (2002). Chemokine signalling: pivoting around multiple phosphoinositide 3-kinases. Immunology. *105*, 125-136.

Danen,E.H., Sonneveld,P., Brakebusch,C., Fassler,R., and Sonnenberg,A. (2002). The fibronectin-binding integrins alpha5beta1 and alphavbeta3 differentially modulate RhoA-GTP loading, organization of cell matrix adhesions, and fibronectin fibrillogenesis. J. Cell Biol. *159*, 1071-1086.

Davis,G.E., Bayless,K.J., Davis,M.J., and Meininger,G.A. (2000). Regulation of tissue injury responses by the exposure of matricryptic sites within extracellular matrix molecules. Am. J. Pathol. *156*, 1489-1498.

Dean,R.A., Cox,J.H., Bellac,C.L., Doucet,A., Starr,A.E., and Overall,C.M. (2008). Macrophage-specific metalloelastase (MMP-12) truncates and inactivates ELR+ CXC chemokines and generates CCL2, -7, -8, and -13 antagonists: potential role of the macrophage in terminating polymorphonuclear leukocyte influx. Blood. *112*, 3455-3464.

Deryugina,E.I., Ratnikov,B., Monosov,E., Postnova,T.I., DiScipio,R., Smith,J.W., and Strongin,A.Y. (2001). MT1-MMP initiates activation of pro-MMP-2 and integrin alphavbeta3 promotes maturation of MMP-2 in breast carcinoma cells. Exp. Cell Res. *263*, 209-223.

Deshmane,S.L., Kremlev,S., Amini,S., and Sawaya,B.E. (2009). Monocyte chemoattractant protein-1 (MCP-1): an overview. J. Interferon Cytokine Res. *29*, 313-326.

Duffield,J.S. (2003). The inflammatory macrophage: a story of Jekyll and Hyde. Clin. Sci. (Lond) *104*, 27-38.

Dunaeva,M., Voo,S., van,O.C., and Waltenberger,J. (2010). Sonic hedgehog is a potent chemoattractant for human monocytes: diabetes mellitus inhibits Sonic hedgehog-induced monocyte chemotaxis. Basic Res. Cardiol. *105*, 61-71.

Dunkelberger,J.R. and Song,W.C. (2010). Complement and its role in innate and adaptive immune responses. Cell Res. *20*, 34-50.

Dupasquier,M., Stoitzner,P., van,O.A., Romani,N., and Leenen,P.J. (2004). Macrophages and dendritic cells constitute a major subpopulation of cells in the mouse dermis. J. Invest Dermatol. *123*, 876-879.

El-Osta,A., Brasacchio,D., Yao,D., Pocai,A., Jones,P.L., Roeder,R.G., Cooper,M.E., and Brownlee,M. (2008). Transient high glucose causes persistent epigenetic changes and altered gene expression during subsequent normoglycemia. J. Exp. Med. *205*, 2409-2417.

Esche,C., Stellato,C., and Beck,L.A. (2005). Chemokines: key players in innate and adaptive immunity. J. Invest Dermatol. *125*, 615-628.

Esposito,C., Fasoli,G., Plati,A.R., Bellotti,N., Conte,M.M., Cornacchia,F., Foschi,A., Mazzullo,T., Semeraro,L., and Dal Canton,A. (2001). Long-term exposure to high glucose up-regulates VCAM-induced endothelial cell adhesiveness to PBMC. Kidney Int. *59*, 1842-1849.

Feezor,R.J., Paddock,H.N., Baker,H.V., Varela,J.C., Barreda,J., Moldawer,L.L., Schultz,G.S., and Mozingo,D.W. (2004). Temporal patterns of gene expression in murine cutaneous burn wound healing. Physiol Genomics. *16*, 341-348.

Feiken,E., Romer,J., Eriksen,J., and Lund,L.R. (1995). Neutrophils express tumor necrosis factor-alpha during mouse skin wound healing. J. Invest Dermatol. *105*, 120-123.

Forough,R., Koyama,N., Hasenstab,D., Lea,H., Clowes,M., Nikkari,S.T., and Clowes,A.W. (1996). Overexpression of tissue inhibitor of matrix metalloproteinase-1 inhibits vascular smooth muscle cell functions in vitro and in vivo. Circ. Res. *79*, 812-820.

Fraley,S.I., Feng,Y., Krishnamurthy,R., Kim,D.H., Celedon,A., Longmore,G.D., and Wirtz,D. (2010). A distinctive role for focal adhesion proteins in three-dimensional cell motility. Nat. Cell Biol. *12*, 598-604.

Frederick,L.A., Matthews,J.A., Jamieson,L., Justilien,V., Thompson,E.A., Radisky,D.C., and Fields,A.P. (2008). Matrix metalloproteinase-10 is a critical effector of protein kinase Ciota-Par6alpha-mediated lung cancer. Oncogene. *27*, 4841-4853.

Friedl,P. and Wolf,K. (2009). Proteolytic interstitial cell migration: a five-step process. Cancer Metastasis Rev. *28*, 129-135.

Friedman,A.D. (2002). Transcriptional regulation of granulocyte and monocyte development. Oncogene *21*, 3377-3390.

Friedman,R.C., Farh,K.K., Burge,C.B., and Bartel,D.P. (2009). Most mammalian mRNAs are conserved targets of microRNAs. Genome Res. *19*, 92-105.

Fujihara,M., Muroi,M., Tanamoto,K., Suzuki,T., Azuma,H., and Ikeda,H. (2003). Molecular mechanisms of macrophage activation and deactivation by lipopolysaccharide: roles of the receptor complex. Pharmacol. Ther. *100*, 171-194.

Galis,Z.S., Sukhova,G.K., Kranzhofer,R., Clark,S., and Libby,P. (1995). Macrophage foam cells from experimental atheroma constitutively produce matrix-degrading proteinases. Proc. Natl. Acad. Sci. U. S. A. *92*, 402-406.

Galkina,E. and Ley,K. (2007). Vascular adhesion molecules in atherosclerosis. Arterioscler. Thromb. Vasc. Biol. *27*, 2292-2301.

Galvez,B.G., Matias-Roman,S., Yanez-Mo,M., Sanchez-Madrid,F., and Arroyo,A.G. (2002). ECM regulates MT1-MMP localization with beta1 or alphavbeta3 integrins at distinct cell compartments modulating its internalization and activity on human endothelial cells. J. Cell Biol. *159*, 509-521.

Gao,C., Cheng,X., Lam,M., Liu,Y., Liu,Q., Chang,K.S., and Kao,H.Y. (2008). Signal-dependent regulation of transcription by histone deacetylase 7 involves recruitment to promyelocytic leukemia protein nuclear bodies. Mol. Biol. Cell. *19*, 3020-3027.

Garton,K.J., Gough,P.J., Blobel,C.P., Murphy,G., Greaves,D.R., Dempsey,P.J., and Raines,E.W. (2001). Tumor necrosis factor-alpha-converting enzyme (ADAM17) mediates the cleavage and shedding of fractalkine (CX3CL1). J. Biol. Chem. *276*, 37993-38001.

Gawden-Bone,C., Zhou,Z., King,E., Prescott,A., Watts,C., and Lucocq,J. (2010). Dendritic cell podosomes are protrusive and invade the extracellular matrix using metalloproteinase MMP-14. J. Cell Sci. *123*, 1427-1437.

Gill,J.H., Kirwan,I.G., Seargent,J.M., Martin,S.W., Tijani,S., Anikin,V.A., Mearns,A.J., Bibby,M.C., Anthoney,A., and Loadman,P.M. (2004). MMP-10 is overexpressed, proteolytically active, and a potential target for therapeutic intervention in human lung carcinomas. Neoplasia. *6*, 777-785.

Gill,S.E. and Parks,W.C. (2008). Metalloproteinases and their inhibitors: regulators of wound healing. Int. J. Biochem. Cell Biol. *40*, 1334-1347.

Gloire,G., Legrand-Poels,S., and Piette,J. (2006). NF-kappaB activation by reactive oxygen species: fifteen years later. Biochem. Pharmacol. *72*, 1493-1505.

Goetzl,E.J., Banda,M.J., and Leppert,D. (1996). Matrix metalloproteinases in immunity. J. Immunol. *156*, 1-4.

Gonzalo,P., Guadamillas,M.C., Hernandez-Riquer,M.V., Pollan,A., Grande-Garcia,A., Bartolome,R.A., Vasanji,A., Ambrogio,C., Chiarle,R., Teixido,J., Risteli,J., Apte,S.S., del Pozo,M.A., and Arroyo,A.G. (2010). MT1-MMP is required for myeloid cell fusion via regulation of Rac1 signaling. Dev. Cell. *%19;18*, 77-89.

Goren,I., Kampfer,H., Podda,M., Pfeilschifter,J., and Frank,S. (2003). Leptin and wound inflammation in diabetic ob/ob mice: differential regulation of neutrophil and macrophage influx and a potential role for the scab as a sink for inflammatory cells and mediators. Diabetes. *52*, 2821-2832.

Goren,I., Muller,E., Schiefelbein,D., Christen,U., Pfeilschifter,J., Muhl,H., and Frank,S. (2007). Systemic anti-TNFalpha treatment restores diabetes-impaired skin repair in ob/ob mice by inactivation of macrophages. J. Invest Dermatol. *127*, 2259-2267.

Greenhalgh,D.G., Sprugel,K.H., Murray,M.J., and Ross,R. (1990). PDGF and FGF stimulate wound healing in the genetically diabetic mouse. Am. J. Pathol. *136*, 1235-1246.

Griffiths-Jones,S., Saini,H.K., van,D.S., and Enright,A.J. (2008). miRBase: tools for microRNA genomics. Nucleic Acids Res. *36*, D154-D158.

Gu,H., Cui,M., Bai,Y., Chen,F., Ma,K., Zhou,C., and Guo,L. (2010). Angiopoietin-1/Tie2 signaling pathway inhibits lipopolysaccharide-induced activation of RAW264.7 macrophage cells. Biochem. Biophys. Res. Commun. *392*, 178-182.

Guha,M. and Mackman,N. (2001). LPS induction of gene expression in human monocytes. Cell Signal. *13*, 85-94.

Gurtner,G.C., Werner,S., Barrandon,Y., and Longaker,M.T. (2008). Wound repair and regeneration. Nature. *453*, 314-321.

Ha,C.H., Jhun,B.S., Kao,H.Y., and Jin,Z.G. (2008). VEGF stimulates HDAC7 phosphorylation and cytoplasmic accumulation modulating matrix metalloproteinase expression and angiogenesis. Arterioscler. Thromb. Vasc. Biol. *28*, 1782-1788.

Haffner,S.M. and Miettinen,H. (1997). Insulin resistance implications for type II diabetes mellitus and coronary heart disease. Am. J. Med. *103*, 152-162.

Han,J., Jiang,Y., Li,Z., Kravchenko,V.V., and Ulevitch,R.J. (1997). Activation of the transcription factor MEF2C by the MAP kinase p38 in inflammation. Nature. *%20;386*, 296-299.

Han,Y.P., Tuan,T.L., Wu,H., Hughes,M., and Garner,W.L. (2001). TNF-alpha stimulates activation of pro-MMP2 in human skin through NF-(kappa)B mediated induction of MT1-MMP. J. Cell Sci. *114*, 131-139.

Hartney,J.M., Brown,J., Chu,H.W., Chang,L.Y., Pelanda,R., and Torres,R.M. (2010). Arhgef1 regulates alpha5beta1 integrin-mediated matrix metalloproteinase expression and is required for homeostatic lung immunity. Am. J. Pathol. *176*, 1157-1168.

Hatley,M.E., Srinivasan,S., Reilly,K.B., Bolick,D.T., and Hedrick,C.C. (2003). Increased production of 12/15 lipoxygenase eicosanoids accelerates monocyte/endothelial interactions in diabetic db/db mice. J. Biol. Chem. *278*, 25369-25375.

Hayashi,T., Juliet,P.A., Miyazaki,A., Ignarro,L.J., and Iguchi,A. (2007). High glucose downregulates the number of caveolae in monocytes through oxidative stress from NADPH oxidase: implications for atherosclerosis. Biochim. Biophys. Acta *1772*, 364-372.

Hembry,R.M., Murphy,G., Cawston,T.E., Dingle,J.T., and Reynolds,J.J. (1986). Characterization of a specific antiserum for mammalian collagenase from several species: immunolocalization of collagenase in rabbit chondrocytes and uterus. J. Cell Sci. *81:105-23.*, 105-123.

Ho,H.H., Antoniv,T.T., Ji,J.D., and Ivashkiv,L.B. (2008). Lipopolysaccharide-induced expression of matrix metalloproteinases in human monocytes is suppressed by IFN-gamma via superinduction of ATF-3 and suppression of AP-1. J. Immunol. *181*, 5089-5097.

Hoffmann,A. and Baltimore,D. (2006). Circuitry of nuclear factor kappaB signaling. Immunol. Rev. *210:171-86.*, 171-186.

Hollingsworth,J.W., Li,Z., Brass,D.M., Garantziotis,S., Timberlake,S.H., Kim,A., Hossain,I., Savani,R.C., and Schwartz,D.A. (2007). CD44 regulates macrophage recruitment to the lung in lipopolysaccharide-induced airway disease. Am. J. Respir. Cell Mol. Biol. *37*, 248-253.

Hotary,K., Li,X.Y., Allen,E., Stevens,S.L., and Weiss,S.J. (2006). A cancer cell metalloprotease triad regulates the basement membrane transmigration program. Genes Dev. *20*, 2673-2686.

Huo,Y. and Xia,L. (2009). P-selectin glycoprotein ligand-1 plays a crucial role in the selective recruitment of leukocytes into the atherosclerotic arterial wall. Trends Cardiovasc. Med. *19*, 140-145.

Ishikawa,F., Miyoshi,H., Nose,K., and Shibanuma,M. (2010a). Transcriptional induction of MMP-10 by TGF-beta, mediated by activation of MEF2A and downregulation of class IIa HDACs. Oncogene *29*, 909-919.

Ishikawa,F., Miyoshi,H., Nose,K., and Shibanuma,M. (2010b). Transcriptional induction of MMP-10 by TGF-beta, mediated by activation of MEF2A and downregulation of class IIa HDACs. Oncogene. *29*, 909-919.

Itoh,Y., Takamura,A., Ito,N., Maru,Y., Sato,H., Suenaga,N., Aoki,T., and Seiki,M. (2001). Homophilic complex formation of MT1-MMP facilitates proMMP-2 activation on the cell surface and promotes tumor cell invasion. EMBO J. *20*, 4782-4793.

Ivetic,A., Florey,O., Deka,J., Haskard,D.O., Ager,A., and Ridley,A.J. (2004). Mutagenesis of the ezrin-radixin-moesin binding domain of L-selectin tail affects shedding, microvillar positioning, and leukocyte tethering. J. Biol. Chem. *279*, 33263-33272.

Ivetic,A. and Ridley,A.J. (2004). The telling tail of L-selectin. Biochem. Soc. Trans. *32*, 1118-1121.

Johnson,J.L., Sala-Newby,G.B., Ismail,Y., Aguilera,C.M., and Newby,A.C. (2008). Low tissue inhibitor of metalloproteinases 3 and high matrix metalloproteinase 14 levels defines a subpopulation of highly invasive foam-cell macrophages. Arterioscler. Thromb. Vasc. Biol. *28*, 1647-1653.

Johnston,S.A., Bramble,J.P., Yeung,C.L., Mendes,P.M., and Machesky,L.M. (2008). Arp2/3 complex activity in filopodia of spreading cells. BMC. Cell Biol. *9:65.*, 65.

Jones,G.E. (2000). Cellular signaling in macrophage migration and chemotaxis. J. Leukoc. Biol. *68*, 593-602.

Kabosova,A., Kramerov,A.A., Aoki,A.M., Murphy,G., Zieske,J.D., and Ljubimov,A.V. (2003). Human diabetic corneas preserve wound healing, basement membrane, integrin and MMP-10 differences from normal corneas in organ culture. Exp. Eye Res. *77*, 211-217.

Kahari,V.M. and Saarialho-Kere,U. (1997). Matrix metalloproteinases in skin. Exp. Dermatol. *6*, 199-213.

Kanitakis,J. (2002). Anatomy, histology and immunohistochemistry of normal human skin. Eur. J. Dermatol. *12*, 390-399.

Kassim,S.Y., Gharib,S.A., Mecham,B.H., Birkland,T.P., Parks,W.C., and McGuire,J.K. (2007). Individual matrix metalloproteinases control distinct transcriptional responses in airway epithelial cells infected with Pseudomonas aeruginosa. Infect. Immun. *75*, 5640-5650.

Kato,T., Haro,H., Komori,H., and Shinomiya,K. (2004). Sequential dynamics of inflammatory cytokine, angiogenesis inducing factor and matrix degrading enzymes during spontaneous resorption of the herniated disc. J. Orthop. Res. *22*, 895-900.

Katoh,K., Kano,Y., Amano,M., Kaibuchi,K., and Fujiwara,K. (2001). Stress fiber organization regulated by MLCK and Rho-kinase in cultured human fibroblasts. Am. J. Physiol Cell Physiol. *280*, C1669-C1679.

Kheir,W.A., Gevrey,J.C., Yamaguchi,H., Isaac,B., and Cox,D. (2005). A WAVE2-Abi1 complex mediates CSF-1-induced F-actin-rich membrane protrusions and migration in macrophages. J. Cell Sci. *118*, 5369-5379.

Killock,D.J. and Ivetic,A. (2010). The cytoplasmic domains of TNFalpha-converting enzyme (TACE/ADAM17) and L-selectin are regulated differently by p38 MAPK and PKC to promote ectodomain shedding. Biochem. J. *428*, 293-304.

Kim,S.Y., Lee,J.G., Cho,W.S., Cho,K.H., Sakong,J., Kim,J.R., Chin,B.R., and Baek,S.H. (2010). Role of NADPH oxidase-2 in lipopolysaccharide-induced matrix metalloproteinase expression and cell migration. Immunol. Cell Biol. *88*, 197-204.

Kimura,K., Kawamoto,K., Teranishi,S., and Nishida,T. (2006). Role of Rac1 in fibronectin-induced adhesion and motility of human corneal epithelial cells. Invest Ophthalmol. Vis. Sci. *47*, 4323-4329.

Kitani,A., Nakashima,N., Izumihara,T., Inagaki,M., Baoui,X., Yu,S., Matsuda,T., and Matsuyama,T. (1998). Soluble VCAM-1 induces chemotaxis of Jurkat and synovial fluid T cells bearing high affinity very late antigen-4. J. Immunol. *161*, 4931-4938.

Kleemann,R., Zadelaar,S., and Kooistra,T. (2008). Cytokines and atherosclerosis: a comprehensive review of studies in mice. Cardiovasc. Res. *79*, 360-376.

Kong,L. and Ge,B.X. (2008). MyD88-independent activation of a novel actin-Cdc42/Rac pathway is required for Toll-like receptor-stimulated phagocytosis. Cell Res. *18*, 745-755.

Kong,W., Yang,H., He,L., Zhao,J.J., Coppola,D., Dalton,W.S., and Cheng,J.Q. (2008). MicroRNA-155 is regulated by the transforming growth factor beta/Smad pathway and contributes to epithelial cell plasticity by targeting RhoA. Mol. Cell Biol. *28*, 6773-6784.

Korpos,E., Wu,C., Song,J., Hallmann,R., and Sorokin,L. (2010). Role of the extracellular matrix in lymphocyte migration. Cell Tissue Res. *339*, 47-57.

Koyama,Y., Norose-Toyoda,K., Hirano,S., Kobayashi,M., Ebihara,T., Someki,I., Fujisaki,H., and Irie,S. (2000). Type I collagen is a non-adhesive extracellular matrix for macrophages. Arch. Histol. Cytol. *63*, 71-79.

Krampert,M., Bloch,W., Sasaki,T., Bugnon,P., Rulicke,T., Wolf,E., Aumailley,M., Parks,W.C., and Werner,S. (2004). Activities of the matrix metalloproteinase stromelysin-2 (MMP-10) in matrix degradation and keratinocyte organization in wounded skin. Mol. Biol. Cell *15*, 5242-5254.

Krampert,M., Kuenzle,S., Thai,S.N., Lee,N., Iruela-Arispe,M.L., and Werner,S. (2005). ADAMTS1 proteinase is up-regulated in wounded skin and regulates migration of fibroblasts and endothelial cells. J. Biol. Chem. *280*, 23844-23852.

Le Gall,S.M., Bobe,P., Reiss,K., Horiuchi,K., Niu,X.D., Lundell,D., Gibb,D.R., Conrad,D., Saftig,P., and Blobel,C.P. (2009). ADAMs 10 and 17 represent differentially regulated components of a general shedding machinery for membrane proteins such as transforming growth factor alpha, L-selectin, and tumor necrosis factor alpha. Mol. Biol. Cell *20*, 1785-1794.

Leibovich,S.J. and Ross,R. (1975). The role of the macrophage in wound repair. A study with hydrocortisone and antimacrophage serum. Am. J. Pathol. *78*, 71-100.

Li,S.L., Reddy,M.A., Cai,Q., Meng,L., Yuan,H., Lanting,L., and Natarajan,R. (2006). Enhanced proatherogenic responses in macrophages and vascular smooth muscle cells derived from diabetic db/db mice. Diabetes *55*, 2611-2619.

Liang,C.P., Han,S., Senokuchi,T., and Tall,A.R. (2007). The macrophage at the crossroads of insulin resistance and atherosclerosis. Circ. Res. *100*, 1546-1555.

Linder,S. (2007). The matrix corroded: podosomes and invadopodia in extracellular matrix degradation. Trends Cell Biol. *17*, 107-117.

Linder,S., Higgs,H., Hufner,K., Schwarz,K., Pannicke,U., and Aepfelbacher,M. (2000). The polarization defect of Wiskott-Aldrich syndrome macrophages is linked to dislocalization of the Arp2/3 complex. J. Immunol. *165*, 221-225.

Liu,L., Marti,G.P., Wei,X., Zhang,X., Zhang,H., Liu,Y.V., Nastai,M., Semenza,G.L., and Harmon,J.W. (2008). Age-dependent impairment of HIF-1alpha expression in diabetic mice: Correction with electroporation-facilitated gene therapy increases wound healing, angiogenesis, and circulating angiogenic cells. J. Cell Physiol. *217*, 319-327.

Lu,B., Rutledge,B.J., Gu,L., Fiorillo,J., Lukacs,N.W., Kunkel,S.L., North,R., Gerard,C., and Rollins,B.J. (1998). Abnormalities in monocyte recruitment and cytokine expression in monocyte chemoattractant protein 1-deficient mice. J. Exp. Med. *187*, 601-608.

Lu,Y. and Wahl,L.M. (2005). Production of matrix metalloproteinase-9 by activated human monocytes involves a phosphatidylinositol-3 kinase/Akt/IKKalpha/NF-kappaB pathway. J. Leukoc. Biol. *78*, 259-265.

Lund,L.R., Romer,J., Bugge,T.H., Nielsen,B.S., Frandsen,T.L., Degen,J.L., Stephens,R.W., and Dano,K. (1999). Functional overlap between two classes of matrix-degrading proteases in wound healing. EMBO J. *18*, 4645-4656.

Luster,A.D., Alon,R., and von Andrian,U.H. (2005). Immune cell migration in inflammation: present and future therapeutic targets. Nat. Immunol. *6*, 1182-1190.

Madison,K.C. (2003). Barrier function of the skin: "la raison d'etre" of the epidermis. J. Invest Dermatol. *121*, 231-241.

Madlener,M., Mauch,C., Conca,W., Brauchle,M., Parks,W.C., and Werner,S. (1996). Regulation of the expression of stromelysin-2 by growth factors in keratinocytes: implications for normal and impaired wound healing. Biochem. J. *320*, 659-664.

Martin,P. and Leibovich,S.J. (2005). Inflammatory cells during wound repair: the good, the bad and the ugly. Trends Cell Biol. *15*, 599-607.

Maruyama,K., Asai,J., Ii,M., Thorne,T., Losordo,D.W., and D'Amore,P.A. (2007). Decreased macrophage number and activation lead to reduced lymphatic vessel formation and contribute to impaired diabetic wound healing. Am. J. Pathol. *170*, 1178-1191.

Matias-Roman,S., Galvez,B.G., Genis,L., Yanez-Mo,M., de la,R.G., Sanchez-Mateos,P., Sanchez-Madrid,F., and Arroyo,A.G. (2005). Membrane type 1-matrix metalloproteinase is involved in migration of human monocytes and is regulated through their interaction with fibronectin or endothelium. Blood. *105*, 3956-3964.

McKnight,A.J., Macfarlane,A.J., Dri,P., Turley,L., Willis,A.C., and Gordon,S. (1996). Molecular cloning of F4/80, a murine macrophage-restricted cell surface glycoprotein with homology to the G-protein-linked transmembrane 7 hormone receptor family. J. Biol. Chem. *271*, 486-489.

Meconi,S., Jacomo,V., Boquet,P., Raoult,D., Mege,J.L., and Capo,C. (1998). Coxiella burnetii induces reorganization of the actin cytoskeleton in human monocytes. Infect. Immun. *66*, 5527-5533.

Meng,L., Park,J., Cai,Q., Lanting,L., Reddy,M.A., and Natarajan,R. (2010). Diabetic conditions promote binding of monocytes to vascular smooth muscle cells and their subsequent differentiation. Am. J. Physiol Heart Circ. Physiol. *298*, H736-H745.

Mestas,J. and Ley,K. (2008). Monocyte-endothelial cell interactions in the development of atherosclerosis. Trends Cardiovasc. Med. *18*, 228-232.

Mirastschijski,U., Impola,U., Karsdal,M.A., Saarialho-Kere,U., and Agren,M.S. (2002). Matrix metalloproteinase inhibitor BB-3103 unlike the serine proteinase inhibitor aprotinin abrogates epidermal healing of human skin wounds ex vivo. J. Invest Dermatol. *118*, 55-64.

Mirza,R., DiPietro,L.A., and Koh,T.J. (2009). Selective and specific macrophage ablation is detrimental to wound healing in mice. Am. J. Pathol. *175*, 2454-2462.

Moser,M., Nieswandt,B., Ussar,S., Pozgajova,M., and Fassler,R. (2008). Kindlin-3 is essential for integrin activation and platelet aggregation. Nat. Med. *14*, 325-330.

Mosesson,M.W. (2005). Fibrinogen and fibrin structure and functions. J. Thromb. Haemost. *3*, 1894-1904.

Mozaffarian,D., Kamineni,A., Carnethon,M., Djousse,L., Mukamal,K.J., and Siscovick,D. (2009). Lifestyle risk factors and new-onset diabetes mellitus in older adults: the cardiovascular health study. Arch. Intern. Med. *169*, 798-807.

Murphy,G., Atkinson,S., Ward,R., Gavrilovic,J., and Reynolds,J.J. (1992). The role of plasminogen activators in the regulation of connective tissue metalloproteinases. Ann. N. Y. Acad. Sci. *667:1-12.*, 1-12.

Murphy,G. and Gavrilovic,J. (1999). Proteolysis and cell migration: creating a path? Curr. Opin. Cell Biol. *11*, 614-621.

Murphy,G. and Knauper,V. (1997). Relating matrix metalloproteinase structure to function: why the "hemopexin" domain? Matrix Biol. *15*, 511-518.

Nagase,H., Visse,R., and Murphy,G. (2006). Structure and function of matrix metalloproteinases and TIMPs. Cardiovasc. Res. *69*, 562-573.

Nareika,A., He,L., Game,B.A., Slate,E.H., Sanders,J.J., London,S.D., Lopes-Virella,M.F., and Huang,Y. (2005). Sodium lactate increases LPS-stimulated MMP and cytokine expression in U937 histiocytes by enhancing AP-1 and NF-kappaB transcriptional activities. Am. J. Physiol Endocrinol. Metab *289*, E534-E542.

Nascimento,A.P. and Costa,A.M. (2006). Overweight induced by high-fat diet delays rat cutaneous wound healing. Br. J. Nutr. *96*, 1069-1077.

Newby,A.C. (2005). Dual role of matrix metalloproteinases (matrixins) in intimal thickening and atherosclerotic plaque rupture. Physiol Rev. *85*, 1-31.

Newby,A.C. (2007). Metalloproteinases and vulnerable atherosclerotic plaques. Trends Cardiovasc. Med. *17*, 253-258.

Ninichuk,V., Khandoga,A.G., Segerer,S., Loetscher,P., Schlapbach,A., Revesz,L., Feifel,R., Khandoga,A., Krombach,F., Nelson,P.J., Schlondorff,D., and Anders,H.J. (2007). The role of interstitial macrophages in nephropathy of type 2 diabetic db/db mice. Am. J. Pathol. *170*, 1267-1276.

Nogales,E. (2000). Structural insights into microtubule function. Annu. Rev. Biochem. *69:277-302.*, 277-302.

Norata,G.D., Bjork,H., Hamsten,A., Catapano,A.L., and Eriksson,P. (2004). High-density lipoprotein subfraction 3 decreases ADAMTS-1 expression induced by lipopolysaccharide and tumor necrosis factor-alpha in human endothelial cells. Matrix Biol. *22*, 557-560.

O'Connell,R.M., Rao,D.S., Chaudhuri,A.A., Boldin,M.P., Taganov,K.D., Nicoll,J., Paquette,R.L., and Baltimore,D. (2008). Sustained expression of microRNA-155 in hematopoietic stem cells causes a myeloproliferative disorder. J. Exp. Med.

O'Connell,R.M., Taganov,K.D., Boldin,M.P., Cheng,G., and Baltimore,D. (2007). MicroRNA-155 is induced during the macrophage inflammatory response. Proc. Natl. Acad. Sci. U. S. A *104*, 1604-1609.

Overall,C.M., McQuibban,G.A., and Clark-Lewis,I. (2002). Discovery of chemokine substrates for matrix metalloproteinases by exosite scanning: a new tool for degradomics. Biol. Chem. *383*, 1059-1066.

Pankov,R., Endo,Y., Even-Ram,S., Araki,M., Clark,K., Cukierman,E., Matsumoto,K., and Yamada,K.M. (2005). A Rac switch regulates random versus directionally persistent cell migration. J. Cell Biol. *170*, 793-802.

Pankov,R. and Yamada,K.M. (2002). Fibronectin at a glance. J. Cell Sci. *115*, 3861-3863.

Parker,K.K., Brock,A.L., Brangwynne,C., Mannix,R.J., Wang,N., Ostuni,E., Geisse,N.A., Adams,J.C., Whitesides,G.M., and Ingber,D.E. (2002). Directional control of lamellipodia extension by constraining cell shape and orienting cell tractional forces. FASEB J. *16*, 1195-1204.

Perttila,J., Salo,M., and Peltola,O. (1990). Plasma fibronectin concentrations in blood products. Intensive Care Med. *16*, 41-43.

Petrie,R.J., Doyle,A.D., and Yamada,K.M. (2009). Random versus directionally persistent cell migration. Nat. Rev. Mol. Cell Biol. *10*, 538-549.

Pasquinelli, A.E., Hunter, S., Bracht, J. (2005). MicroRNAs: a developing story. Curr Opin Genet Dev. *15*, 200-5.

Pilcher,B.K., Dumin,J.A., Sudbeck,B.D., Krane,S.M., Welgus,H.G., and Parks,W.C. (1997). The activity of collagenase-1 is required for keratinocyte migration on a type I collagen matrix. J. Cell Biol. *137*, 1445-1457.

Pixley,F.J. and Stanley,E.R. (2004). CSF-1 regulation of the wandering macrophage: complexity in action. Trends Cell Biol. *14*, 628-638.

Pollard,J.W. (1997). Role of colony-stimulating factor-1 in reproduction and development. Mol. Reprod. Dev. *46*, 54-60.

Proksch,E., Brandner,J.M., and Jensen,J.M. (2008). The skin: an indispensable barrier. Exp. Dermatol. *17*, 1063-1072.

Rawlings,N.D. and Barrett,A.J. (1993). Evolutionary families of peptidases. Biochem. J. *290*, 205-218.

Rawlings,N.D., Barrett,A.J., and Bateman,A. (2010). MEROPS: the peptidase database. Nucleic Acids Res. *38*, D227-D233.

Rechardt,O., Elomaa,O., Vaalamo,M., Paakkonen,K., Jahkola,T., Hook-Nikanne,J., Hembry,R.M., Hakkinen,L., Kere,J., and Saarialho-Kere,U. (2000). Stromelysin-2 is upregulated during normal wound repair and is induced by cytokines. J. Invest Dermatol. *115*, 778-787.

Redd,M.J., Kelly,G., Dunn,G., Way,M., and Martin,P. (2006). Imaging macrophage chemotaxis in vivo: studies of microtubule function in zebrafish wound inflammation. Cell Motil. Cytoskeleton. *63*, 415-422.

Reijerkerk,A., Kooij,G., van der Pol,S.M., Khazen,S., Dijkstra,C.D., and de Vries,H.E. (2006). Diapedesis of monocytes is associated with MMP-mediated occludin disappearance in brain endothelial cells. FASEB J. *20*, 2550-2552.

Reiss,K., Ludwig,A., and Saftig,P. (2006). Breaking up the tie: disintegrin-like metalloproteinases as regulators of cell migration in inflammation and invasion. Pharmacol. Ther. *111*, 985-1006.

Ren,X.D., Kiosses,W.B., and Schwartz,M.A. (1999). Regulation of the small GTP-binding protein Rho by cell adhesion and the cytoskeleton. EMBO J. *18*, 578-585.

Ridley,A.J. (2001). Rho GTPases and cell migration. J. Cell Sci. *114*, 2713-2722.

Ridley,A.J., Schwartz,M.A., Burridge,K., Firtel,R.A., Ginsberg,M.H., Borisy,G., Parsons,J.T., and Horwitz,A.R. (2003). Cell migration: integrating signals from front to back. Science. *302*, 1704-1709.

Robinson,J.M. and Vandre,D.D. (1995). Stimulus-dependent alterations in macrophage microtubules: increased tubulin polymerization and detyrosination. J. Cell Sci. *108*, 645-655.

Rodriguez,A., Vigorito,E., Clare,S., Warren,M.V., Couttet,P., Soond,D.R., van Dongen,S., Grocock,R.J., Das,P.P., Miska,E.A., Vetrie,D., Okkenhaug,K., Enright,A.J., Dougan,G., Turner,M., and Bradley,A. (2007). Requirement of bic/microRNA-155 for normal immune function. Science *316*, 608-611.

Rodriguez,J.A., Orbe,J., Martinez,d.L., Calvayrac,O., Rodriguez,C., Martinez-Gonzalez,J., and Paramo,J.A. (2008). Metalloproteinases and atherothrombosis: MMP-10 mediates vascular remodeling promoted by inflammatory stimuli. Front Biosci. *13*, 2916-2921.

Roldan,E., Garcia-Pardo,A., and Brieva,J.A. (1992). VLA-4-fibronectin interaction is required for the terminal differentiation of human bone marrow cells capable of spontaneous and high rate immunoglobulin secretion. J. Exp. Med. *175*, 1739-1747.

Ronald,J.A., Ionescu,C.V., Rogers,K.A., and Sandig,M. (2001). Differential regulation of transendothelial migration of THP-1 cells by ICAM-1/LFA-1 and VCAM-1/VLA-4. J. Leukoc. Biol. *70*, 601-609.

Rosmarin,A.G., Yang,Z., and Resendes,K.K. (2005). Transcriptional regulation in myelopoiesis: Hematopoietic fate choice, myeloid differentiation, and leukemogenesis. Exp. Hematol. *33*, 131-143.

Sabeh,F., Shimizu-Hirota,R., and Weiss,S.J. (2009). Protease-dependent versus -independent cancer cell invasion programs: three-dimensional amoeboid movement revisited. J. Cell Biol. *185*, 11-19.

Saghizadeh,M., Brown,D.J., Castellon,R., Chwa,M., Huang,G.H., Ljubimova,J.Y., Rosenberg,S., Spirin,K.S., Stolitenko,R.B., Adachi,W., Kinoshita,S., Murphy,G., Windsor,L.J., Kenney,M.C., and Ljubimov,A.V. (2001). Overexpression of matrix metalloproteinase-10 and matrix metalloproteinase-3 in human diabetic corneas: a possible mechanism of basement membrane and integrin alterations. Am. J. Pathol. *158*, 723-734.

Saghizadeh,M., Kramerov,A.A., Yaghoobzadeh,Y., Hu,J., Ljubimova,J.Y., Black,K.L., Castro,M.G., and Ljubimov,A.V. (2010). Adenovirus-driven overexpression of proteinases in organ-cultured normal human corneas leads to diabetic-like changes. Brain Res. Bull. *81*, 262-272.

Salmela,M.T., Pender,S.L., Karjalainen-Lindsberg,M.L., Puolakkainen,P., Macdonald,T.T., and Saarialho-Kere,U. (2004). Collagenase-1 (MMP-1), matrilysin-1 (MMP-7), and stromelysin-2 (MMP-10) are expressed by migrating enterocytes during intestinal wound healing. Scand. J. Gastroenterol. *39*, 1095-1104.

Schapira,K., Lutgens,E., de,F.A., Sprague,A., Roemen,A., Gardner,H., Koteliansky,V., Daemen,M., and Heeneman,S. (2005). Genetic deletion or antibody blockade of alpha1beta1 integrin induces a stable plaque phenotype in ApoE-/- mice. Arterioscler. Thromb. Vasc. Biol. *25*, 1917-1924.

Schneider,F., Sukhova,G.K., Aikawa,M., Canner,J., Gerdes,N., Tang,S.M., Shi,G.P., Apte,S.S., and Libby,P. (2008). Matrix metalloproteinase-14 deficiency in bone marrow-derived cells promotes collagen accumulation in mouse atherosclerotic plaques. Circulation *117*, 931-939.

Shanmugam,N., Reddy,M.A., Guha,M., and Natarajan,R. (2003). High glucose-induced expression of proinflammatory cytokine and chemokine genes in monocytic cells. Diabetes *52*, 1256-1264.

Shimoda,M., Hashimoto,G., Mochizuki,S., Ikeda,E., Nagai,N., Ishida,S., and Okada,Y. (2007). Binding of ADAM28 to P-selectin glycoprotein ligand-1 enhances P-selectin-mediated leukocyte adhesion to endothelial cells. J. Biol. Chem. *282*, 25864-25874.

Shivdasani,R.A. (2006). MicroRNAs: regulators of gene expression and cell differentiation. Blood *108*, 3646-3653.

Si,J., Ge,Y., Zhuang,S., and Gong,R. (2010). Inhibiting nonmuscle myosin II impedes inflammatory infiltration and ameliorates progressive renal disease. Lab Invest. *90*, 448-458.

Singh,R.J., Mason,J.C., Lidington,E.A., Edwards,D.R., Nuttall,R.K., Khokha,R., Knauper,V., Murphy,G., and Gavrilovic,J. (2005). Cytokine stimulated vascular cell adhesion molecule-1 (VCAM-1) ectodomain release is regulated by TIMP-3. Cardiovasc. Res. *67*, 39-49.

Sithu,S.D., English,W.R., Olson,P., Krubasik,D., Baker,A.H., Murphy,G., and D'Souza,S.E. (2007). Membrane-type 1-matrix metalloproteinase regulates intracellular adhesion molecule-1 (ICAM-1)-mediated monocyte transmigration. J. Biol. Chem. *282*, 25010-25019.

Song,S.H. and Vieille,C. (2009). Recent advances in the biological production of mannitol. Appl. Microbiol. Biotechnol. *84*, 55-62.

Sorrell,J.M. and Caplan,A.I. (2004). Fibroblast heterogeneity: more than skin deep. J. Cell Sci. *117*, 667-675.

Stahl,P.D. and Ezekowitz,R.A. (1998). The mannose receptor is a pattern recognition receptor involved in host defense. Curr. Opin. Immunol. *10*, 50-55.

Stefanidakis,M., Ruohtula,T., Borregaard,N., Gahmberg,C.G., and Koivunen,E. (2004). Intracellular and cell surface localization of a complex between alphaMbeta2 integrin and promatrix metalloproteinase-9 progelatinase in neutrophils. J. Immunol. *172*, 7060-7068.

Stringa,E., Knauper,V., Murphy,G., and Gavrilovic,J. (2000). Collagen degradation and platelet-derived growth factor stimulate the migration of vascular smooth muscle cells. J. Cell Sci. *113*, 2055-2064.

Sunderkotter,C., Steinbrink,K., Goebeler,M., Bhardwaj,R., and Sorg,C. (1994). Macrophages and angiogenesis. J. Leukoc. Biol. *55*, 410-422.

Suzuki,T., Hashimoto,S., Toyoda,N., Nagai,S., Yamazaki,N., Dong,H.Y., Sakai,J., Yamashita,T., Nukiwa,T., and Matsushima,K. (2000). Comprehensive gene expression profile of LPS-stimulated human monocytes by SAGE. Blood. *96*, 2584-2591.

Sweet,M.J., Campbell,C.C., Sester,D.P., Xu,D., McDonald,R.C., Stacey,K.J., Hume,D.A., and Liew,F.Y. (2002). Colony-stimulating factor-1 suppresses responses to CpG DNA and expression of toll-like receptor 9 but enhances responses to lipopolysaccharide in murine macrophages. J. Immunol. *168*, 392-399.

Szalai,C., Duba,J., Prohaszka,Z., Kalina,A., Szabo,T., Nagy,B., Horvath,L., and Csaszar,A. (2001). Involvement of polymorphisms in the chemokine system in the susceptibility for coronary artery disease (CAD). Coincidence of elevated Lp(a) and MCP-1 -2518 G/G genotype in CAD patients. Atherosclerosis. *158*, 233-239.

Taganov,K.D., Boldin,M.P., Chang,K.J., and Baltimore,D. (2006). NF-kappaB-dependent induction of microRNA miR-146, an inhibitor targeted to signaling proteins of innate immune responses. Proc. Natl. Acad. Sci. U. S. A *103*, 12481-12486.

Takahashi,K., Takeya,M., and Sakashita,N. (2002). Multifunctional roles of macrophages in the development and progression of atherosclerosis in humans and experimental animals. Med. Electron Microsc. *35*, 179-203.

Tester,A.M., Cox,J.H., Connor,A.R., Starr,A.E., Dean,R.A., Puente,X.S., Lopez-Otin,C., and Overall,C.M. (2007). LPS responsiveness and neutrophil chemotaxis in vivo require PMN MMP-8 activity. PLoS. One. *2*, e312.

Thompson,R.D., Noble,K.E., Larbi,K.Y., Dewar,A., Duncan,G.S., Mak,T.W., and Nourshargh,S. (2001). Platelet-endothelial cell adhesion molecule-1 (PECAM-1)-deficient mice demonstrate a transient and cytokine-specific role for PECAM-1 in leukocyte migration through the perivascular basement membrane. Blood. *97*, 1854-1860.

Tili,E., Michaille,J.J., Cimino,A., Costinean,S., Dumitru,C.D., Adair,B., Fabbri,M., Alder,H., Liu,C.G., Calin,G.A., and Croce,C.M. (2007). Modulation of miR-155 and miR-125b levels following lipopolysaccharide/TNF-alpha stimulation and their possible roles in regulating the response to endotoxin shock. J. Immunol. *179*, 5082-5089.

Trial,J., Baughn,R.E., Wygant,J.N., McIntyre,B.W., Birdsall,H.H., Youker,K.A., Evans,A., Entman,M.L., and Rossen,R.D. (1999). Fibronectin fragments modulate monocyte VLA-5 expression and monocyte migration. J. Clin. Invest. *104*, 419-430.

Tsuboi,R. and Rifkin,D.B. (1990). Recombinant basic fibroblast growth factor stimulates wound healing in healing-impaired db/db mice. J. Exp. Med. *172*, 245-251.

Uchida,K.S., Kitanishi-Yumura,T., and Yumura,S. (2003). Myosin II contributes to the posterior contraction and the anterior extension during the retraction phase in migrating Dictyostelium cells. J. Cell Sci. *116*, 51-60.

Urban,E., Jacob,S., Nemethova,M., Resch,G.P., and Small,J.V. (2010). Electron tomography reveals unbranched networks of actin filaments in lamellipodia. Nat. Cell Biol. *12*, 429-435.

Ussar,S., Wang,H.V., Linder,S., Fassler,R., and Moser,M. (2006). The Kindlins: subcellular localization and expression during murine development. Exp. Cell Res. *312*, 3142-3151.

Uzui,H., Harpf,A., Liu,M., Doherty,T.M., Shukla,A., Chai,N.N., Tripathi,P.V., Jovinge,S., Wilkin,D.J., Asotra,K., Shah,P.K., and Rajavashisth,T.B. (2002). Increased expression of membrane type 3-matrix metalloproteinase in human atherosclerotic plaque: role of activated macrophages and inflammatory cytokines. Circulation *106*, 3024-3030.

Valledor,A.F., Borras,F.E., Cullell-Young,M., and Celada,A. (1998). Transcription factors that regulate monocyte/macrophage differentiation. J. Leukoc. Biol. *63*, 405-417.

Van,G.E., Poincloux,R., Gauffre,F., Maridonneau-Parini,I., and Le,C., V (2010). Matrix architecture dictates three-dimensional migration modes of human macrophages: differential involvement of proteases and podosome-like structures. J. Immunol. *184*, 1049-1061.

Van,T.C., Alain,T., Kossakowska,A.E., Urbanski,S., Potworowski,E.F., and St-Pierre,Y. (2004). Stromelysin-2 (matrix metalloproteinase 10) is inducible in lymphoma cells and accelerates the growth of lymphoid tumors in vivo. J. Immunol. *173*, 3605-3611.

Velnar,T., Bailey,T., and Smrkolj,V. (2009). The wound healing process: an overview of the cellular and molecular mechanisms. J. Int. Med. Res. *37*, 1528-1542.

Vicente-Manzanares,M., Webb,D.J., and Horwitz,A.R. (2005). Cell migration at a glance. J. Cell Sci. *118*, 4917-4919.

Voisin,M.B., Woodfin,A., and Nourshargh,S. (2009). Monocytes and neutrophils exhibit both distinct and common mechanisms in penetrating the vascular basement membrane in vivo. Arterioscler. Thromb. Vasc. Biol. *29*, 1193-1199.

Wagsater,D., Bjork,H., Zhu,C., Bjorkegren,J., Valen,G., Hamsten,A., and Eriksson,P. (2007). ADAMTS-4 and -8 are inflammatory regulated enzymes expressed in macrophage-rich areas of human atherosclerotic plaques. Atherosclerosis.

Walker,E.B., Akporiaye,E.T., Warner,N.L., and Stewart,C.C. (1985). Characterization of subsets of bone marrow-derived macrophages by flow cytometry analysis. J. Leukoc. Biol. *37*, 121-136.

Wall,S.J., Bevan,D., Thomas,D.W., Harding,K.G., Edwards,D.R., and Murphy,G. (2002). Differential expression of matrix metalloproteinases during impaired wound healing of the diabetes mouse. J. Invest Dermatol. *119*, 91-98.

Wang,L., Zheng,J., Bai,X., Liu,B., Liu,C.J., Xu,Q., Zhu,Y., Wang,N., Kong,W., and Wang,X. (2009). ADAMTS-7 mediates vascular smooth muscle cell migration and neointima formation in balloon-injured rat arteries. Circ. Res. *104*, 688-698.

Wang,S., Voisin,M.B., Larbi,K.Y., Dangerfield,J., Scheiermann,C., Tran,M., Maxwell,P.H., Sorokin,L., and Nourshargh,S. (2006). Venular basement membranes contain specific matrix protein low expression regions that act as exit points for emigrating neutrophils. J. Exp. Med. *203*, 1519-1532.

Webb,S.E., Pollard,J.W., and Jones,G.E. (1996). Direct observation and quantification of macrophage chemoattraction to the growth factor CSF-1. J. Cell Sci. *109 (Pt 4)*, 793-803.

Webster,N.L. and Crowe,S.M. (2006). Matrix metalloproteinases, their production by monocytes and macrophages and their potential role in HIV-related diseases. J. Leukoc. Biol. *80*, 1052-1066.

Weisberg,S.P., McCann,D., Desai,M., Rosenbaum,M., Leibel,R.L., and Ferrante,A.W., Jr. (2003). Obesity is associated with macrophage accumulation in adipose tissue. J. Clin. Invest. *112*, 1796-1808.

Wells, C.M., Walmsley, M., Ooi, S., Tybulewicz, V., Ridley, A.J. (2004). Rac1-deficient macrophages exhibit defects in cell spreading and membrane ruffling but not migration. J. Cell Sci. *17*, 1259-68.

Wendt,T., Harja,E., Bucciarelli,L., Qu,W., Lu,Y., Rong,L.L., Jenkins,D.G., Stein,G., Schmidt,A.M., and Yan,S.F. (2006). RAGE modulates vascular inflammation and atherosclerosis in a murine model of type 2 diabetes. Atherosclerosis. *185*, 70-77.

West,M.A., Prescott,A.R., Chan,K.M., Zhou,Z., Rose-John,S., Scheller,J., and Watts,C. (2008). TLR ligand-induced podosome disassembly in dendritic cells is ADAM17 dependent. J. Cell Biol. *182*, 993-1005.

Wheeler,A.P. and Ridley,A.J. (2007). RhoB affects macrophage adhesion, integrin expression and migration. Exp. Cell Res. *313*, 3505-3516.

Wheeler,A.P., Wells,C.M., Smith,S.D., Vega,F.M., Henderson,R.B., Tybulewicz,V.L., and Ridley,A.J. (2006). Rac1 and Rac2 regulate macrophage morphology but are not essential for migration. J. Cell Sci. *119*, 2749-2757.

Wierzbicka-Patynowski,I. and Schwarzbauer,J.E. (2003). The ins and outs of fibronectin matrix assembly. J. Cell Sci. *116*, 3269-3276.

Wiktor-Jedrzejczak,W., Bartocci,A., Ferrante,A.W., Jr., Ahmed-Ansari,A., Sell,K.W., Pollard,J.W., and Stanley,E.R. (1990). Total absence of colony-stimulating factor 1 in the macrophage-deficient osteopetrotic (op/op) mouse. Proc. Natl. Acad. Sci. U. S. A *87*, 4828-4832.

Williams,L.M. and Ridley,A.J. (2000). Lipopolysaccharide induces actin reorganization and tyrosine phosphorylation of Pyk2 and paxillin in monocytes and macrophages. J. Immunol. *164*, 2028-2036.

Wojciak-Stothard,B., Williams,L., and Ridley,A.J. (1999). Monocyte adhesion and spreading on human endothelial cells is dependent on Rho-regulated receptor clustering. J. Cell Biol. *145*, 1293-1307.

Wolf,K., Mazo,I., Leung,H., Engelke,K., von Andrian,U.H., Deryugina,E.I., Strongin,A.Y., Brocker,E.B., and Friedl,P. (2003a). Compensation mechanism in tumor cell migration: mesenchymal-amoeboid transition after blocking of pericellular proteolysis. J. Cell Biol. *%20;160*, 267-277.

Wolf,K., Muller,R., Borgmann,S., Brocker,E.B., and Friedl,P. (2003b). Amoeboid shape change and contact guidance: T-lymphocyte crawling through fibrillar collagen is independent of matrix remodeling by MMPs and other proteases. Blood. *102*, 3262-3269.

Worthylake,R.A. and Burridge,K. (2001). Leukocyte transendothelial migration: orchestrating the underlying molecular machinery. Curr. Opin. Cell Biol. *13*, 569-577.

Worthylake,R.A., Lemoine,S., Watson,J.M., and Burridge,K. (2001). RhoA is required for monocyte tail retraction during transendothelial migration. J. Cell Biol. *154*, 147-160.

Xia,H., Qi,Y., Ng,S.S., Chen,X., Li,D., Chen,S., Ge,R., Jiang,S., Li,G., Chen,Y., He,M.L., Kung,H.F., Lai,L., and Lin,M.C. (2009). microRNA-146b inhibits glioma cell migration and invasion by targeting MMPs. Brain Res. *1269:158-65. Epub;%2009 Mar 3.*, 158-165.

Xie,B., Laouar,A., and Huberman,E. (1998). Fibronectin-mediated cell adhesion is required for induction of 92-kDa type IV collagenase/gelatinase (MMP-9) gene expression during macrophage differentiation. The signaling role of protein kinase C-beta. J. Biol. Chem. *273*, 11576-11582.

Yeop,H.C., Kargi,A.Y., Omer,M., Chan,C.K., Wabitsch,M., O'Brien,K.D., Wight,T.N., and Chait,A. (2010). Differential effect of saturated and unsaturated free fatty acids on the generation of monocyte adhesion and chemotactic factors by adipocytes: dissociation of adipocyte hypertrophy from inflammation. Diabetes. *59*, 386-396.

Yu,W.H., Yu,S., Meng,Q., Brew,K., and Woessner,J.F., Jr. (2000). TIMP-3 binds to sulfated glycosaminoglycans of the extracellular matrix. J. Biol. Chem. *275*, 31226-31232.

Yurchenco,P.D. and Schittny,J.C. (1990). Molecular architecture of basement membranes. FASEB J. *4*, 1577-1590.

Zhang,H., Sun,C., Glogauer,M., and Bokoch,G.M. (2009). Human neutrophils coordinate chemotaxis by differential activation of Rac1 and Rac2. J. Immunol. *183*, 2718-2728.

Zhao,B., Bowden,R.A., Stavchansky,S.A., and Bowman,P.D. (2001). Human endothelial cell response to gram-negative lipopolysaccharide assessed with cDNA microarrays. Am. J. Physiol Cell Physiol. *281*, C1587-C1595.

Zimmet,P., Alberti,K.G., and Shaw,J. (2001). Global and societal implications of the diabetes epidemic. Nature *414*, 782-787.

Zykova,S.N., Jenssen,T.G., Berdal,M., Olsen,R., Myklebust,R., and Seljelid,R. (2000). Altered cytokine and nitric oxide secretion in vitro by macrophages from diabetic type II-like db/db mice. Diabetes *49*, 1451-1458.